

SPUTTER DEPOSITION OF Y-Ba-Cu-O SUPERCONDUCTOR
AND SrTiO_3 BARRIER LAYER THIN FILMS

By

JAMES KELLY TRUMAN

A DISSERTATION PRESENTED TO THE GRADUATE SCHOOL
OF THE UNIVERSITY OF FLORIDA IN PARTIAL FULFILLMENT
OF THE REQUIREMENTS FOR THE DEGREE OF
DOCTOR OF PHILOSOPHY

UNIVERSITY OF FLORIDA

1992

To my family

ACKNOWLEDGEMENTS

I wish to extend boundless gratitude to Dr. Paul Holloway for being the most patient, challenging, understanding, supportive, and helpful advisor and friend I could have imagined. The University of Florida should grant him a bonus sabbatical year, restricted to long, relaxed fishing excursions, for having had to work with me for so long.

I am thankful for the advise, time, and efforts of the other members of my doctoral committee who include Drs. Joseph Simmons, Robert DeHoff, and Rolf Hummel of the Department of Materials Science and Engineering and David Tanner of the Department of Physics. Their insights and enlightened critiques have made my education a more enriched experience.

The various staff personnel in the Department of Materials Science and Engineering who worked with me over the years were a great help. I would like to acknowledge Wayne Acree for electron microprobe analysis, Amy Holtzer for X-ray diffraction work, and Eric Lambers for Auger analysis and training. I would especially like to thank Joe Rojo for keeping me connected to UF while I was in Rochester

and Ludie Hampton for being a good secretary and a good friend.

I went through a lot over the years with other graduate students and made many friends who have unique places in my memories. I would like to single out my good friends Steve Wallace and Tom Bussing for being long-time sources of support, commiseration, entertainment and irreverence. Further, I would like to thank Carl Mueller for making many of the sputter targets used in my work and for being my partner in all aspects of high temperature superconductor work in our laboratory. I would also like to thank Greg Lindauer for writing the software which controlled the resistance versus temperature system and Ed Clausen for invaluable help when I first delved heavily into personal computers. Finally, I am grateful for the experience of having worked and socialized with people from a variety of cultures, since doing so greatly expanded the views of this small-town midwesterner.

I have been fortunate that my advisor brought in a steady stream of visiting scientists and post-doctoral associates, since I benefited greatly from their presence. In particular, Dr. Markku Leskela was mainly responsible for getting me involved in the high temperature superconductivity field and became a good friend. Also Dr. Georg Thurner's negative SIMS and Auger analysis work was invaluable and I really enjoyed our political discussions and musical shared interests.

I have often found it useful to get on the telephone and ask questions to those whom I considered to be the best source of answers. Over the years I especially relied on Dr. Bill Westwood and Grant Este of Bell-Northern Research and Mike Wagner of Tektronix. They were always willing to entertain (and were sometimes entertained by) my questions on sputter deposition and vacuum equipment.

My summer at IBM Watson provided me a unique opportunity to work with a true sage in Dr. Norm Braslau. The technical activities of that summer were rewarding, but Norm's reflections on being a scientist caused me to reevaluate my own professional attitudes and the role of the scientist in today's world.

My employer during the past two years, CVC Products, has been very supportive while I chipped away at my dissertation among the trivial activities of work, marriage, and parenting. My boss, Paul Ballentine, and the company's president, Christine Whitman, provided a good work environment and steady encouragement. Also, Dr. Alan Kadin of the University of Rochester essentially assumed the role of my local advisor, and his persistent pressure on me to finish my dissertation was a needed motivation. I am grateful for all of his assistance and the friendship we established.

Finally, my family has been unbelievably patient throughout my seemingly never-ending doctoral program. I owe my wife Cristina a million back rubs and my daughter Isabel

a house full of kittens for all they have had to sacrifice for the past few years (although those long holidays on the beach with Grandma while I was writing could not have been too bad). Their love and support were invaluable. I am especially grateful for the encouragement and support my mother, Suzanne Higgins, has provided throughout my entire education and particularly while I finished my dissertation. I never would have done any of this if it were not for her.

TABLE OF CONTENTS

| | |
|--|-----|
| ACKNOWLEDGEMENTS..... | iii |
| ABSTRACT..... | xi |
| CHAPTERS | |
| 1 INTRODUCTION..... | 1 |
| 2 LITERATURE REVIEW..... | 12 |
| Sputter deposition of $\text{YBa}_2\text{Cu}_3\text{O}_{7-x}$ Thin Films..... | 12 |
| Principles of Sputter Deposition..... | 14 |
| Deviation of the Compositions of Sputter Target and Sputtered Films..... | 18 |
| Processing Variations for $\text{YBa}_2\text{Cu}_3\text{O}_{7-x}$ Thin Films..... | 30 |
| <i>In Situ</i> Growth of $\text{YBa}_2\text{Cu}_3\text{O}_{7-x}$ | 36 |
| Explanations for Deviation of Y-Ba-Cu-O Film and Target Compositions..... | 40 |
| Run-to-Run Irreproducibility of Film Composition..... | 49 |
| Summary..... | 55 |
| Barrier Layers for the Growth of $\text{YBa}_2\text{Cu}_3\text{O}_{7-x}$ on Practical Substrates..... | 56 |
| Directions for Research..... | 61 |
| 3 EXPERIMENTAL PROCEDURES..... | 63 |
| Identification of Negative Ions by SIMS..... | 63 |
| AES Study of Long Time Sputtering Effects on $\text{YBa}_2\text{Cu}_3\text{O}_{7-x}$ Targets..... | 67 |
| Processing of Y-Ba-Cu-O Thin Films..... | 69 |

| | | |
|---|---|-----|
| | Sputter Target Fabrication..... | 69 |
| | RF Sputter Deposition of Y-Ba-Cu-O and Barrier Layer Thin Films..... | 71 |
| | Post-deposition Heat Treatment..... | 76 |
| | Physical Characterization of Thin Films..... | 78 |
| | Electrical Characterization of the Y-Ba-Cu-O Films..... | 81 |
| 4 | MECHANISMS OF FILM AND TARGET COMPOSITION DEVIATION FOR SPUTTER DEPOSITED Y-Ba-Cu-O..... | 90 |
| | SIMS Study of Negative Ions Sputtered from Y-Ba-Cu-O..... | 91 |
| | Effect of Oxygen Addition..... | 97 |
| | Temperature Dependence of O ⁻ Yield..... | 98 |
| | Discussion of Negative Ion Data..... | 100 |
| | Summary of SIMS Negative Ion Study..... | 118 |
| | AES Depth Profiling Study for Ba Migration..... | 120 |
| 5 | Y-Ba-Cu-O THIN FILM PROCESSING..... | 124 |
| | Towards a 1:2:3 Film Composition by RF Sputter Deposition from a Single Y-Ba-Cu-O Target..... | 125 |
| | Experimental..... | 125 |
| | Sputter Target Preparation and Condition..... | 129 |
| | Composition of Y-Ba-Cu-O Films..... | 132 |
| | Discussion of Y-Ba-Cu-O Film Composition Data..... | 146 |
| | Summary of Sputtered Y-Ba-Cu-O Film Composition Data..... | 159 |
| | Towards Superconducting Y-Ba-Cu-O Films..... | 160 |
| | Heat Treatments to Form Superconducting Y-Ba-Cu-O..... | 161 |
| | Properties of Superconducting Y-Ba-Cu-O Films..... | 162 |
| | Discussion of Properties of Superconducting Y-Ba-Cu-O Films..... | 174 |
| | Summary..... | 180 |

| | | |
|------------|---|-----|
| 6 | STRONTIUM TITANATE BARRIER LAYERS FOR Y-Ba-Cu-O FILMS ON SILICON AND SAPPHIRE SUBSTRATES..... | 182 |
| | Sample Fabrication..... | 183 |
| | Results and Discussion..... | 185 |
| | Y-Ba-Cu-O on Si or Sapphire Without a Barrier Layer..... | 185 |
| | SrTiO ₃ Films on Si and Sapphire Substrates..... | 188 |
| | Y-Ba-Cu-O/SrTiO ₃ /Sapphire..... | 195 |
| | Y-Ba-Cu-O/SrTiO ₃ /Si..... | 198 |
| | Summary..... | 203 |
| 7 | SUGGESTIONS FOR FUTURE STUDY..... | 204 |
| 8 | SUMMARY AND CONCLUSIONS..... | 210 |
| APPENDICES | | |
| A | HOME-BUILT MULTISOURCE SPUTTER DEPOSITION SYSTEM..... | 214 |
| | General Description..... | 214 |
| | Description of Equipment..... | 217 |
| | Vacuum..... | 217 |
| | Gas Flow and Control..... | 220 |
| | Sputter Sources and Power Supplies..... | 221 |
| | Baffles and Shields..... | 224 |
| | Substrate Mounting and Positioning..... | 226 |
| | Operation..... | 230 |
| | Cold Start-Up..... | 230 |
| | Regular Start-Up..... | 231 |
| | Target Mounting..... | 232 |
| | Sample Loading..... | 233 |
| | Pump-Down..... | 234 |
| | Presputtering and Deposition..... | 235 |
| | Sample Removal..... | 237 |

| | | |
|---|--|-----|
| | Shut Down..... | 238 |
| B | HOME-BUILT RESISTIVITY VERSUS TEMPERATURE MEASUREMENT SYSTEM..... | 240 |
| | Description of System..... | 240 |
| | Operating Procedure..... | 244 |
| | REFERENCES..... | 247 |
| | BIOGRAPHICAL SKETCH..... | 257 |

Abstract of Dissertation Presented to the Graduate School
of the University of Florida in Partial Fulfillment of the
Requirements for the Degree of Doctor of Philosophy

SPUTTER DEPOSITION OF Y-Ba-Cu-O SUPERCONDUCTOR
AND SrTiO_3 BARRIER LAYER THIN FILMS

By

JAMES KELLY TRUMAN

DECEMBER 1992

Chairman: Paul H. Holloway
Major Department: Materials Science and Engineering

The commercial application of superconducting $\text{YBa}_2\text{Cu}_3\text{O}_{7-x}$ thin films requires the development of deposition methods which can be used to reproducibly deposit films with good superconducting properties on insulating and semiconducting substrates. Sputter deposition is the most popular method to fabricate Y-Ba-Cu-O superconductor thin films, but when used in the standard configuration suffers from a deviation between the compositions of the Y-Ba-Cu-O sputter target and deposited films, which is thought to be primarily due to resputtering of the film by negative ions sputtered from the target. In this study, the negative ions were explicitly identified and were found to consist of predominantly O^- . The sputter yield of O^- was found to depend on the Ba compound used in the fabrication of Y-Ba-Cu-O targets and was related to the electronegativity difference between the

components. An unreacted mixture of Y_2O_3 , CuO , and BaF_2 was found to have the lowest O^- yield among targets with $Y:Ba:Cu = 1:2:3$. The high yield of O^- from $YBa_2Cu_3O_{7-x}$ was found to depend on the target temperature and be due to the excess oxygen present. The SIMS negative ion data supported the composition data for sputter-deposited Y-Ba-Cu-O films. Targets using BaF_2 were found to improve the Ba deficiency, the run-to-run irreproducibility and the nonuniformity of the film composition typically found in sputtered Y-Ba-Cu-O films. Superconducting Y-Ba-Cu-O films were formed on $SrTiO_3$ substrates by post-deposition heat treatment of Y-Ba-Cu-O-F films in humid oxygen.

The growth of superconducting $YBa_2Cu_3O_{7-x}$ thin films on common substrates such as sapphire or silicon requires the use of a barrier layer to prevent the deleterious interaction which occurs between Y-Ba-Cu-O films and these substrates. Barrier layers of $SrTiO_3$ were studied and found to exhibit textured growth with a preferred (111) orientation on (100) Si substrates. However, $SrTiO_3$ was found to be unsuitable as a barrier layer for the growth of $YBa_2Cu_3O_{7-x}$ on Si since Ba reacted with the Si after migrating through the $SrTiO_3$ layer. For sapphire, no textured growth of $SrTiO_3$ was observed but it was found to be a suitable barrier layer since it prevented any interaction between Y-Ba-Cu-O films and sapphire substrates.

CHAPTER 1 INTRODUCTION

The discovery of high critical temperature (T_c) La-Ba-Cu-O superconductors by Bednorz and Mueller [1] and of the $\text{YBa}_2\text{Cu}_3\text{O}_{7-x}$ compound with a T_c of 90 K by Wu et al. [2] heralded the onset of an unprecedented amount of research activity in a single area. High temperature superconductivity became one of the rare scientific subjects which attracted the attention of the general public and garnered coverage by the popular press. The promise of economical levitating trains and lossless power transmission seemed to have moved beyond the realm of science fiction. Even proven superconductor applications such as magnet wire and magnetic detectors could clearly benefit from the cost reductions of operation in liquid nitrogen, rather than in liquid helium as required by conventional superconductors. Furthermore, the integration of high temperature superconductors with conventional semiconductor technology could have important consequences for microelectronics. Passive superconductor applications such as interconnects offer the possibility of low-loss signal transmission, while active devices such as Josephson junctions offer the possibility of fast switching speeds with low heat

generation [3]. Because of its predominance in the semiconductor industry, Si is the primary candidate for these integrated applications with superconductors.

However, the processing of high T_c materials with the desired chemical, mechanical, and superconducting properties has proven to be a formidable task, even with most efforts concentrating on one material, $\text{YBa}_2\text{Cu}_3\text{O}_{7-x}$. The processing of high quality bulk $\text{YBa}_2\text{Cu}_3\text{O}_{7-x}$ has shown progress but the quality of the material is still not suitable for most applications. The limitations are due to brittleness, low critical current density (J_c) values, and instability in ambient [4]. On the other hand, applications involving superconducting thin films are in the early stages of commercialization and the processing of thin films is now capable of producing extremely high quality material. In particular, thin films with good microwave properties, $T_c \geq 90$ K and J_c values in excess of 10^6 A/cm² at 77 K, are now commonly reported [5]. However, the processing of $\text{YBa}_2\text{Cu}_3\text{O}_{7-x}$ thin films is still not without its problems and a good deal of work remains to be done.

During the first few years after the discovery of high temperature superconductors, most processes for the fabrication of superconducting $\text{YBa}_2\text{Cu}_3\text{O}_{7-x}$ thin films consisted of depositing a film with a Y:Ba:Cu ratio of 1:2:3, heating the film to 800 - 900 °C in oxygen to obtain the tetragonal $\text{YBa}_2\text{Cu}_3\text{O}_{7-x}$ crystal structure, and slowly

cooling the film in oxygen to increase the oxygen concentration and form orthorhombic, superconducting $\text{YBa}_2\text{Cu}_3\text{O}_{7-x}$ [5, 6]. Since 1989 most efforts have concentrated on growing superconducting $\text{YBa}_2\text{Cu}_3\text{O}_{7-x}$ films *in situ* by depositing at substrate temperatures of 600 - 800 °C to form tetragonal $\text{YBa}_2\text{Cu}_3\text{O}_{7-x}$, then backfilling the deposition chamber with oxygen and slowly cooling to form orthorhombic $\text{YBa}_2\text{Cu}_3\text{O}_{7-x}$. This *in situ* deposition avoids the high temperatures of a post-deposition heat treatment and produces films with properties better suited for device applications [7].

The crystal structure of the superconducting $\text{YBa}_2\text{Cu}_3\text{O}_{7-x}$ phase is orthorhombic with $0 \leq x < 0.7$, which is illustrated in Figure 1-1a [8]. When the temperature is raised and the oxygen stoichiometry is less than approximately 6.3 [9], the material becomes non-superconducting and transforms to the tetragonal $\text{YBa}_2\text{Cu}_3\text{O}_{7-x}$ phase illustrated in Figure 1-1b [8]. In Figure 1-1b a composition of $\text{YBa}_2\text{Cu}_3\text{O}_6$ is illustrated, which is completely depleted of excess oxygen. During slow cooling in oxygen to form the superconducting, orthorhombic $\text{YBa}_2\text{Cu}_3\text{O}_{7-x}$ phase, oxygen is incorporated into the structure between the Cu atoms along the b-axis, resulting in the formation of Cu-O chains as indicated in Figure 1-1a. The incorporation or removal of this excess oxygen occurs reversibly with thermal cycling [9]. In spite of an incredible amount of effort, no theory has been developed to

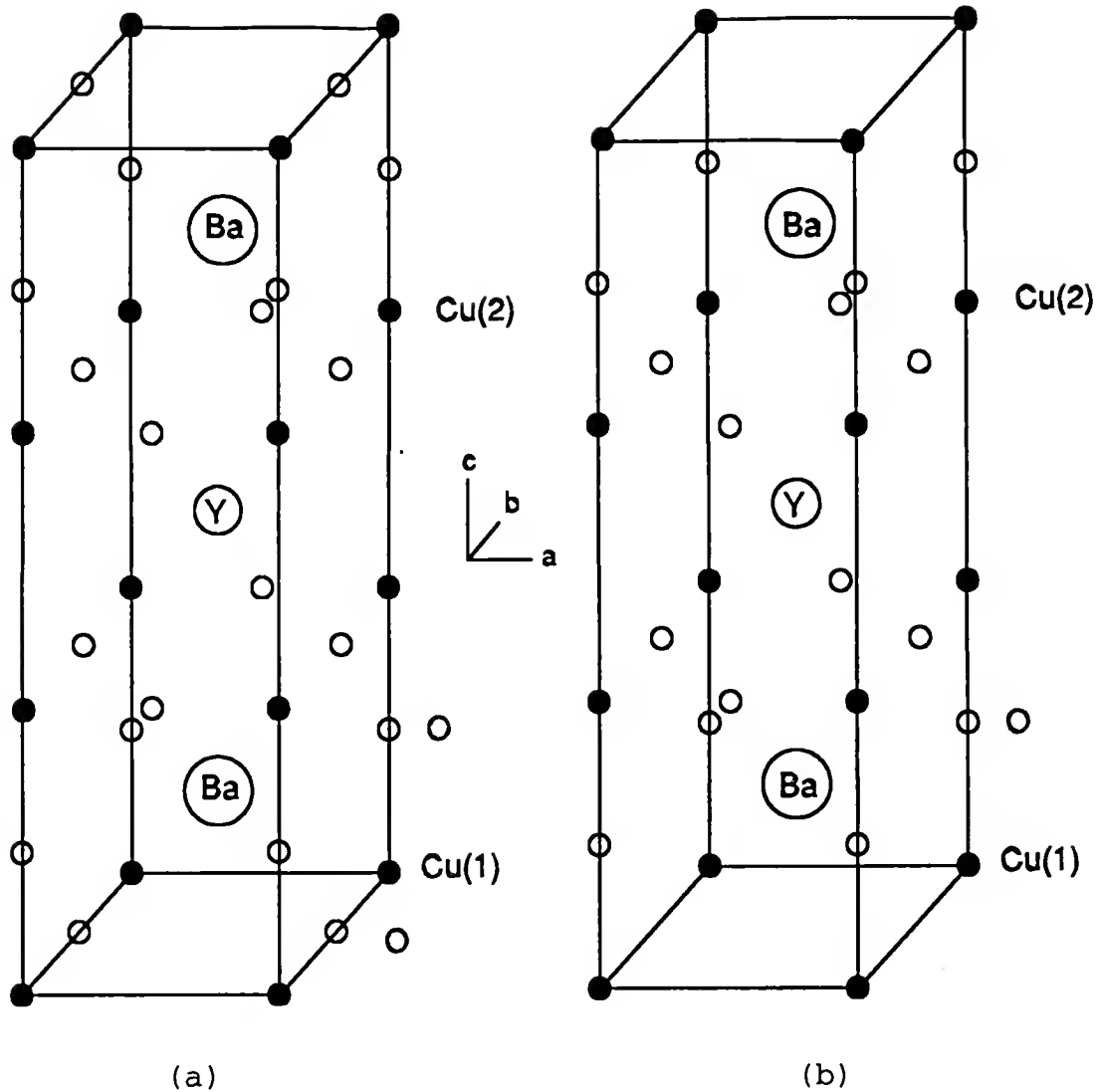


Figure 1-1. Structure of the two phases in the $\text{YBa}_2\text{Cu}_3\text{O}_{7-x}$ family. Orthorhombic $\text{YBa}_2\text{Cu}_3\text{O}_{7-x}$, illustrated in a), is superconducting, whereas tetragonal $\text{YBa}_2\text{Cu}_3\text{O}_6$, illustrated in b), is insulating. After reference [8].

suitably explain high temperature superconductivity in $\text{YBa}_2\text{Cu}_3\text{O}_{7-x}$. Regardless, the incorporation of excess oxygen and the transformation to an orthorhombic crystal structure are necessary conditions for superconductivity to occur.

Throughout this dissertation, the following convention will be adopted to distinguish between orthorhombic and tetragonal $\text{YBa}_2\text{Cu}_3\text{O}_{7-x}$: the use of $\text{YBa}_2\text{Cu}_3\text{O}_{7-x}$ implies the orthorhombic superconducting phase, whereas the tetragonal, insulating phase will be designated $\text{YBa}_2\text{Cu}_3\text{O}_6$, even though the tetragonal phase may actually be $\text{YBa}_2\text{Cu}_3\text{O}_{6+y}$, as discussed above.

The desired superconducting properties of $\text{YBa}_2\text{Cu}_3\text{O}_{7-x}$ films are a sharp resistive transition with a T_c near 90 K and a J_c of 10^6 A/cm² or greater. To achieve these properties, the films must have the correct metallic stoichiometry Y:Ba:Cu of 1:2:3 and consist of only the orthorhombic $\text{YBa}_2\text{Cu}_3\text{O}_{7-x}$ structure and no impurity phases. Further, the critical current in superconducting $\text{YBa}_2\text{Cu}_3\text{O}_{7-x}$ is anisotropic and depends on the crystalline quality of the material. Specifically, the critical current is higher along the a-b planes than in the direction of the c axis [7]. Thus for most applications it is desirable to grow thin films with the c-axis oriented normal to the plane of the film. The elimination of grain boundaries and other crystalline defects also increases J_c [4, 10]. Hence a single crystal, c-axis oriented, epitaxial $\text{YBa}_2\text{Cu}_3\text{O}_{7-x}$ film is desired. This dictates the lattice parameter of materials to be used as substrates for $\text{YBa}_2\text{Cu}_3\text{O}_{7-x}$ films.

Since lattice matching to $\text{YBa}_2\text{Cu}_3\text{O}_{7-x}$ is one of the primary criteria in the choice of a substrate material,

SrTiO_3 and LaAlO_3 have been the most popular substrates for the growth of high quality $\text{YBa}_2\text{Cu}_3\text{O}_{7-x}$ films [5, 11]. Although these substrates are useful for certain applications, the large-scale commercialization of $\text{YBa}_2\text{Cu}_3\text{O}_{7-x}$ will require applications utilizing more common, low-cost substrates. However, the temperatures of post-deposition heating are sufficiently high to promote harmful interactions between $\text{YBa}_2\text{Cu}_3\text{O}_{7-x}$ and some substrates. Unfortunately this is true for substrates such as sapphire ($\alpha\text{-Al}_2\text{O}_3$) and the semiconductor Si, which react with $\text{YBa}_2\text{Cu}_3\text{O}_{7-x}$ to such an extent as to destroy superconductivity [5]. To permit the growth of $\text{YBa}_2\text{Cu}_3\text{O}_{7-x}$ on Si or sapphire, an idea which has received much study is the insertion of an intermediate barrier layer to prevent the reaction between the film and the substrate. The lower temperatures used for *in situ* processing will limit but not stop the reaction between Si and $\text{YBa}_2\text{Cu}_3\text{O}_{7-x}$. Furthermore, very little is known about the effects of the reaction on the semiconducting properties of Si or on Si devices. Thus a barrier layer will probably be needed even for *in situ* $\text{YBa}_2\text{Cu}_3\text{O}_{7-x}$ film growth on Si or sapphire.

Many different thin film growth techniques have been employed in the processing of $\text{YBa}_2\text{Cu}_3\text{O}_{7-x}$ thin films with varying degrees of success in satisfying the demands discussed above. Sputter deposition has been the most commonly used technique, but laser ablation, and to a much

lesser extent electron beam evaporation, are also commonly used. Sputter deposition potentially offers the benefit of being able to grow stoichiometric films from a single multicomponent target. Electron beam evaporation requires the simultaneous control of three different sources and has been found to be impractical beyond research applications. Laser ablation can produce the $\text{YBa}_2\text{Cu}_3\text{O}_{7-x}$ films of the same high quality as sputter deposition, while more easily obtaining the correct film composition and having potentially higher deposition rates [12]. However, films grown by laser ablation suffer from poor thickness uniformity and poor surface smoothness over large areas. Comparatively, sputter deposition can produce high quality films at moderate deposition rates with good thickness uniformity and excellent surface smoothness on substrates presently as large as three inches in diameter [13]. Thus sputtering appears to be the best-suited physical deposition technique for manufacturing-scale production of $\text{YBa}_2\text{Cu}_3\text{O}_{7-x}$ films. However, for reasons to be discussed below, consistently obtaining the desired Y-Ba-Cu-O film stoichiometry by sputter deposition is not as simple as is usually the case for the sputter deposition of other multicomponent thin films.

The goal of the present work was to address two issues which could lead to improved processing and manufacturability of $\text{YBa}_2\text{Cu}_3\text{O}_{7-x}$ thin films grown by sputter

deposition. First, a study was performed to better understand the mechanics of the sputter deposition of $\text{YBa}_2\text{Cu}_3\text{O}_{7-x}$ thin films from single multicomponent oxide targets. As will be discussed in more detail below, the reproducible deposition of Y-Ba-Cu-O thin films with a 123 composition has been a major problem encountered in the sputter deposition of Y-Ba-Cu-O. However, very few diagnostic studies have been done to explicitly identify the reason(s) for this lack of control. Further definition of these reasons was an objective of this study. The results would serve as a guide for improving control of the film composition. Second, as discussed above, the growth of $\text{YBa}_2\text{Cu}_3\text{O}_{7-x}$ on practical substrates will require the use of barrier layers. This is also true for the growth of $\text{YBa}_2\text{Cu}_3\text{O}_{7-x}$ on the most common single crystal oxide substrate, sapphire. An investigation of one possible barrier layer material was performed in this study.

In the balance of this dissertation, a review of the literature is presented in Chapter 2 which emphasizes the sputter deposition of $\text{YBa}_2\text{Cu}_3\text{O}_{7-x}$ thin films and the issues associated with this method. Possible explanations for the deviation of film and target compositions are discussed as well as methods to obtain the desired film composition. The requirements for barrier layers on Si for $\text{YBa}_2\text{Cu}_3\text{O}_{7-x}$ are then presented along with a discussion of various barrier layer materials reported in the literature.

In Chapter 3 the experimental methods used in this study are described. Additional information on the sputter deposition system used in this study and on the resistivity versus temperature measurement apparatus are presented in Appendix A and Appendix B, respectively.

Presented in Chapter 4 are the results and discussion of studies of two possible mechanisms for the deviation of the composition of Y-Ba-Cu-O thin films and targets observed in sputter deposition. These mechanisms are the resputtering of the growing film by negative ions and the migration of atoms to the target surface during sputtering. First, the results of a secondary ion mass spectroscopy (SIMS) study show that the dominant negative ion sputtered from Y-Ba-Cu-O targets is O^- . The proper choice of starting compounds in the sputter target will be shown to influence the O^- yield. A discussion on the formation of negative ions is presented. Secondly, the results of an Auger electron spectroscopy (AES) study of the surface composition of $YBa_2Cu_3O_{7-x}$ sputter targets as a function of sputter time and substrate temperature are presented. The migration of target components, specifically Ba, to the surface during sputtering is found not to occur.

Chapter 5 contains a description of efforts to deposit Y-Ba-Cu-O films with a 123 composition by rf planar magnetron sputter deposition and to form superconducting $YBa_2Cu_3O_{7-x}$ by post-deposition heat treatment. Electron

microprobe analysis showed that films sputter deposited from targets using BaO_2 or BaCO_3 precursors were Ba deficient and exhibited very poor run-to-run reproducibility of the film composition. The use of sputter targets containing unreacted mixtures of Y_2O_3 , BaF_2 , and CuO was found to improve the Ba deficiency in Y-Ba-Cu-O films, the run-to-run reproducibility in the film composition, and the uniformity of the film composition across two inch diameter substrates. As suggested by the results of the negative SIMS study in Chapter 4, the use of BaF_2 in unreacted targets reduced the Ba deficiency problem as result of a decreased O^- yield. Finally, the properties of superconducting $\text{YBa}_2\text{Cu}_3\text{O}_{7-x}$ films on SrTiO_3 substrates are described.

In Chapter 6 is presented a study of the suitability of SrTiO_3 barrier layers for preventing interaction between Y-Ba-Cu-O films and substrates of Si or sapphire. The SrTiO_3 layers were found to exhibit textured growth with a (111) preferred orientation on the (100) Si substrates. However, SrTiO_3 was not a suitable barrier layer for Si since Ba still reacted with the Si after migrating through the SrTiO_3 layer. For sapphire, SrTiO_3 was found to be a suitable barrier layer since it prevented any interaction between the Y-Ba-Cu-O film and the sapphire substrate.

Chapter 7 contains suggestions for future work based on the review of the literature and the questions raised by the experiments in this effort.

Finally, in Chapter 8 is presented a summary of the results from the previous chapters.

CHAPTER 2

LITERATURE REVIEW

Presented in this chapter is a review of published literature relating to the sputter deposition of $\text{YBa}_2\text{Cu}_3\text{O}_{7-x}$ thin films and the growth of $\text{YBa}_2\text{Cu}_3\text{O}_{7-x}$ on barrier layers on practical substrates, particularly Si. In addition, the reactions between the superconductor thin films and these substrates are reviewed. The number of publications since 1987 in the area of $\text{YBa}_2\text{Cu}_3\text{O}_{7-x}$ thin film fabrication and reactions, including journal articles and conference proceedings, is easily in excess of one thousand. Thus a comprehensive review of every paper is simply impossible. Hence, this review is general in scope, but focuses on relevant important publications.

2.1 Sputter Deposition of $\text{YBa}_2\text{Cu}_3\text{O}_{7-x}$ Thin Films

Sputter deposition is typically the method of choice when depositing multicomponent thin films since the desired film composition can usually be obtained from a single target with the same composition. For targets containing compounds in which one of the elements is highly volatile, such as oxygen in oxides, the film is usually deficient in the volatile element unless special steps are taken.

However, the ratio of metallic species in the film usually equals that in the target for steady state conditions [14]. Certain exceptions arise, as discussed below, when even the ratio of metallic species in the film does not equal that in the target. This problem has been the bane of investigators studying sputter deposition of $\text{YBa}_2\text{Cu}_3\text{O}_{7-x}$ thin films.

Generally, films deposited from Y-Ba-Cu-O sputter targets (where Y-Ba-Cu-O represents any combination of Y, Ba, Cu, and O) onto unheated substrates are deficient in Ba relative to the target, with Cu deficiencies sometimes being reported. Furthermore, the reproducibility of film compositions between successive depositions, even with all deposition parameters kept constant, has been marginal at best unless special precautions are taken.

The Y:Ba:Cu ratio needed in a film to get a superconducting transition is not strictly 1:2:3, since a film made of less than 50% $\text{YBa}_2\text{Cu}_3\text{O}_{7-x}$ can have a continuous superconducting network due to percolation effects [15]. However, the closer to a uniform 1:2:3 stoichiometry, the more desirable are the properties of the film, including a sharper resistive transition and a higher critical current density. Furthermore, when deposited on an unheated substrate, sputtered Y-Ba-Cu-O films are insulating and require post-deposition heat treatment at 800 - 900 °C in oxygen to form the superconducting $\text{YBa}_2\text{Cu}_3\text{O}_{7-x}$ phase [6]. Many reports during the past two years have emphasized the *in situ* growth of superconducting $\text{YBa}_2\text{Cu}_3\text{O}_{7-x}$ during which the

substrate temperature is elevated during deposition to 600 - 800 °C [7]. The heating of substrates has also been found to affect the film composition. Hence, much of the work in the sputter deposition of $\text{YBa}_2\text{Cu}_3\text{O}_{7-x}$ has centered on controllably obtaining a 123 film composition in as-deposited thin films.

A brief overview of the basic principles of sputter deposition will be given. Four general explanations for the deviation of the sputtered film compositions from that of the sputter target will be outlined. These will provide the background necessary for understanding the summary of the many processing variations presented in the literature in attempts to grow stoichiometric $\text{YBa}_2\text{Cu}_3\text{O}_{7-x}$ thin films.

2.1.1 Principles of Sputter Deposition

The basic principles of sputter deposition are best understood by examining the simplest configuration, the planar diode, which is illustrated in Figure 2-1 [16]. Sputtering is a process in which energetic particles strike the surface of a material and eject particles from the material's surface by a momentum exchange process. For film deposition by sputtering, the ejected particles M are collected on a substrate. A heavy inert gas, usually Ar, is backfilled into a vacuum chamber to a pressure of 1 to 100 mTorr. A power supply maintains a potential between cathode and anode electrodes in order to sustain an Ar plasma. The plasma provides the Ar^+ ions which sputter the target. The

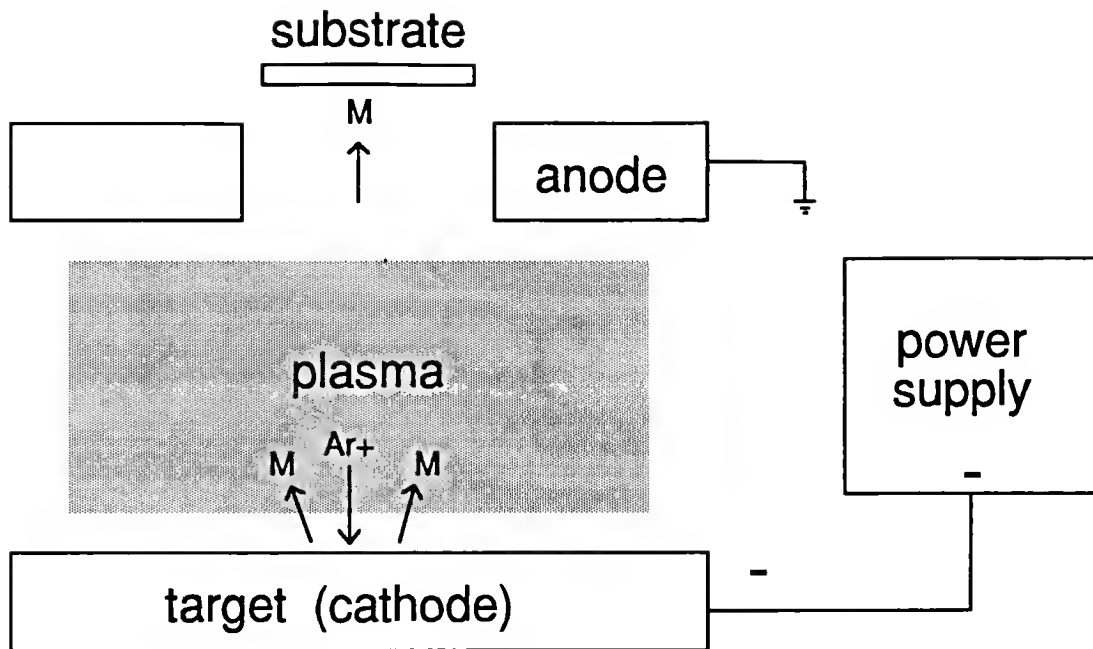


Figure 2-1. Schematic illustration of planar diode sputter deposition. Ar^+ ions are accelerated to the negatively charged target. Target particles M are ejected and travel to the substrate, thereby forming a film. After ref. [16].

target, which is the source of material to be deposited, is the cathode and is negatively biased to accelerate Ar^+ ions from the plasma so that its surface is sputtered by the ions. A conducting target can be biased using a DC potential, and the target can double as the cathode. A nonconducting target requires the use of a RF potential and the target is usually attached to a conducting cathode electrode. Material sputtered from the target, M in Figure 2-1, collects on a substrate, which is usually positioned beyond an opening in the anode. The sputtered species are primarily low energy atoms, although energetic neutral atoms

molecules as well as low and high energy positive and negative ions are also observed [17]. Also created in the sputtering process are the secondary electrons necessary to sustain the plasma. The deposition rates from diodes are generally low. Also, bombardment of the substrate by electrons and the plasma leads to undesirable heating when a diode source is used.

Limitations of the planar diode have led to the development and widespread use of magnetron sputter cathodes [18]. A magnetron is essentially a diode apparatus with specially configured magnets placed beneath the cathode electrode. The resulting magnetic field, combined with the electric field from the applied potential on the cathode, confines the electrons in the plasma to a net motion in a closed loop above the cathode. The most common magnetron configuration is the circular magnetron, for which the target is a flat disk. The magnetic field and resulting $\vec{E} \times \vec{B}$ electron drift path for a circular magnetron are illustrated in Figure 2-2 [19]. Since most of the electrons in the plasma are confined to motion in an annular path, the probability of collisions with gas atoms is much greater and the plasma is much denser within this region. This results in the brightly glowing ring which can be seen in the plasma above a circular magnetron cathode and also in a greatly increased Ar^+ density in this region. Thus an increased flux of Ar^+ is incident on the target and an increased sputter

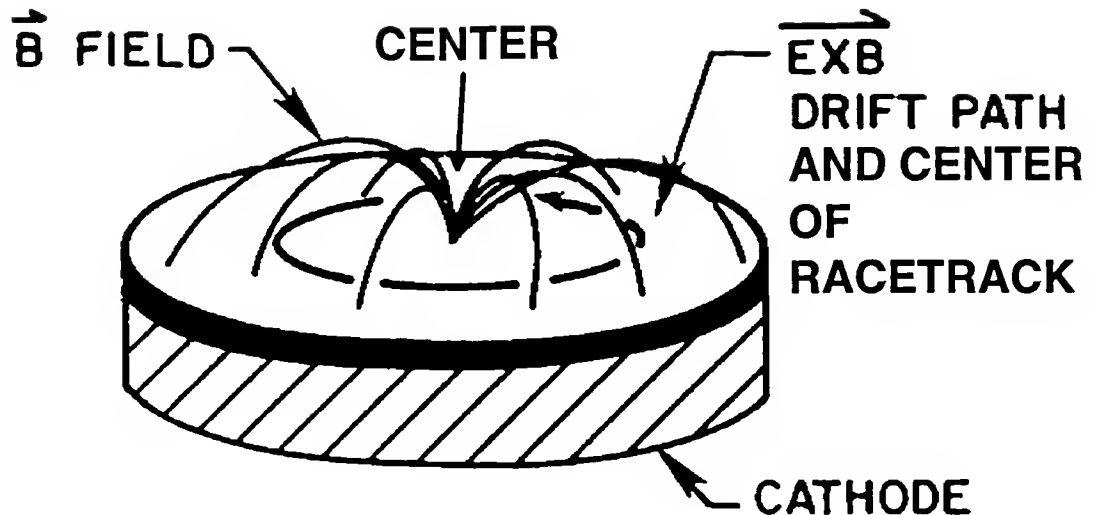


Figure 2-2. Schematic of circular planar magnetron cathode, illustrating the shape of the magnetic field and the drift path of the electrons resulting from the combined magnetic and electric fields. After reference [19].

rate results beneath the ring in the plasma. The sputtering pattern in the magnetron results in the formation of a circular groove in the target, which is commonly called the racetrack. Finally, the sputter rate in the central area of the target can be low enough that a net redeposition from the racetrack region can occur [20].

Compared to a diode source, the confined motion of electrons in a magnetron results in the formation of a far greater number of Ar^+ ions for a given pressure and potential. Thus, magnetrons can give an order of magnitude or more increase in the deposition rate [18]. Also, the confinement of the electrons greatly reduces the substrate heating due to electron and plasma bombardment.

2.1.2 Deviation of the Compositions of Sputter Target and Sputtered Films

As pointed out above, one of the main advantages of sputtering is that the composition of a film is usually the same as that of the target. The reason is the formation of an altered layer on the target surface which is depleted and enriched in the high and low sputtering rate constituent(s), respectively [17, 21]. After a stabilization period of typically a few minutes (i.e. sputter depths of about 100 Å) during which the altered layer is formed, the sputtered flux usually has the same composition as the target. To explain this, a few concepts will be briefly discussed. The incident flux, F_{Ar} , is the number of Ar^+ ions per unit time per unit area striking the target. (It is assumed that only Ar is being used as the sputter gas). The total flux of component i sputtered from the target by the incident Ar^+ ions is represented by F_i^{Ar} . The total sputter yield, Y_T , is defined as the total flux of particles sputtered from the target per incident ion [22]. For a single component target comprised of element M , the total sputter yield equals the yield of M , or

$$Y_T = \frac{F_M^{Ar}}{F_{Ar}}. \quad (2.1)$$

For a multicomponent target, it is typically assumed the sputter yields for each component are equal to those determined from elemental targets for sputtering with Ar^+ of a specified energy and angle of incidence [22]. To account

for different concentrations of each component in a multicomponent target, the fractional concentration of component i in the surface region of the target, c_i , is included in the expression for the flux of i sputtered from a multicomponent target [22],

$$F_1^{Ar} = F_{Ar} Y_1^{Ar} c_i. \quad (2.2)$$

To understand the formation of the altered layer during sputtering, consider a target made of an alloy AB with a surface composition initially equal to that of the bulk. Let the sputter yield of component A, Y_A , be twice that of component B, Y_B , for sputtering with Ar^+ of a specified energy and angle of incidence. The initial sputtered flux will be rich in component A and the target surface will become depleted in A. Eventually a steady state condition will be reached in which the surface concentration of A will become half the fraction of A in the bulk with a concomitant rise in the surface concentration of B. In other words,

$$\frac{c_A}{c_B} = \frac{Y_B^{Ar} c_A^b}{Y_A^{Ar} c_B^b} \quad (2.3)$$

where c_A^b and c_B^b are the bulk concentrations of A and B, respectively [21]. The region near the surface is the desired altered layer. Thus after an initial transient period, the steady state sputtered flux and the deposited thin film will have the same composition as the target bulk.

In general, the composition of sputter deposited films equals that of the multicomponent target. However, there are four main mechanisms, to be discussed in more detail below,

which can prevent the sputtered film composition from being equal to that of the target. The first mechanism involves migration of one or more of the target specie(s) to the target surface during sputtering independent of sputter rate [21]; this will be discussed in Section 2.1.2.1. The second mechanism entails differing non-unity sticking coefficients of the components on the substrate [21]. The sticking coefficient, S_i , is defined as the ratio of the number of particles of specie i incident on a surface to the number of particles of specie i which stick to the surface, or as the probability that a single incident particle will stick to a surface [23]. The importance of this will be discussed in Section 2.1.2.2. The third mechanism involves a variation in the angular distribution of species sputtered from a multicomponent target [24]. The angular distribution of a sputtered flux usually follows a cosine distribution. However, for some multicomponent targets, the sputtered angular distributions of some specie(s) may not follow a simple cosine distribution, as will be discussed below in Section 2.1.2.3. The fourth and final mechanism involves an unexpectedly high sputter yield of negatively charged ions, which is the number of negative ions sputtered per incident Ar^+ ion [25]. This issue will be discussed in Section 2.1.2.4. Any combination of these mechanisms may be present, but the exact contribution of each is difficult to predict.

2.1.2.1 Migration of species to the target surface

The typical power dissipation during sputtering is several hundred watts. As a result, sputter targets are kept cool by water which flows across the back side of the cathode. To effectively cool, the target must be in good thermal contact with water or the conducting cathode on which it rests. However, the surface of poor thermal conductors (e.g. most insulators) may still get hot even though the bottom of the target is adequately cooled. Even metal targets with high thermal conductivity can reach temperatures of 200 - 300 °C when sputtering at a high rate. During the initial stages of sputtering of a multicomponent target, the target surface becomes depleted in the component with the highest sputter yield, as discussed above. The formation of an altered layer, with the composition necessary to produce a sputtered flux with the same composition as the target bulk, would require that the surface remain depleted in this component. The depletion of a component at the target surface represents a driving force for the migration of atoms from deeper in the target to the surface. In an adequately cooled target, the rate of migration of the depleted component is low compared to the sputter rate, and the altered layer maintains the correct stoichiometry. However, in a hot target, a mobile component may migrate to the target surface at a rate faster than the sputter rate can keep the surface depleted in the component.

This will prevent the formation of an altered layer with the desired composition and the sputtered flux would not have the same composition as the bulk. Rather, the sputtered flux and the resulting film composition would be rich in the mobile component [21].

2.1.2.2 Sticking coefficient variations

Non-unity sticking coefficients can result in the deficiency of a component in the deposited film. A highly volatile element in a target, such as oxygen, will commonly be deficient in deposited films. The oxygen which is not sputtered from the target as an oxide molecule or which does not rapidly react with a deposited electropositive element often does not stick to the substrate and is pumped away [26]. When substrates are at room temperature, it is usually safe to assume that the sticking coefficient of all nonvolatile components sputtered from a target, i.e. most cationic species, is approximately equal to unity [27]. However, the substrate temperature, even for a planar magnetron apparatus, can easily reach 200 °C due to bombardment by electrons and reflected excited state neutral Ar [28]. At this temperature the sticking coefficients for high vapor pressure components such as Pb may be less than one, resulting in a film composition not equal to that of the target.

2.1.2.3 Angular distribution variations

A variation in the angular distribution of species sputtered from a multicomponent target can result in unexpected deviations and non-uniformities in film composition. For normal incidence ions, the flux of sputtered atoms from a single component target follows a cosine distribution centered about the normal to the target surface [22]. However, for a binary alloy target, significant differences between the angular distributions of the components have been reported [24]. The difference in angular distributions is more pronounced at lower ion energies (< 1 keV) and for greater differences in the mass of the components [29]. Specifically, the lower mass component is preferentially sputtered along the target surface normal and the heavier component is sputtered along more oblique angles. For a two component target, there must exist an angle at which a substrate can be positioned which will result in a film with the same composition as the target. However, this is not necessarily the case for an alloy target with three or more components, particularly when their masses differ significantly. For most compound targets, the angular distribution cannot always be predicted from the mass difference of the components, as was reported for $\text{WSi}_{2.3}$ [29].

2.1.2.4 Resputtering by negative ions

The species sputtered from a target by Ar^+ are mostly atoms, but can also include high energy excited state neutral atoms as well as molecular clusters and positive and negative ions. Also, molecules are often sputtered from compound targets [26]. Positively charged particles are attracted to the target because of its large negative potential. Conversely, negative ions are accelerated away from the target towards the substrate due to repulsion by the large negative potential, which is the same potential which attracts the Ar^+ ions. The negative ions then enter the plasma where they may collide with electrons, other ions, atoms, or excited species and lose their additional electron, depending on the mean free path for collision. This mean free path in turn depends on the target potential and the pressure [30]. The collision with electrons is most likely to remove the extra electron from a negative ion. The energetic, now neutral atom has a small collision cross-section and can travel through the plasma to the substrate, with the number of energy-reducing collisions again depending on the mean free path [30]. For mean free paths on the order of the target-to-substrate distance, which are possible at low operating pressures or high target potentials, energetic negative ions can pass through the plasma without collision and bombard the substrate.

The yield of negative ions during sputtering is usually less than 1% [26] and their effects are generally not critical. However, large yields of negative ions have been observed from certain compounds, particularly those which are highly ionic and contain a strongly electronegative element such as F or O bonded to a strongly electropositive element. In such cases, the negative ions can bombard the substrate with a flux comparable to the deposition rate of the film and thus greatly resputter the growing film or even cause etching of the substrate. Hanak and Pellicane [31] were the first to identify the cause of such effects during the sputtering of TbF_3 , as the negative ion F^- . An additional problem with negative ions is that when the target contains more than two elements, the resputtering of the growing film by negative ions can result in the depletion of one (or more) of the elements. For example, films deposited from $\text{BaPb}_{1-x}\text{Bi}_x\text{O}_3$ targets were found to be strongly deficient in Ba [32]. Resputtering by negative ions was conjectured to be the cause, although no further verification was reported.

The only model predicting the degree of film resputtering by negative ions was published by Cuomo et al. [25]. During the sputter deposition of films from targets consisting of selected compounds of gold and a rare earth (RE) metal such as Sm, the deposition rate on the substrate ranged from unexpectedly low to a negative rate, i.e., substrate etching had occurred. Analysis by SIMS found that

the Au^- negative ion yield from SmAu was four orders of magnitude greater than that from Au. It was concluded that the unexpectedly low deposition rates were due to resputtering of the depositing film by negative ions formed during sputtering of the Au-RE targets.

Cuomo et al. developed a model which attributed the formation of Au^- to the high electron affinity of Au in combination with the low ionization potential of a given rare earth metal. In generalizing the model, the target material was simplistically treated as a simple ionic compound AB, in which negative B ions were present in the solid. Negative ions were suggested to be sputtered from AB because of the high electron affinity of the B atom, such that sputtered B retained the negative charge it possessed in the lattice. During the formation of the solid, the energy required to remove an electron from the A atom was assumed to be equal to the ionization potential of A, I_A . Forming the negative ion B^- resulted in a gain of energy equal to the electron affinity of B, EA_B . Thus the total energy difference $I_A - \text{EA}_B$ was suggested to be a measure of the difficulty in transferring an electron from A to B during the formation of the ionic solid. Among a series of compounds, comparing the values of $I_A - \text{EA}_B$ was suggested to provide an estimate for the ease of charge transfer in AB and the likelihood of removing negative ions by sputtering.

Conceptually, the explanation of Cuomo et al. suggested how a negative ion could be created during sputtering of a target material. However, this model did not provide a realistic picture since no solid, including Au-RE compounds, is perfectly ionic with complete localization of charge. Further, although the model suggested how negative ions may be sputtered from the target, it was not able to predict a threshold voltage for the formation of negative ions. Rather, the model was used to empirically predict the degree of film resputtering during deposition from a variety of Au-RE target materials. Specifically, it was found that if the value of $I_A - EA_B$ was less than 3.4 eV for Au-RE compounds, where component A was the rare earth element and component B was Au, sputter deposition with Ar at an accelerating voltage of -1000 V would result in substrate etching by Au^- ions. However, the rate of resputtering by negative ions was found to be low enough in some cases that substrate etching did not occur but the net deposition rate decreased. No attempt was made to explain this. Also, for a given value of $I_A - EA_B$, the degree of resputtering was found to depend strongly on the negative accelerating potential on the target. Thus the value of $I_A - EA_B$ alone was not sufficient to predict when negative ion rates would be observed or significant. However, this value did provide a helpful qualitative comparison among similar Au-RE compounds.

Kester and Messier [33] compared the predictions of the model of Cuomo et al. [25] for the formation of negative ions to qualitative effects of resputtering of a large number of oxides, including changes in deposition rate and film morphology. Negative ion resputtering effects were observed for RF magnetron sputter deposition of BaTiO_3 and other titanate perovskites, zirconate perovskites, niobates and other oxides. All of the oxide compounds which exhibited negative ion resputtering had values of $I_A - EA_B$ greater than 3.4 eV, in contrast to the prediction of the empirical model of Cuomo et al. Furthermore, for just one material, BaTiO_3 , the degree of resputtering varied from none to severe depending on the RF power, i.e. the accelerating potential on the target. Thus, in agreement with the results of Cuomo et al., the value of $I_A - EA_B$ was not alone sufficient to predict negative ion effects. However, for the same deposition conditions and among similar materials (e.g. zirconates or titanates), the amount of resputtering was found to increase with a decreasing value of $I_A - EA_B$. The applicability of this binary compound model to predict sputtering of ternary oxides has been attempted, but the calculation of a meaningful $I_A - EA_B$ value remains. It was assumed that only the $I_A - EA_B$ value between the element with the lowest ionization potential and oxygen was important, whereas negative ions may have also formed between the other element and oxygen. In summary, it was found that the $I_A - EA_B$

values was but one of many factors that influence whether resputtering by negative ions will occur, and to what degree.

The formation of negative ions has understandably received considerable attention from the Secondary Ion Mass Spectroscopy (SIMS) analysis community [22]. In SIMS analysis, the information sought is the mass-to-charge ratio versus the intensity of ionic species sputtered from a material's surface, as will be discussed below in Chapter 3. In order to apply SIMS in quantitative surface compositional analyses, much effort has gone into relating the sputtered ion intensities to the actual surface compositions. However, most of these efforts are at least partially empirical, and a first-principles theory relating sputtered ion intensities to actual surface composition has not been developed. Semi-quantitative models have been developed to predict the the sputtered ion yield from metallic materials, for which the emission of ions is understood to be due to the tunneling of electrons from the surface of metals to sputtered particles [22]. On the other hand, only a qualitative understanding, based on the concept of bond breaking, exists for the emission of ions during the sputtering of ionic compounds. In general, it is observed that the more ionic the character of the bonds in a compound, the more likely the sputtered species are to retain their charge from the lattice [22]. An increased ionic bond character is obtained with an increasing

electronegativity difference between species in the compound. Thus the more electronegative a specie is in the compound, the greater the probability that it will retain the negative charge in the lattice and be sputtered as a negative ion [22]. However, this provides no basis for calculating the fraction of the specie which will be sputtered as a negative ion.

2.1.3 Processing Variations for $\text{YBa}_2\text{Cu}_3\text{O}_{7-x}$ Thin Films

As discussed above, the reproducible sputter deposition of Y-Ba-Cu-O thin films with a 1:2:3 composition from a $\text{YBa}_2\text{Cu}_3\text{O}_{7-x}$ target is very difficult. An additional complication is that the film composition as well as the thickness depends on the position above a $\text{YBa}_2\text{Cu}_3\text{O}_{7-x}$ sputter target, as shown in Figure 2-3 [34]. In all such data a depletion of Ba is seen in the film above the magnetron racetrack region of the target, which is where the sputter rate is the highest. Thus the first step in the sputter deposition of $\text{YBa}_2\text{Cu}_3\text{O}_{7-x}$ is the establishment of processing conditions for a particular system to obtain a 1:2:3 film composition. A large variety of sputter configurations and geometries have been used in the growth of $\text{YBa}_2\text{Cu}_3\text{O}_{7-x}$ thin films. Almost every conceivable sputter deposition technique has been employed and for each of these a large matrix of deposition parameters have been varied. Also, unconventional sputtering geometries and different types of

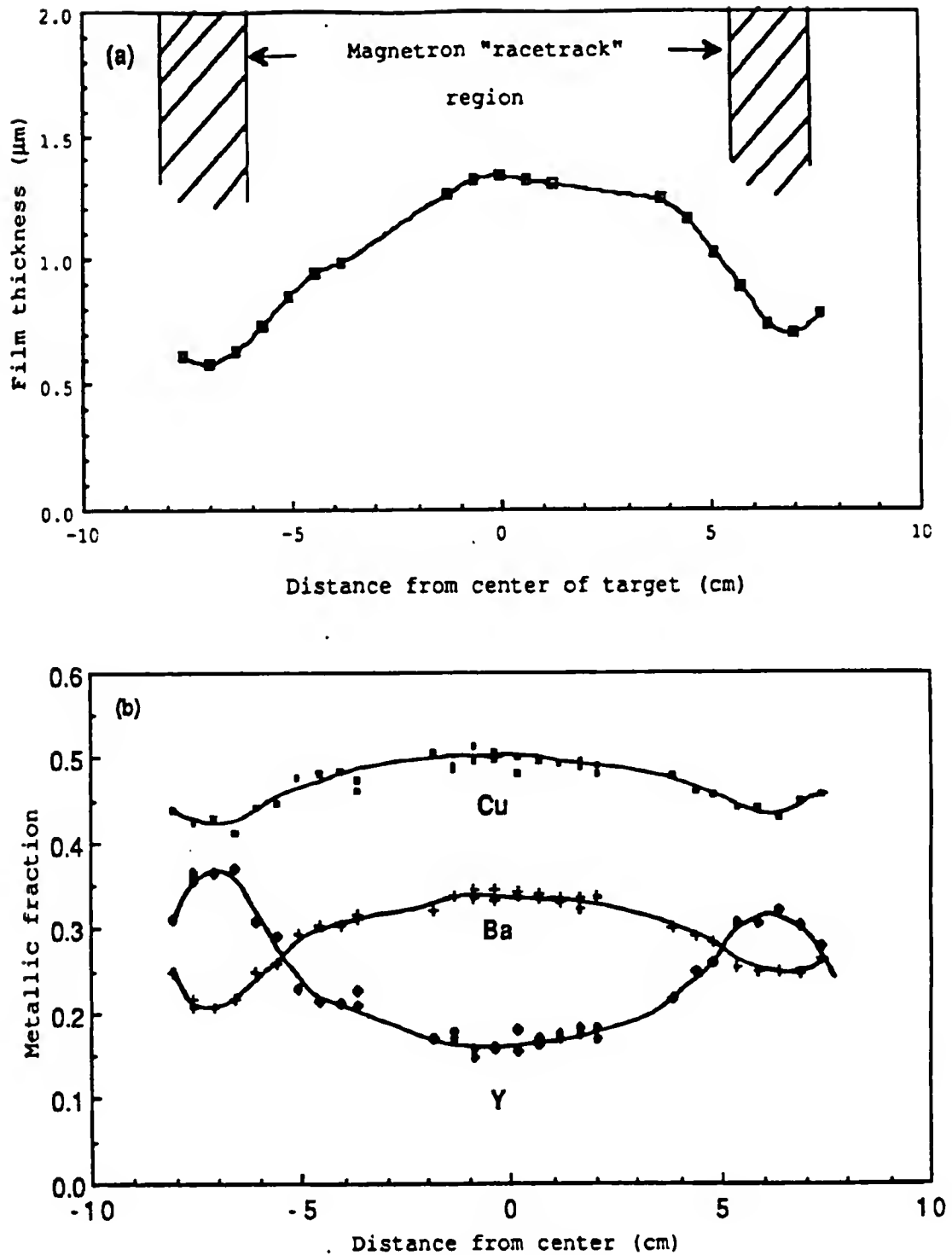


Figure 2-3. Variation in composition and thickness of Y-Ba-Cu-O film as a function of position above sputter target [34].

targets have been studied. These processing variations will be briefly reviewed; more detailed discussion is given in a review by Leskela et al. [35].

All types of sputter deposition techniques, including, but not limited to, DC planar diode [36] and magnetron [37], unbalanced DC magnetron [38], RF planar diode [39] and magnetron [40], RF cylindrical magnetron [41], and ion beam deposition [42] have been successfully employed in the growth of $\text{YBa}_2\text{Cu}_3\text{O}_{7-x}$ thin films. The most commonly used technique has by far been RF planar magnetron sputtering, and the reasons for its popularity will be discussed. Any RF sputtering technique is more versatile for depositing Y-Ba-Cu-O films than the related DC technique (i.e. diode or magnetron) since either insulating or conducting targets may be used, and Y-Ba-Cu-O targets are conducting only when reacted to form orthorhombic $\text{YBa}_2\text{Cu}_3\text{O}_{7-x}$. Further, among RF methods, the RF magnetron's magnetic field confines electrons and reduces the substrate heating which occurs with RF diodes [41]. For a given power, a magnetron source also allows lower pressure sputtering as compared to a diode source. Lower pressure sputtering results in line-of-sight deposition with higher rates, which is important for patterning of thin films [43]. For ion beam sputtering the deposition rates are generally quite low [44]. The RF planar magnetron also offers the convenience of using easy-to-fabricate flat, round targets, unlike the targets required for a cylindrical magnetron.

The most common method for obtaining 1:2:3 film compositions has been to use RF planar magnetron sputter deposition from a single oxide target enriched in those components found to be deficient in the deposited film, while keeping all other deposition parameters constant [5, 35]. However, choosing the correct target composition is not simple. This process is iterative and usually requires several different target compositions until a 1:2:3 film composition is obtained. Target compositions reported in the literature are nearly as numerous as the number of publications. The addition of excess Ba and Cu are common, but the amounts vary from system to system.

Many groups found the fabrication of oxide sputter targets with a variety of compositions to be too painstaking. Attempts to fabricate a metallic target with a Y:Ba:Cu ratio equal to 1:2:3 were unsuccessful because neither an alloy or compound with this stoichiometry could be formed and sintered targets of mixed Y, Ba, and Cu were highly unstable in air, typically corroding and crumbling in a short time [45]. On the other hand, the film composition was controlled *in situ* by simultaneous or sequential deposition from multiple sources containing either oxide or metallic targets. Target combinations used include $\text{YBa}_2\text{Cu}_3\text{O}_{7-x}$ and Ba or Cu [46], $\text{Y}_2\text{Cu}_2\text{O}_5$ and BaCuO_2 [47], Y and Ba_2Cu_3 [48], and YCu and BaCu [49]. Films were deposited with the deposition rates from each source set in the correct ratio

to give a 1:2:3 composition. However, the control of film composition over reasonably large area ($\cong 1 \text{ cm}^2$) using multiple sources proved to be difficult due to the need to precisely control deposition rates and geometrical factors. Further, the composition of the films were still found to deviate from the values predicted from deposition rates. Also, the atmospheric stability of metal targets containing Ba, such as Ba and Ba_2Cu_3 , was found to be extremely poor [45]. Thus the amount of effort in using multiple sputter targets has greatly decreased during the past two years.

Sputter deposition parameters which have been varied systematically include sputter gas pressure and percent of oxygen in the sputter gas [50], power [51], substrate bias [52], source-to-substrate distance [53], length of presputter time [54, 34], and substrate temperature [55, 56]. Substrate temperature has also been controlled for the purpose of *in situ* superconducting $\text{YBa}_2\text{Cu}_3\text{O}_{7-x}$ depositions, which will be discussed below. The effect of varying each parameter is difficult to isolate since it can depend on other parameters as well, but general trends can be observed. Higher Ar pressures [50] and lower accelerating voltages [51] give film compositions closer to that of the target. The addition of oxygen to the Ar sputter gas can lead to severe deficiencies of Ba and lesser deficiencies of Cu in films [57]. Increasing the substrate temperature causes an larger depletion of Cu in films sputter deposited

onto substrates positioned directly above the target [55, 56, 58]. In fact, it was found necessary to keep the substrate constantly cooled to obtain the same Cu/Y ratio in the film as in the target [58]. Negatively biasing the substrate had no effect at higher Ar pressures, but at low Ar pressure a small negative bias improved the film composition [59]. On the other hand, too large of a negative substrate bias caused resputtering of the film by Ar^+ from the plasma. Systematic trends due to source-to-substrate distance are difficult to quantify among different deposition systems, but film compositions nonetheless are sensitive to this parameter.

Selinder et al. [54] and Kadin et al. [34] found very long presputtering times of 30 - 60 hours, depending on the target, to be necessary to obtain a 1:2:3 film composition from a $\text{YBa}_2\text{Cu}_3\text{O}_{7-x}$ target. The long sputtering times were suggested to be necessary due to the slow loss of oxygen from the target as it converted from orthorhombic $\text{YBa}_2\text{Cu}_3\text{O}_{7-x}$ to tetragonal $\text{YBa}_2\text{Cu}_3\text{O}_6$, which is completely depleted of excess oxygen, as discussed in Chapter 1. No test was performed to actually observe oxygen leaving the target, nor was the target analyzed to determine that tetragonal $\text{YBa}_2\text{Cu}_3\text{O}_6$ had formed.

Unconventional, off-axis sputtering geometries have been successfully implemented to obtain films with a 1:2:3 composition from a slightly compensated target [60, 61, 62, 63]. The substrates were positioned at an angle to the

substrate normal such that they were not directly above the target. The off-axis angle depended on the geometry of the particular deposition chamber and reported values vary from 30 to 90 degrees from the target normal. The film composition was found to depend on the off-axis angle [63]. The substrates required rotation during deposition to obtain a uniform composition. The main disadvantage of off-axis substrate positions has been low deposition rates. Regardless, since 1990 the use of off-axis substrate positioning has emerged as the most popular variation of sputter deposition of $\text{YBa}_2\text{Cu}_3\text{O}_{7-x}$ films. The concern for compositional reproducibility has overshadowed the drawback of low deposition rates.

2.1.4 In Situ Growth of $\text{YBa}_2\text{Cu}_3\text{O}_{7-x}$

As pointed out in Chapter 1, *in situ* growth of superconducting $\text{YBa}_2\text{Cu}_3\text{O}_{7-x}$ films has received much attention since 1989, with the number of $\text{YBa}_2\text{Cu}_3\text{O}_{7-x}$ films grown by post-deposition annealing greatly decreasing. The *in situ* formation of $\text{YBa}_2\text{Cu}_3\text{O}_{7-x}$ films is desirable because of the lower temperature seen by the substrate and a much smoother film morphology. The smoother film morphology results from the growth of either strongly textured films with low angle grains boundaries or epitaxial, nearly single-crystal films and is particularly important for microwave applications. Further, most implementations of *in situ* sputter deposition

of $\text{YBa}_2\text{Cu}_3\text{O}_{7-x}$ have also utilized off-axis substrate positions [64, 65, 66].

The temperatures used in the typical post-deposition heat treatment, 800 - 900 °C, are undesirably high for two main reasons. First, such heat treatments can cause interdiffusion or reaction of the Y-Ba-Cu-O film and the substrate, thereby destroying superconductivity and/or damaging the substrate. Second, many potential applications of $\text{YBa}_2\text{Cu}_3\text{O}_{7-x}$ require its growth on silicon substrates. Any Si devices already present would be damaged by heating to such temperatures. For *in situ* growth of $\text{YBa}_2\text{Cu}_3\text{O}_{7-x}$, substrate temperatures of 650 - 800 °C are typically used during deposition for crystallization of the perovskite-like structure [67]. Substrate temperatures as low as 450 °C have also been reported [68], although the quality of the $\text{YBa}_2\text{Cu}_3\text{O}_{7-x}$ films was not very high and post-deposition heat treatment was still required. This is not surprising since the crystallization temperature for $\text{YBa}_2\text{Cu}_3\text{O}_6$ is reported to be in the range 500 - 600 °C [67].

In addition to elevated substrate temperatures, the *in situ* formation of $\text{YBa}_2\text{Cu}_3\text{O}_{7-x}$ also requires the addition of oxygen to the Ar sputter gas, with reported values ranging from 20 to 50% O_2 [64, 65, 66]. The deposition is followed by slow cooling in the chamber in an oxygen background in order to increase the oxygen content of the film [64, 65, 66]. Very high quality, epitaxial films have been grown on substrates including SrTiO_3 , MgO , and LaAlO_3 . Fair quality

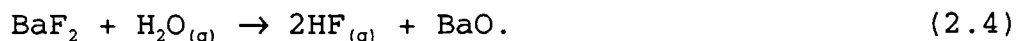
$\text{YBa}_2\text{Cu}_3\text{O}_{7-x}$ films have been grown directly on Si, but interface reactions and lattice mismatch have limited T_c and J_c values [69, 70].

An additional benefit of the *in situ* growth of $\text{YBa}_2\text{Cu}_3\text{O}_{7-x}$ films which has been observed is an improved resistance to environmental degradation [5]. This probably results from the formation of nearly epitaxial, smooth $\text{YBa}_2\text{Cu}_3\text{O}_{7-x}$ films with decreased exposed grain boundary area [71]. Films of $\text{YBa}_2\text{Cu}_3\text{O}_{7-x}$ formed by post-deposition heat treatment have a rougher film surface morphology and a greater grain boundary area, which makes them more susceptible to atmospheric degradation [71], as discussed in Section 2.1.6. Further, in a conventional post-deposition annealing process, the as-deposited Y-Ba-Cu-O films can suffer environmental degradation prior to annealing, which in turn prevents the complete reaction to form $\text{YBa}_2\text{Cu}_3\text{O}_{7-x}$ films after annealing [72]. The resulting impurity phases can limit T_c and J_c .

Control of the film composition for *in situ* $\text{YBa}_2\text{Cu}_3\text{O}_{7-x}$ growth has added complications. During sputter deposition, the substrate temperature and the oxygen in the sputter gas synergistically affect the film composition [57, 63]. For a constant percent oxygen, increasing substrate temperature leads to a Cu deficiency. Increasing the percent of oxygen for a given substrate temperature causes a shortage of Ba in the film. These factors must be accounted for in the

iteratively determined composition of a target to compensate for the deficient elements.

As discussed above, the majority of $\text{YBa}_2\text{Cu}_3\text{O}_{7-x}$ thin films, whether deposited by sputtering, laser ablation, or co-evaporation, are now grown by *in situ* processes. However, a process in which films are grown without intentional substrate heating and then heated after deposition to form $\text{YBa}_2\text{Cu}_3\text{O}_{7-x}$ would be advantageous for coating non-uniformly shaped objects or large areas, due to the difficulty of uniformly heating such substrates *in situ*. One notable process exists in which post-deposition annealing is used to form $\text{YBa}_2\text{Cu}_3\text{O}_{7-x}$ films with surface morphology, T_c and J_c equivalent to the best *in situ* grown films. In this process, Y, Cu, and BaF_2 are co-evaporated from electron-beam sources and then subjected to a post-deposition heat treatment to form $\text{YBa}_2\text{Cu}_3\text{O}_{7-x}$ [73, 74]. The use of BaF_2 as the Ba source adds the complication of a post-deposition heat treatment in humid oxygen, which is necessary to reduce the BaF_2 by the reaction [75]



The resulting BaO then reacts with CuO, Y_2O_3 and/or ternary Y-Cu-O oxides to form $\text{YBa}_2\text{Cu}_3\text{O}_{7-x}$. A temperature of 850 °C or above is required for the reduction of BaF_2 and the formation of $\text{YBa}_2\text{Cu}_3\text{O}_{7-x}$ with humid oxygen. However, recent data show that decreased oxygen partial pressure during post-deposition annealing (e.g. annealing in mixtures of

humidified O_2 and Ar) leads to a lower anneal temperature to form $YBa_2Cu_3O_{7-x}$ from Y, Cu, and BaF_2 . In fact the temperature can be lowered to values equal to those employed for *in situ* film growth (e.g. 730 °C) [74]. Thus the additional difficulty of *in situ* processing may not ultimately be necessary to achieve films of the highest quality. However, a caveat in the use of BaF_2 is its greater toxicity than $BaCO_3$ or BaO_2 , of which one must be aware when handling the materials [76].

2.1.5 Explanations for Deviation of Y-Ba-Cu-O Film and Target Compositions

Deviations of the compositions of sputter deposited films from Y-Ba-Cu-O target compositions has been discussed in the literature in terms of all four of the mechanisms described in Section 2.1.1, namely, 1) migration of one or more of the target specie(s) to the target surface during sputtering, 2) differing sticking coefficients of the components on the substrate, 3) angular distribution variation of sputtered species, and 4) unexpectedly high negative ion yields from sputtering. These four reasons will be discussed here relative to their effects and probability during magnetron sputter deposition of Y-Ba-Cu-O superconductor thin films.

2.1.5.1 Migration of Ba in Y-Ba-Cu-O target

Liou et al. [77] suggested that the Ba deficiency in sputtered Y-Ba-Cu-O films may be due to the migration of Ba to the surface of the $\text{YBa}_2\text{Cu}_3\text{O}_{7-x}$ target during sputtering. Very little explanation was given as to why the migration of Ba in the target would occur, but the point bears further consideration. Since sintered $\text{YBa}_2\text{Cu}_3\text{O}_{7-x}$ or off-stoichiometric Y-Ba-Cu-O targets are not good thermal conductors, they could reach temperatures as high as 300 °C during sputtering. As discussed above in Section 2.1.2.1, such higher temperatures could accelerate migration of components to the target surface, prevent the formation of an altered layer on the surface with the desired composition, and result in a sputtered flux with a composition different from that of the target bulk. Considering Ba migration in a Y-Ba-Cu-O target, the sputtered flux and film composition would be rich in Ba compared to the target. However, sputtered Y-Ba-Cu-O films have usually been reported to be Ba-deficient [57], whereas films rich in Ba relative to the target have never been reported. It is conceivable that the length of a typical deposition (three or more hours) may be greater than the time it takes to deplete Ba from the target, which could account for the Ba deficiency in the films. If this were true, eventually the flux of Ba migrating to the target surface would not be able to compensate for the removal of

Ba from the surface by sputtering, and the amount of Ba in the sputtered flux would decrease. Thus a Ba deficiency in the film composition would be seen. Further, if Ba continued to be more and more depleted from the target with additional sputtering, a time-dependent surface composition could develop. As a result of this, in successive depositions the film compositions could differ. A study of the composition of the surface of Y-Ba-Cu-O sputter targets after extended periods of sputtering has not been reported, which would be necessary to test the suggestion of Ba migration of Liou et al. Experiments to test this suggestion are presented in Section 4.2.

2.1.5.2 Sticking coefficient variations for Cu

The decrease in Cu concentration in Y-Ba-Cu-O films with increased substrate temperature discussed above has been suggested to result from a decreased sticking coefficient for CuO due only to higher substrate temperature [78]. This hypothesis appeared to be supported by the report of Argana et al. [58] of the need to cool the substrate in order to obtain the same Cu/Y ratio in RF planar magnetron sputter-deposited films as in the target. Authors supporting the lower sticking coefficient argument appeared to implicitly assume that CuO_x was being sputtered, which could have had a lower coefficient. This assumption ignored the fact that metallic Cu could have been sputtered, with CuO_x

reformed by surface reaction on the film. In addition, the deficiency of Cu should not be strictly a thermal sticking coefficient effect, since no such deficiency has been reported for $\text{YBa}_2\text{Cu}_3\text{O}_{7-x}$ deposited *in situ* by laser ablation, even though the substrate temperature has been taken as high as 800 °C [5, 6, 35]. Thus the decrease in Cu concentration with increasing substrate temperature must also have been related to the sputtering process itself. Furthermore, the authors do not suggest whether CuO should be sputtered as a molecule or form on the substrate. If metallic Cu was sputtered, then a thermal sticking coefficient argument would not be reasonable since the coefficient for Cu would be expected to unity at temperatures up to 500 °C [79].

An alternative explanation for the decrease in Cu concentration with increasing substrate temperature for sputtered Y-Ba-Cu-O thin films is suggested by the optical emission data of Fledderman [80]. Optical emission spectroscopy was used to study the excited-state atoms and molecules created during the ion beam sputtering of $\text{YBa}_2\text{Cu}_3\text{O}_{7-x}$ targets. Species present included Y, Ba, Ba⁺, Cu, YO, BaO, and CuO. The intensity of emission was monitored as a function of sputter ion energy, oxygen content of the beam, and target temperature. As the $\text{YBa}_2\text{Cu}_3\text{O}_{7-x}$ target temperature was increased above 200 °C, the intensity of the Cu emission lines increased. Although not acknowledged by Fledderman, this suggests that the sputter yield of Cu from $\text{YBa}_2\text{Cu}_3\text{O}_{7-x}$ increased as a function of temperature. As

discussed below, a Y-Ba-Cu-O thin film being deposited by sputter deposition may be subjected to resputtering by energetic O^- ions or neutralized O, whose energy and impingement rate depend on the plasma conditions. Increasing the substrate temperature would result in an increase in the yield of Cu sputtered from the film by the O^- ions or O atoms. Thus, the decrease in the Cu concentration in Y-Ba-Cu-O films with increasing substrate temperature could be due to a temperature-dependent resputter rate of Cu from the film, rather than due to a decreasing sticking coefficient. A study of this issue is suggested for future work, as discussed below in Chapter 7.

2.1.5.3 Angular distribution variation for Y, Ba, and Cu

The significant differences in atomic mass among Y, Ba, and Cu would make them good candidates for differing sputtered angular distributions. Wehner et al. [81] measured the composition of a Y-Ba-Cu-O film deposited on a curved Ta foil substrate by DC triode sputter deposition from a planar $YBa_2Cu_3O_{7-x}$ target. The curved substrate was flattened out and the composition of the Y-Ba-Cu-O measured as a function of the angle from substrate normal. These data indicate that Y and Cu were ejected preferentially in the normal direction, while the heavier Ba atoms were ejected more obliquely. Similar results were observed by Burbidge et al. [82] for films deposited by DC planar magnetron sputtering from a

$\text{YBa}_2\text{Cu}_3\text{O}_{7-x}$ target onto 1 cm^2 substrates located at various angular positions. Wehner et al. explained the deviations in Y-Ba-Cu-O film compositions in terms of angular distribution variations. However, no effort was made in either study to account for the effect of negative ions impinging on the films above the target. As discussed below, the angular variation in negative ion flux above the target could have caused the observed Ba deficiency, rather than angular variations in the sputtered flux of target atoms. Also, the data of Kageyama and Taga [83] showed sputtered angular distributions of Y, Ba, and Cu which did not agree with those of Wehner et al., with the distributions being strongly dependent on the deposition conditions including RF power, substrate-target distance, and sputter gas pressure. This is not surprising since, as discussed above in Section 2.1.2.3, the angular distribution of components sputtered from a compound target does not always follow the prediction of those of heavy mass being ejected more strongly along the target normal.

Furthermore, an interesting result of Kageyama and Taga, which has also been observed in studies of off-axis deposition [63], was that regardless of the angular distribution patterns of Y, Ba, and Cu, the film compositions always converged to the target composition at an angle of 90° to the target normal. Also, the higher the sputter gas pressure, the closer the film composition to the

target composition [62]. None of these authors offered explanations why such results were observed. These data suggest that the Y-Ba-Cu-O film compositions were not simply determined by the mass-dependent angular distribution variations of Y, Ba and Cu. It is suggested below in Chapter 7 that a valuable future study would be to isolate the composition variation in Y-Ba-Cu-O films due only to the angular variations in the sputtered flux of target atoms.

2.1.5.4 Negative ion effects for sputtered Y-Ba-Cu-O

Negative ions have been considered to be the major reason for the difficulty in obtaining 1:2:3 film compositions by sputter deposition from $\text{YBa}_2\text{Cu}_3\text{O}_{7-x}$ targets [5, 35]. The fact that $\text{YBa}_2\text{Cu}_3\text{O}_{7-x}$ contains highly electropositive Ba and Y bonded to highly electronegative oxygen led to the suggestion that the dissociation of Ba-O and Y-O bonds during sputtering of $\text{YBa}_2\text{Cu}_3\text{O}_{7-x}$ led to the formation of negative ions, namely O^- [57]. Thus negative ion effects, particularly film resputtering, were thought to be primarily responsible for the film composition deviations. Also, the results of many of the process variations could be interpreted in terms of their effect(s) on the negative ions, as will be discussed below. A few groups attributed most of the problems to bombardment of the substrate with electrons [84, 85, 86]. Electron effects do not seem likely since similar problems were observed for

both magnetron and diode sources, and the electrons would largely be confined away from the substrate in the magnetron source.

Rossnagel and Cuomo [57] were the first to explicitly show that sputtering of $\text{YBa}_2\text{Cu}_3\text{O}_{7-x}$ produced a large yield of negative ions. The negative ions were accelerated by a grid placed closely over the target. The particles were then energy analyzed and counted in a four-grid energy analyzer. Thus the analysis could only identify a particle's charge; it could not identify the ionic specie. Ion beam sputtering of a fresh $\text{YBa}_2\text{Cu}_3\text{O}_{7-x}$ target with Ar^+ was found to give a negative ion yield of 0.3. In other words, for every 10 Ar^+ ions which bombarded the target, approximately three negative ions were created. More oxygen in the sputter gas resulted in an increased negative ion yield. Also, the deposition rates of Y-Ba-Cu-O films deposited by RF planar magnetron sputtering from a $\text{YBa}_2\text{Cu}_3\text{O}_{7-x}$ target were found to decrease with an increasing percentage of oxygen in the sputter gas. A 100% oxygen sputter gas resulted in etching of the substrates rather than film growth. These phenomenological results led to the conclusion that the dominant negative ion was O^- . No explicit identification of O^- or any other negative ion was obtained. It was suggested that BaO or Y_2O_3 were responsible for the generation of O^- since they were reported to have high O^- yields in SIMS [87]. A fact not addressed by Rossnagel and Cuomo was that neither compound was present in the single phase $\text{YBa}_2\text{Cu}_3\text{O}_{7-x}$

target. However, Shah and Garcia [85] reported that resputtering of films occurred when using either a BaO or a Y_2O_3 target but not a CuO target, although they did not attribute the effect to O^- . This suggests that the dissociation of Ba-O or Y-O bonds during sputtering can lead to resputtering by negative ions.

That negative ion effects can best explain the deviation of Y-Ba-Cu-O film and target compositions is strengthened by the fact that many of the results obtained from variations in sputter deposition parameters can be interpreted in terms of their effect(s) on negative ions. For example, increasing the sputter gas pressure or decreasing the RF power would increase the probability of scattering of the negative ions [26] and reduce the energy with which they bombarded the substrate, thereby decreasing the amount of resputtering. Many of the changes in sputtering parameters were enacted in attempts to reduce the deleterious effects of negative ions on film composition and properties. For example, substrates were biased with negative voltages to in efforts to repel the negative ions [59]. Although not acknowledged by the authors, the success of this biasing depended on the sputter gas pressure and the power applied to the target because scattering of the negative ions could cause loss of the extra electron and formation of a neutral particle, which would not be repelled by the negative bias. Also, off-axis substrate locations were used to avoid the direct path of negative ions

accelerated away from the target surface by the negative voltage on the target. Although never stated in the literature, the effectiveness of off-axis substrate locations also depended on the sputter gas pressure and power, because scattering of the negative ions would cause their trajectory to be diverted away from the target normal. In summary, attempts to avoid film resputtering by negative ions have been based on either reducing the energy of the negative ions striking the substrate or preventing the negative ions from striking the substrate altogether.

2.1.6 Run-to-Run Irreproducibility of Film Composition

Once an optimum target composition had been obtained for a given single oxide target sputter deposition process, even if all other parameters were kept constant, the film composition could still vary between successive depositions. This irreproducibility was found to depend on the target firing temperature and target material(s) [77], and was more of a problem for systems without load-locked chambers [54]. Firing pressed oxide targets at only 500 °C prevented reaction among the starting compounds, nominally Y_2O_3 , CuO , and BaCO_3 [88], and was reported to improve the stability of the targets and the reproducibility of the film composition [77, 89]. The 500 °C firing resulted in just enough sintering to allow handling and mounting of the targets. Thus these targets essentially consisted of mechanical mixtures of the starting compounds. In fact, an unsintered,

loose powder target was reported to result in easy fabrication and improved run-to-run composition control [34, 58].

There have been essentially three reasons suggested in the literature for the run-to-run variation in film compositions: 1) the atmospheric instability of $\text{YBa}_2\text{Cu}_3\text{O}_{7-x}$, 2) the time-dependent loss of excess oxygen from $\text{YBa}_2\text{Cu}_3\text{O}_{7-x}$ during sputtering, and 3) the migration of Ba in $\text{YBa}_2\text{Cu}_3\text{O}_{7-x}$ targets during sputtering. Each of these suggestions will be discussed below.

First, a brief discussion of the atmospheric stability of $\text{YBa}_2\text{Cu}_3\text{O}_{7-x}$ and related Ba-containing compounds is in order, particularly with regard to understanding the run-to-run irreproducibility of film compositions. The main issue is that $\text{YBa}_2\text{Cu}_3\text{O}_{7-x}$ and related Ba-containing compounds such as BaO_2 are hygroscopic and react with water [77]. The amount of water present in the air as humidity in a typical laboratory is sufficient to degrade the surface of a bulk $\text{YBa}_2\text{Cu}_3\text{O}_{7-x}$ sample, resulting in a loss of superconductivity at the surface. The reaction of $\text{YBa}_2\text{Cu}_3\text{O}_{7-x}$ with water results in an enrichment of Ba at the surface, due primarily to the formation of $\text{Ba}(\text{OH})_2$ at the expense of $\text{YBa}_2\text{Cu}_3\text{O}_{7-x}$ [90]. Other atmospheric degradation products on the surface can include hydrated $\text{Ba}(\text{OH})_2$, BaO_2 , hydrated BaC_xO_y , and adsorbed water. Eventually the $\text{Ba}(\text{OH})_2$ may react with CO_2 in the air and convert to BaCO_3 [72]. Thus the surface of a superconducting $\text{YBa}_2\text{Cu}_3\text{O}_{7-x}$ sample becomes insulating. Also, the atmospheric

degradation of $\text{YBa}_2\text{Cu}_3\text{O}_{7-x}$ is often accompanied by cracking and crumbling of the surface of the samples [40].

For thin films, it has been observed that the resistance to atmospheric degradation is improved for *in situ* deposited $\text{YBa}_2\text{Cu}_3\text{O}_{7-x}$ films versus $\text{YBa}_2\text{Cu}_3\text{O}_{7-x}$ films formed by post-deposition heat treatment. As discussed in Section 2.1.4, this is probably due to the smoother film morphology and decreased grain boundary area of *in situ* deposited $\text{YBa}_2\text{Cu}_3\text{O}_{7-x}$ films. This is supported by the results of Zandbergen et al. [71] and Buyukliamanli [90], who suggested that the atmospheric degradation of $\text{YBa}_2\text{Cu}_3\text{O}_{7-x}$ is dominated by the reaction of water at particle or grain boundaries, and decreasing the particle or grain boundary area greatly improves the resistance to environmental degradation. A single crystal, epitaxial $\text{YBa}_2\text{Cu}_3\text{O}_{7-x}$ thin film would be much more stable in air than a typical $\text{YBa}_2\text{Cu}_3\text{O}_{7-x}$ target, which is typically sintered from a polycrystalline powder with a particle size of $\leq 50 \mu\text{m}$ and after firing has a density equal to 50% - 80 % of the theoretical maximum, depending on the firing temperature [88]. The particle surface area in such a case would be relatively large.

Based on the above discussion of atmospheric degradation, the improved run-to-run reproducibility observed with unreacted targets made of Y_2O_3 , CuO , and BaCO_3 is probably due to the improved atmospheric stability of these compounds relative to $\text{YBa}_2\text{Cu}_3\text{O}_{7-x}$. However, the firing at 500 °C in air used to sinter the unreacted targets would

convert some of the BaCO_3 on the surface to Ba(OH)_2 or other compounds [90]. This must be taken into account when using such targets. For unreacted targets, the amount of material on the surface with a composition different from the bulk of the target would be less, and less sputtering would be required to remove the degradation products.

The use of BaF_2 rather than the usual BaCO_3 as the Ba source in unreacted Y-Ba-Cu-O sputter targets has been found to improve the run-to-run control of the film composition [77]. Also, the use of BaF_2 as the Ba source greatly improved the atmospheric stability of the as-deposited Y-Ba-Cu-O-F films as well as the annealed, superconducting $\text{YBa}_2\text{Cu}_3\text{O}_{7-x}$ films [91]. In the as-deposited films, the use of BaF_2 has been suggested to make them non-hygroscopic, in contrast to as-deposited films containing other Ba compounds [75]. However, BaF_2 actually does react with the water in air to form a thin surface layer of Ba(OH)_2 , which essentially passivates BaF_2 from further reaction [92]. For superconducting $\text{YBa}_2\text{Cu}_3\text{O}_{7-x}$ films, the improved atmospheric stability gained by the use of BaF_2 has been suggested to be due to the formation of an oxyfluoride overlayer, which passivates the $\text{YBa}_2\text{Cu}_3\text{O}_{7-x}$ surface [93].

Klein and Yen [94] studied the emission spectra resulting from ion beam sputtering of $\text{YBa}_2\text{Cu}_3\text{O}_{7-x}$. The emission data provided the identification of hydrogen as it was sputtered away from the $\text{YBa}_2\text{Cu}_3\text{O}_{7-x}$. The emission spectra was collected for a $\text{YBa}_2\text{Cu}_3\text{O}_{7-x}$ sample which had been left in

ambient laboratory conditions for several weeks. It was found that more than 30 minutes of ion beam sputtering at an accelerating voltage of 800 V and a beam current of 40 mA was required to bring the intensity of the H peak to near zero. Although not suggested by the authors, the source of the H was most likely Ba(OH)_2 formed by the reaction of $\text{YBa}_2\text{Cu}_3\text{O}_{7-x}$ with water. This data illustrates that removal of the atmospheric degradation products from a $\text{YBa}_2\text{Cu}_3\text{O}_{7-x}$ target requires substantial presputtering.

The length of time which the target is exposed to atmosphere and the relative humidity of the ambient air can both affect the degree to which surface degradation products are formed [90]. The degradation products must be sputtered away before the sputtered flux has the same composition as the target bulk. The amount of presputtering needed for a given target will depend on many factors including the density of the target, the firing conditions, the humidity of the environment in which the target was fired and stored, and the sputtering conditions. This will be discussed further below in Section 5.1.4.

Second, as discussed above in Section 2.1.3, Selinder et al. [54] and Kadin et al. [34] found that very long presputtering of a $\text{YBa}_2\text{Cu}_3\text{O}_{7-x}$ sputter target was necessary to get a 1:2:3 film composition. This was suggested, although never proven, to be necessary to completely remove the excess oxygen in $\text{YBa}_2\text{Cu}_3\text{O}_{7-x}$ in order to form tetragonal $\text{YBa}_2\text{Cu}_3\text{O}_6$. Until the excess oxygen was completely removed,

the Y-Ba-Cu-O film composition would be dependent on the amount of time spent presputtering prior to deposition. Selinder et al. [54] thus suggested that a run-to-run irreproducibility in the film composition would occur as a result of the time-dependent loss of the excess oxygen from $\text{YBa}_2\text{Cu}_3\text{O}_{7-x}$ during sputtering. No suggestion was given as to how the loss of excess oxygen from the target actually affected the film composition. This will be discussed further in Chapter 4 below.

Third, the run-to-run irreproducibility in the film composition has been suggested to be due to the possible migration of Ba to the target surface during sputtering and the resulting time-dependent concentration of Ba on the target surface [77], as was discussed above in Section 2.1.5.1. In fact, the run-to-run irreproducibility due to Ba migration to the target surface can be viewed as a time-dependent manifestation of the same mechanism suggested for the deviation between the film and target composition: If more Ba were depleted from the target during successive depositions, the degree of Ba deficiency would vary from run to run.

The improvement in the reproducibility of film compositions due to the use of unreacted composite targets of Y_2O_3 , BaF_2 , and CuO was suggested to be due to the minimizing of the segregation of Ba in the target due to its tighter bonding in BaF_2 [77]. However, no data were presented to support this proposition.

2.1.7 Summary

In summary, for films deposited under typical conditions, a deviation of the Y-Ba-Cu-O target and sputtered film compositions usually exists with films deficient in Ba and also possibly Cu. The exact film composition is strongly dependent on the sputter deposition parameters including RF power, target composition, sputter gas pressure, substrate temperature, percent of oxygen in the sputter gas, and the angle between the target and substrate normals. The deviation of the Y-Ba-Cu-O film composition has been discussed in the literature in terms of four possible explanations: 1) migration of Ba to the target surface and the eventual depletion of Ba from the target, 2) sticking coefficient differences of the components striking the substrate, particularly at increasing substrate temperatures, 3) variations in the angular distribution of sputtered components due to differences in their masses and 4) negative ion effects, particularly resputtering of the growing film. The first explanation may be viable but has never been experimentally tested. The second explanation, as suggested above, is probably incorrect since an explanation for the decrease in Cu with increasing substrate temperature must also account for why this only occurs above a sputtering source. The third explanation could account for some data presented in the literature, but the results were not consistent among different researchers. Also, the effect

of variations in angular distributions were never clearly isolated from those of negative ions, so their magnitudes are unknown. Finally, the fourth explanation for the deviation of film and target compositions has been considered the dominant mechanism, since most experimental results pointed to resputtering of the film by negative ions accelerated away from the sputter target. However, no explicit identification of the deleterious negative ion(s) has been reported. Further, although much effort has gone into avoiding the effects of negative ions, little work has been published on trying to lower the number of negative ions sputtered from the target in the first place.

2.2 Barrier Layers for $\text{YBa}_2\text{Cu}_3\text{O}_{7-x}$ on Practical Substrates

The growth of very high quality $\text{YBa}_2\text{Cu}_3\text{O}_{7-x}$ thin films on ceramic oxide substrates such as SrTiO_3 , MgO , and LaAlO_3 is well documented [5, 6, 11, 35]. However, from the viewpoint of applications and cost, it is highly desirable to grow superconducting $\text{YBa}_2\text{Cu}_3\text{O}_{7-x}$ films on substrates such as Si and sapphire (Al_2O_3), which are more affordable and more commonly used. The potential importance for high speed operation by integration of superconducting $\text{YBa}_2\text{Cu}_3\text{O}_{7-x}$ thin films with conventional semiconductor technology is formidable.

When a conventional post-deposition heat treatment process of 800 - 900 °C is used, films of $\text{YBa}_2\text{Cu}_3\text{O}_{7-x}$ react to

some degree with all substrates on which it has been deposited. For successful substrates such as SrTiO_3 and MgO , the reaction does not appear to degrade the superconducting properties because it is either limited to near the $\text{YBa}_2\text{Cu}_3\text{O}_{7-x}$ /substrate interface or results in substitution (e.g.) of Sr for Ba in the lattice with only marginal net consequences on T_c and J_c [95]. On the other hand, for heat treatments in oxygen at $\geq 900^\circ\text{C}$ the reaction with other oxides such as Al_2O_3 proceeds as much as $0.5\text{ }\mu\text{m}$ into the $\text{YBa}_2\text{Cu}_3\text{O}_{7-x}$ and films thinner than this would no longer be superconducting [95]. Even for thicker films, the superconducting cross-section is reduced, lowering the total current necessary to exceed J_c . The reaction between $\text{YBa}_2\text{Cu}_3\text{O}_{7-x}$ and Si or GaAs is severe and leads to complete loss of superconductivity [96]. The reaction of a Y-Ba-Cu-O film and a Si substrate leads to the formation of BaSiO_3 at the Si interface and depletion of Ba from the Y-Ba-Cu-O [97]. Even if an *in situ* growth process is used, the lower temperatures do not eliminate reaction between the $\text{YBa}_2\text{Cu}_3\text{O}_{7-x}$ film and Si and the thickness of the film must be greater than the reaction layer. For example, a $200\text{ }\text{\AA}$ thick interface reaction layer forms between Y-Ba-Cu-O and Si at a substrate temperature of 600°C during the typical four hours required to deposit a $\approx 0.5\text{ }\mu\text{m}$ thick Y-Ba-Cu-O film by off-axis sputtering [98]. While the effects of Si on the superconductor are clear, the effects of Ba, Y, or Cu on any

semiconductor device on the substrate have been less well studied. It would seem however that a barrier layer would be equally necessary for avoiding degradation of the semiconductor.

The obvious method of preventing deleterious interaction between Y-Ba-Cu-O films and substrates has been the insertion of an intermediate layer between them. The terms barrier layer and buffer layer have been used interchangeably in the literature to describe the intermediate layer. In this work the term barrier layer will be used. The ideal barrier layer should 1) be chemically passivating and prevent interaction between $\text{YBa}_2\text{Cu}_3\text{O}_{7-x}$ and the substrate, and 2) not harm the $\text{YBa}_2\text{Cu}_3\text{O}_{7-x}$ film or the substrate, such as creating electrically active defects in Si. It has become clear over the last two years that with the strong anisotropy in the critical current, the ideal barrier layer would also 3) grow very strongly textured or epitaxially on the substrate to in turn allow epitaxial growth of $\text{YBa}_2\text{Cu}_3\text{O}_{7-x}$ with a c-axis orientation as needed for maximizing J_c . Data presented over the last two years have shown that grain boundaries may be sources of resistance destroying superconductivity. Therefore epitaxial growth, which eliminates grain boundaries, would also be very desirable. Finally, the ideal barrier should 4) have a matched thermal expansion coefficient between that of

$\text{YBa}_2\text{Cu}_3\text{O}_{7-x}$ and the substrate in order to reduce the stress generated by thermal cycling and thereby prevent cracking.

A large number of barrier layer/substrate combinations have been reported in the literature, with the majority of work focusing on barrier layers on Si or sapphire, as expected. Much of the early work was very Edisonian in nature, with groups apparently trying almost every source material available in their laboratories as barrier layers [35]. Barrier layer materials reported include fluorides, nitrides, oxides, and metals (e.g. BaF_2 , CaF_2 , BN, WN, VN, NbN, Ta_2O_5 , Y_2O_3 , SiO_2 , BaTiO_3 , MgO, ITO, TiO_2 , ZrO_2 , Cu, Ag, Au, Pt, Nb, Ni, and Ti) [35]. In most of these studies, preventing interface reactions was the only objective. No regard made to growing textured or epitaxial barrier or superconductor layers. Most of the barrier layers were not successful, particularly on Si and sapphire. The best results on Si substrates were obtained with a ZrO_2 barrier layer [99], whereas for sapphire, the best improvements in the superconducting properties of $\text{YBa}_2\text{Cu}_3\text{O}_{7-x}$ were obtained using Pt [100] and ZrO_2 [101]. Although barrier layers of Ag on sapphire and other oxide substrates yielded high quality $\text{YBa}_2\text{Cu}_3\text{O}_{7-x}$ films, Ag was not stable against interaction with $\text{YBa}_2\text{Cu}_3\text{O}_{7-x}$ [102]. In fact, Ag was found throughout the $\text{YBa}_2\text{Cu}_3\text{O}_{7-x}$ films. However, silver's incorporation into $\text{YBa}_2\text{Cu}_3\text{O}_{7-x}$ did not cause degradation of the superconducting properties. Rather, Ag apparently improved the

superconducting properties (T_c , J_c) by a proposed mechanism of lowering the grain boundary resistance [102].

Recent barrier layer studies have emphasized the growth of strongly textured $\text{YBa}_2\text{Cu}_3\text{O}_{7-x}$ films on Si (100) substrates. The best results reported presented two different barrier layers which came close to being ideal. First, a bilayer barrier consisting of an initial layer of MgAl_2O_4 on Si followed by a layer of BaTiO_3 facilitated the growth of strongly textured $\text{YBa}_2\text{Cu}_3\text{O}_{7-x}$ with complete c-axis orientation [98]. An *in situ* $\text{YBa}_2\text{Cu}_3\text{O}_{7-x}$ growth process was used. The lattice mismatch between the first layer and Si, the first and second layers, and the second layer and $\text{YBa}_2\text{Cu}_3\text{O}_{7-x}$ were all small enough to permit the $\text{YBa}_2\text{Cu}_3\text{O}_{7-x}$ to grow with its c-axis normal to the surface of the (100) oriented Si substrate. Also, the thermal mismatch among the layers, Si, and $\text{YBa}_2\text{Cu}_3\text{O}_{7-x}$ was small enough to avoid microcrack formation in the $\text{YBa}_2\text{Cu}_3\text{O}_{7-x}$. A sharp transition at $T_c = 87$ K and a J_c at 77 K of 10^5 A/cm² were measured. Secondly, by optimizing the amount of Y_2O_3 in the film, barriers of Y_2O_3 -stabilized ZrO_2 (Y-ZrO₂) were grown epitaxially on Si and epitaxial $\text{YBa}_2\text{Cu}_3\text{O}_{7-x}$ was grown on the barrier [103]. The Y_2O_3 concentration was optimized to adjust the lattice parameter of the Y-ZrO₂. The Si surface preparation was found to be crucial and consisted of an innovative procedure to hydrogen passivate the freshly-cleaned Si surface prior to deposition. The clean, ordered Si surface was then exposed by heating above 500 °C *in situ*.

2.3 Directions for Research

In order to develop sputter deposition processes for $\text{YBa}_2\text{Cu}_3\text{O}_{7-x}$ with improved compositional control, in light of the literature it is clear that a better understanding of the mechanisms behind the deviation of the film and target compositions are needed. In an RF planar magnetron sputtering system the situation is very complicated, and it is difficult to sort out which mechanism(s), whether one or more of those presented in the literature or one not yet suggested, is (are) affecting the film composition. It is likely that more than one mechanism may be acting synergistically to influence the Y-Ba-Cu-O film composition. Experiments are needed to independently study the effect and magnitude of each possible mechanism. Also needed are explanations of the deviation between the target and film compositions which account for the effects of more than one mechanism acting simultaneously. It would then be possible to intelligently design sputter deposition processes with control over the Y-Ba-Cu-O film composition, rather than following the Edisonian approach which has dominated the literature to date.

In this study it was desired to evaluate two of the suggested mechanisms for the deviation between the composition of Y-Ba-Cu-O targets and sputtered films. First, an explicit identification of the negative ion(s) proposed to cause film resputtering and to be the primary reason for

the deviation of the film and targets compositions was clearly needed. This information could then be used to choose target materials and/or fabrication procedures which minimized the number of negative ions created during sputtering. Secondly, it was considered valuable to experimentally determine if the migration of Ba to the target surface during sputtering and its subsequent depletion were in fact occurring. Such information would offer guidelines on the requirements for target fabrication, mounting, and cooling.

In this study it was also desired to study barrier layers for the growth of superconducting $\text{YBa}_2\text{Cu}_3\text{O}_{7-x}$ films on practical substrates. In the barrier layer study presented below it was desired to combine the best substrate for growing $\text{YBa}_2\text{Cu}_3\text{O}_{7-x}$, SrTiO_3 , with both the most widely used semiconductor substrate, Si, and the most common single crystal oxide substrate, sapphire ($\alpha\text{-Al}_2\text{O}_3$). Since $\text{YBa}_2\text{Cu}_3\text{O}_{7-x}$ was known to be relatively stable with SrTiO_3 , it was thought that SrTiO_3 might make a stable barrier layer between $\text{YBa}_2\text{Cu}_3\text{O}_{7-x}$ and Si or sapphire. At the start of this study, chemical stability was the key issue with the growth of strongly textured $\text{YBa}_2\text{Cu}_3\text{O}_{7-x}$ on a barrier layer on Si or sapphire being a secondary issue. However, as the study progressed, the importance of the textured growth of the barrier layer on Si became important and was addressed as well.

CHAPTER 3 EXPERIMENTAL PROCEDURES

The general experimental procedures used in the course of this work are presented in this chapter; more specific experimental procedures are presented as needed in other chapters. First, a secondary ion mass spectroscopy (SIMS) study of the negative ions sputtered from $\text{YBa}_2\text{Cu}_3\text{O}_{7-x}$ and related compounds is discussed. Second, an Auger electron spectroscopy (AES) sputter depth profiling study, performed to determine if Ba is migrating to the target surface during sputtering of $\text{YBa}_2\text{Cu}_3\text{O}_{7-x}$, is presented. Third, the processing system and steps required for the sputter deposition of Y-Ba-Cu-O and barrier layer thin films, including the fabrication of sputter targets, RF planar magnetron sputter deposition parameters, and post-deposition heat treatment, are covered. The sputter deposition system is described in more detail in Appendix A. Finally, the physical and electrical characterization of the Y-Ba-Cu-O thin films are discussed.

3.1 Identification of Negative Ions by SIMS

In order to identify the species and determine the relative yield of the negative ions being created by the

sputtering of Y-Ba-Cu-O targets, a negative SIMS study was carried out, the results of which are presented in Chapter 4. For a complete discussion of the principles of SIMS characterization, the reader is referred to an excellent, comprehensive book recently written by Benninghoven et al. [22]. A brief explanation will suffice for understanding the data presented here. The information provided by SIMS is related to the composition of a sample's surface. An ion beam is used to sputter the surface, and an analyzer is used to mass separate the secondary ions created during sputtering. The secondary ions which are ejected come from the uppermost layers (15 Å) of a solid's surface, thereby giving SIMS an excellent surface sensitivity. The mass-to-charge ratio (m/e) of the sputtered species versus the intensity of each specie provide direct information on the composition of the sputtered area. For accurate quantitative analysis, correction factors generally must be applied to the raw data.

A 3M model 610 static SIMS was used in the negative secondary ion detection mode with a primary ion beam voltage of 0.5 kV, an Ar pressure of 5×10^{-5} Torr, and a constant beam current of 5 nA, typically. Samples were all mounted simultaneously on a multiposition carousel and analyzed under the same vacuum conditions in order to eliminate artifacts in the data, particularly with regard to beam alignment. The analysis system contained both a 3M SIMS and

a Perkin Elmer Phi model 545 scanning Auger spectrometer. The sample normal on the carousel was 60° away from the Auger electron analyzer axis, in the plane defined by the analyzer and the UHV manipulator axis. The manipulator was located on top of the stainless steel chamber and mounted with the axis vertical. The ion gun was mounted on a 2.75 inch diameter flange on top of the chamber, 15° away from the analyzer axis. The quadrapole mass analyzer was mounted on a 4.5 inch diameter flange 15° from the manipulator axis on the other side on the plane formed by the manipulator and analyzer axes. The incident angle of the ion beam on the sample was about 30° and the take-off angle to the quadrapole was approximately the same. The distance from the sample to the quadrapole mass analyzer was about 5 inches. A modified Bessel box filter was used to energy select secondary ions and an extraction voltage was used to attract ions from the sample to the mass analyzer.

Cylindrical targets of 0.25 inch diameter and 0.25 inch thick were produced using the same process as for the two inch diameter sputter targets used in film deposition, as discussed below. Starting powders for the SIMS targets were $\text{YBa}_2\text{Cu}_3\text{O}_{7-x}$ and 123 mixtures of CuO , Y_2O_3 , and either BaF_2 , BaO_2 , or BaCO_3 . A $\text{YBa}_2\text{Cu}_3\text{O}_6$ target was formed by reducing a $\text{YBa}_2\text{Cu}_3\text{O}_{7-x}$ target at 600 °C for six hours in 90% N_2 /10% H_2 forming gas. The orthorhombic $\text{YBa}_2\text{Cu}_3\text{O}_{7-x}$ target was fired at 950 °C in air for 168 hours to maximize formation of the

superconducting phase, as verified by X-ray diffraction. The 1:2:3 mixtures were fired at 500 °C for 12 hours to promote sintering but to avoid reaction. Quickly after the firing process, the back side of the targets was sanded down to reduce the thickness to 0.125 inch, as needed to fit under the clips on the SIMS' sample carousel. The samples were immediately loaded into the SIMS' UHV vacuum chamber and pumpdown was begun.

The UHV chamber was pumped by sorption roughing and ion pumps down to a base pressure of $\leq 1 \times 10^{-9}$ Torr. The poppet valve to the ion pump was then partially closed to a small conductance and ultra-high purity (99.9999%) Ar was backfilled into the chamber to establish the typical Ar sputtering pressure of 5×10^{-5} Torr for sputtering. To study the effect of oxygen on the negative ion yield, 10% O₂ (99.9995%) was sometimes added to the sputter gas. As will be discussed below in Chapter 4, it was desired to determine if Ba with its low work function on a freshly sputtered YBa₂Cu₃O_{7-x} surface could supply electrons to thermal O₂ and form O⁻. To test this, the YBa₂Cu₃O_{7-x} target was sputtered with Ar⁺ and then the chamber was backfilled with O₂ to 1×10^{-6} Torr with the mass spectrometer operating. Finally, to simulate the heating of targets during sputtering deposition, the SIMS targets were sometimes sputtered while being heated up to 300 °C by a Ta foil envelope heater.

To collect SIMS data, the sample alignment was first checked by observing the location of an electron beam on the target surface. The sample position was then adjusted using a cylindrical mirror analyzer to locate the elastically reflected electrons at the incident beam energy of 2 keV. The target surface was presputtered for two minutes with an ion beam voltage of 3 keV to remove surface contamination and artifacts. An AES survey was then taken to check the cleanliness of the sample surface. For SIMS analysis, the ion beam voltage was reduced to 0.5 keV to simulate voltages closer to those used in sputter deposition. The Ar pressure, emission current, and beam voltage were kept constant to keep the ion beam current constant at 5 nA. The raw SIMS data were collected on an x-y recorder. The mass/charge range was set at 1 to 50 amu, while the y-axis counts per second (cps) range was varied to optimize the resolution of the data plot, but was typically $10^4 - 10^5$ cps. The intensity of the O^- peak was characterized by the maximum peak intensity. Only relative O^- yield data were compared among samples. The results of these experiments are presented in Chapter 4.

3.2 AES Study of Long Time Sputter Effects on $YBa_2Cu_3O_{7-x}$ Targets

In order to determine if the deviation of film and target composition was due to the migration of Ba or other species to the target surface during sputtering, an Auger

electron spectroscopy (AES) sputter depth profiling study of a heated $\text{YBa}_2\text{Cu}_3\text{O}_{7-x}$ target was performed. To simulate the conditions of actual magnetron sputter deposition, the target was heated to a temperature for deposition (300°C) and sputtered with Ar ions for extended periods of time. If changes in the surface concentration of Ba or other species were measured with increasing sputter time, it would indicate that migration of Ba from the bulk to the target surface was occurring.

A cylindrical 0.25 inch diameter by 0.25 inch thick $\text{YBa}_2\text{Cu}_3\text{O}_{7-x}$ target was fabricated as described in Section 3.1. The $\text{YBa}_2\text{Cu}_3\text{O}_{7-x}$ target was mounted in a Ta envelope and heated to 300°C by passing a controlled DC current through Ta wire leads spot-welded to the envelope. The temperature was monitored by a type K thermocouple spot-welded to the envelope. The analysis was performed in the same UHV vacuum system as the negative SIMS measurements and similar vacuum conditions were obtained. The Physical Electronics Model 545 scanning Auger Electron Spectrometer described above was used for AES analysis while sputtering with Ar ions with a voltage of 3 keV and current of 5 nA. AES depth profiling was performed for sputter times from 0.1 to 30 hours. The electron beam was rastered over an area of $\approx 0.25\text{ mm}^2$ and the ion beam diameter was approximately 1 mm, versus an average grain (particle) size of $\approx 50\text{ }\mu\text{m}$ in the target. Thus the area sputtered and analyzed contained a large number of

grains and grain boundaries, as is the situation in actual magnetron sputtering. The raw AES first derivative data were output in real time to a strip chart recorder. The peak-to-peak heights of the Ba, Cu, and O Auger signals were monitored as a function of sputter time. The intensity of the Y peak was too low to accurately measure changes. The results of this study are presented in Chapter 4.

3.3 Processing of Y-Ba-Cu-O Thin Films

Thin films of Y-Ba-Cu-O were grown by RF planar magnetron sputter deposition from single targets. Cold-pressed, sintered targets were prepared from Y_2O_3 , CuO, $BaCO_3$, BaO_2 , or BaF_2 . A BaF_2 precursor was chosen to determine if improvements suggested by the results of the negative SIMS study presented in Chapter 4 could be realized in actual sputter deposition of Y-Ba-Cu-O films. The various aspects of Y-Ba-Cu-O film processing and characterization are described below. Since the growth and characterization of barrier layer films are very similar, the barrier layers are discussed along with the Y-Ba-Cu-O films.

3.3.1 Sputter Target Fabrication

Powders for Y-Ba-Cu-O sputter targets were combined in the desired Y:Ba:Cu ratio using Y_2O_3 , CuO, and $BaCO_3$, BaO_2 , or BaF_2 powders of 99.5% purity or better from either AESAR, Aldrich, or Alfa Chemicals. The particle diameter of each

powder was 5 μm or less. Acetone was added to the mixtures and the resulting slurry was shaken by hand in a sealed plastic jar. The mixtures were transferred to a glass beaker and carefully heated at 160 $^{\circ}\text{C}$ for three hours in a fume hood to remove the acetone. A binder solution of polyvinyl alcohol, deionized water, and glycerine was added to the powders to improve the strength of cold-pressed targets. The powders were transferred to a plastic jar along with 0.5 cm diameter ZrO_2 milling media. Complete mixing was obtained by ball milling for 12 hours. The powder mixture was poured into a two inch diameter stainless steel die. The powder was cold pressed at a pressure of 13,000 psi into a two inch diameter by 0.125 inch thick target.

For unreacted, composite targets, green targets were heated at 500 $^{\circ}\text{C}$ for 12 hours in air in order to burn off the binder and to promote sufficient sintering for mechanical stability. For targets in which reaction of the starting compounds was desired, for example to form orthorhombic $\text{YBa}_2\text{Cu}_3\text{O}_{7-x}$, firing in air was done at temperatures up to 950 $^{\circ}\text{C}$ for times ranging from 12 to 120 hours. The phases formed in the targets as a function of temperature were determined by X-ray diffraction, as reported below in Chapter 5.

After firing, targets were bonded with CERAC Ag epoxy to a copper backing plate for improved thermal conductivity to prevent cracking. The total thickness of the target,

epoxy, and backing plate was kept at about 3/16 inch due to mounting restrictions in the sputter source.

3.3.2 RF Sputter Deposition of Y-Ba-Cu-O and Barrier Layer Thin Films

All Y-Ba-Cu-O and barrier layer thin films used in this study were grown in the same home-built multisource sputter deposition system. The system, described in detail in Appendix A, contained two US Gun model I DC and two US Gun model II RF planar magnetron sputter sources. All films discussed in this study were deposited using an RF source. Home-made and/or commercially obtained two inch diameter sputter targets, bonded to a Cu backing plate as discussed above, were mounted in the sources. Conductive Ag paste was applied to both the Cu backing plate and the mounting stage of the sputter source to insure good thermal contact. Cooling water flowing beneath the stage of the sputter source thus kept the targets cool during sputtering.

Prior to loading for deposition, substrates were cleaned to remove hydrocarbon contaminants, metallic impurities, and native oxide in the case of Si. Substrates used in this study included (100) Si, (100) SrTiO₃, and (11 $\bar{2}$ 0) (A-plane) sapphire, which were obtained from Virginia Semiconductor, Commercial Crystal Laboratories, and Sapphikon, respectively. All substrates were given a minimum degreasing clean of five minutes in ultrasonically agitated methanol, followed by blow drying with nitrogen or freon.

For sputter rate calibration or films deposited for compositional analysis by electron probe for microanalysis (discussed below), a Si substrate was used and no other cleaning or etching was done. However, for the growth of superconducting Y-Ba-Cu-O films or of barrier layers, a more thorough cleaning was usually performed. The exception was SrTiO₃ substrates, which were purchased precleaned and thus were only given a methanol degreasing. A more complete degreasing included an additional first two steps of two minutes in trichloroethane followed by two minutes in acetone prior to methanol cleaning. The containers of both solvents were placed in an ultrasonic tank. Sapphire substrates were then cleaned in a 1:1:10 HF:HCl:H₂O mixture for 10 minutes to remove metallic surface contaminants, rinsed in flowing deionized water and blow dried with N₂. Silicon substrates, after being degreased and then rinsed in deionized water, were etched in a 10:1 deionized water:buffered oxide solution to remove the native oxide. This etch was followed by rinsing in flowing deionized water.

After cleaning, all substrates were immediately loaded onto the home-built substrate holder described in Appendix A. For verification of the anticipated film thicknesses and to establish sputter rates, a portion of a Si substrate was masked with a cleaved piece of a Si wafer and held in place on the substrate holder by a tungsten clip, as described in

Appendix A. The substrates and the holder were blown clean with N_2 filtered to remove particulates $> 0.5 \mu m$. The substrate holder was then attached to the arm of the substrate rotation assembly, as illustrated in Figure A-5. The distance between the target and the substrate and the position of the substrate above the target were set as desired. Typically, the substrate was 6 cm directly above the target.

The diffusion-pumped, liquid nitrogen trapped glass bell jar, with a stainless steel clam shell liner, high vacuum system was typically pumped to a base pressure of 1×10^{-6} Torr for depositions. Argon or $Ar+O_2$ sputter gas was backfilled into the chamber at a controlled flow rate. In conjunction with a limiting of the pumping speed by a throttle valve, a constant pressure of 10 mTorr was typically established. The RF plasma was then ignited and the reflected RF power minimized with a tuning network. The desired RF power (typically 50 W) was established and the target was presputtered with a shutter protecting the substrate. New Y-Ba-Cu-O targets were sputtered for at least three hours prior to use. A presputter of at least one hour was used for all subsequent depositions from a target, with three hours not being uncommon. For reacted Y-Ba-Cu-O targets, the amount of presputtering was found to strongly effect the film composition.

After presputtering, the shutter was opened and Y-Ba-Cu-O deposited for the estimated length of time needed to grow a film of the desired thickness (based on the sputter rate of a deposition with the same parameters). Frequent manual retuning of the RF matching network was used during deposition to maintain constant deposition power. Substrates were electrically floating and nominally unheated, although during deposition a temperature of up to 200 °C was possible due to electron, ion, and neutral bombardment of the substrate. After deposition, the shutter was closed and the RF power and the sputter gas flow were brought to zero. The substrates and target were allowed to cool under vacuum at a pressure of $\leq 2 \times 10^{-6}$ Torr for at least 15 minutes. The pumping system was valved off and the chamber backfilled with nitrogen gas to bring it up to atmospheric pressure. Finally, the substrates coated with newly grown Y-Ba-Cu-O films were removed.

After a deposition, the film thickness was determined by removing the Si mask and measuring the height of the resulting step with a Sloan Dektak Model I profilometer. Typical film thicknesses were 0.5 to 1.0 μm . The sputter rate was calculated by dividing the thickness by the time of the deposition in minutes. Since RF power, gas pressure, and other deposition parameters were held constant, the sputter rate was assumed to remain constant throughout a deposition

[20]. Deposition rates for RF power of 50 W were typically 30 - 50 Å/min.

The deposition parameters of a typical Y-Ba-Cu-O deposition were as follows: 50 W RF power, 10 mTorr Ar, 6 cm substrate-to-target (S-T) distance, and substrate electrically floating, nominally unheated, and positioned face-down directly above target center. The prime emphasis of this study was to control the film composition by using these typical deposition parameters and varying the target composition, the starting Ba compound, and the target firing temperature.

Different target compositions were used to iteratively approach a cationic Y:Ba:Cu ratio of 1:2:3 in the film, as will be discussed in Chapter 5. Barium precursor compounds of BaCO_3 , BaO_2 , or BaF_2 were studied to determine their effect(s) on film composition. Target compositions for all Ba compounds included 1:2:3 and 1:4:4 (indicating the ratio of Y:Ba:Cu). After BaF_2 was found to give the most consistent results among the Ba precursor compounds, the target composition using BaF_2 was iteratively refined to 1:1.6:2 in order to get a film composition near 1:2:3.

Barrier layer films of SrTiO_3 were RF sputter deposited from commercially obtained stoichiometric oxide targets onto Si (100) and sapphire ($11\bar{2}0$) substrates. Initial depositions used the standard deposition parameters established for Y-Ba-Cu-O films, since this allowed

presputtering of the Y-Ba-Cu-O target while the barrier layer was being grown. These included 50 W RF power, 10 mTorr Ar, 6 cm substrate-to-target (S-T) distance, and substrate electrically floating, nominally unheated, and positioned face-down directly above target center. However, when a pure Ar sputter gas was used, SrTiO₃ films were found to be highly stressed in the as-deposited condition and exhibited cracking and even peeling, as discussed in Chapter 6. Oxygen was added to the sputter gas to reduce the stress in the SrTiO₃ films. The deposition rate for SrTiO₃ was typically 40 - 50 Å/min and the thickness of the barrier layer films was typically 0.4 - 0.5 μm. After the growth of the barrier layer, either the substrate was rotated over the second RF source and Y-Ba-Cu-O was deposited without breaking vacuum, or the sample was removed from the vacuum chamber and subjected to heat treatment prior to Y-Ba-Cu-O growth. The heat treatment was intended to relieve stress in the barrier layer and to promote crystallization and/or grain growth.

3.3.3 Post-deposition heat treatment

As-deposited Y-Ba-Cu-O thin films were not superconducting but rather were insulating and amorphous. In order to form superconducting YBa₂Cu₃O_{7-x}, the films required a post deposition heat treatment. The heat treatments were done in a three-zone Applied Test Systems tube furnace with

an enclosed 51 mm diameter quartz tube for containing the desired ambient gas. Samples were loaded onto a quartz boat and positioned in the center of the quartz tube. A cap was placed on the end of the tube and gas regulated by a valve was flowed through the tube and exited through an oil bubbler. The furnace was powered by three Leeds and Northrup model 11906-223 zero voltage power packs and was controlled by an Omega model CN-2010 microprocessor, which regulated both setpoints and heating and cooling rates.

The heating cycle was similar for all Y-Ba-Cu-O films. The samples were brought from room temperature to the desired high temperature setpoint of 850 - 900 °C in 1 to 2 hours. Then the temperature was held constant for a one hour soak. After the soak, the temperature was lowered very slowly (≤ 3 °C/min.) to room temperature by either simply shutting off power to the furnace or by having the controller regulate the cooling. Occasionally, during cooling an additional 2 to 6 hour soak was performed at 500 °C in an attempt to improve the oxygen stoichiometry of the $\text{YBa}_2\text{Cu}_3\text{O}_{7-x}$ film. For films deposited from targets with BaO_2 or BaCO_3 precursor compounds, heat treatments were performed in 99.995% purity oxygen flowing at 10 - 30 sccm. For BaF_2 containing targets, the films required heating in humid oxygen in order to reduce the BaF_2 to BaO and permit formation of $\text{YBa}_2\text{Cu}_3\text{O}_{7-x}$ [75], as discussed in Chapter 2. Oxygen was humidified by passing it at an accelerated flow

rate of 200 sccm through a 1000 ml flask of deionized water at room temperature. The humid oxygen was used during heating from room temperature and during the high temperature soak, but dry oxygen at a reduced flow rate of 30 sccm was used during cooling.

3.3.4 Physical Characterization of Thin Films

The composition of as-deposited Y-Ba-Cu-O thin films was determined by Electron Probe Microanalysis (EPMA) on a JEOL Superprobe model 733 EPMA System. All EPMA work was performed by MAIC staff at the University of Florida. To assure the surface smoothness which is critical to quantitative EPMA and to avoid secondary fluorescence of the elements in the film due to emission from the substrate, 0.5 - 1 μm thick films were deposited for composition analysis on two inch diameter Si (100) substrates. The EPMA analysis was performed using wavelength dispersive spectroscopy with an 8 keV electron accelerating voltage, a 20 μm beam diameter, and a 40° tilt between the crystals and the normal to the sample surface. The 8 keV voltage was used to prevent the electron beam from penetrating beyond the films into the substrate. Data was collected for 60 seconds to obtain a quantitative accuracy of ± 2 atomic percent. Calibration standards were chosen with Y, Ba, and Cu bonded to oxygen in order to approximate the bonding condition in the oxide targets: YAG for Y, CuO or Cu for Cu, and BaSO₄

for Ba. Also, CaF_2 was used as the calibration standard for F. Tracor Northern phi-rho-z correction software was applied to the K values to obtain quantitative composition. Analysis of a bulk, textured $\text{YBa}_2\text{Cu}_3\text{O}_{7-x}$ sample obtained from David Tanner in the Department of Physics at the University of Florida yielded a 1:2:3 composition, thereby verifying the accuracy of the measurement. Further, the composition values determined by EPMA for two films were verified by Rutherford Backscattering Spectroscopy. The film thicknesses had to be at least $0.4\text{ }\mu\text{m}$ to prevent fluorescence from the substrate. To assign a single composition value for a given deposition, five data points were averaged for a substrate of 1 cm^2 positioned 0.5 inches from the center of the substrate holder, which was in turn centered directly above the target. For composition profiles across two inch diameter substrates, an EPMA line scan was performed with 25 data points spaced $2000\text{ }\mu\text{m}$ apart. Data were plotted as atomic percent versus position from substrate center.

The crystallinity and structure of thin films was determined by X-ray diffraction (XRD). Samples were mounted with double-stick tape onto a 1" by 3" glass slide. All XRD data collection were performed by MAIC staff at the University of Florida. A Phillips model APD 3720 diffractometer was used with Cu K_α radiation and generator settings of 40 kV and 20 mA. The angle 2θ was varied from 15° to 90° at a rate of $3^\circ/\text{min}$. A typical full-scale

intensity of 1000 cps was plotted versus 2θ . Phase and structure identification were done by comparing the d-spacing data to standard values from a JCPDS [104] card file and from values in the recent Y-Ba-Cu-O literature.

The morphology of the Y-Ba-Cu-O and barrier layer thin films was studied by scanning electron microscopy (SEM) and optical microscopy. A JEOL model JSM-35C SEM was used to obtain images of the film surface at magnifications up to 10,000 times. Both Y-Ba-Cu-O and barrier layer films had to be coated with 100 Å of gold to prevent charging of nonconductive regions. Optical microscopy provided complementary information at lower magnifications and required no sample preparation. In particular, identifying microcracks in barrier layer and Y-Ba-Cu-O thin films required both SEM and optical microscopy. A Nikon model Epiphot-TME optical microscope was used at magnifications up to 1000X.

The distribution of elements across the surface and throughout the thickness of the films was determined by Auger Electron Spectroscopy (AES) surveys, images, and/or depth profiles. The distribution of Y, Ba, Cu, O and sometimes F was studied for as-deposited and heat treated Y-Ba-Cu-O films. The ability of barrier layer films to prevent interaction of Y-Ba-Cu-O and a given substrate was also determined by AES sputter profiling. The AES analysis was done on a Perkin Elmer model 660 Scanning Auger

Microprobe. An electron beam accelerating voltage of 10 keV and a current of 30 nA was used. The peak energies used for each element were as follows (values in eV): Y = 1746, Ba = 584, Cu = 920, O = 510, F = 650, Si = 1619, Sr = 1649, Ti = 418, and Al = 1396. For sputtering, an Ar⁺ beam produced in an ion gun with a 25 mA emission current and an Ar pressure of 1.1×10^{-4} Torr was accelerated by a voltage of 3 keV and rastered in a standard 3 mm x 3 mm area. Sputter rates were estimated from calibrated values on Ta₂O₅ known for the accelerating voltage used. The data collection and reduction was computer-controlled by a Perkin Elmer personal computer and software written by Perkin Elmer. The Auger surveys and depth profiles were plotted on either a Hewlett Packard laser printer or pen plotter.

3.3.5 Electrical Characterization of the Y-Ba-Cu-O Films

Resistivity versus temperature characterization is the most common way to obtain information about the superconducting transition properties of a thin film or bulk material [3, 5]. In this approach, the resistivity of a material is measured as a function of a decreasing temperature. At a specific temperature value, the resistivity may begin to drop suddenly, indicating the onset of superconductivity. As the temperature is lowered a resistivity of zero may eventually be observed, indicating complete transition to the superconducting state. The

temperature at which the resistivity equals zero is the critical transition temperature, T_c . Of course, a measurement of zero resistivity cannot truly be made. The "zero" value is typically taken as the lowest resistivity value measurable by a given system, which can either be limited by the equipment at hand or by noise. For the common DC four point probe technique used in this study, discussed below, the equipment limitations were usually the output range of the current source and the sensitivity of the voltmeter available. Since the resistive transition for high quality superconducting $\text{YBa}_2\text{Cu}_3\text{O}_{7-x}$ samples usually drops steeply, the exact definition for zero resistivity may not be critical. However, many authors have reported on $\text{YBa}_2\text{Cu}_3\text{O}_{7-x}$ samples for which the resistive transition was not sharp and extended over several degrees, as discussed below. In such cases, a clear statement of what comprises zero resistance, or zero voltage for DC four contact measurements, is necessary to be able to compare reported T_c values. In this study, for reasons discussed below, the value for zero voltage was $0.9 \mu\text{V}$. Unfortunately, in the literature the definition for zero resistivity or voltage is rarely given. To avoid the issue of what comprises zero resistivity, T_c values are often reported as the temperature at the midpoint of the superconductor resistive transition. This was especially true during the first few years of the high temperature superconductor field, since the quality of

much of the material was not high and the resistive transitions were often not sharp. Even today T_c values based on either the midpoint of the transition or on zero resistivity are utilized. However, the basis for the T_c value is often not stated.

Resistivity versus temperature data for a good quality post-deposition heat treated $\text{YBa}_2\text{Cu}_3\text{O}_{7-x}$ thin film on SrTiO_3 are shown in Figure 3-1 [105]. In this figure, the normal state resistivity decreases linearly from room temperature, 300 K, to an extrapolated intercept on the resistivity axis near a value of zero at 0 K, as expected for metallic conduction. The superconducting transition occurs near 90 K and the resistivity drops to zero within a narrow temperature range which is nominally less than 5 K. The relatively soft shoulder on the transition is typical of $\text{YBa}_2\text{Cu}_3\text{O}_{7-x}$. The room temperature resistivity is about $900 \mu\Omega\text{cm}$, which is high considering the relatively sharp superconducting transition, even for post-deposition heat treated films. During the last few years, room temperature resistivity values less than $200 \mu\Omega\text{cm}$ have been reported for *in situ* grown $\text{YBa}_2\text{Cu}_3\text{O}_{7-x}$ films [5, 13, 65].

At the end of the superconducting transition a small tail can appear in which the final drop to zero resistivity may take several degrees. The extent of the tail portion of the R-T data depends on the definition of zero resistivity, which depends on the measurement capabilities, as discussed

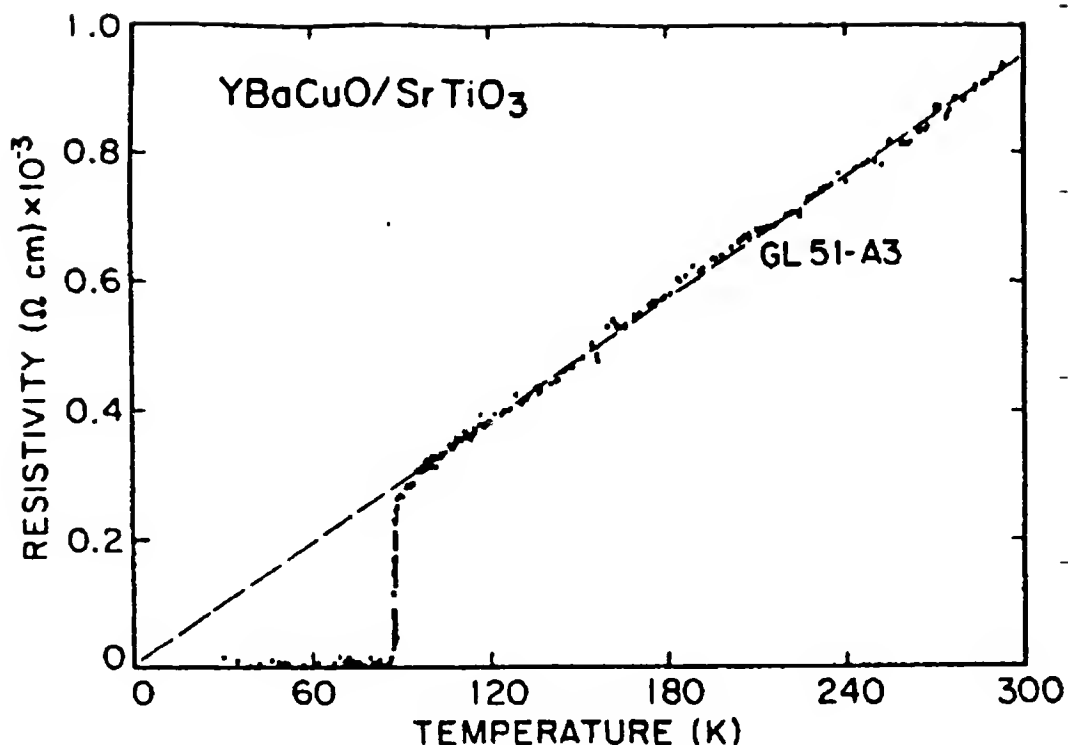


Figure 3-1. Example of good quality resistance versus temperature data for post-deposition heat treated Y-Ba-Cu-O film [105].

above. As a result, the data in the tail portion of the R-T plot are often ignored in the literature.

Several parameters are commonly used to compare high temperature superconductor R-T data, including the critical transition temperature, T_c , the transition width, ΔT , and the resistivities at room temperature (300 K) and 0 K, ρ_{rt} and ρ_0 , respectively. The relationship of these parameters to physical properties of superconducting Y-Ba-Cu-O thin films will be discussed in Chapter 5. As pointed out above, T_c can be defined either as the midpoint of the

superconductive transition, $T_{C,mid}$, or as where the resistivity goes to zero, $T_{C,0}$. The determination of $T_{C,mid}$ will be discussed below. The value for ρ_0 is taken as where the linear extrapolation of the normal state portion of the curve intersects the resistivity axis. This parameter gives an indication of the residual normal state resistivity in a sample.

Similar to the case for T_c , the definition of ΔT is not consistent among publications. Strictly, ΔT is defined as the difference of the temperature at the onset of superconductivity, T_{onset} , which is nominally where the resistivity begins to drop, and the temperature where the resistivity goes to zero, $T_{C,0}$. The problems with the definition of zero resistivity were discussed above. The definitions of T_{onset} are inconsistent because of the soft shoulder between the normal state and superconducting transition portions of the R-T data for $YBa_2Cu_3O_{7-x}$. As a result, in some samples a T_{onset} of above 100 K would be obtained, when in reality the transition to the superconducting state does not occur until about 92 K. It then follows that the values of ΔT could be unexpectedly large.

To solve the problem for the determination of T_{onset} , one of a few methods is commonly used [106]. The method used in this study is illustrated in Figure 3-2, using R-T data

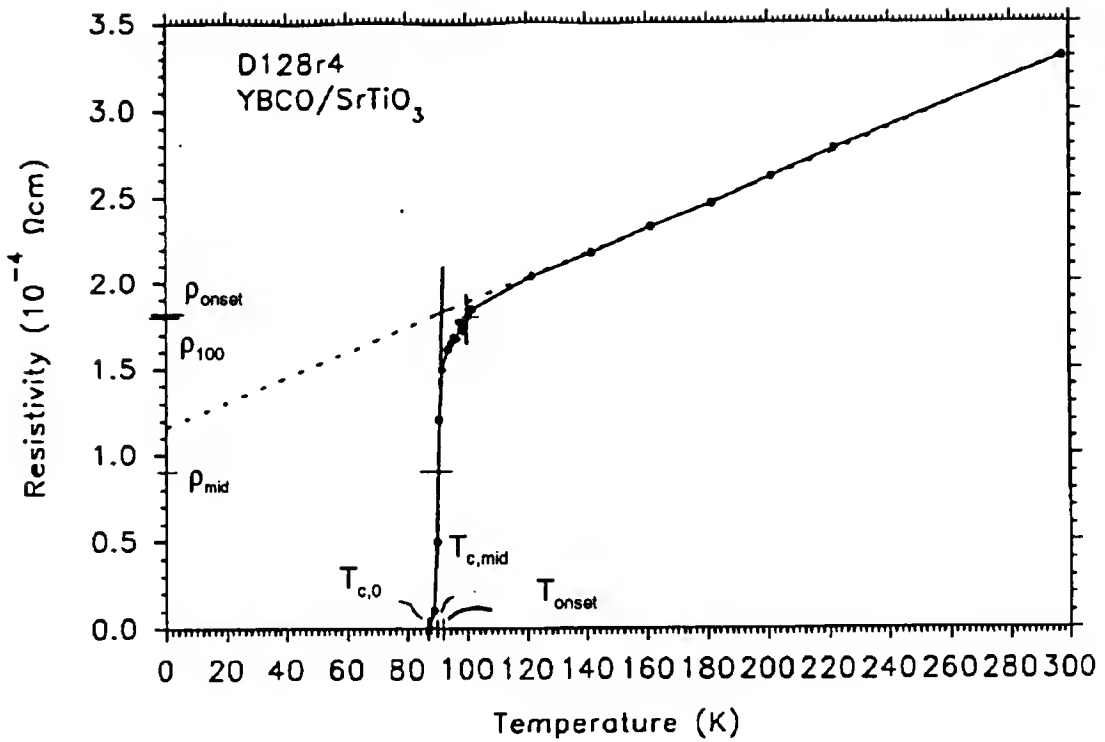


Figure 3-2. Illustration of graphical method used to calculate T_c and ΔT from R-T data.

presented in Chapter 5. The linear extrapolation of the normal state portion of the curve is drawn to determine ρ_0 , as discussed above. A line is then drawn through the superconducting transition region of the curve. Where the two lines intersect is taken to be T_{onset} . In this way, the uncertainty due to a soft shoulder on the transition is removed. Further, once T_{onset} has been defined, the resistivity corresponding to the onset, ρ_{onset} , can be determined. Subsequently, values of $T_{c,\text{mid}}$ and ΔT can be determined. Another common practice is to take ΔT be the

difference between the temperatures corresponding to the resistivity values equal to 90% and 10% ρ_{onset} [106]. The value for $T_{c,\text{mid}}$ is taken to be the temperature where the R-T data crosses the value of 50% of ρ_{onset} .

Data in the literature are presented either as resistance versus temperature or resistivity versus temperature plots. Either type of data presentation allows the determination of T_c and ΔT . However, recent publications have more frequently presented resistivity versus temperature data, since the normal state resistivity values are also indicative of film quality.

In this study, room temperature resistivity values for Y-Ba-Cu-O thin films were determined using a home-built four point probe measurement system. Room temperature resistivity data were used as a first screening test for the superconductivity of a film. If a film was insulating or a very poor conductor, it was unlikely to exhibit a superconducting transition and further electrical testing was not performed. An Alessi model CPS four point probe test fixture and model C4S four point probe head, with collinear spring-loaded osmium probe tips of 0.005 inch diameter spaced 0.05 inch apart, were used. A Lake Shore Cryotronics model 120 current supply provided a constant current to the outer two of the four contacts. A Keithley model 196 voltmeter was used to measure the resulting voltage across

the inner two contacts. The polarity of the current was then reversed and the voltage remeasured. The film sheet resistance was calculated by the relationship [107]

$$R_s = \frac{4.532 \text{ V}}{I} (\Omega/\text{square}). \quad (3.1)$$

The film resistivity in Ωcm was then calculated by multiplying R_s by the film thickness in centimeters.

Superconducting properties of a film were determined by direct current (DC) resistivity versus temperature (R-T) data. The home-built, computer-controlled R-T system and the operating procedure are discussed more fully in Appendix B. In brief, the R-T system performed the same resistance measurement as the room temperature four point apparatus but with a controlled variation in temperature from room temperature down to 12 K, if necessary. Thin film samples of Y-Ba-Cu-O were loaded into a holder and contacted by four collinear rhodium-tipped copper probes. The holder was then inserted into a cryostat cooled by a closed-cycle He refrigerator and the temperature automatically brought to the desired value. A constant DC current was applied to the outer two contacts and the resultant DC voltage across the inner contacts was measured. The polarity of the current was reversed and the voltage remeasured. An average resistance was calculated from the opposite polarity voltage measurements as discussed in Appendix B. The temperature was successively lowered until a zero voltage measurement was obtained, at which time the measurement was terminated by

the controlling computer. The zero voltage value for this study was 0.9 μV . This value was primarily limited by noise, not by the capabilities of the instrumentation. At the completion of the measurement, the computer calculated resistance values relative to the resistance at room temperature (R/R_{rt}) and plotted these values versus temperature. Resistivity values were calculated by multiplying the relative resistance values from the R-T measurement by the room temperature resistivity value obtained from the four point probe measurement using the Alessi probe station.

CHAPTER 4

MECHANISMS OF FILM AND TARGET COMPOSITION DEVIATION FOR SPUTTER DEPOSITED Y-Ba-Cu-O

In this chapter are presented the results of studies to address the two most probable mechanisms to explain the deviation between the film and target composition for sputter deposited Y-Ba-Cu-O films. First, in order to identify the negative ion species created by the sputtering of $\text{YBa}_2\text{Cu}_3\text{O}_{7-x}$ and related compounds and to determine their relative yields, a negative SIMS study was performed. As discussed in the Chapter 2, O^- has been postulated to be the primary cause of negative ion effects in the sputter deposition of Y-Ba-Cu-O films, including non-uniform thickness and composition, but no explicit identification of O^- has been reported. In the results that follow, the formation of O^- by sputtering Y-Ba-Cu-O targets will be clearly illustrated. Also, it will be shown that the yield of O^- can be affected by the choice of the sputter target material(s). Second, the results of an AES depth profiling study performed to determine the time-dependence of the composition of $\text{YBa}_2\text{Cu}_3\text{O}_{7-x}$ sputter targets are presented. It is clearly shown that the migration of Ba to the target surface can be ruled out as a mechanism for the deviation of the film and target compositions.

4.1 SIMS Study of Negative Ions Sputtered from Y-Ba-Cu-O

SIMS data were collected as described in Chapter 3. A SIMS spectra for a superconducting $\text{YBa}_2\text{Cu}_3\text{O}_{7-x}$ target sputtered by 0.5 keV Ar^+ is presented in Figure 4-1. The scale on the abscissa, m/e , is the mass-to-charge ratio of detected negative ions, while that of the ordinate is the intensity in counts per second. Because the incident ion current was kept constant, the intensity is proportional to a yield, defined as in Section 2.1.2 as the ratio of the number of sputtered species to the number of incident ions. The peaks with the highest intensity were at m/e values of 16 and 17, corresponding to O^- and OH^- . Other peaks were obtained at m/e values of 12, 14, 19, 28, 32 and 35, as illustrated in Figure 4-1. The identification of the ionic specie(s) corresponding to each peak is presented along with its relative yield in Table 4-1. In order to measure the yield of peaks beyond a m/e value of 20, the cps scale was magnified by a factor of 10.

The main point of these data is that the dominant negative ion sputtered from $\text{YBa}_2\text{Cu}_3\text{O}_{7-x}$ is O^- , with a relative yield approximately an order of magnitude greater than that of any other specie. The presence of OH^- may be due to residual water or hydrogen in the vacuum chamber, which illustrates the importance of maintaining a good vacuum. However, the OH^- may also result from the presence of atmospheric degradation products, specifically $\text{Ba}(\text{OH})_2$, on

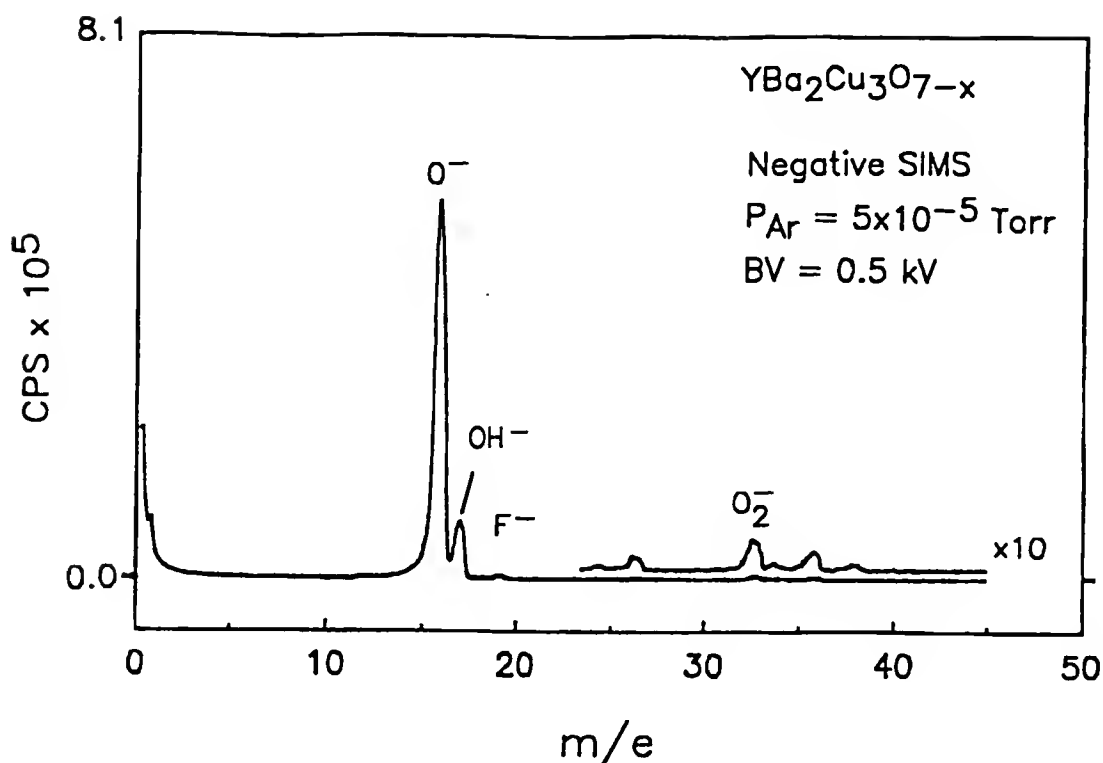


Figure 4-1. Raw SIMS data for $\text{YBa}_2\text{Cu}_3\text{O}_{7-x}$ bulk sample.

the surface of the sintered powder particles. This will be discussed further in Chapter 5. Also of note are the presence of C, Cl, and F. These were not impurities in the target, but rather were residual contaminants in the vacuum chamber, since these peaks were seen for all SIMS analyses in this system regardless of the target material. Since O^- is the dominant specie, it is clear that any attempt at controlling the effects of negative ions on the composition of sputter deposited Y-Ba-Cu-O films must emphasize controlling O^- .

As discussed in Section 2.1.6, the use of unreacted or reduced Y-Ba-Cu-O targets had been reported to improve

Table 4-1. Identity of ions in negative SIMS data for orthorhombic $\text{YBa}_2\text{Cu}_3\text{O}_{7-x}$.

| Mass/Charge | Negative Ion(s) | Relative Yield |
|-------------|-------------------|----------------|
| 12 | C | 0.004 |
| 14 | N | 0.007 |
| 16 | O | 1.000 |
| 17 | OH | 0.150 |
| 19 | F | 0.010 |
| 28 | N_2 , CO | 0.004 |
| 32 | O_2 | 0.007 |
| 35 | Cl | 0.005 |

reproducibility and control of the film composition. To determine if these improvements could be related to a decrease in the O^- yield from the unreacted starting compounds, and to determine if the O^- yield could be minimized by the choice of the compound(s) in the target, four targets with a Y:Ba:Cu ratio equal to 1:2:3 were mounted together on a multiposition carousel and negative SIMS data were collected. The incident Ar^+ ion current was kept constant for all of the targets. To a first approximation, having the same cationic ratio in each target should have resulted in the same sputter rate for each and permitted direct comparison of negative ion yield data. The compound(s) in the targets were as follows:

1) superconducting, orthorhombic $\text{YBa}_2\text{Cu}_3\text{O}_{7-x}$, 2) tetragonal

YBa₂Cu₃O₆ formed by the reduction of YBa₂Cu₃O_{7-x}, 3) an unreacted 1:2:3 mixture of Y₂O₃, CuO and BaCO₃, fired at 500 °C, referred to as the BaCO₃-123 mixture and 4) an unreacted 1:2:3 mixture of Y₂O₃, BaF₂, and CuO, fired at 500 °C, referred to as the BaF₂-123 mixture. The O⁻ yield data are summarized in Figure 4-2, where it can be seen that the O⁻ yield decreased in the order: orthorhombic YBa₂Cu₃O_{7-x}, BaCO₃-123 mixture, tetragonal YBa₂Cu₃O₆, and BaF₂-123 mixture. The BaCO₃-123 mixture had an O⁻ yield about half that obtained for orthorhombic YBa₂Cu₃O_{7-x}. Reducing a YBa₂Cu₃O_{7-x} target to form tetragonal YBa₂Cu₃O₆ resulted in about a threefold decrease in the O⁻ yield. The O⁻ yield for the BaF₂-123 mixture, in which Ba was not bonded to oxygen, was nearly an order of magnitude less than that for YBa₂Cu₃O_{7-x}. Hence a significant decrease in the O⁻ yield was obtained by avoiding superconducting YBa₂Cu₃O_{7-x}, and an additional decrease was realized by avoided compounds in which Ba and O were bonded.

As discussed above in Section 2.1.5.4, the large electronegativity difference between Ba and O has been postulated to be the main reason for the formation of O⁻ during sputtering of YBa₂Cu₃O_{7-x} [57]. If this reasoning is extended, then the sputtering of BaF₂ would be expected to produce a high yield of F⁻, since F is even more electronegative than O. This could cause the same resputtering problems as suggested to be due to O⁻. However, as shown in Figure 4-3, the F⁻ yield from the BaF₂-123

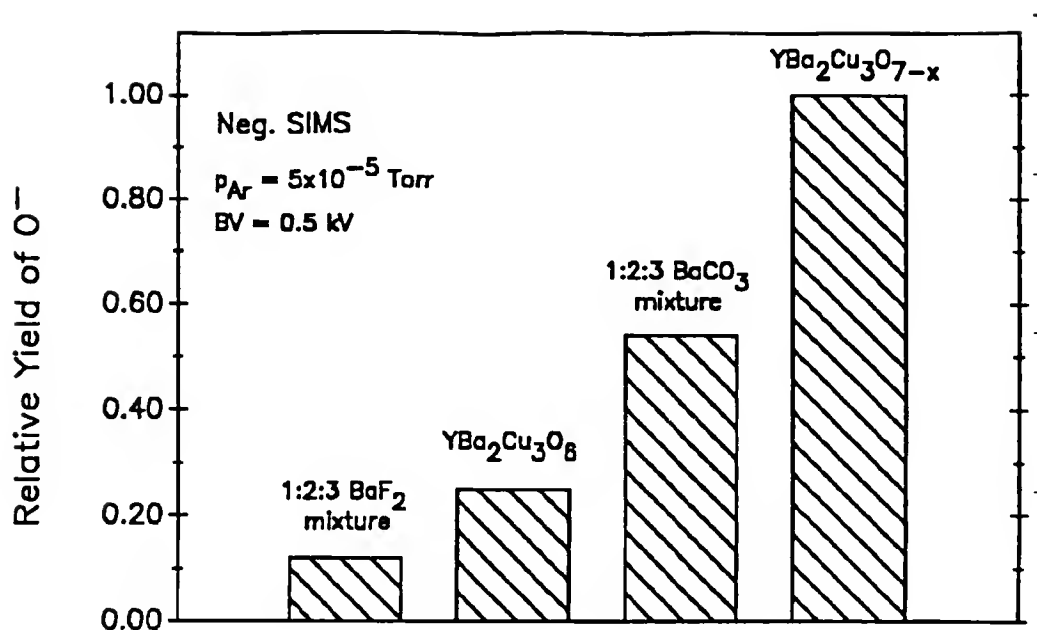


Figure 4-2. Summary of SIMS O^- yield data.

mixture is much lower than the O^- yield. The relative yield of F^- to O^- is 0.12, which is approximately an order of magnitude greater than the background value for $YBa_2Cu_3O_{7-x}$ presented in Table 4-1. The O^- from the BaF_2 -123 mixture must have come from Y_2O_3 and CuO , in both of which oxygen was bonded to an element much less electropositive than Ba. Thus the use of BaF_2 instead of $BaCO_3$ as the Ba precursor compound resulted in a substantially decreased O^- yield and a small increase in the yield of F^- . As discussed in Chapter 5, crystalline BaF_2 was observed in as-deposited Y-Ba-Cu-O films sputtered from unreacted targets using the fluoride precursor. This suggested that the BaF_2 was sputtered as a molecule, which may explain why a large

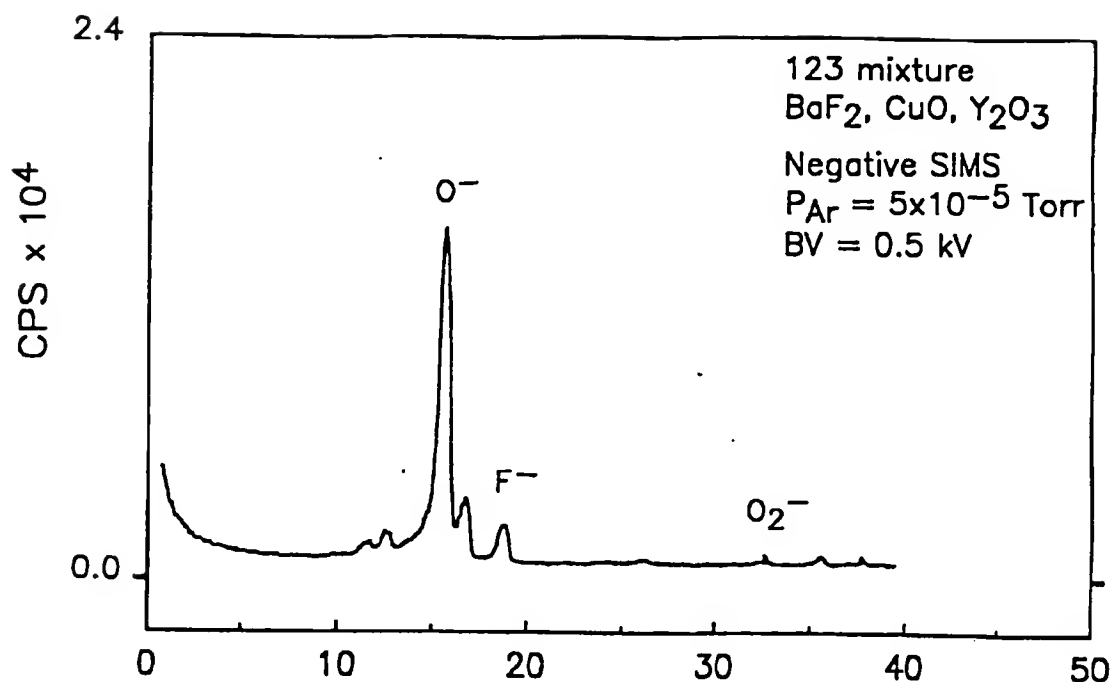


Figure 4-3. Raw SIMS data for BaF₂-123 bulk sample.

increase in the F⁻ yield was not observed. Furthermore, although F is highly electronegative, it is known to be sputtered from some sample surfaces with a high yield of positive ions [108]. This has been suggested to be due to electron rearrangement through Auger transitions. Thus it is possible that part of the F in the target was being sputtered as F⁺ ions. In sputter deposition, the F⁺ ions would be collected by the negatively biased target and would not reach the substrate.

4.1.1 Effect of Oxygen Addition

The addition of O_2 to the gas during planar magnetron sputtering of $YBa_2Cu_3O_{7-x}$ was shown to result in more dramatic negative ion effects [57], as discussed in Section 2.1.5.4. This implied that the addition of O_2 to the sputter gas resulted in an increase in the sputter yield of O^- from the $YBa_2Cu_3O_{7-x}$ target, or an increase in the number of O^- or O_2^- formed in the plasma. To test this hypothesis, 10% O_2 was added to the Ar sputter gas during negative SIMS analysis of a $YBa_2Cu_3O_{7-x}$ target. The partial pressure of Ar was 1×10^{-5} Torr, while that of oxygen was 1×10^{-6} Torr. No increase in either the O^- or O_2^- yield was observed. These results apparently contradicted the observation of Rossnagel and Cuomo [57] that increased resputtering resulted from the addition of O_2 to the sputter gas. The increased resputtering was attributed to an increased negative ion yield. However, as discussed below, this apparent discrepancy can also be explained by a difference in the sputter rate relative to the oxidation rate of the target surface.

Barium is reported to have a low work function of 2.7 eV [109]. A Ba atom on the surface of a sputter target could in principle easily pass an electron to oxygen to create O^- . The hypothesis that oxygen could become a negative ion by picking up an electron from Ba on the surface of freshly sputtered $YBa_2Cu_3O_{7-x}$ was tested. After

sputtering a $\text{YBa}_2\text{Cu}_3\text{O}_{7-x}$ target surface with 3 keV Ar, thermal O_2 at a pressure of 1×10^{-6} Torr was backfilled into the chamber while negative SIMS data were being collected. No O^- or O_2^- were detected even on a transient basis, implying that O_2 did not pick up an electron from the Ba on the surface and form a negative ion. Thus, based on these experiments, the formation of O^- was not due to gas phase oxygen acquiring an extra electron, but rather was due to the sputtering process itself.

4.1.2 Temperature Dependence of O^- Yield

During planar magnetron sputter deposition, the target is heated due to bombardment by energetic Ar^+ as discussed in Chapter 2. For target materials with poor thermal conductivity, it is not unusual for the temperature of the target surface to reach 300 °C, even if the back of the target is cooled. To replicate these actual sputter deposition conditions, the O^- yield from $\text{YBa}_2\text{Cu}_3\text{O}_{7-x}$ was measured as a function of the target temperature. Also, since a reduced $\text{YBa}_2\text{Cu}_3\text{O}_{7-x}$ target was shown to give better control of film composition [54], it was of interest to determine if a $\text{YBa}_2\text{Cu}_3\text{O}_6$ target exhibited less of a temperature dependence on O^- yield as a result of the removal of excess oxygen. The yield of O^- from negative SIMS data is presented as a function of target temperature for $\text{YBa}_2\text{Cu}_3\text{O}_{7-x}$ and $\text{YBa}_2\text{Cu}_3\text{O}_6$ in Figure 4-4. The O^- yield for $\text{YBa}_2\text{Cu}_3\text{O}_{7-x}$ was found to increase with increasing temperature,

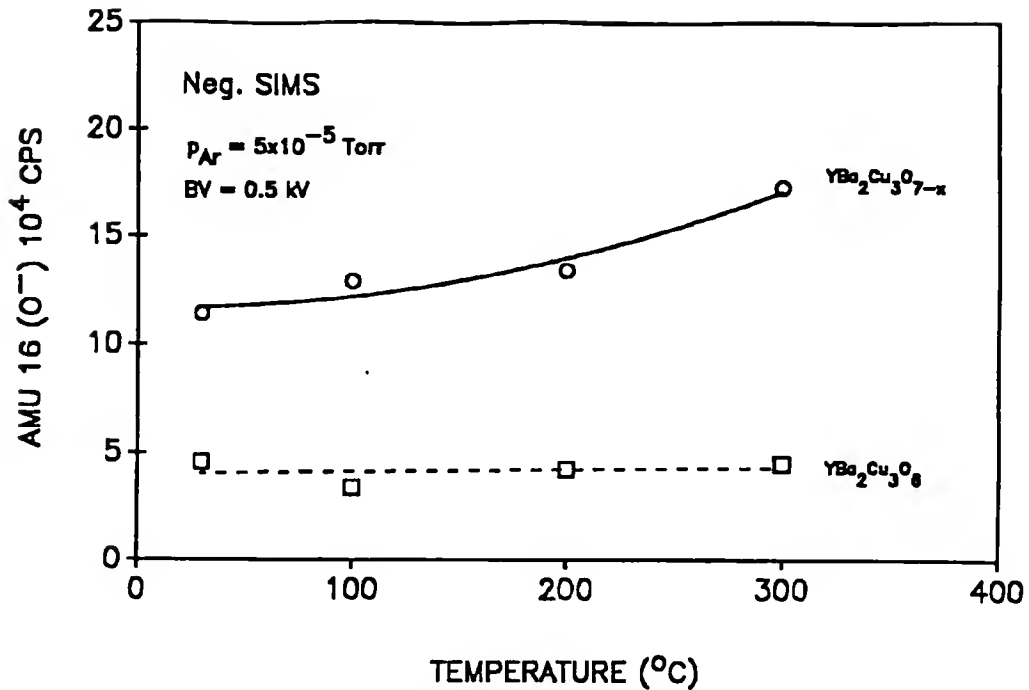


Figure 4-4. SIMS O⁻ yield for YBa₂Cu₃O_{7-x} and YBa₂Cu₃O₆ as a function of target temperature.

while the O⁻ yield for YBa₂Cu₃O₆ was essentially temperature independent. The results imply that at an elevated temperature the excess oxygen in YBa₂Cu₃O_{7-x} would eventually be depleted and a YBa₂Cu₃O₆ condition achieved. To observe this *in situ*, both YBa₂Cu₃O_{7-x} and YBa₂Cu₃O₆ samples were held at 300 °C and sputtered for extended periods of time. After 13, 35, 36, and 105 hours the O⁻ yield was measured by SIMS. The data for O⁻ yield versus sputter time are summarized in Figure 4-5. As expected, the O⁻ yield for YBa₂Cu₃O_{7-x} showed a decrease toward the value for YBa₂Cu₃O₆. Unfortunately, after 105 hours the heater filament failed before the O⁻ yield from YBa₂Cu₃O_{7-x} had completely dropped to the value of

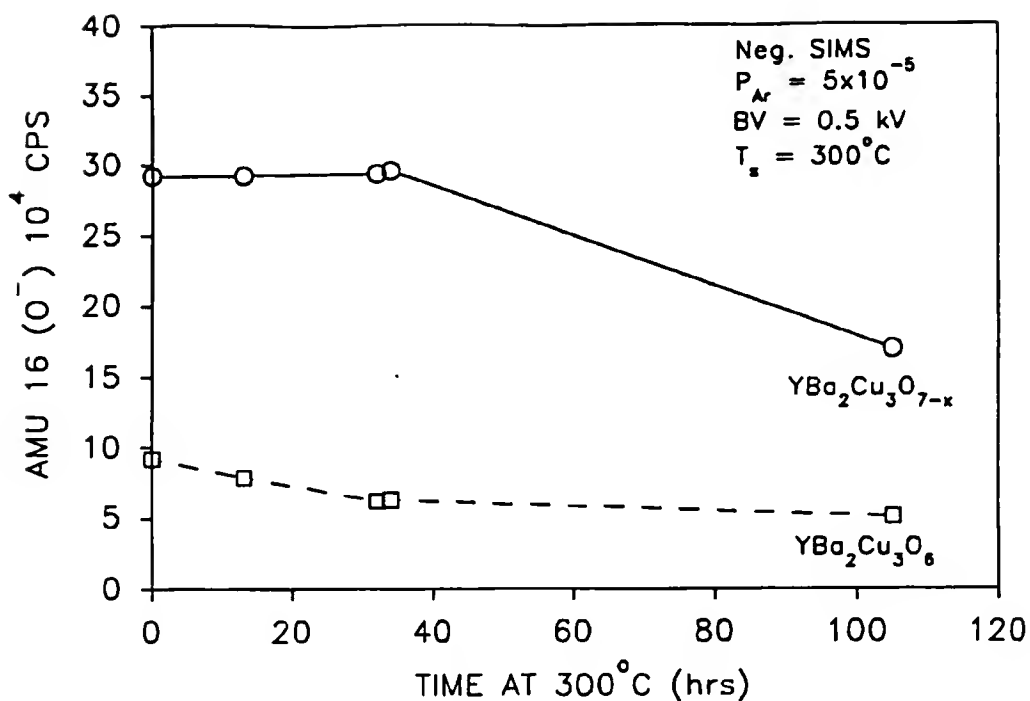


Figure 4-5. SIMS O^- yield at 300 °C for $YBa_2Cu_3O_{7-x}$ and $YBa_2Cu_3O_6$ as a function of sputter time.

$YBa_2Cu_3O_6$. The trend was clear, however, the small decrease in the O^- yield from $YBa_2Cu_3O_6$ with increasing sputter time was not expected. This suggests that excess oxygen had not been completely removed during the 600 °C heat treatment of $YBa_2Cu_3O_{7-x}$ in $N_2/10\%H_2$ to form $YBa_2Cu_3O_6$, i.e. that the sample was really $YBa_2Cu_3O_{6+y}$, where y is a small fraction.

4.1.3 Discussion of Negative Ion Data

The data presented above clearly show that O^- is the dominant negative ion sputtered from $YBa_2Cu_3O_{7-x}$ and related compounds. Therefore to control the effects of negative ion resputtering on the growth of $YBa_2Cu_3O_{7-x}$ films, the number

and energy of O^- striking the growing film must be controlled. As discussed in Chapter 2, many variations in sputter deposition processes have been made to avoid resputtering of the growing film by negative ions, which this work clearly identified for the first time to be essentially exclusively O^- . However, the data presented in this chapter illustrate that besides reducing the energy or avoiding the trajectory of O^- (which had been accomplished by sputtering at lower accelerating voltages, higher pressures, or off-axis substrate positions), the number of O^- which were generated by sputtering a Y-Ba-Cu-O target could be lowered by the choice of the target condition and material(s). The lowest O^- yield for the 1:2:3 targets was obtained for the BaF_2 -123 mixture, as illustrated in Figure 4-2. This suggested that the use of such a target would result in less resputtering of the film and give a film composition closer to that of the target. More specifically, this would give films with less Ba depletion as compared to a $YBa_2Cu_3O_{7-x}$ target or a mixed 1:2:3 target made with $BaCO_3$, since less resputtering of the growing film would occur. This hypothesis was tested and shown to be true; the results are reported in Chapter 5. Also, the lower O^- yield for the $BaCO_3$ -123 mixture compared to $YBa_2Cu_3O_{7-x}$ indicates why unreacted targets give improved film stoichiometries, as discussed in Chapter 2.

The data presented in Figure 4-2 illustrate that the O^- yield for $YBa_2Cu_3O_{7-x}$ was the greatest among the targets studied with a 1:2:3 composition. Thus to prevent a high flux of O^- from striking the substrate, the use of a $YBa_2Cu_3O_{7-x}$ sputter target should be avoided. If a $YBa_2Cu_3O_{7-x}$ target is used, it is important that the target temperature be well regulated since the O^- yield is temperature dependent, as illustrated in Figure 4-4. Otherwise, the O^- flux could vary between successive depositions, resulting in unpredictable film compositions.

The most mobile oxygen in $YBa_2Cu_3O_{7-x}$ is that for which $0 \leq x < 1$ [110]. This oxygen is reversibly incorporated into the sites along the Cu chains illustrated in Figure 1.1a [111]. The complete loss of this oxygen results in the formation of $YBa_2Cu_3O_6$, in which the oxygen atoms are bound in an immobile configuration. Even if the target temperature is kept constant, the O^- flux sputtered from $YBa_2Cu_3O_{7-x}$ will eventually decrease over the sputter lifetime of the target as the excess oxygen content is decreased until $YBa_2Cu_3O_6$ forms. Normally, during the initial stages of sputtering an altered layer would be formed, which would most likely be depleted in oxygen. This altered layer would normally be maintained in a steady-state condition if the target were kept cool. However, an elevated target temperature might allow oxygen from the target bulk to diffuse to the surface in response to the concentration gradient. Even at typical target temperatures of about 300 °C, the diffusion

coefficient for excess oxygen in $\text{YBa}_2\text{Cu}_3\text{O}_{7-x}$ has been reported to be as high as $4.9 \times 10^{-17} \text{ cm}^2/\text{s}$ [110]. Thus the diffusion of oxygen to the surface of the target during normal sputtering conditions could be expected. Once at the target surface, the excess oxygen could be removed by sputtering or volatilization. Hence a depletion of the bulk oxygen concentration in the target would be observed to be a function of time, which would in turn lead to a decrease in the flux of O^- sputtered from the $\text{YBa}_2\text{Cu}_3\text{O}_{7-x}$ target. This decrease in the O^- flux will also cause variations in the film composition between successive depositions until it stabilized when a target composition of $\text{YBa}_2\text{Cu}_3\text{O}_6$ was obtained. This observation illustrates that the run-to-run variation in film composition discussed in Section 2.1.6 can be viewed as a time-dependent manifestation of the mechanisms suggested for the deviation between the film and target compositions, which in this case was the resputtering of the film by negative ions.

As discussed in Section 2.1.3, Selinder et al. [54] and Kadin et al. [34] reported that presputtering times of up to 60 hours were needed to stabilize the film composition at a value near the target composition. Selinder et al. suggested this was due to depletion of excess oxygen from the target. Although no explicit mention of the conversion of $\text{YBa}_2\text{Cu}_3\text{O}_{7-x}$ to $\text{YBa}_2\text{Cu}_3\text{O}_6$ was given, the data in Figure 4-5 suggest this conversion was the reason for the long presputtering times needed. However, the amount of presputtering needed would be

dependent on the target temperature, since at higher temperatures the oxygen in the target would diffuse faster to the target surface and be depleted sooner. A better option to control O^- would be to reduce $YBa_2Cu_3O_{7-x}$ by heating in a reducing ambient at temperatures of 500-600 °C in order to form $YBa_2Cu_3O_6$ [112]. As illustrated in Figures 4-4 and 4-5, a $YBa_2Cu_3O_6$ target would have a lowered, consistent O^- flux, resulting in film compositions closer to that of the target and in improved temporal stability for film composition. However, as reported by Selinder et al. [54], a reduced target would react during exposure to air and must be kept in a load-locked vacuum chamber to ensure consistent film compositions.

As mentioned above, to make comparisons of O^- fluxes valid it must be assumed that the total sputtered flux from the 1:2:3 targets was equal. Prime considerations for this to be correct were that the incident Ar^+ current was held constant and the targets all contained the same ratio of Y:Ba:Cu. Measurements of the total sputter flux from the targets were not performed, but are suggested for future work. In fact, the parameter of most fundamental interest is the sputter yield. As discussed in Section 2.1.2, the total yield is the total number of particles sputtered per incident Ar^+ . Because of the direct proportionality, the sputter rate provides equivalent information to yield for a constant Ar^+ voltage and current. As long as the total sputter yields are equal, then the same rate of Y, Ba, and

Cu will leave each target and reach the substrate. This point is pertinent to interpreting negative SIMS yield data in terms of their relevance to the potential for resputtering of RF magnetron sputter deposited films by negative ions, as will be discussed below.

In order to determine how the SIMS O^- yield data relate to resputtering, the net accumulation rate of the growing Y-Ba-Cu-O film should be known, as suggested by Cuomo et al. [25]. The net accumulation rate is the difference between the deposition rate of the growing film and the resputtering rate of the film components. With significant resputtering, the net accumulation rate is actually determined when the measured film thickness is divided by the elapsed time to determine the deposition rate. The nominal deposition rate, when no resputtering occurs, is equal to the sputter rate from the target times a geometrical factor and a sticking coefficient. The sticking coefficient was defined in Section 2.1.2. The geometrical factor, K_i , represents the fraction of the sputtered flux of component i which reaches the substrate and is related to the angular distribution variation discussed in Section 2.1.2.3. The resputtering rate is the rate of removal of film components due to sputtering of the growing film by negative ions, which in this study have been shown conclusively to be predominantly O^- .

A general expression, suggested by similar work by Cuomo et al. [25], will be derived for the accumulation rate

in order to be able to identify the effect of various factors, including the O^- yield, on the accumulation rate. The net accumulation rate can be represented by

$$A = D - R \quad (4.1)$$

where A is defined as the net accumulation rate, D is defined as the nominal deposition rate of Y, Ba, Cu, and O, and R is defined as the resputter rate of Y, Ba, Cu, and O from the growing film. For film growth, a positive net accumulation rate is required. This means that the nominal deposition rate must be greater than the rate of resputtering. A zero accumulation rate means that the nominal deposition rate and resputtering rates are equal. A negative accumulation rate means that the resputtering rate is greater than the nominal deposition rate, and thus substrate etching occurs.

Expansion of each term will lead to an indication of how the sputter rates of the targets and the SIMS O^- yield data affect the net accumulation rate. It is assumed that only Ar is being used as the sputter gas. The nominal deposition rate can be represented by

$$D = \sum F_i^{Ar} K_i S_i \quad (4.2)$$

where F_i^{Ar} is the flux, in number/cm²-s, of particle i sputtered from the target by Ar^+ ions. Particle i can be Y, Cu, Ba, all possible metal-oxygen combinations MO_y , O, or O^- . The term $\sum F_i^{Ar}$ is thus the total sputtered flux from the

target. The term K_i is the geometrical factor, which may vary with specie, and S_i is the sticking coefficient particle i . It is assumed that all positively charged species which are sputtered are collected by the negatively biased target. The flux term F_i^{Ar} can be expanded as given in expression (2.2).

The specie giving rise to a sputtered component must be carefully evaluated, e.g. as in c_{O^-} , since there is probably not any oxygen truly present in the solid as O^- . In the Y-Ba-Cu-O solid target, the oxygen which is sputtered as O^- is assumed to exist in the solid as O. Thus the value for c_{O^-} can be substituted for the value of c_{O^-} .

The resputtering rate, R , represents the sputter rate of Y, Ba, Cu, and O from the growing film for incident O^- ions. Resputtering of the film by Ar^+ ions is assumed to be negligible due to bias voltages that are present. The resputtering rate can be represented as

$$R = \sum F_i^{O^-} \quad (4.3)$$

where the term $F_i^{O^-}$ is the flux of component i resputtered from the growing film by O^- . Each resputtering flux term can be expanded as

$$F_i^{O^-} = F_{O^-}^{Ar} c'_i Y_i^{O^-}, \quad (4.4)$$

where $F_{O^-}^{Ar}$ is the flux of O^- sputtered from the target by Ar^+ , c'_i is the concentration of specie i in the film which yields resputtered component i , and $Y_i^{O^-}$ is the yield of component i resputtered from the film by O^- . $F_{O^-}^{Ar}$ is defined using expression (2.2) as

$$F_{O^-}^{Ar} = F_{Ar} c_O Y_{O^-}^{Ar} \quad (4.5)$$

where these terms have been defined above.

Substituting (2.2) into (4.2), (4.5) into (4.4), (4.4) into (4.3), and (4.2) and (4.3) into (4.1) yields for the net accumulation rate,

$$A = F_{Ar} (\sum K_i S_i c_i Y_i^{Ar} - c_O Y_{O^-}^{Ar} \sum c_i' Y_i^{O^-}). \quad (4.6)$$

The deposition rate of oxygen can be neglected since the only oxygen which sticks to the substrate is that which bonds with Y, Ba, and/or Cu; i.e., the sticking coefficient of unbonded oxygen is much less than one. Further, resputtering of oxygen from the film can be neglected since it is the ratio of Y, Ba, and Cu which are critical in the as-deposited film. Additional oxygen will be added during the post-deposition heat treatment. It is thus assumed that resputtering is only important for cations in the film.

The first term in the parentheses in expression (4.6) represents the variables in the deposition rate of all components containing Y, Ba, and Cu, which can include metallic Y, Ba, and Cu and all metal-oxide compounds. For example, it was reported in the emission spectroscopy studies of Fledderman [80] and Klein and Yen [94] that the particles sputtered from a $YBa_2Cu_3O_{7-x}$ target included Y, Ba, Cu, BaO, CuO and YO. In expression (4.6), the composition in the target of the respective cation c_i is used for each MO_y compound which is sputtered from the target.

The second term in the parentheses in expression (4.6) represents the resputtering rate of Y, Ba, and Cu from the

growing film by O^- . From this term it can be seen that to decrease the rate of resputtering, either the concentration of oxygen in the target or the yield of O^- sputtered by Ar^+ needs to be decreased. Based on the results of this chapter, both would result in reduced resputtering. For example, the negative SIMS data showed that removing the excess oxygen from $YBa_2Cu_3O_{7-x}$ to form $YBa_2Cu_3O_6$ resulted in a decreased flux of O^- sputtered from the target. However, this is only true if the other terms remain constant among different target materials. If the deposition rate terms for Y, Ba, and Cu also decrease, then the decrease in the rate of resputtering could have no net effect on the accumulation rate. Similarly, if the sputter yield of O^- is measured by SIMS to have increased, the resputtering rate would increase. However, if a concomitant increase in the sputter yield of Y, Ba, and/or Cu could occur, the deposition rate would also increase. In this case an increase in the yield of O^- between different target materials, as measured by SIMS, would not guarantee a decrease in the net accumulation rate. The sputter yields of cations in the target either must be known to be the same among different samples or the differences in cationic sputter yields must be accounted for to draw very sound conclusions.

For the $YBa_2Cu_3O_{7-x}$ and $YBa_2Cu_3O_6$ targets used in this study, the assumption of equal sputter rates was good since the bonding for Y, Ba, and Cu and the crystal structure in each was essentially the same, with the only difference

being the oxygen concentration. However, for the BaCO_3 -123 and BaF_2 -123 mixtures, with the cationic ratios both being equal to 1:2:3, the Y, Ba and Cu were not bonded together in a single structure. Rather, the targets consisted of particles of Y_2O_3 , CuO , and BaCO_3 or BaF_2 , with a diameter $\leq 5 \mu\text{m}$ which were mechanically mixed. Thus it was very likely that the total yields were not equal to that of $\text{YBa}_2\text{Cu}_3\text{O}_{7-x}$. Sputter rate measurements have not been performed and data are not available in the literature. However, the film composition results presented in Chapter 5 for mixed targets using BaF_2 show that the film composition was closer to that of the target than for a $\text{YBa}_2\text{Cu}_3\text{O}_{7-x}$ target, as expected since the negative SIMS O^- yield data show the O^- flux was reduced. Thus the sputter rate for the 1:2:3 mixtures and the rate of Y, Ba, and Cu reaching the substrate must be reasonably close to that of the $\text{YBa}_2\text{Cu}_3\text{O}_{7-x}$ target. Accordingly, the SIMS O^- yields for the 1:2:3 targets can be interpreted as reflecting the ratio of O^- to all particles reaching the substrate. In this study, the lowest O^- yield apparently does indicate the least potential amount of resputtering.

In terms of the effect of resputtering by O^- on the composition of Y-Ba-Cu-O films, the key term in expression (4.6) is $Y_1^{\text{O}^-}$. If the yields for the sputtering of Y, Ba, or Cu in the film by O^- are not equal, preferential resputtering of one or more of the components will occur and the remaining Y:Ba:Cu in the film will not equal that which

was deposited. This is the most likely reason why Ba is deficient in Y-Ba-Cu-O films relative to the target. The reason why Ba is preferentially sputtered by O^- is not understood and is suggested in Chapter 7 as a subject for future study. Regardless, this suggests that in addition to decreasing the flux of O^- , another way to decrease the effect of resputtering on the deposition rate and the film composition is to decrease $Y_1^{O^-}$ to the same value for all components. This can be accomplished by decreasing the energy of the incident O^- (or neutralized O) particles, which can be done by increasing the sputter gas pressure or decreasing the accelerating voltage on the sputter target. These would decrease the mean free path for O^- , thereby causing more energy-reducing collisions prior to reaching the substrate. A completely thermalized O^- would not have enough incident energy to cause resputtering of the film. However, as discussed in Chapter 2, the deposition rate would be greatly decreased.

For unheated substrates, the sticking coefficient S_i can be assumed to be equal to one for Y, Ba, Cu, and MO_y molecules. For oxygen, S_i is probably less than one, but this is not critical since additional oxygen is added to the film during post-deposition heat treatment. At elevated substrate temperatures, it is possible that S_i is less than one for Y, Ba, and/or Cu, as discussed in Chapter 2. This

may cause further deviations between the film and target compositions which would have to be compensated accordingly.

The above discussion illustrates the important point that any model which predicts the yield of negative ions formed by sputtering but does not account for deposition parameters such as sputter gas pressure, target accelerating voltage, system geometry and substrate temperature will not be able to predict the degree of resputtering which occurs. This was seen in Section 2.1.2.4 to be the case for the model of Cuomo et al. [25], where the degree of resputtering based on values of $I_A - EA_B$ was also found to depend strongly on the target accelerating voltage.

As discussed in Section 2.1.2.4, the model of Cuomo et al. for the formation of negative ions suggested how a negative ion may be formed during sputtering. In the above discussion, the negative ion yield, i.e. the O^- yield, would essentially be what should be predicted using the model of Cuomo et al. However, this model was only used to empirically predict the net accumulation rate for a series of Au-RE compounds, since it was found that for a value of $I_A - EA_B$ less than 3.4 eV substrate etching occurred. In other words, the net accumulation rate was less than zero. Since the model did not account for the deposition rate of the neutral species nor the resputtering rate from the film, it appears almost circumstantial that the model predicted the net accumulation rate. However, among a series of isostructural Au-RE compounds, it is possible that the sputter rates may

be similar enough that the dominant variable is the negative ion yield. In this case, direct comparisons of the negative ion yields, such as the negative SIMS data presented above, could be used to predict the net accumulation rate. Cuomo et al. did not acknowledge this issue.

As discussed in Section 2.1.2.4, in SIMS analysis it is observed that the more ionic the character of the bonds in a compound, the more likely the sputtered species are to retain their charge from the lattice [22]. The more electronegative a specie is in the compound, the greater the probability that it will retain the negative charge in the lattice and be sputtered as a negative ion. It is suggested that a model for the yield of negative ions be developed which explicitly takes into account the ionic character of the bonds, i.e., Pauling's percent ionicity [113]. The percent ionicity, Π , for a binary compound AB is calculated as

$$\Pi = 1 - e^{-0.25(\chi_A - \chi_B)^2}, \quad (4.7)$$

where χ_A and χ_B are the electronegativity of components A and B, respectively. The values for the electronegativity difference ($\Delta\chi$), percent ionicity, and SIMS O^- yield for the binary oxides BaO, CuO, and Y_2O_3 are presented in Table 4-2. The O^- yield data for BaO and CuO were reported by Benninghoven and Weidmann [87]; data were not available for Y_2O_3 . The relationship between percent ionicity and negative ion yield is clear in Table 4-2. The large electronegativity

Table 4.2 Electronegativity difference, percent ionicity, and negative ion yield for BaO, Y₂O₃ and CuO. Negative ion yield data are from reference [87].

| Compound | $\Delta\chi$ | Percent Ionicity | SIMS Negative Ion Yield |
|-------------------------------|--------------|------------------|-------------------------|
| BaO | 2.55 | 97 | 0.94 |
| Y ₂ O ₃ | 2.22 | 71 | - |
| CuO | 1.54 | 45 | 0.04 |

difference between Ba and O correlates well with the high O⁻ yield due to breaking bonds between Ba and O, as discussed above. The O⁻ yield for Y₂O₃ would be expected to be between those of BaO and CuO, based on the value of Π . A model based on the percent ionicity of the bonds in ionic compounds would present a more realistic picture of the material being sputtered than the model of Cuomo et al., in which the compounds were assumed to be completely ionic. Also, a model incorporating the percent ionicity would explicitly account for the electronegativity difference of the components in ionic compounds, as larger value for which has been correlated with an increased negative ion yield, as discussed above.

Cuomo et al. [25] suggested that their parameter $I_A - EA_B$ was related to the electronegativity difference between A and B, based on the definition of electronegativity according to the Mulliken scale [114], which is

$$\chi_M = \frac{(I + EA)}{2}. \quad (4.8)$$

The electronegativity difference for compound AB would then be

$$\Delta\chi_M = \frac{(I_B + EA_B)}{2} - \frac{(I_A + EA_A)}{2} \quad (4.9)$$

which can be rewritten as

$$\Delta\chi_M = \frac{[(I_B - EA_A) - (I_A - EA_B)]}{2} \quad (4.10)$$

where the appearance of the parameter $I_A - EA_B$ of Cuomo et al. suggests the relationship. The Mulliken scale is based on the ionization and electron affinity energies of free electrons, in contrast to the more commonly used Pauling scale, which is based on the heats of formation of ionic compounds and describes the power of atoms to attract electrons in the bonded condition. The electronegativity values from the Mulliken and Pauling scales follow similar trends except for the transition metals, where the Mulliken scale has been reported to be more appropriate [114]. Although not discussed by the Cuomo et al., it can be found by substituting values for I and EA for various elements, such as Y, Ba, Cu and O, that as $I_A - EA_B$ decreases, the electronegativity difference increases. Thus the model of Cuomo et al., which suggests the ease of electron transfer, would be complementary to a model based on electronegativity differences in understanding the sputtering of negative ions.

As discussed above, the large electronegativity difference between Ba and O is the main reason for the high sputter yield of O^- from Y-Ba-Cu-O. However, as also

discussed above, the greater O^- yield of $YBa_2Cu_3O_{7-x}$ versus that of $YBa_2Cu_3O_6$ is thought to be due to the presence of excess oxygen when $0 \leq x < 1$. What is of particular interest is the location of the excess oxygen atoms, which is illustrated in Figure 1-1a. The excess oxygen atoms are positioned between the Cu atoms along the b axis, resulting in the formation of CuO chains. In other words, the additional oxygen atoms, which are the cause of the enhanced resputtering effect observed for $YBa_2Cu_3O_{7-x}$ targets, are weakly bonded only to Cu. However, the data in Table 4-2 showed that the yield of O^- from a CuO target is only 0.04. Further, as discussed in Section 2.1.5.4, Shah and Garcia [85] reported that resputtering occurred above BaO and Y_2O_3 targets but not above a CuO target. This would imply that the yield of O^- from the additional oxygen atoms could not be high enough to cause the resputtering observed. However, even though the additional oxygen are bonded to Cu in the equilibrium structure, during sputtering of the $YBa_2Cu_3O_{7-x}$ surface the situation is probably different. Dangling Ba and Y bonds would probably be available on the surface of the sputtered target. Further, the surface of a $YBa_2Cu_3O_{7-x}$ target sputtered by Ar^+ has been reported to be depleted in Cu after the formation of the steady state altered layer [78]. The resulting enrichment of Ba and Y on the target surface could result in some of the additional oxygen atoms which had been bound to Cu becoming bonded to Ba and/or Y. Thus the large degree of resputtering observed above the

$\text{YBa}_2\text{Cu}_3\text{O}_{7-x}$ target would be consistent with the expectations discussed above.

The final issue to be addressed in this discussion is the apparent discrepancy between the effects of adding oxygen to the sputter gas during RF planar magnetron sputtering of $\text{YBa}_2\text{Cu}_3\text{O}_{7-x}$ reported by Rossnagel and Cuomo [57] and the lack of an increase in the SIMS O^- yield when 10% oxygen is mixed in with Ar as discussed in Section 4.1.1. As discussed in Chapter 2, Rossnagel and Cuomo reported that increasing the amount of oxygen in the sputter gas results in a decreasing sputter rate and eventual etching of the substrate. As is known from reactive sputtering studies [26], increasing the amount of oxygen in the gas replenishes the oxygen depleted from the surface of the target during sputtering. In other words, the target surface is continually reoxidized, whereas without oxygen in the gas a steady state condition is reached in which an altered layer on the target surface is formed which is deficient in easily-sputtered oxygen. For a $\text{YBa}_2\text{Cu}_3\text{O}_{7-x}$ target, the reoxidation of the target surface would result in an increase in the O^- yield. Accordingly, one would expect to see an increase in the SIMS O^- yield when 10% oxygen was added to the Ar sputter gas, but this increase was not observed. This apparent discrepancy can be explained by the difference between the RF planar magnetron deposition and the SIMS experiment in the rate of reoxidation versus the sputter rate of the target surface. For the same proportion

of oxygen in the sputter gas, the rate of reoxidation of the target surface would be far greater for the RF planar magnetron deposition for two reasons. First, the plasma in the planar magnetron or the electrons in the ion source of the SIMS dissociate O_2 into atomic O, which is far more reactive than O_2 . The O formed in the ion gun are not accelerated toward the target because they are neutral rather than O^+ and are mostly confined in the ion source. The unconstrained plasma in the planar magnetron allows a larger fraction of the O to strike the target surface. Secondly, the oxygen partial pressure in the planar magnetron is on the order of 1 mTorr, whereas that for the SIMS is only 10^{-4} mTorr, so the rate of impingement of oxygen for the planar magnetron would be a factor of 10^3 greater. Also, the higher pressure for the planar magnetron system results in a shorter mean free path for dissociating collisions for O_2 , producing a larger fraction of atomic O. Hence, relative to the sputter rate, the reoxidation of the target surface for the SIMS must have been far slower than that for the planar magnetron. In fact, the lack of any increase in the SIMS O^- yield indicates that 0.5 keV Ar^+ sputtered away surface material at a greater rate than reoxidation was occurring.

4.1.4 Summary of SIMS Negative Ion Study

In this chapter the results of a negative SIMS study to identify the negative ions sputtered from $YBa_2Cu_3O_{7-x}$ and

related compounds were presented. The primary negative ion sputtered from $\text{YBa}_2\text{Cu}_3\text{O}_{7-x}$ was found to be O^- . The yield of O^- was found to be dependent on the compounds present in targets with a Y to Ba to Cu ratio of 1:2:3. For $\text{YBa}_2\text{Cu}_3\text{O}_{7-x}$ targets, the target temperature and heat treatment of the target in a reducing ambient were shown to influence the O^- yield. These dependencies were the result of the excess oxygen in $\text{YBa}_2\text{Cu}_3\text{O}_{7-x}$. The use of a mixed 1:2:3 target using BaF_2 as the source of Ba was found to greatly lower the O^- yield compared to $\text{YBa}_2\text{Cu}_3\text{O}_{7-x}$. These data suggested that targets containing BaF_2 would give improved film stoichiometries; experimental confirmation of this is presented in the next chapter.

Proper interpretation of SIMS O^- yield data in terms of its relevance to predicting the degree of resputtering from a target material was discussed. It was pointed out that sputter yield of negative ions was not the only issue of importance in determining the degree of resputtering; the sputter rate of metal-containing particles as well as the deposition parameters such as the pressure and accelerating voltage were also suggested to be controlling factors. The model of Cuomo et al. [25] for the formation of and resputtering by negative ions was addressed and used in the understanding of the SIMS data.

4.2 AES Depth Profiling Study for Ba Migration

As discussed above, the observation of a temperature and time dependent O^- yield supported the suggestions of Selinder [57] and Kadin [34] presented in Section 2.1.6 that loss of excess oxygen could cause the Ba deficiency and run-to-run variations in the composition of films sputter deposited from a $YBa_2Cu_3O_{7-x}$ target. A second explanation for the Ba deficiency and the run-to-run irreproducibility in sputtered Y-Ba-Cu-O film compositions was offered by Liou et al. [77], who suggested that these could be caused by the migration of Ba to the target surface during sputtering, as discussed in Section 2.1.5.1 and 2.1.6.

As discussed, if Ba was migrating to the target surface during sputtering, a depletion in Ba from the bulk of the target would eventually develop. Since a Ba deficiency was observed in sputter-deposited Y-Ba-Cu-O films and the length of the first sputter deposition was typically three to six hours [35], then if the Ba deficiency was due to depletion of Ba from the target, a decrease in the Ba concentration in the target should be found after three to six hours of sputtering. This would depend on the temperature of the target, which affects the mobility of Ba, and the current density of the incident Ar^+ ions, which affects the sputter rate. But with these two parameters controlled, the Ba depletion should be seen.

To test for a decrease in the Ba concentration in the target after extended periods of sputtering, a 0.25 inch thick by 0.25 inch diameter cylindrical $\text{YBa}_2\text{Cu}_3\text{O}_{7-x}$ target was heated to 300 °C to approximate target temperatures reached during magnetron sputtering. Auger depth profiling was performed for times up to 7 hours with Ar^+ ions at an accelerating voltage of 3 keV and a current density on the order of 10^2 A/cm^2 , which was approximately an order of magnitude greater than that for actual magnetron sputter deposition. The greater current density resulted in a greater sputter rate from the target and would have accelerated the depletion of Ba from the target compared to magnetron sputter deposition, since the Ba would have been more quickly removed from the target surface. The area sputtered was approximately 1 mm^2 versus an average powder particle size of about $50 \text{ }\mu\text{m}$ in the target, so the area sputtered and analyzed contained a large number of particles and particle boundaries, as in actual magnetron sputtering. The peak-to-peak heights of the Ba and Cu Auger signals were monitored as a function of sputter time. The Y signal was too low to accurately measure changes. The data are summarized in Figure 4-6. The data are presented as a ratio to normalize changes in the data for changing sample topography of the sintered target and variations in the electron beam current over time.

It can be seen that no systematic decrease in the Ba concentration in the target occurred for sputter times up to

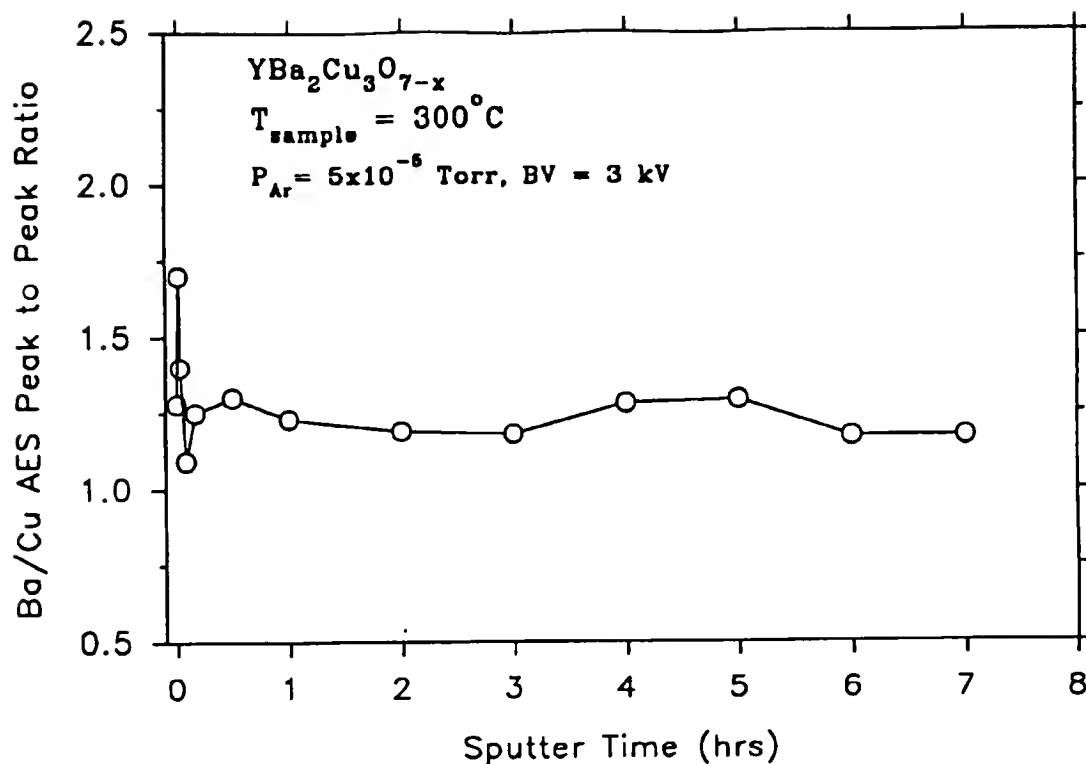


Figure 4-6. Ratio of Ba/Cu AES peak to peak data as function of sputter time for YBa₂Cu₃O_{7-x} heated to 300 °C.

7 hours. The changes in the initial surface composition during the first three minutes of sputtering were due to the removal of carbon-containing surface contaminants, as is typically seen in AES data. The value for Ba/Cu after seven hours of sputtering is about the same value as after the carbon-containing surface contaminants were removed.

Thus these data strongly suggest that migration of Ba to the target surface during sputter deposition does not occur, as had been suggested by Liou et al. [77]. Accordingly, depletion of Ba from a YBa₂Cu₃O_{7-x} target does not result after extended periods of sputtering and the Ba

deficiency observed in sputtered Y-Ba-Cu-O films is not due to the migration of Ba to the target surface. Similarly, the run-to-run irreproducibility of sputter deposited Y-Ba-Cu-O film compositions is not due to the migration of Ba, since a time-dependent Ba depletion in a $\text{YBa}_2\text{Cu}_3\text{O}_{7-x}$ target is not observed.

CHAPTER 5

Y-Ba-Cu-O THIN FILM PROCESSING

Presented in this chapter are efforts to fabricate thin films of superconducting $\text{YBa}_2\text{Cu}_3\text{O}_{7-x}$ by RF planar magnetron sputter deposition from a single multicomponent target. As discussed above, sputter deposition of Y-Ba-Cu-O films with a specific composition is difficult due to preferential resputtering of Ba, and to a lesser extent Cu, from the growing films by O^- ions accelerated away from the Y-Ba-Cu-O sputter target. Thus, the major emphasis of the work presented in this chapter was controllably depositing Y-Ba-Cu-O thin films with a composition close to 1:2:3. In addition, also presented is the development of the post-deposition heat treatments which were required to form superconducting $\text{YBa}_2\text{Cu}_3\text{O}_{7-x}$ from the insulating as-deposited Y-Ba-Cu-O films. Characterizations of the properties of the superconducting $\text{YBa}_2\text{Cu}_3\text{O}_{7-x}$ films are then presented, and the data presented includes room temperature resistivity, T_c , morphology and crystal structure.

As discussed in Chapter 4, a goal of the thin film deposition efforts presented in this chapter was to determine if the results of the negative SIMS study could be used to explain the data for the effects of target parameters on deposited film compositions. Specifically, it

will be shown if the use of BaF_2 as the source of Ba in sputter targets, rather than the commonly used BaCO_3 or BaO_2 , resulted in an improvement in the Ba deficiency, presumably due to less negative ion resputtering. In order to directly gauge the improvements gained by the use of BaF_2 versus BaCO_3 and BaO_2 , thin films were sputter deposited from targets utilizing each of the Ba precursor compounds. During the course of these studies, variations in the fabrication of the sputter targets and in the sputter deposition parameters were also explored. Electron microprobe analysis showed that films from BaO_2 and BaCO_3 precursors were Ba deficient, whereas with a BaF_2 precursor films were slightly Y deficient. Target compositions were compensated to bring the film composition towards 1:2:3 for BaF_2 , but this was more difficult for BaCO_3 and BaO_2 . The use of BaF_2 was found to improve the correlation between film and target composition, compositional reproducibility and uniformity.

5.1 Towards a 1:2:3 Film Composition by RF Sputter Deposition from a Single Y-Ba-Cu-O Target

5.1.1 Experimental

The development of a process to sputter deposit Y-Ba-Cu-O thin films with a 1:2:3 composition from a single target followed the sequence shown in Figure 5-1. As discussed in Chapter 2, almost every imaginable deposition

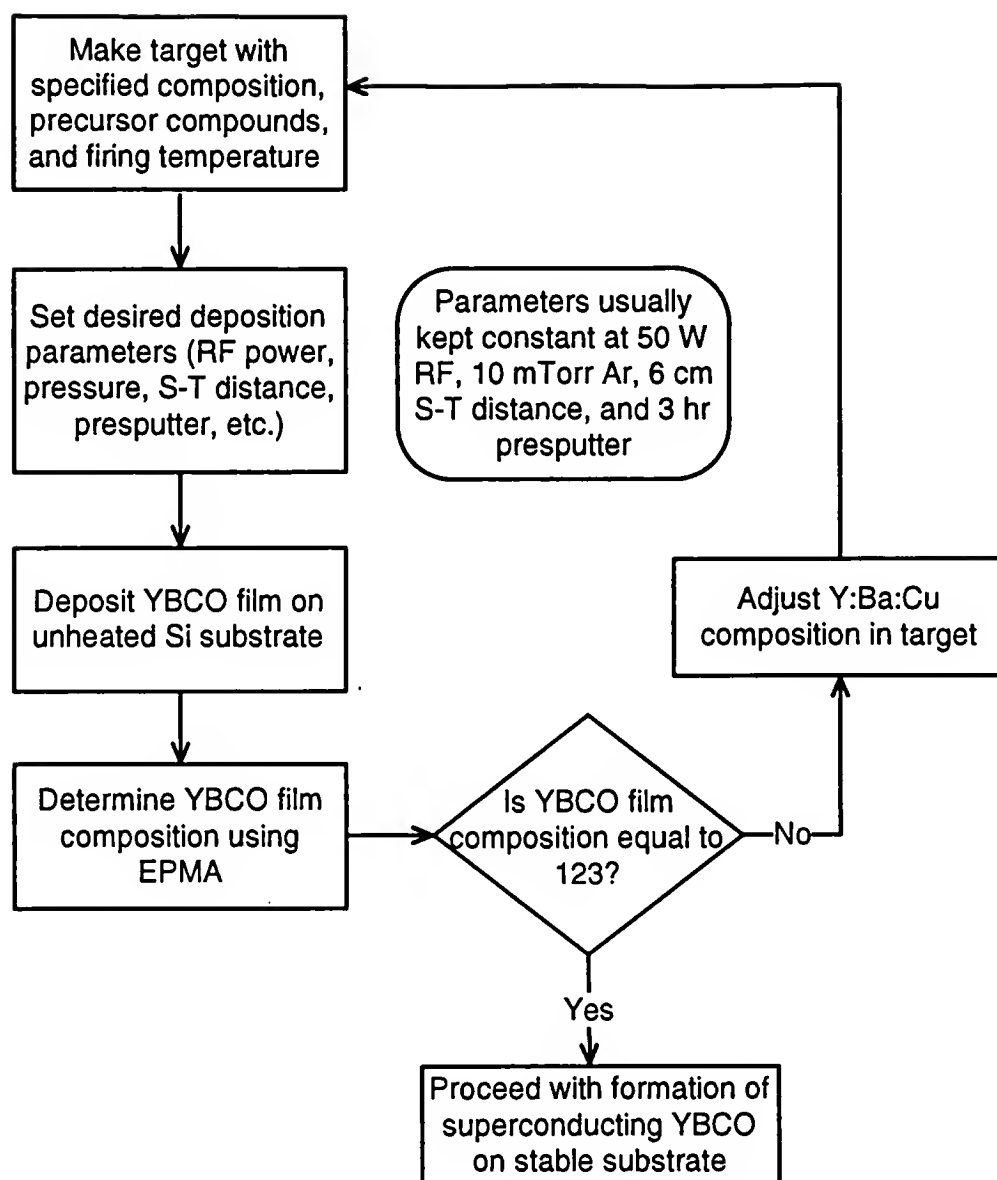


Figure 5-1. Process flow used in this study for iteratively reaching a Y-Ba-Cu-O film composition of 1:2:3 by sputter deposition of Y-Ba-Cu-O from a single target.

parameter has been reported to have been varied by different authors in an attempt to controllably obtain a 1:2:3 film composition. These parameters include sputter gas pressure and stoichiometry, power to the target, substrate

temperature, substrate-target distance, and position of the substrate relative to the target. A number of these variations were also explored in the early stages of this study. However, it was desired to determine primarily the effect of the target preparation variables of composition, Ba precursor, and target firing temperature on film composition, with all other controllable sputter deposition parameters kept constant. The Ba precursors were varied among BaCO_3 , BaO_2 , and BaF_2 . The target composition was iteratively varied to bring the film composition closer to 1:2:3. Also, the target firing temperatures were varied to avoid full reaction to superconducting $\text{YBa}_2\text{Cu}_3\text{O}_{7-x}$ and to determine if decreasing the oxygen content of the target and/or altering the phases present would allow better film composition control. Furthermore, to better understand the chemical and microstructural variations in targets with different Ba precursors, the sequence of phases formed in air as a function of temperature was studied using X-ray diffraction.

Circular sputter targets two inches in diameter and 0.125 inch thick were fabricated using Y_2O_3 , CuO , and BaCO_3 , BaO_2 , or BaF_2 precursor powders as discussed in Chapter 3. Barium carbonate was chosen since it was the commonly used Ba precursor. Barium peroxide was chosen since in hot stage XRD studies it was found to react to form $\text{YBa}_2\text{Cu}_3\text{O}_{7-x}$ at lower temperatures than BaCO_3 [88]. Further, it was thought that the lower melting temperature of BaO_2 , 450 °C, versus that

of BaCO_3 , 1740 °C, [109] might result in denser targets. Barium flouride was initially chosen because of its low reactivity with air. Target stoichiometries which were eventually utilized included (Y:Ba:Cu) 1:2:3, 1:4:4, 1:4:3, and 1:1.6:2.2. These stoichiometries were chosen iteratively to approach a 1:2:3 film composition, since the initial films from a superconducting $\text{YBa}_2\text{Cu}_3\text{O}_{7-x}$ target were always strongly Ba deficient. The targets were fired for 12 hours or longer in air at temperatures of 500, 800, or 950 °C and cooled. The firing temperatures were chosen as follows. A temperature of 800 °C was found in previous hot-stage XRD studies of powders to be the temperature where BaCO_3 reacts with Y_2O_3 and CuO [88], whereas 950 °C was the commonly reported heat treatment temperature for the formation of $\text{YBa}_2\text{Cu}_3\text{O}_{7-x}$. A firing temperature of 500 °C was chosen for two reasons: first, to verify that the results of the negative SIMS study in Chapter 4 could be applied to actual sputter deposition and second, to test the suggestions of Liou et al. [77] and Bruyere et al. [89] discussed Section 2.1.6 that targets fired at temperatures in which reaction of the starting compounds was avoided might provide improved control of the film stoichiometry. Finally, a two inch diameter $\text{YBa}_2\text{Cu}_3\text{O}_6$ sputter target was not available for this study.

The Y-Ba-Cu-O films compositions were determined by EPMA as described in Chapter 3. The Y-Ba-Cu-O thin films were grown on (100) Si substrates by RF planar magnetron

sputter deposition, also as described above in Chapter 3. The two inch diameter Si substrates were either cleaved into 0.5 inch square pieces or used whole, and centered above the sputter target. Two inch diameter substrates were used in order to determine the composition as a function of position over substrates of the size which would be necessary to scale up Y-Ba-Cu-O film growth for practical applications.

As discussed in Chapter 3, the standard sputtering parameters were 50 W RF power, 10 mTorr Ar, 6 cm substrate-target distance, and the substrate electrically floating and nominally unheated. New targets were presputtered at least 3 hours before depositing, and before every subsequent deposition the target was given at least a one hour presputter. Since two depositions were performed for every pumpdown, the second deposition received the extra presputtering of the first deposition. Deposition rates were typically 40 - 50 Å/min and film thicknesses were 0.5 - 1.0 µm.

5.1.2 Sputter Target Preparation and Condition

Immediately after cold pressing, unfired targets did not exhibit cracks or warping and had the desired dimensions. Targets fired to 500°C, even though not reacted, were strong enough to be handled without breaking. However, targets with BaO₂ and BaCO₃ precursors would warp and crack while just sitting for extended periods in the laboratory. Targets containing BaO₂ and BaCO₃ and fired at 800 or 950 °C

occasionally had problems with warping or cracking during heating, possibly due to binder distribution, temperature nonuniformities, or reactions along the pore surfaces. With a BaF_2 precursor, targets exhibited no warping or cracking during firing and were very stable in air, presumably due to the comparative stability of BaF_2 to air and water versus BaCO_3 and BaO_2 , as discussed in Section 2.1.6. After firing, the densities achieved for the targets ranged from 55% of theoretical density for targets fired at 500 °C to 80% for firing at 950 °C.

Results of XRD characterization of sputter targets of varying composition prepared with BaO_2 , BaCO_3 , or BaF_2 precursors and fired in air are presented in Table 5-1. After firing at 500 °C, the original starting compounds were detected and no new phases were identified in any of the targets, except for the conversion of BaO_2 to BaCO_3 . The conversion of BaO_2 was probably due to reaction with CO_2 in the ambient.

Firing at 800 °C, performed only for targets using BaO_2 and BaCO_3 , resulted in a mixture of original compounds and Y-Ba-O, Ba-Cu-O, and Y-Cu-O ternary phases, but no $\text{YBa}_2\text{Cu}_3\text{O}_{7-x}$ was formed. This was in agreement with the hot-stage XRD study of powders by Leskela et al. [88].

After extended firing at 950 °C, a target with a 1:2:3 composition and a BaO_2 precursor yielded single phase, $\text{YBa}_2\text{Cu}_3\text{O}_{7-x}$, whereas with a BaCO_3 precursor small amounts of BaCO_3 and $\text{Y}_2\text{Cu}_2\text{O}_5$ were still present along with the $\text{YBa}_2\text{Cu}_3\text{O}_{7-x}$

Table 5-1. XRD data indicating phases in sputter target after firing 12 hours in air (except where noted) versus Ba precursor, target composition and firing temperature.

| Ba Precursor | Target Composition (Y:Ba:Cu) | Firing Temperature (°C) | Phases Identified |
|-------------------|------------------------------|-------------------------|---|
| BaCO ₃ | 1:2:3 | 500 | BaCO ₃ , CuO, Y ₂ O ₃ |
| | 1:2:3 | 950 (90 h) | YBa ₂ Cu ₃ O _{7-x} , BaCO ₃ , Y ₂ Cu ₂ O ₅ |
| | 1:4:3 | 800 | BaCO ₃ , Y ₂ O ₃ , CuO, BaCuO ₂ , Ba ₂ Y ₂ O ₅ |
| BaO ₂ | 1:2:3 | 500 | BaCO ₃ , CuO, Y ₂ O ₃ |
| | 1:2:3 | 950 (90 h) | YBa ₂ Cu ₃ O _{7-x} |
| | 1:4:4 | 800 | BaCO ₃ , CuO, Y ₂ O ₃ , Y ₂ Cu ₂ O ₅ , Ba ₂ Y ₂ O ₅ , BaCuO ₂ |
| | 1:4:3 | 800 | BaCuO ₂ , Y ₂ O ₃ , Y ₃ Ba ₈ Cu ₅ O ₁₈ |
| BaF ₂ | 1:2:3 | 500 | BaF ₂ , Y ₂ O ₃ , CuO |
| | 1:2:3 | 950 (120 h) | BaF ₂ , Y ₂ O ₃ , Y ₂ Cu ₂ O ₅ , YBa ₄ Cu ₃ O ₉ |
| | 1:4:4 | 500 | BaF ₂ , Y ₂ O ₃ , CuO |
| | 1:1.6:2.2 | 500 | BaF ₂ , Y ₂ O ₃ , CuO |

phase. This suggests that during the ramping of the furnace from room temperature to 950 °C, the BaO₂ precursor did not completely convert to BaCO₃, as it had during the 12 hour firing at 500 °C. If this had occurred, then the same phases would be expected after firing at 950 °C.

Two targets, a 1:4:3 composition target starting with a BaO₂ precursor (BaO₂-143) and a 1:2:3 target with a BaF₂

precursor (BaF_2 -123), which were fired at 800 and 950 °C, respectively, contained quaternary phases other than $\text{YBa}_2\text{Cu}_3\text{O}_{7-x}$, as predicted by the ternary CuO - Y_2O_3 - BaO_2 phase diagram reported by De Leeuw et al. [115]. Even after firing at 950 °C for 120 hours in air, the BaF_2 precursor in the BaF_2 -123 target had not been fully reduced. The BaF_2 which had reacted with the Y and Cu oxides formed the quaternary $\text{YBa}_4\text{Cu}_3\text{O}_9$ phase rather than $\text{YBa}_2\text{Cu}_3\text{O}_{7-x}$. As discussed in Section 2.1.4, the reduction of BaF_2 to form $\text{YBa}_2\text{Cu}_3\text{O}_{7-x}$ required a substantial partial pressure of water along with oxygen in the heat treatment ambient [75]. The partial pressure of water in the air in the laboratory, which during these experiments had a relative humidity of about 75% at room temperature, was apparently not high enough to reduce the BaF_2 .

5.1.3 Composition of Y-Ba-Cu-O Films

Composition data for a majority of the sputter deposited Y-Ba-Cu-O films are presented in Figures 5-2, 5-3, and 5-4 for targets listed in Table 5-1 with BaCO_3 , BaO_2 , or BaF_2 precursors, respectively. Unless otherwise specified, the films were deposited with the standard parameters reported in Chapter 3. Figures 5-2, 5-3, and 5-4 provide a simple visual indication of the statistical spread in the film composition from a given target. In each figure are shown the target composition, using solid symbols, and the composition data for films deposited from each target, using

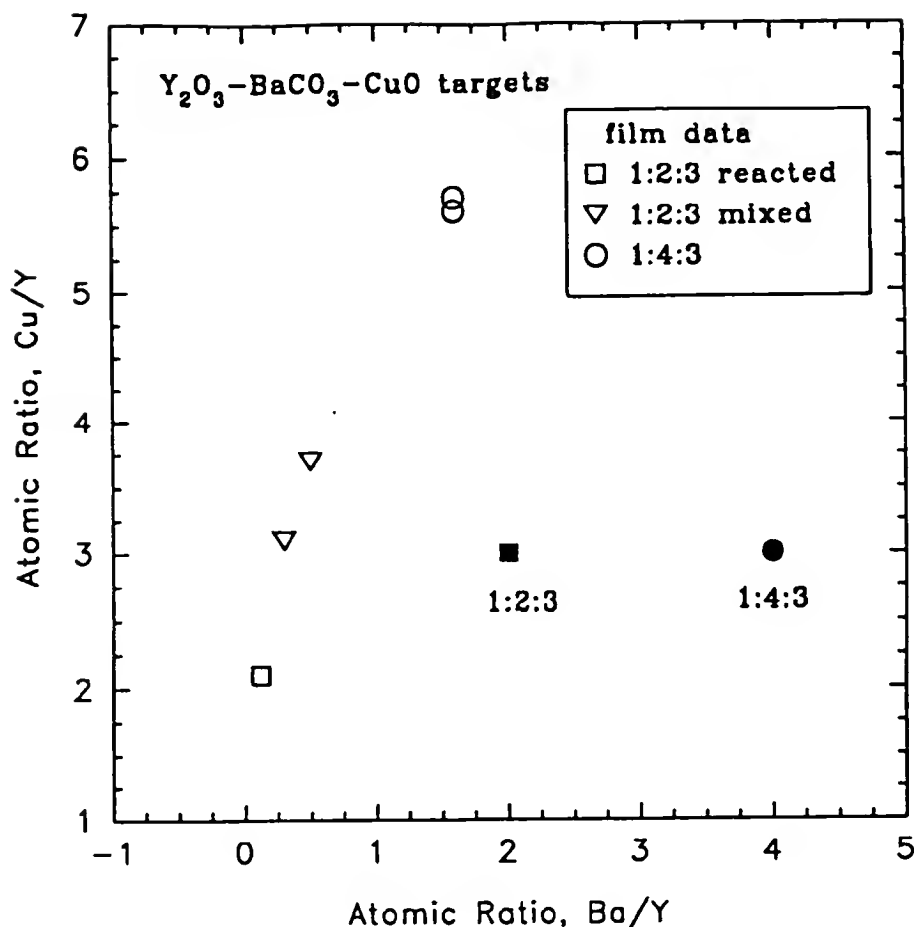


Figure 5-2. Relationship of film composition to target composition and variation among film compositions for targets using BaCO₃. Solid symbols represent target compositions.

hollow symbols. Each film composition data point represents the average of five EPMA measurements along a 0.5 inch trace centered directly above the center of the target.

In Figure 5-2, the composition data are presented for films deposited from three different targets using BaCO₃, including two targets with a 1:2:3 composition but subjected to different thermal processing, as given in Table 5-1. The composition data for films deposited from four different

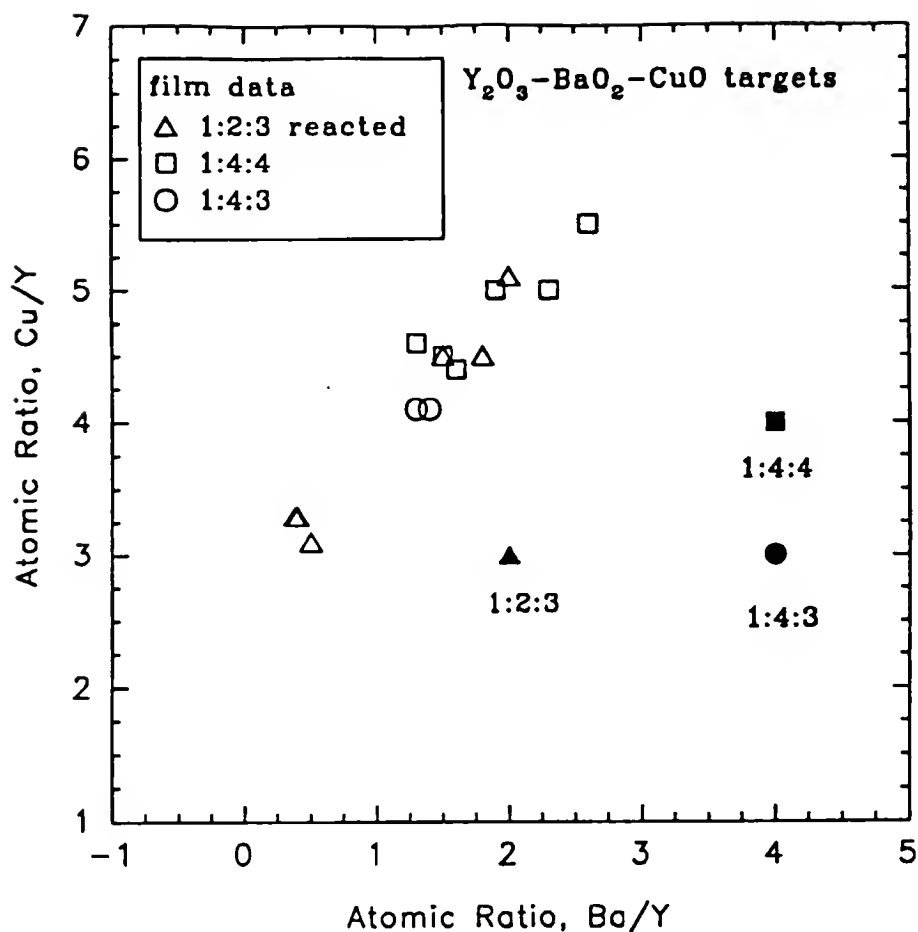


Figure 5-3. Relationship of film composition to target composition and variation among film compositions for targets using BaO₂. Solid symbols represent target compositions.

targets using BaO₂, are presented in Figure 5-3. The 1:2:3 composition targets fired at 950 °C in air and Ar, respectively, were used, but not the 1:2:3 target fired at 500 °C, since the latter target contained the same phases as the target using BaCO₃, which was fired at 500 °C. Presented in Figure 5-4 are composition data for films deposited from four different targets using BaF₂, all of which were fired at 500 °C and thus consisted of unreacted mixtures. The

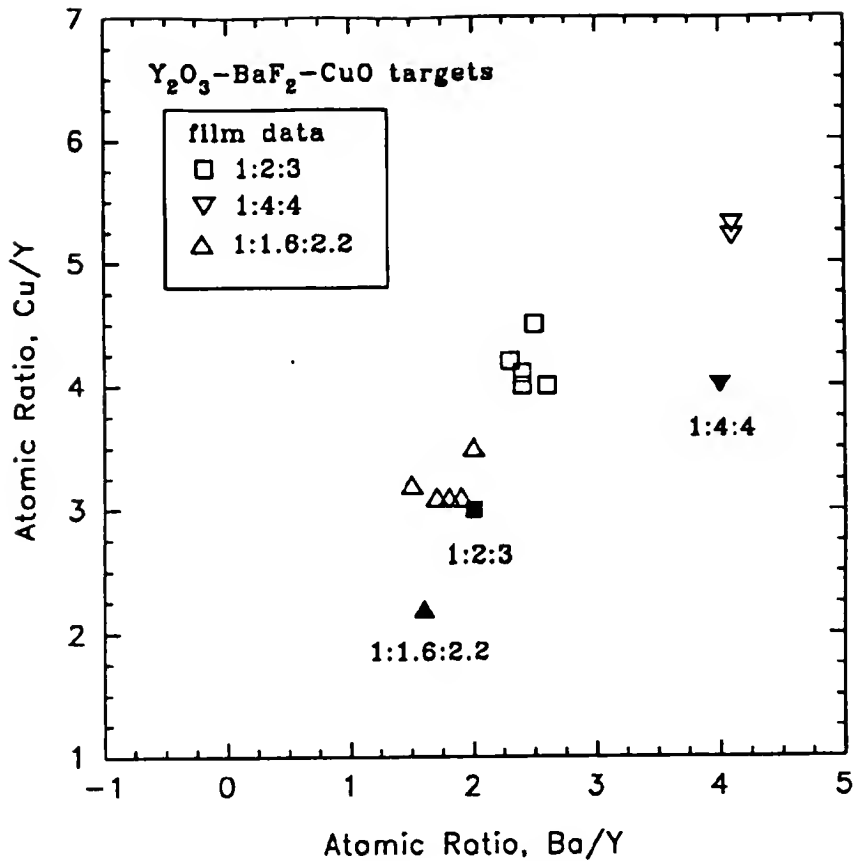


Figure 5-4. Relationship of film composition to target composition and variation among film compositions for targets using BaF₂. Solid symbols represent target compositions.

target compositions represent iterations chosen to bring the film composition closer to 1:2:3.

The most prevalent aspects of the film composition data for films deposited from targets using BaO₂ or BaCO₃ precursors, presented in Figures 5-2 and 5-3, are a substantial variation in the film compositions from a given target and a strong Ba deficiency relative to the target composition. Also, almost all of the films were rich in Cu

relative to the target compositions. Comparatively, the variation in the composition of the films deposited from a given target using a BaF_2 precursor was much less, as seen in Figure 5-4. Further, although films deposited from targets using a BaF_2 precursor were also Cu rich, most of these films were Ba rich rather than Ba deficient. Looked at another way, films deposited from targets using BaF_2 were Y deficient, but to a lesser degree than the Ba deficiency seen for targets using BaCO_3 or BaO_2 . These observations are further supported by comparing the average of the film compositions deposited from each target, which are presented in Table 5-2. In this table, the composition data are normalized to Y = 1. Among the variables of Ba precursor, firing temperature, and target composition, the one with the most dramatic effect on the film composition was the use of a BaF_2 precursor, since the Ba deficiency seen for all other films from BaO_2 or BaCO_3 was eliminated and the deviation between the target and film composition was reduced. Further, when the composition of a target using BaF_2 was altered, the film composition changed accordingly. This was certainly not the case for targets using BaCO_3 or BaO_2 , as will be discussed below.

For films sputtered from targets with BaCO_3 or BaO_2 precursors, the effect of target composition, Ba precursor, and firing temperature on film composition do not describe the complete picture. It is possible to conclude though that films deposited from a 1:2:3 target fired at 950 °C, whether

Table 5-2. Summary of average film compositions, from data presented in Figures 5-1, 5-2, and 5-3. The data are normalized to Y=1.

| Ba Precursor | Target Composition | | Firing Temp. (°C) | Average Film Composition | | No. of films |
|-------------------|--------------------|-------|----------------------|--------------------------|-------|--------------|
| | Y:Ba:Cu | Cu/Ba | | Y:Ba:Cu | Cu/Ba | |
| BaCO ₃ | 1:2:3 | 1.5 | 950 | 1:0.1:2.1 | 17.5 | 1 |
| | 1:2:3 | 1.5 | 500 | 1:0.4:3.4 | 8.5 | 2 |
| | 1:4:3 | 0.75 | 800 | 1:1.6:5.6 | 3.5 | 2 |
| BaO ₂ | 1:2:3 | 1.5 | 950 | 1:1.1:4.0 | 3.6 | 6 |
| | 1:4:4 | 1 | 800 | 1:1.9:4.8 | 2.5 | 6 |
| | 1:4:3 | 0.75 | 800 | 1:1.4:4.1 | 2.9 | 2 |
| BaF ₂ | 1:2:3 | 1.5 | 500 | 1:2.4:4.2 | 1.8 | 5 |
| | 1:4:4 | 1 | 500 | 1:4.1:5.3 | 1.3 | 2 |
| | 1:1.6:2.2 | 1.38 | 500 | 1:1.8:3.2 | 1.8 | 5 |

the Ba precursor was BaCO₃ or BaO₂, were strongly deficient in Ba and only slightly Cu deficient. Attempts to get a 1:2:3 composition film by compensating for the Ba deficiency by using off-stoichiometric 1:4:3 or 1:4:4 targets improved the situation, but were not totally successful. For targets using BaO₂, a 1:4:4 composition was chosen to double the amount of Ba in the target, and since the amount of Cu in the film was expected to decrease, the amount in the target was increased. However, the ratio of Cu/Y in the film increased far more than expected. Efforts to decrease the amount of Cu in the films using a 1:4:3 target composition resulted in films which actually had a higher Cu/Ba ratio. The correlation between the film and target compositions for

a 1:4:3 target using BaCO_3 was even worse. Regardless of the changes made in the target composition, all films were deficient in Ba and rich in Cu relative to the target.

Among the targets using BaCO_3 or BaO_2 , the BaO_2 -144 target fired at 800 °C yielded the best run-to-run film composition reproducibility, as can be seen in Figure 5-3. Further, the target was very stable and never cracked or warped. Although the film compositions were not very close to 1:2:3 or to the target composition, the relative stability of this target made it the most useful among the targets using BaCO_3 or BaO_2 .

For targets using a BaCO_3 precursor, changes in target composition did result in some corresponding film changes: increasing the ratio of Ba/Y and decreasing Cu/Ba led to changes in the same direction but of unequal value in the film. However, keeping Cu/Y constant between a 1:2:3 and a 1:4:3 target led to a large increase in Cu/Y in the film. Apparently the sputter yields at the target and/or sticking coefficients of Cu and Ba are synergetic or the different phases had different stabilities with respect to atmospheric degradation. Also, a change in firing temperature for a 1:2:3 target to 800 °C to avoid full reaction to superconducting $\text{YBa}_2\text{Cu}_3\text{O}_{7-x}$ did not improve the Ba deficiency but corrected the Cu deficiency.

For all targets using BaO_2 or BaCO_3 precursors, if the initial presputter time during target burn-in was not at least three hours long (with the exact amount being

target-dependent), then the first few films would have wildly inconsistent compositions. It was empirically found that once a target was presputtered for at least three hours, the Ba deficiency would improve somewhat and more consistent film compositions would be obtained. However, once the initial erratic film compositions were eliminated, the film composition still only showed a marginal reproducibility among depositions, as illustrated in Figures 5-2 and 5-3. Even for a target with over 30 hours of accumulated sputter time (e.g. the BaO_2 -144 target fired at 800°C), the amount of presputtering time while under vacuum was found to affect the film composition, with a longer presputtering time resulting in slightly increased Ba/Y and Ba/Cu ratios. The run-to-run and long-term variation in the composition of films deposited from targets using BaCO_3 or BaO_2 will be discussed below.

The uniformity of the composition of a Y-Ba-Cu-O film across a two inch diameter Si wafer, which was mounted directly over the center of a BaO_2 -144 target, is presented in Figure 5-5. The term D84A in the figure refers to the deposition number. The data in Figure 5-5 show that the amount of Ba is nearly uniform across the center 0.75 inch of the substrate, but then increases sharply and even doubles the center value at the edges of the substrate. Yttrium shows a complementary but far less pronounced decrease at the edge, while Cu only drops off at the edges. The stronger drop for Cu at the left edge is probably due to

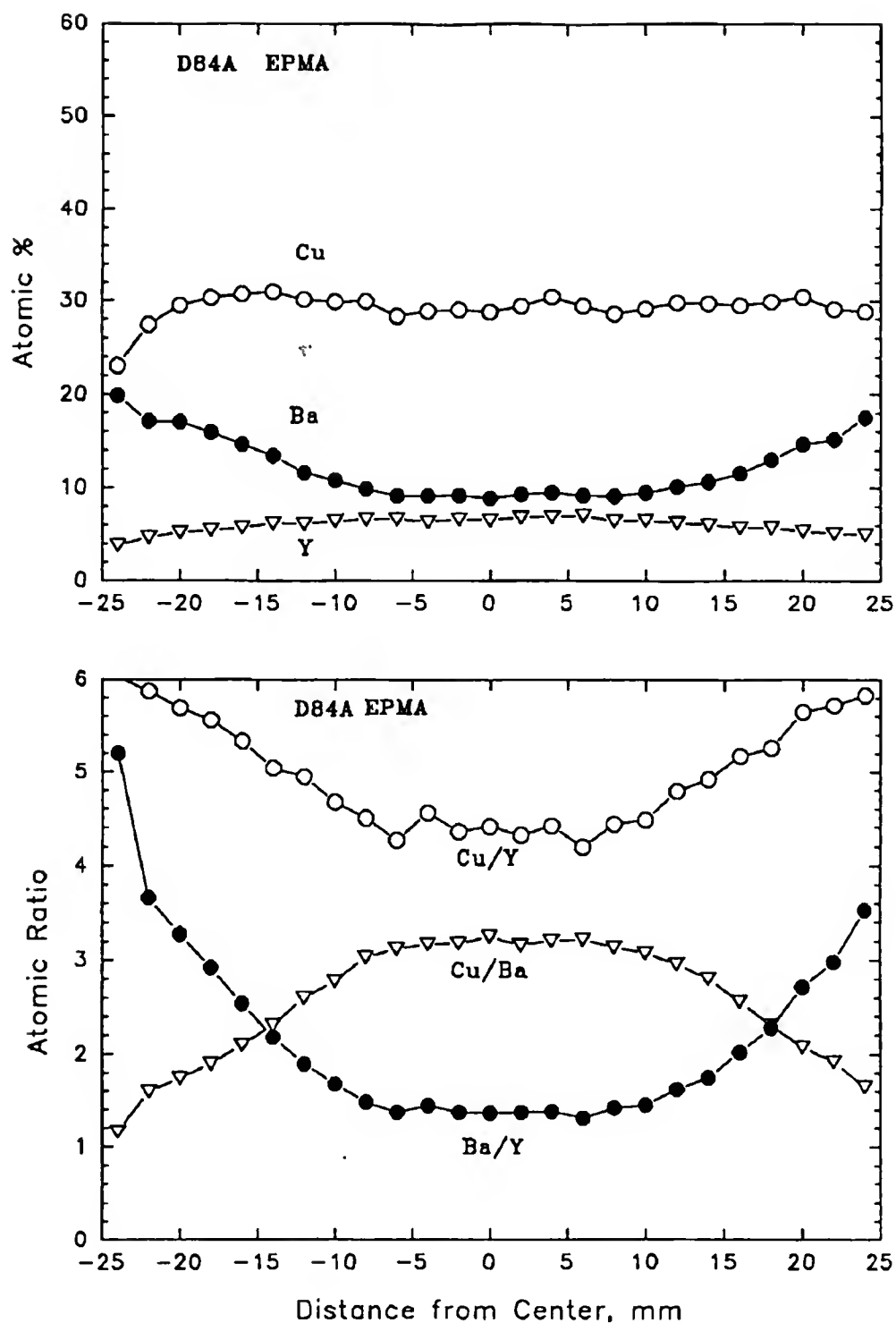


Figure 5-5. Uniformity of Y-Ba-Cu-O film composition across a 2 inch diameter Si substrate, as determined by EPMA. Film sputter deposited from BaO₂-144 target.

the EPMA scan not being correctly centered. Reasons for the compositional uniformity variation will be discussed below.

Compared to the instability and tendency toward cracking of targets using BaCO_3 or BaO_2 precursors, and the film composition problems encountered with their use (e.g. irreproducibility, large deviation between target and film composition, poor correlation of film composition with changing target composition, and nonuniformity), the use of BaF_2 greatly improved the controllability of the deposition of Y-Ba-Cu-O thin films. First, after only an initial three hour burn-in, the composition of films from any target using BaF_2 , regardless of additional exposures of the target to air, remained near a stabilized value, as illustrated in Figure 5-4. Second, the data in Figure 5-4 and Table 5-2 illustrate that the deviation between the film composition and the starting target composition for targets using BaF_2 is clearly smaller than for films from almost all targets using BaCO_3 or BaO_2 . Only for films deposited from the reduced BaCO_3 -123 target were the deviation values comparable.

Third, changes in the target composition for targets using BaF_2 were followed by related changes in the film composition. For example, when the target composition was changed from 1:2:3 to 1:4:4, the film composition showed a clear increase in Ba/Y, Cu/Y, and Cu/Ba, contrary to the effect of changing the target composition when BaO_2 or BaCO_3 were used. However, the change in film composition still did

not equal the change in the BaF_2 -containing target composition, so determining the target composition necessary to give a 1:2:3 required an iterative process. However, the third target composition tried, 1:1.6:2.2, gave a film composition close to 1:2:3.

Fourth, the use of a BaF_2 precursor greatly improved the reproducibility of the film composition from a given target over a number of depositions, as can be seen by comparing Figures 5-2 and 5-3 to Figure 5-4. For example, the films deposited from the BaO_2 -144 target yielded reproducibilities of about $\pm 30\%$, $\pm 10\%$, and $\pm 20\%$ for Ba/Y, Cu/Y, and Cu/Ba, respectively. In comparison, the respective values from the BaF_2 -123 target were about $\pm 6\%$, $\pm 6\%$, and $\pm 9\%$.

Fifth and finally, the use of a BaF_2 precursor improved the uniformity of the composition across a two inch diameter substrate, as illustrated in Figure 5-6. Compared to the data for the film deposited from the BaO_2 -144 target shown in Figure 5-5, the film deposited from the BaF_2 -123 target shows a much smaller drop in the Ba concentration above the center of the target. Also, the Cu and Y compositional profiles are both more uniform in Figure 5-6. These improvements will be discussed below.

Substrate rotation would be useful for improving film thickness uniformity and sample throughput. The effect of substrate rotation on the uniformity of the Y-Ba-Cu-O film composition on a two inch diameter substrate is presented in

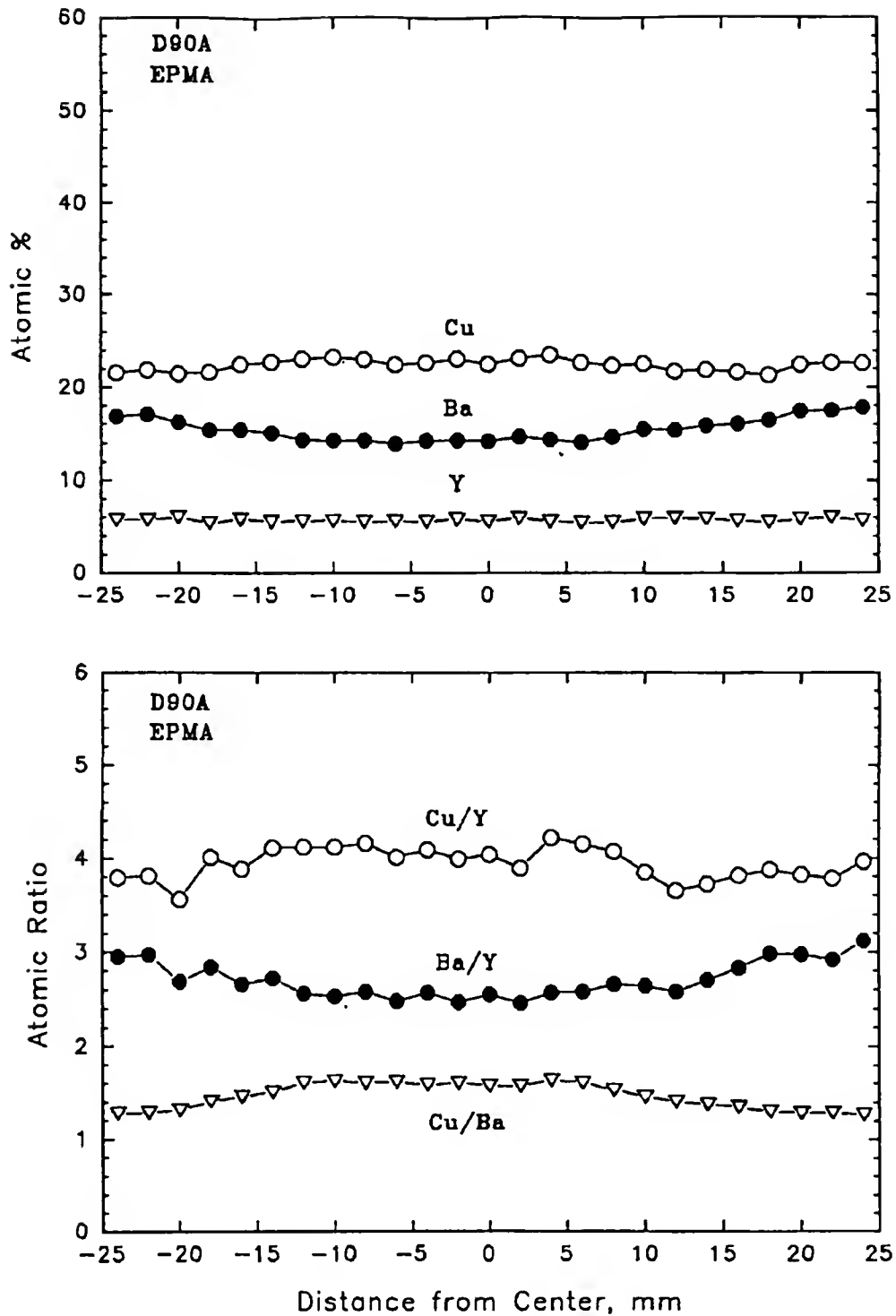


Figure 5-6. Uniformity of Y-Ba-Cu-O film composition across 2 inch diameter Si substrate, as determined by EPMA. Film sputter deposited from unreacted BaF_2 -123 target.

Figure 5-7. The term D134t in the plot refers to the deposition number. The substrate was rotated past the BaF_2 -1:1.6:2.2 target using the substrate rotation assembly described in Appendix A. The compositional uniformity was excellent for Y, Ba, and Cu. However, the average film composition, 1:2.5:2.2, did not equal either the target composition or a value of 1:2:3. These data will be discussed further below.

The reproducibility of film compositions from BaF_2 -based targets was good enough to spot a problem. Films from two successive depositions from the BaF_2 -1:1.6:2.2 target exhibited an unexpected depletion of Ba, as measured by EPMA. The film compositions were determined to be about 1:0.8:3.2, as compared to the average value from the BaF_2 -1:1.6:2.2 target of 1:1.8:3.2, as given in Table 5-2. It was found after the second deposition that the vacuum system had developed a leak, which was allowing air into the chamber during deposition at a partial pressure of about 1×10^{-6} Torr. It was postulated that oxygen from the air leak was responsible for the Ba depletion. To test this, 10% O_2 was deliberately added to the Ar sputter gas. The resulting composition for a Y-Ba-Cu-O film positioned above the center of the substrate was 1:0:2.6; in other words, Ba had been completely depleted from the film. Compared to the average composition for this target, 1:1.8:3.2, the amount of Cu had also decreased. This emphasized the importance of a good vacuum during the sputter deposition of Y-Ba-Cu-O.

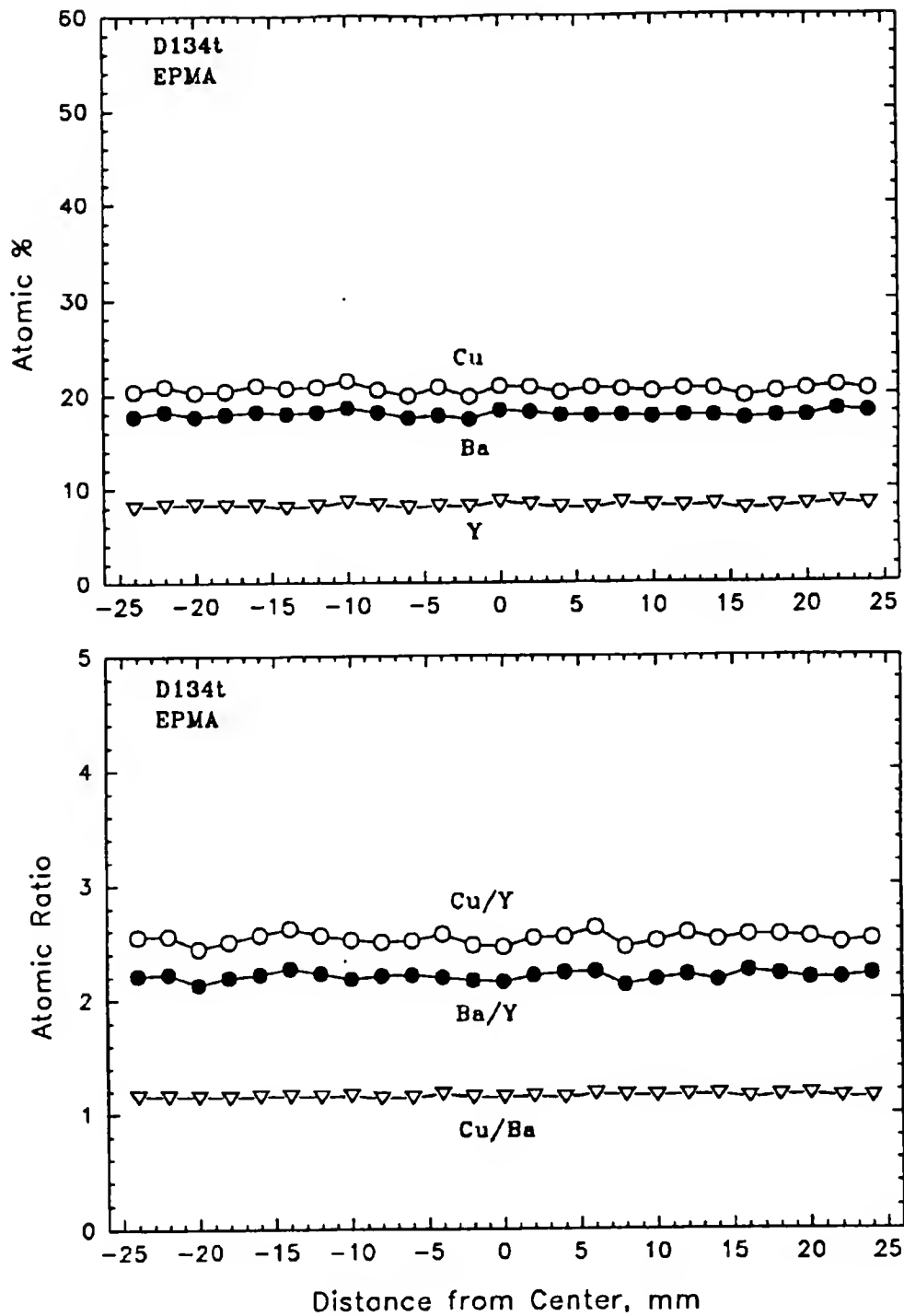


Figure 5-7. Uniformity of Y-Ba-Cu-O film composition across 2 inch diameter Si substrate, as determined by EPMA. Film sputter deposited from unreacted BaF_2 -1:1.6:2.2 target onto substrate rotated past target.

Further, these data agreed with the results of Rossnagel and Cuomo [57] discussed in Section 2.1.5.4, in which an increasing amount of oxygen in the sputter gas was found to cause an increase amount of resputtering of Y-Ba-Cu-O films. As discussed in Chapter 4, the addition of oxygen in the sputter gas probably resulted in the oxidation of the target surface during sputtering and the formation of Ba-O and Y-O bonds, the dissociation of which in turn led to an increased O^- yield. The complete depletion of Ba and slight decrease in Cu was probably due to oxidation of the target surface, an increased O^- yield, and subsequent resputtering of Ba and Cu from the growing film.

5.1.4 Discussion of Y-Ba-Cu-O Film Composition Data

In Figure 4-2 it was shown that the O^- yield from negative SIMS data for Y-Ba-Cu-O targets with a 1:2:3 composition decreased in the order: $YBa_2Cu_3O_{7-x}$, $BaCO_3$ -123 mixture, $YBa_2Cu_3O_6$, and BaF_2 -123 mixture. It was suggested in Section 4.1.3 that as the yield of O^- decreased among Y-Ba-Cu-O targets with a 1:2:3 composition, the deviation between the target and sputtered film compositions would decrease. The film composition data presented in Figures 5-2, 5-3, and 5-4 and in Table 5-2 allow this suggestion to be tested. Compositions are given for films deposited from targets with the same phases as were present in three of the four pellets used in the SIMS study. The BaO_2 -123 target fired at 950 °C consists of $YBa_2Cu_3O_{7-x}$, while the $BaCO_3$ -123

and BaF_2 -123 targets fired at 500 °C both consist of unreacted mixtures of the starting compounds. Whether the film compositions followed the expected pattern will be discussed.

By comparing the composition data in Figures 5-2, 5-3, and 5-4 and Table 5-2 for the three targets of interest, it is clear that the use of BaF_2 greatly improved the Ba deficiency in sputter deposited Y-Ba-Cu-O films. In fact, films deposited from the mixed BaF_2 -123 target had an average Ba/Y value of 2.4, which is greater than that in the target. The deviation for Ba/Y between the target and average film composition, about 17%, is less than half the value between the average film composition and the $\text{YBa}_2\text{Cu}_3\text{O}_{7-x}$ target, which is 45%. As discussed in Chapter 2, a deficiency in Ba is reported for most sputtered Y-Ba-Cu-O films and is attributed to negative ion resputtering. In Chapter 4 it was explicitly shown that the dominant negative ion sputtered from Y-Ba-Cu-O targets is O^- and the yield among targets with a 1:2:3 composition was lowest for one using BaF_2 . The use of unreacted BaF_2 in the sputter target results in less resputtering of the growing Y-Ba-Cu-O film and an improvement in the Ba deficiency normally seen in sputter deposited Y-Ba-Cu-O films, as suggested by the negative SIMS results from Chapter 4.

A new issue brought on by the use of unreacted targets containing BaF_2 -123 is a slight deficiency in Y in films. The films deposited from the mixed BaF_2 -123 target exhibited

an increase in both Ba/Y and Cu/Y relative to the target. As discussed above, this can be interpreted as a decrease in the Y concentration in the films. The source of the Y deficiency is most likely not due to resputtering by O^- , since no reports of a Y deficiency were found in the literature; only deficiencies of Ba or Cu have been reported. Due to the complexity of sputtering of Y-Ba-Cu-O, an obvious solution is not apparent. However, two alternative speculations will be offered. First, the deficiency in Y may be due to a decrease in sputter yield of Y from the mixed BaF_2 -123 target. The cause of this could be Y on the surface of the target recombining with available F, rather than remaining bound to O or partially bound. This could put Y in a more strongly bound state and thus make it more difficult for Y to be sputtered away. Second, it is also possible that the use of the mixed BaF_2 -123 target affects the angular distribution variation of the sputtered species, as was discussed in Sections 2.1.2.3 and 2.1.5.3. Typically, the lighter species are sputtered more along the normal to the target surface and heavier species are sputtered with their distributions skewed to larger angles. For Y-Ba-Cu-O, one would expect the sputtered distribution of Cu to be normal to the target, the distribution of Y to be at a larger angle, and the distribution of Ba to be at the largest angle. However, as discussed in Sections 2.1.2.3 and 2.1.5.3, the angular distributions do not always follow the values expected from the masses of the species. It is

conceivable that the angular distribution of Y was distorted to larger angles due to the sputtering from the mixed BaF_2 -123 target. This would result in the composition of Y in films positioned above the target to drop. Determining the reason for the deficiency in Y in films sputtered from unreacted targets using BaF_2 is an area requiring further study. Regardless, as discussed above, the deficiency in Y from targets using BaF_2 is much less than the Ba deficiency for targets using BaCO_3 or BaO_2 . Thus as suggested in Chapter 4, avoiding Ba-O bonding leads to a decrease in the O⁻ yield and less depletion of Ba in sputter deposited films due to resputtering by O⁻.

The negative SIMS results presented in Figure 4-2 also suggest that the composition of films deposited from a mixed BaCO_3 -123 target should be closer to the target composition than films deposited from an $\text{YBa}_2\text{Cu}_3\text{O}_{7-x}$ target, since the O⁻ yield is lower for the former. Based on the average film composition values presented in Table 5-2, 1:0.4:3.4 for the mixed BaCO_3 -123 target versus 1:1.1:4.0 for the $\text{YBa}_2\text{Cu}_3\text{O}_{7-x}$ target, the reverse of this prediction was observed. The Ba deficiency for films from the mixed BaCO_3 -123 target is worse than films from the $\text{YBa}_2\text{Cu}_3\text{O}_{7-x}$ target. However, as can be seen in Figure 5-3, the film composition values for the $\text{YBa}_2\text{Cu}_3\text{O}_{7-x}$ target have a variation wide enough to include the composition values for the mixed BaCO_3 -123 target presented in Figure 5-2. In other words, this reversal may be

fortuitous and not representative of a violation of the predicted trend.

As discussed in Section 2.1.6, the run-to-run irreproducibility in the film composition for $\text{YBa}_2\text{Cu}_3\text{O}_{7-x}$ sputter targets can either be attributed to a decreasing amount of excess oxygen until a $\text{YBa}_2\text{Cu}_3\text{O}_6$ composition is reached, as also discussed in Chapter 4, or to atmospheric degradation. For sputter targets which do not contain the $\text{YBa}_2\text{Cu}_3\text{O}_{7-x}$ phase, the excess oxygen is not a concern and only atmospheric degradation should control the run-to-run irreproducibility in film composition. Another suggested explanation for the run-to-run variation, the migration of Ba in the target, was shown in Section 4.2 not to be an issue.

As discussed in Section 2.1.6, atmospheric degradation of $\text{YBa}_2\text{Cu}_3\text{O}_{7-x}$ results in the formation of compounds on the surface which do not have the same composition as the bulk of the target. The most prevalent degradation product is $\text{Ba}(\text{OH})_2$ [90], the formation of which results in an enrichment of Ba on the surface of $\text{YBa}_2\text{Cu}_3\text{O}_{7-x}$. Other Ba-containing compounds such as BaCO_3 and BaO_2 are also susceptible to reaction with water, and $\text{Ba}(\text{OH})_2$ can form on the surface of targets containing these compounds [90]. Further, barium fluoride can also react with water to form a surface $\text{Ba}(\text{OH})_2$ layer, as discussed in Section 2.1.6, but the extent of the reaction is less for BaF_2 than for BaCO_3 or BaO_2 [92].

The presence of atmospheric degradation products on the surface of a sputter target would result in a sputtered flux which does not have the same composition as the bulk of the target. Unless the degradation products are completely removed during the presputtering prior to deposition, the composition of sputtered films will deviate from that of the target. The amount of presputtering necessary is difficult to predict since it depends on the conditions under which the atmospheric degradation products were formed, the materials in the target and, for sintered targets, the density of the target. For example, the extent of atmospheric degradation has been reported to be greater for higher temperatures, higher relative humidities, and longer exposure times [90]. The temperature and relative humidity in the laboratory in which the depositions were performed could vary anywhere from 21 - 29 °C and 50 - 85%, respectively, depending on the weather and the status of the climate control system. The length of time the chamber was open while loading substrates or performing routine maintenance was not consistent, either. As discussed above, each target in this study for which a Ba source of BaCO_3 or BaO_2 was used required an initial presputting of at least three hours or wildly erratic film compositions would be obtained. These initial film compositions were probably due to the domination of the surface of the targets and the sputtered flux by the atmospheric degradation products formed during firing in air and subsequent storage.

Furthermore, a sintered target with a low density could require extra presputtering compared to a high density target since more porosity could mean a greater surface area on a target. Thus the thickness of the degraded layer on the surface of the Y-Ba-Cu-O targets was an unpredictable quantity.

Another issue to consider is that during planar magnetron sputter deposition, the incident flux of Ar^+ ions is not equal across the surface of the target, as discussed in Section 2.1.1. The annular shape of the plasma results in a much greater sputter rate from a circular area on the target directly beneath the plasma, which leads to the formation of the racetrack in the target. The atmospheric degradation products would be sputtered away soonest from the area of the target directly beneath the annular region in the plasma with the highest density of Ar^+ , while the rest of the racetrack region would require longer to clean. This would complicate predicting the amount of presputtering time needed to remove the atmospheric degradation products.

An additional issue to consider with regard to the atmospheric degradation products formed on Y-Ba-Cu-O is that not only do these compounds have a different composition than the target, but they are also a probable source of O^- . This is particularly true for $\text{Ba}(\text{OH})_2$. As discussed in Sections 2.1.5.4, the dissociation of Ba-O bonds is the most likely source of O^- during the sputtering of Y-Ba-Cu-O

targets. The dissociation of Ba(OH)_2 during sputtering would thus probably result in a significant yield of O^- .

The final issue with regard to the atmospheric degradation of Y-Ba-Cu-O targets is that the degradation made testing of the results of the negative SIMS study difficult. As discussed above, for the $\text{YBa}_2\text{Cu}_3\text{O}_{7-x}$ and mixed BaCO_3 -123 targets, the proposed effect of the atmospheric degradation products on the film composition probably masked any changes due to a decreased sputter yield of O^- . In order to properly test if the 1:2:3 Y-Ba-Cu-O target with the lowest O^- yield does in fact produce the least deviation between the film and target compositions, atmospheric degradation of the targets should be avoided in future experiments. For example, the targets should be fired in dry oxygen rather than in air. After firing, the targets should be stored in an effective dessicator. Before the first deposition, targets should be presputtered for 12 hours to be certain the surfaces are clean. Also, the sputter deposition system should have a load-lock capability for introducing substrates into the vacuum chamber without exposing the target to atmosphere. Even with these precautions, some presputtering will be needed to remove the contaminants which would collect on the target surface between depositions. These precautions are suggested for future study in Chapter 7.

The next item to be addressed is the uniformity of the Y-Ba-Cu-O film composition across the two inch diameter

substrates mounted directly above the two inch diameter targets, with the center of each aligned. As can be seen in Figure 5-5, the Ba concentration in a film sputter deposited from the BaO₂-144 target showed a substantial decrease toward the center of the substrate. A film deposited from the unreacted BaF₂-123 target also exhibited a decrease in the Ba concentration toward the center of the substrate, but of a smaller magnitude, as illustrated in Figure 5-6. In both cases the pattern for the depletion of Ba can be explained by the trajectory of the O⁻ flux sputtered from the targets.

As discussed above and in Section 2.1.1, the annular shape of the plasma in a circular magnetron results in a much greater sputter rate from a circular area on the target directly beneath the annular region, which leads to the formation of the racetrack in the target. The distributions of Y, Ba, and Cu sputtered from the racetrack versus that of O⁻ is schematically illustrated in Figure 5-8 in which M represents Y, Ba, and Cu atoms. The Y, Ba, and Cu atoms are sputtered from the racetrack region with an approximate $\cos\theta$ angular distribution, with the exact distribution being dependent on the mass of each as discussed above. These atoms continue outward in their respective trajectories, although some scattering in the plasma occurs and broadens the distributions. On the other hand, after O⁻ ions are sputtered from the target, they do not follow a $\cos\theta$ angular distribution [30]. Rather, the O⁻ ions are accelerated by

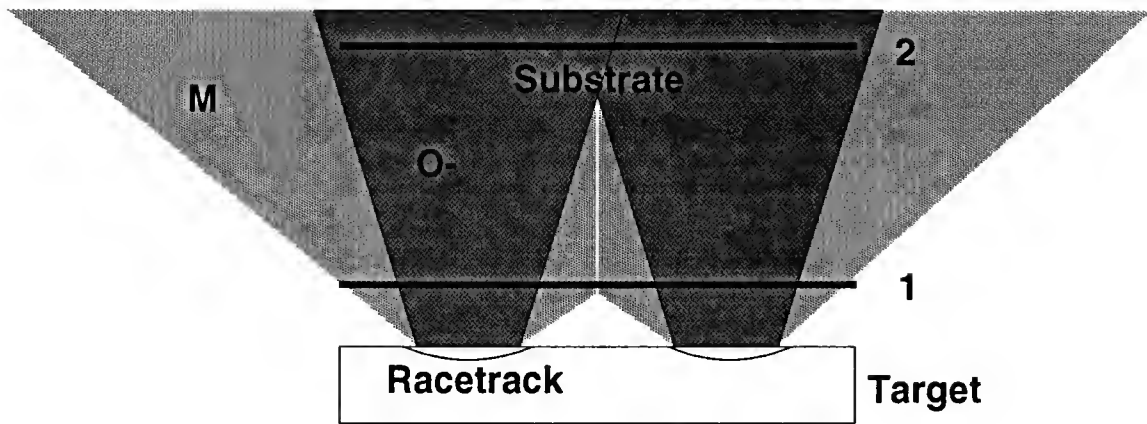


Figure 5-8 Illustration of distributions of atoms M versus O^- ions sputtered from the racetrack in a circular magnetron. The atoms are sputtered with a $\cos\theta$ distribution, while the O^- are confined by acceleration by the electric field to a trajectory more perpendicular to the target. The substrate positions 1 and 2 are discussed in the text.

the electric field perpendicular to the target surface and travel away from the target in this direction. The O^- ions then enter the plasma where they may be scattered by atoms, molecules, and other ions, which results in a broadening of the O^- distribution, as illustrated in Figure 5-7. The probability of scattering depends on the accelerating voltage on the target and the sputter gas pressure. As discussed in Section 2.1.2.4, collisions with electrons in the plasma may strip the O^- ions of the extra electron, resulting in a beam of mostly neutral oxygen which may also sputter the substrate.

In Figure 5-8, the substrate in position 2 is located at a substrate-target distance which is beyond the point where the O^- "beams" from each side of the racetrack cross

over. In the area where the beams cross over, which in this case coincides with the center of the substrate, the O^- flux will be high due to the additive contribution of O^- from each portion of the racetrack. Correspondingly, the amount of resputtering will increase and the Ba concentration in the film will decrease towards the center of the substrate. The profile of O^- flux versus position on a substrate depends on the position of the substrate relative to the point where the O^- beams cross over, as well as the distribution of O^- within the beams. The distribution of O^- within each beam would not be uniform since the flux sputtered from the center of the racetrack would be greater than at the outer and inner diameters of the racetrack. At a substrate-target distance well beyond the crossover point, the area of increased O^- flux in the center of the substrate could be as large as the target diameter. In this case, the O^- flux could be greatest at the center of the substrate and decrease continuously out to the edge of the substrate. This situation apparently corresponds to the substrate-target distance used for the deposition of the films in Figures 5-5 and 5-6. The greater decrease in the Ba concentration towards the center of the substrate in Figure 5-5 compared to that in Figure 5-6 is certainly due to the greater O^- sputter yield from the BaO_2 -144 target than from the BaF_2 -123 target. Although the use of BaF_2 results in a greatly decreased O^- yield by eliminating Ba-O bonds, the

presence of Y_2O_3 in the target will still result in some resputtering by O^- , as discussed in Section 4.1.3.

The substrate in position 1 in Figure 5-8 is located just beyond the point where the M distributions cross over. A film would be deposited across all of the substrate, although the thickness uniformity would probably not be good. The incident O^- flux at this substrate-target distance would be high on the areas of the substrate directly above the racetrack, but would be greatly decreased at the center and edges of the substrate with a value approaching zero. Thus directly above the racetrack the film would be expected to be depleted in Ba and also possibly Cu. This corresponds exactly to the data of Kadin et al. [34] presented in Figure 2-3. Note also in Figure 2-3 that the film thickness decreases above the racetrack, where it would normally be expected to increase due to the increased sputter rate of Y, Ba, and Cu. This was due to a rate of resputtering by O^- greater than the deposition rate.

The data presented in Figure 5-7 illustrate that rotating the substrate past the target during deposition resulted in greatly improved compositional uniformity across a two inch diameter substrate. The reason for this improvement was simply that the nonuniformities observed in Figures 5-5 and 5-6 for static substrates were averaged out by rotating the substrate past the target. Rather than the increased O^- flux being incident on only the center of the substrate in position 2 in Figure 5-8, it was essentially

scanned across the substrate. The film composition did not equal the target position because of resputtering by the O^- . With further iterations of the target composition, a 1:2:3 film composition could have been obtained across the two inch diameter substrate, with all other parameters kept constant. This is suggested for further study, particularly since deposition on large area substrates will be important for practical applications of $YBa_2Cu_3O_{7-x}$. However, the time required to deposit the film in Figure 5-7, which was approximately $0.8\text{ }\mu\text{m}$ thick, was about 24 hours versus about 4 hours for a static deposition of equivalent thickness. This long time was required since the substrate was only spending about one sixth of its rotation period over the sputter source. Such long deposition times would seem to be incompatible with manufacturing scale deposition of $YBa_2Cu_3O_{7-x}$ films.

It is clear from the discussions in this chapter and in Chapter 4 that the dominant mechanism for the deviation between the composition of sputtered Y-Ba-Cu-O films and sputter targets is resputtering of the films by O^- ions. It is also possible that the angular distribution variations among sputtered Y, Ba, and Cu atoms may be playing a role in the composition deviation. This is particularly true for the compositional uniformity measurements on two inch diameter substrates, where the angular distribution variations would more likely be evident. For example, as discussed in Sections 2.1.2.3 and 2.1.5.3, since Ba has the heaviest mass

among Y, Ba and Cu, it should be sputtered with a distribution enhanced along oblique angles away from the normal to the target surface, as suggested by the data of Wehner et al. [81]. Such a sputtered distribution is consistent with the data in Figures 5-5 and 5-6. Also, in most of the films deposited in this study, the Cu concentration was enhanced relative to the target. Since Cu has the lightest mass among Y, Ba, and Cu, it would be expected to be preferentially sputtered along the normal to the target surface. This could account for the excess Cu seen in the films, but it does not explain the relatively uniform Cu concentrations in Figures 5-5 and 5-6. However, as discussed in Section 2.1.5.3, it is difficult to separate the effects of the angular distribution variations from those due to resputtering by O^- . Separation of these effects has never been properly done for sputtering from Y-Ba-Cu-O and is suggested for future work, with the experimental procedures discussed in Chapter 7.

5.1.5 Summary of Sputtered Y-Ba-Cu-O Film Composition Data

Barium deficiency and run-to-run irreproducibility were found to be the most serious problems in the sputter deposition of Y-Ba-Cu-O thin films. Electron microprobe analysis showed that films deposited from targets using BaO_2 or $BaCO_3$ precursors were Ba deficient, whereas with a BaF_2 precursor films were Y deficient, but less so. Target compositions were compensated to bring the film composition

towards 1:2:3, but for targets using BaCO_3 and BaO_2 this was difficult. Testing the results of the negative SIMS study in Chapter 4 was difficult for a $\text{YBa}_2\text{Cu}_3\text{O}_{7-x}$ target and a mixed BaCO_3 -123 target due to the run-to-run variation in the film compositions, which was probably caused by the poor atmospheric stability of these materials. As suggested by the results of the negative SIMS study in Chapter 4, the use of BaF_2 in unreacted targets reduced the Ba deficiency problem as result of a decreased O^- yield. The uniformity of the film composition across two inch diameter substrates was also improved as a result of the decreased O^- yield. Further, the better atmospheric stability of BaF_2 resulted in an improvement in the run-to-run variation in the film composition.

5.2 Towards Superconducting Y-Ba-Cu-O Films

Once a process had been established to controllably sputter deposit Y-Ba-Cu-O films with a composition close to 1:2:3, the next step was to develop a post-deposition heat treatment process to convert the insulating as-deposited films to superconducting $\text{YBa}_2\text{Cu}_3\text{O}_{7-x}$. In actuality, even prior to getting close to a 1:2:3 film composition, heat treatments were performed on films deposited from targets made using BaCO_3 , BaO_2 , or BaF_2 precursors. This was primarily done to study the suitability of SrTiO_3 as a barrier layer to prevent the reaction between Y-Ba-Cu-O and Si, as will be discussed in Chapter 6. However, attempts to

get superconducting Y-Ba-Cu-O from films deposited from targets using BaCO_3 or BaO_2 were not successful. This was due both to the poor compositions of the films as well as the heat treatment not being optimized. Once a Y-Ba-Cu-O film composition close to 1:2:3 was deposited from a BaF_2 -1:1.6:2.2 target, development of a heat treatment process to form $\text{YBa}_2\text{Cu}_3\text{O}_{7-x}$ was addressed.

5.2.1 Heat Treatments to Form Superconducting Y-Ba-Cu-O

As discussed in Section 3.3.3, the heat treatment cycle was similar for all films, consisting of a one to two hour ramp from room temperature to the desired high temperature setpoint of 850 - 900 °C, a soak of one hour, and a slow (≤ 3 °C/min.) cool down to room temperature. Prior to heating, samples were positioned inside of a capped quartz tube and the tube was purged with the desired ambient gas. For films deposited from targets using BaCO_3 or BaO_2 , the ambient gas consisted of 99.995% purity oxygen flowing at 10 - 30 sccm.

Films deposited from targets using a BaF_2 precursor required an ambient gas of humid oxygen, as discussed in Section 2.1.4. Oxygen was humidified by passing it through a flask of deionized water (i.e. a water bubbler) at room temperature. A flow rate of humidified oxygen of 30 sccm was initially tried but found to be insufficient to facilitate the reduction of BaF_2 and formation of $\text{YBa}_2\text{Cu}_3\text{O}_{7-x}$. A high flow rate of oxygen, 200 sccm, was found to be necessary

during the ramp-up and soak at high temperature for the formation of $\text{YBa}_2\text{Cu}_3\text{O}_{7-x}$. This can be understood by examining expression (2.4). An increasing flow rate would result in faster purging of gaseous HF, thereby ensuring faster removal of the reaction products from the film surface and increasing the driving force for the reaction from BaF_2 to BaO or $\text{YBa}_2\text{Cu}_3\text{O}_{7-x}$. It can also be noted from expression (2.4) that increasing the partial pressure of water would also drive the reaction to the right. This could have been accomplished by heating the water in the flask, but it was easier to increase the flow rate of the oxygen.

After the high temperature heat treatment in humidified oxygen, the ambient gas during cooling was changed to dry oxygen at a flow rate of 30 sccm. The wet oxygen was no longer needed since all of the BaF_2 should have reacted to form oxidized Ba, which in turn should have reacted with the compounds containing Y and Cu to form $\text{YBa}_2\text{Cu}_3\text{O}_6$. The dry oxygen was needed to increase the oxygen content of the $\text{YBa}_2\text{Cu}_3\text{O}_6$ during cooling in order to form $\text{YBa}_2\text{Cu}_3\text{O}_{7-x}$.

5.2.2 Properties of Superconducting Y-Ba-Cu-O Films

As discussed above, the emphasis of the work presented in this chapter was controlling the composition of sputter-deposited Y-Ba-Cu-O films. It was desired to verify that superconducting Y-Ba-Cu-O films with reasonable R-T properties could be fabricated by sputter deposition from a

BaF₂-based target. Extensive measurements of the properties of superconducting films were not the objective of this study. Thus the properties of only three representative superconducting films will be presented.

All three of the film samples to be discussed in the section that follows, samples D128r2, D128r4, and D128r3, were deposited during the same deposition on 10 mm x 5 mm (100) SrTiO₃ substrates. SrTiO₃ is an excellent substrate for the formation of superconducting YBa₂Cu₃O_{7-x}, due to a good lattice match. The films were deposited from the BaF₂-1:1.6:2.2 target at the standard deposition parameters of 50 W RF, 10 mTorr Ar, 6 cm substrate-to-target distance, and a nominally unheated and electrically floating substrate. The samples were positioned within 0.5 inch of the center of the substrate holder, together with an adjacent piece of (100) Si to be used for each as the substrate for measurement of the film composition by EPMA.

The thickness of each film was approximately 1.1 μ m. The film compositions determined by EPMA on the Si pieces were 1:1.9:3.1, 1:1.7:3.1, and 1:1.8:3.1, for samples D128r1, D128r2, and D128r3, respectively. These compositions were close enough to 1:2:3 that after heat treatment the film should have consisted predominantly of YBa₂Cu₃O_{7-x}. After deposition, each Y-Ba-Cu-O/SrTiO₃ sample was heated at 900 °C in humidified oxygen in one of three successive heat treatments.

5.2.2.1 Electrical properties of Y-Ba-Cu-O films

The room temperature resistivity of the films was determined by DC four-point probe measurements, as discussed in Section 3.3.5. All as-deposited films were electrically insulating. After heat treatment, resistivity versus temperature (R-T) measurements were performed as described in Section 3.3.5 and Appendix B. Presented in Figures 5-9, 5-10, and 5-11 are R-T data for samples D128r2, D128r3, and D128r4, respectively. The dotted line in each R-T plot represents a linear regression through the normal state data above 120 K extrapolated to the intersection with the resistivity axis, in order to determine the residual resistivity at 0 K, ρ_0 , as discussed in Section 3.3.5. The nonlinear normal state R-T data for sample D128r2 and the noisy data below 120 K for sample D128r3 probably resulted from poor or intermittent electrical contact between the spring-loaded Pogo contacts and the samples.

The values for $T_{c,0}$, ΔT , ρ_{rt} , and ρ_0 for each sample are summarized in Table 5-3. The room temperature resistivity values were comparable with values near $330 \mu\Omega\text{cm}$, which is nearly twice as high as the best values reported in the literature for *in situ*, epitaxial films, which are usually around $180 \mu\Omega\text{cm}$ [13]. However, these ρ_{rt} values are equivalent to good post-deposition heat treated superconducting films, as illustrated in Figure 3-1 [105]. Similarly, ρ_{rt} values of greater than $300 \mu\Omega\text{cm}$ were reported

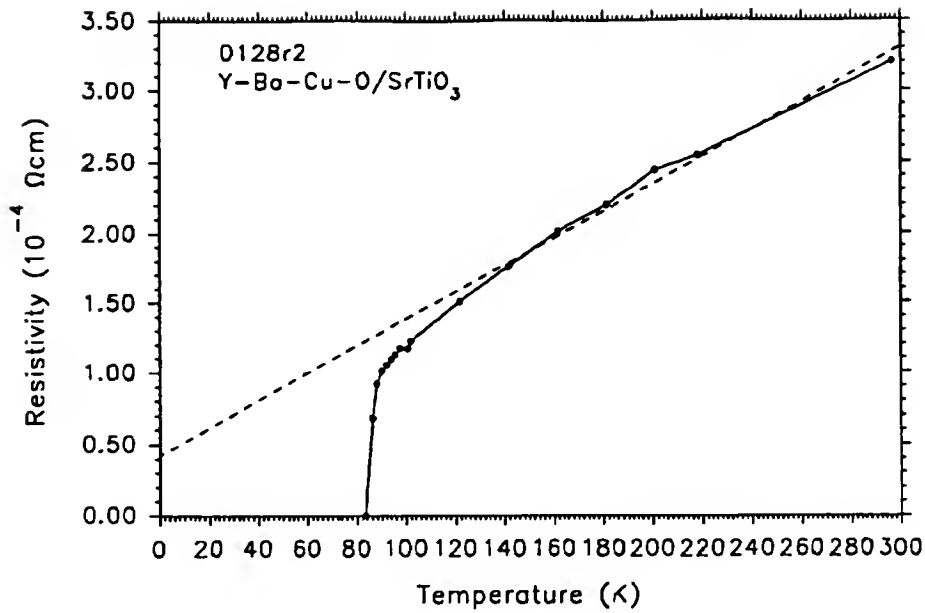


Figure 5-9. R-T data for sample D128r2, consisting of a 1.1 μm thick Y-Ba-Cu-O film on a (100) SrTiO₃ substrate.

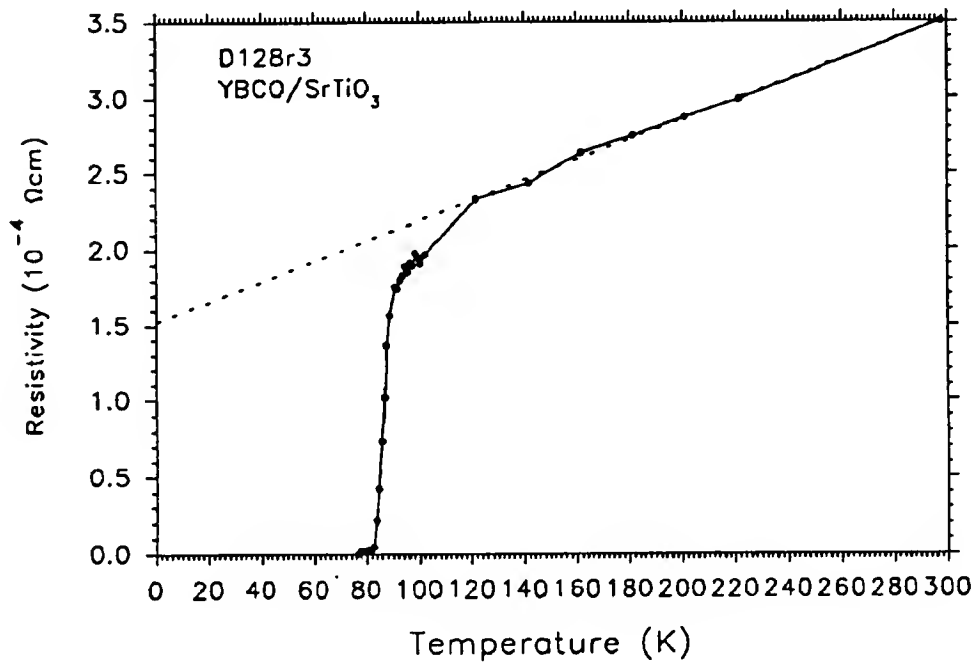


Figure 5-10. R-T data for sample D128r3, consisting of a 1.1 μm thick Y-Ba-Cu-O film on a (100) SrTiO₃ substrate.

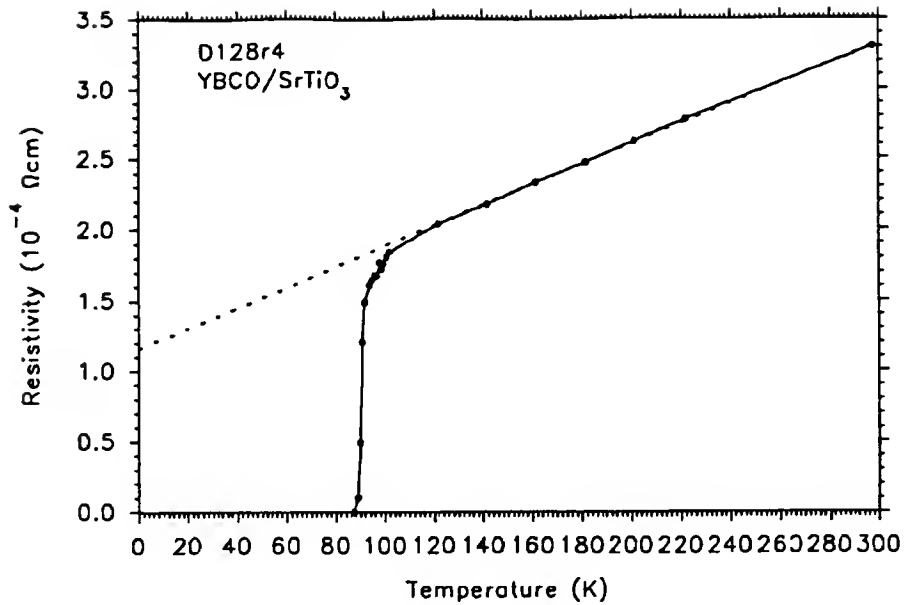


Figure 5-11. R-T data for sample D128r4, consisting of a 1.1 μm thick Y-Ba-Cu-O film on a (100) SrTiO₃ substrate.

Table 5-3. Summary of room temperature resistivity and R-T data for Y-Ba-Cu-O films deposited from BaF₂-1:1.6:2.2 target onto SrTiO₃ substrates. Post-deposition heat treatment performed in humid oxygen for 1 hr at 900 °C, followed by slow cooling in dry oxygen.

| Sample I.D. | T _{onset} (K) | T _{C,0} (K) | T _{C,mid} (K) | ΔT (K) | ρ_{rt} ($\mu\Omega\text{cm}$) | ρ_0 ($\mu\Omega\text{cm}$) |
|-------------|------------------------|----------------------|------------------------|----------------|---|-----------------------------------|
| D128r2 | 90 | 83 | 86 | 6 | 330 | 45 |
| D128r3 | 90 | 80 | 86 | 8 | 350 | 190 |
| D128r4 | 92 | 86 | 90 | 2 | 330 | 115 |

for $\text{YBa}_2\text{Cu}_3\text{O}_{7-x}$ films formed by the co-evaporation of Y, Cu, and BaF_2 and heat treatment in humidified O_2 after deposition [116]. Further, it can be seen in Table 5-3 that $T_{c,0}$ for all samples was ≥ 80 K and ΔT was less than 10 K. The best value for $T_{c,0}$ did not necessarily correspond to the best values for ΔT and ρ_0 , which was also typical for post-deposition heat treated films [5, 35].

Very similar values and inconsistencies for $T_{c,0}$ and ΔT were reported by Garzon et al. [117] for stoichiometric $\text{YBa}_2\text{Cu}_3\text{O}_{7-x}$ films formed by co-evaporation of Y, BaF_2 , and Cu and post-deposition heat treatment in humidified oxygen. The film fabrication procedure was the same in all cases and yet the film properties were inconsistent, with ΔT values ranging from 3 to 8 K. The inconsistencies were suggested to be due to degradation of the $\text{YBa}_2\text{Cu}_3\text{O}_{7-x}$ by excessively long heat treatments in humidified oxygen.

5.2.2.2 Physical properties of Y-Ba-Cu-O films

After R-T measurements, films were analyzed by X-ray diffraction (XRD) and Scanning Electron Microscopy (SEM), as described in Chapter 3. As-deposited films were dark brown in color and were found by XRD to be amorphous except for the presence of crystalline BaF_2 . The presence of crystalline BaF_2 in as-deposited, sputtered Y-Ba-Cu-O films on nominally unheated substrates was also reported by Liou et al. [77]. The presence of crystalline BaF_2 in the

as-deposited films suggested that BaF_2 had been sputtered from the target as a molecule.

After heat treatment the films were dark black in color. The XRD pattern for sample D128r2 after heat treatment is presented in Figure 5-12, which indicated that the Y-Ba-Cu-O film consisted almost entirely of $\text{YBa}_2\text{Cu}_3\text{O}_{7-x}$ with a (00 ℓ), or c-axis, preferred orientation. This was the expected structure for high-quality $\text{YBa}_2\text{Cu}_3\text{O}_{7-x}$ films [5]. Since the film had a composition of 1:1.7:3.1 and was rich in Cu, compounds such as CuO or $\text{Y}_2\text{Cu}_2\text{O}_5$ might be expected to be present. The unidentified peaks at 28.4° and 64° could not be attributed to any known compounds, but it was probable these peaks were due to one or more compounds which could account for the excess Cu. Similar XRD data were obtained for samples D128r3 and D123r4.

In contrast to the as-deposited films, the presence of BaF_2 in the heat treated films was not detected by XRD data. However, F was detected at concentrations of a few atomic percent by X-ray photoelectron spectroscopy, performed by Buyuklimanli [90], in a heat treated Y-Ba-Cu-O film. The presence of F in the heat treated Y-Ba-Cu-O film suggested that either the BaF_2 had not been completely reduced to BaO, after the reaction given in expression (2.4), or an oxyfluoride had formed on the film surface as suggested by Vasquez et al. [93]. Unreduced BaF_2 , if present, must have generated an XRD signal below the noise level.

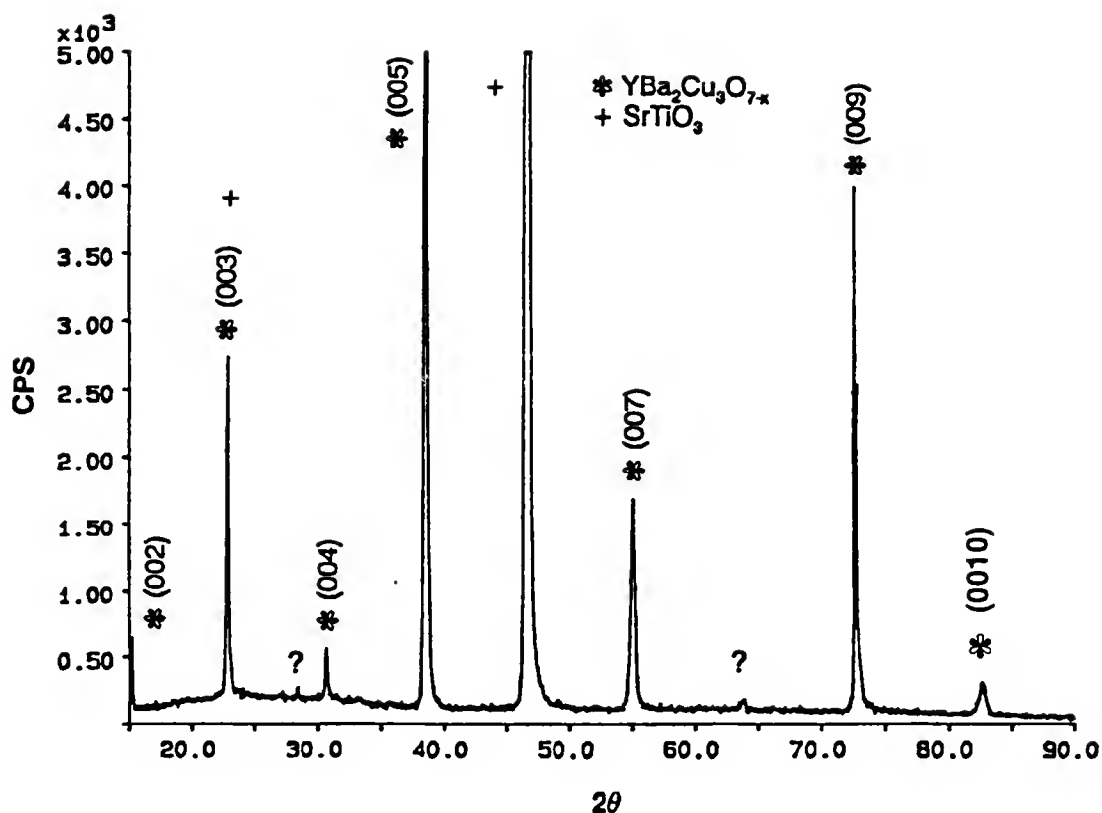


Figure 5-12. XRD data for Y-Ba-Cu-O thin film on SrTiO_3 substrate. The only identifiable peaks in the film are $\text{YBa}_2\text{Cu}_3\text{O}_{7-x}$ (00 ℓ).

The c-axis lattice parameter value has been reported to be correlated with the oxygen concentration and T_c in $\text{YBa}_2\text{Cu}_3\text{O}_{7-x}$ [118]. Specifically, as the oxygen concentration decreased, the c-axis lattice parameter increases and T_c decreased. For bulk Y-Ba-Cu-O samples, the c-axis lattice parameter has been compared directly to the optimal value for fully oxygenated $\text{YBa}_2\text{Cu}_3\text{O}_{7-x}$, 11.68 Å [8], as an indication of the oxygen concentration. In this study, c-axis lattice parameters were determined from (00 ℓ) XRD peaks using a method for diffractometer data described by

Cullity [119]. Briefly, c-axis lattice parameters were calculated from each (00 ℓ) peak using Bragg's law, the values were plotted versus $\cos^2\theta/\sin\theta$, a linear regression was plotted through the calculated values, and the line was extrapolated to zero. The procedure is illustrated for sample D128r2 in Figure 5-13. The calculated c-axis lattice parameters for samples D128r2, D128r3, and D128r4 were 11.71 Å, 11.71 Å, and 11.69 Å, respectively. These values were slightly higher than that for bulk $\text{YBa}_2\text{Cu}_3\text{O}_{7-x}$, 11.68 Å, suggesting the films were not completely oxygenated, which could have contributed to the T_c values being less than the ideal value of 92 K. However, the difference among the lattice parameter values and the optimum bulk value was not larger than the expected error in the values resulting from the resolution limit of the XRD measurement itself, the graphical technique used to determine the values, and probable strain in the films due to thermal expansion mismatch between $\text{YBa}_2\text{Cu}_3\text{O}_{7-x}$ and SrTiO_3 [35, 119]. Thus, based on the XRD data, the effect of incomplete oxidation of $\text{YBa}_2\text{Cu}_3\text{O}_{7-x}$ on the T_c values was not clearly significant. Further, the values for T_{onset} were all close to 90 K, which suggests that the oxygen content for all the films was comparable. The depressed and varying T_c values are suggested to be due to intergranular impurity phases, as discussed below.

A SEM micrograph of the surface of the Y-Ba-Cu-O film from sample D128r2 is presented in Figure 5-14. The film

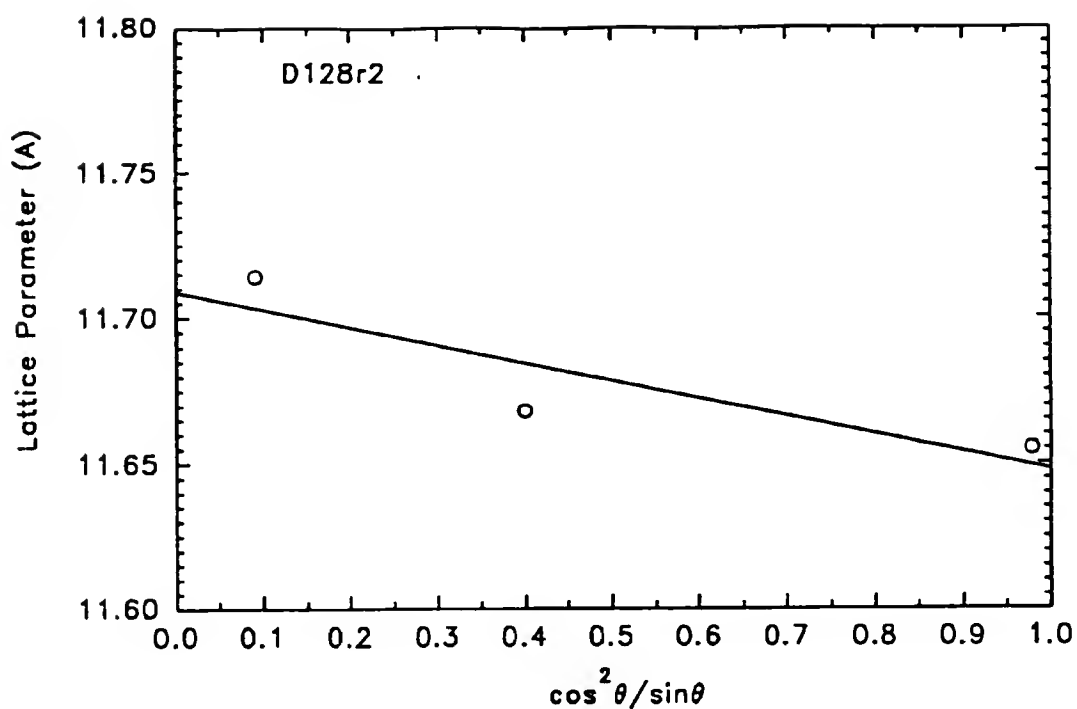


Figure 5-13. Determination of c-axis lattice parameter for $\text{YBa}_2\text{Cu}_3\text{O}_{7-x}$ film on SrTiO_3 substrate.

surface consisted of a mixture of material with a "basketweave" morphology, protruding pebble-grained material, and small boulders. This morphology was also observed for samples D128r3 and D128r4. A similar morphology has been reported by other groups for Y-Ba-Cu-O films formed by the co-evaporation of Cu, Y, and BaF_2 and post-deposition heat treatment in humid oxygen [120, 121, 122]. The pebble-grained structure has been attributed to polycrystalline $\text{YBa}_2\text{Cu}_3\text{O}_{7-x}$ with a preferred orientation of its c-axis parallel to the substrate normal, whereas the basketweave structure has been attributed to $\text{YBa}_2\text{Cu}_3\text{O}_{7-x}$ with

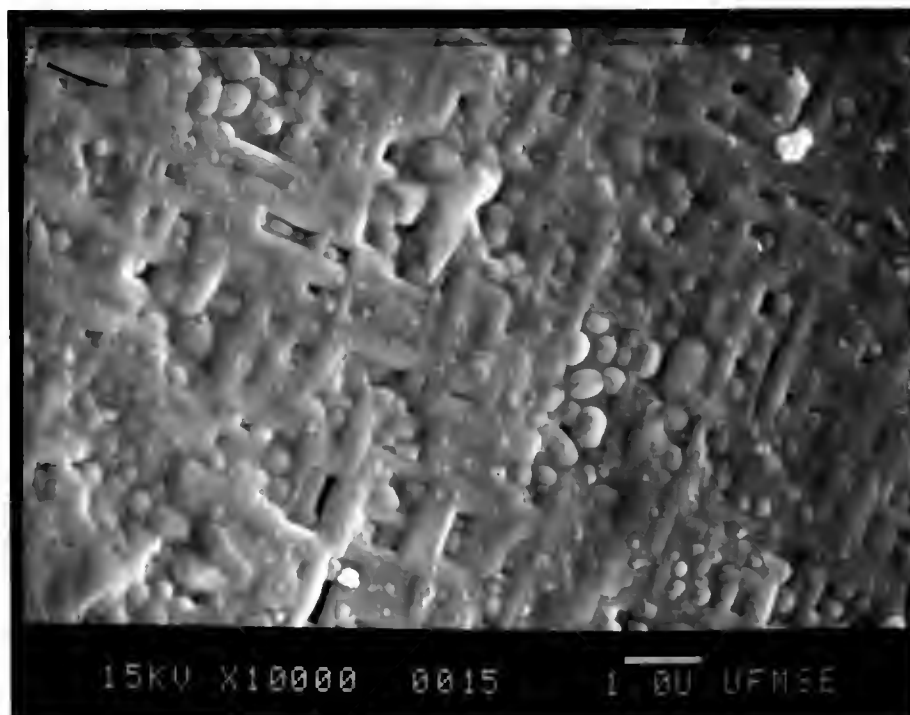


Figure 5-14. SEM micrograph of surface of Y-Ba-Cu-O film from sample D128r2. Present are a mix of pebble-grained c-axis oriented $\text{YBa}_2\text{Cu}_3\text{O}_{7-x}$, basketweave a-axis oriented $\text{YBa}_2\text{Cu}_3\text{O}_{7-x}$, and impurity phase boulders.

its a-axis preferentially oriented parallel to the face of the substrate [62, 122]. The small boulders on the surface of the film in Figure 5-14 were probably due to Cu-rich impurity phases such as CuO , as has been reported by other groups [13, 65, 120, 121] and which would have been consistent with the 1:1.9:3.1 film composition. The impurity phase boulders may have accounted for the unknown peaks in the XRD data in Figure 5-12, but as discussed above these peaks could not be attributed to CuO or other known phases. Additionally, impurity phases have also been reported to

precipitate at or segregate to grain boundaries [123], so the unknown peaks in the XRD data may have produced by material not visible in the SEM micrograph. Finally, distinguishing between pebble-grained $\text{YBa}_2\text{Cu}_3\text{O}_{7-x}$ and impurity phase boulders was difficult.

Although a-axis oriented $\text{YBa}_2\text{Cu}_3\text{O}_{7-x}$ with a basketweave morphology was present on the surface on sample D128r2, as seen in Figure 5-14, no (h00) peaks were present in the XRD data in Figure 5-12. This possibly resulted from the volume of a-axis oriented $\text{YBa}_2\text{Cu}_3\text{O}_{7-x}$ in the films being too small to generate a detectable diffraction intensity. This is supported by reports that a-axis oriented $\text{YBa}_2\text{Cu}_3\text{O}_{7-x}$ with the basketweave structure grows on the surface of c-axis oriented $\text{YBa}_2\text{Cu}_3\text{O}_{7-x}$ films after the c-axis material has reached a critical thickness, which depends strongly on the growth conditions [116, 124]. This was true for $\text{YBa}_2\text{Cu}_3\text{O}_{7-x}$ films co-evaporated from Y, BaF_2 , and Cu sources and heat treated after deposition [116] as well as for films formed *in situ* by sputter deposition onto heated substrates [124]. The reported thickness at which c-axis oriented $\text{YBa}_2\text{Cu}_3\text{O}_{7-x}$ switched over to a-axis oriented material ranged from 2500 Å [116] to over 1 μm [124]. In both cases, if the layer of a-axis oriented material was thin enough, XRD data indicated a film comprised entirely of c-axis oriented $\text{YBa}_2\text{Cu}_3\text{O}_{7-x}$, while SEM analysis found the film surfaces to consist almost entirely of a-axis oriented $\text{YBa}_2\text{Cu}_3\text{O}_{7-x}$. Thus in sample D128r2, the a-axis oriented basketweave $\text{YBa}_2\text{Cu}_3\text{O}_{7-x}$ was

probably confined to the top portion of the film, in which case the volume fraction could be too low for detection by XRD.

In summary, physical characterization showed that the Y-Ba-Cu-O films in samples D128r2, D128r3, and D128r4 were predominantly c-axis oriented $\text{YBa}_2\text{Cu}_3\text{O}_{7-x}$ as evidenced by XRD data, while SEM showed the film surfaces to be comprised of a mix of c-axis oriented $\text{YBa}_2\text{Cu}_3\text{O}_{7-x}$, a-axis oriented $\text{YBa}_2\text{Cu}_3\text{O}_{7-x}$, and possibly impurity phase boulders.

5.2.3 Discussion of Properties of Superconducting Y-Ba-Cu-O Films

The electrical and physical properties of the superconducting Y-Ba-Cu-O films discussed above in this chapter were typical for Y-Ba-Cu-O films subjected to a post-deposition heat treatment in order to form $\text{YBa}_2\text{Cu}_3\text{O}_{7-x}$, and were especially similar to Y-Ba-Cu-O films deposited by the co-evaporation of Y, BaF_2 , and Cu. Common electrical properties for post-deposition heat treated films have included somewhat inconsistent values for T_c of 80 - 90 K, ΔT of 1 - 8 K, and ρ_{rt} in excess of 200 $\mu\Omega\text{cm}$ [5, 35, 105, 116, 120, 121, 122]. Similar physical properties for post-deposition heat treated films have included a somewhat rough, granular film morphology, possibly with regions of a-axis oriented basketweave material, and a strongly c-axis oriented $\text{YBa}_2\text{Cu}_3\text{O}_{7-x}$ structure on lattice-matched substrates such as SrTiO_3 [116, 120, 121, 122]. On the other hand, the

recent *in situ* growth of epitaxial $\text{YBa}_2\text{Cu}_3\text{O}_{7-x}$ films has greatly improved the surface morphology and consistency of the electrical properties of the films. However, even $\text{YBa}_2\text{Cu}_3\text{O}_{7-x}$ films grown by *in situ* sputter deposition suffer, albeit to a lesser degree, from problems of surface roughness and inconsistent electrical properties [13, 64, 65].

The highest quality $\text{YBa}_2\text{Cu}_3\text{O}_{7-x}$ thin films exhibit superconducting properties which include $T_c \geq 90$ K, $\Delta T \leq 1$ K, $\rho_{rt} \approx 180 \mu\Omega\text{cm}$, and $\rho_0 = 0 \mu\Omega\text{cm}$ [5, 7, 13, 64, 65, 66]. The physical properties of such films include a uniform 1:2:3 cation stoichiometry, an oxygen stoichiometry greater than 6.5, an epitaxial, single phase $\text{YBa}_2\text{Cu}_3\text{O}_{7-x}$ crystal structure, and a smooth surface morphology. The correlation between these physical properties and good superconducting properties has been well established, and these properties provide a baseline for comparison.

The films in this study exhibited physical nonidealities including, a cation stoichiometry slightly different from 1:2:3, impurity phases, a granular film structure, a-axis oriented $\text{YBa}_2\text{Cu}_3\text{O}_{7-x}$ on the film surface, and the presence of residual F in unreacted BaF_2 or an oxyfluoride compound. The presence of a large area of exposed grain boundaries area also suggested that atmospheric degradation products would have formed at the grain boundaries, as discussed above. Since a successful theory explaining the mechanism(s) responsible for high

temperature superconductivity in $\text{YBa}_2\text{Cu}_3\text{O}_{7-x}$ has yet to be developed, relating all the physical nonidealities with specific electrical properties is not possible. However, the electrical properties of the films are generally consistent with the physical properties, and some qualitative observations can still be made.

A model published by Halbritter [123] described variations in the resistivity as a function of temperature for $\text{YBa}_2\text{Cu}_3\text{O}_{7-x}$ and related superconducting compounds in terms of increases in intragrain elastic scattering of carriers, increases in grain boundary (intergrain) resistances, and lengthening or area reduction of the current paths. The intragrain scattering was suggested to result from point defects such as impurity atoms and planar defects such as small angle grain boundaries and twins, which would have been dominant in single crystal, epitaxial films. The increases in intergranular resistances were suggested to be due to high angle grain boundaries or impurity phases, which would have had a greater effect than intragranular defects and would have been dominant in polycrystalline, granular films. All of the intragranular and intergranular defects were suggested to contribute to the lengthening or area reduction of the current paths. This model included a larger set of defects than was normally accounted for in the residual resistivity term in Matthiessen's rule for electron conduction in metals [125].

The normal state resistivity values, ρ_{rt} and ρ_0 , of the three superconducting Y-Ba-Cu-O films from this study were higher than those of high quality, *in situ* $\text{YBa}_2\text{Cu}_3\text{O}_{7-x}$ films. This was consistent with the physical properties of the films discussed above, including a granular film structure, the presence of a-axis oriented basketweave material on the film surface, and impurity phases at the grain boundaries. Furthermore, the pebble-grained, c-axis oriented film structure probably contained high angle grain boundaries which acted as scattering sites for carriers between the grains of $\text{YBa}_2\text{Cu}_3\text{O}_{7-x}$ and increased both ρ_{rt} and ρ_0 . Similarly, the open basketweave structure of the a-axis oriented $\text{YBa}_2\text{Cu}_3\text{O}_{7-x}$ certainly contained high angle grain boundaries. This was consistent with the report that a-axis oriented $\text{YBa}_2\text{Cu}_3\text{O}_{7-x}$ films have ρ_{rt} values over four times greater than epitaxial c-axis oriented $\text{YBa}_2\text{Cu}_3\text{O}_{7-x}$ films due to increased grain boundary scattering [126]. The grain boundary areas of both the pebble-grained and basketweave $\text{YBa}_2\text{Cu}_3\text{O}_{7-x}$ probably contained atmospheric degradation products such as $\text{Ba}(\text{OH})_2$ and BaCO_3 , as discussed above, and these compounds would have been electrically insulating. Further, the atmospheric degradation problem would have been worse for the more open-grained structure of the basketweave material. In addition to the atmospheric degradation products, other impurity phases at the grain boundaries could have included a Cu-rich phase and BaF_2 , as discussed above. All of the intergranular impurity phases could have caused increases in

ρ_{rt} and ρ_0 due to increased resistance between the conducting $\text{YBa}_2\text{Cu}_3\text{O}_{7-x}$ grains. The inconsistency in the values of ρ_0 was probably not an anomaly but rather a reflection of a combination the different film compositions and different conditions of atmospheric exposure resulting in the formation of varying amounts of intergranular impurity phases.

The depressed values of $T_{c,0}$ for the superconducting Y-Ba-Cu-O films in this study can also be understood in terms of the physical properties of the films. High angle grain boundaries and intergranular impurity phases would cause weak links between the grains of superconducting $\text{YBa}_2\text{Cu}_3\text{O}_{7-x}$ which would impede the coupling of the superconducting current across the grain boundaries [3]. At temperatures near T_c , the critical current density across the intergranular region would be decreased by the weak links and a lower temperature would be required to overcome thermal fluctuations and maintain the flow of superconducting current [3], i.e. to reach zero resistivity. As a result, rather than a sharp drop in ρ from the value at T_{onset} to zero at $T_{c,0}$, the value of $T_{c,0}$ would be depressed, ΔT would be accordingly increased, and a tail could appear near $T_{c,0}$ in the R-T data. The variation in the values for $T_{c,0}$ and ΔT among the three samples was probably due to the slightly different film compositions and conditions of atmospheric exposure together resulting in the formation of varying amounts of intergranular impurity phases.

An additional cause for the tail in the R-T data near $T_{c,0}$ could have been the high contact resistance between the contact probes and the Y-Ba-Cu-O films. This could have resulted in localized heating and the applied current being in excess of J_c in some regions of the film. The contact resistance between the Pogo contact probes used in the R-T measurement system (see Appendix B) and the Y-Ba-Cu-O films was probably high due to the small contact area. Comparatively, the contact area of other commonly used contacts to $YBa_2Cu_3O_{7-x}$, such as painted or evaporated Ag, would be larger and the contact resistance smaller. Also, if the Pogo contacts had contacted basketweave $YBa_2Cu_3O_{7-x}$ or impurity phases, the contact resistance would be even higher due to the higher resistivity of these materials.

Finally, the processing steps required to improve the properties of the superconducting Y-Ba-Cu-O films formed by the method discussed in this chapter are clear and include reproducibly depositing films with a composition equal to 1:2:3 and optimizing the heat treatment. Further, as discussed in Section 2.1.4, the use of a lowered partial pressure of oxygen during post-deposition heat treatment has been reported to permit the use of lower temperatures and produce high quality $YBa_2Cu_3O_{7-x}$ films with improved surface morphology [74]. Experiments to implement these processing improvements are discussed in Chapter 7.

5.3 Summary

Thin films of Y-Ba-Cu-O were sputter deposited from sputter targets of a variety of compositions and heat treatments in an effort to reproducibly deposit films with a 1:2:3 composition. The targets were prepared from Y_2O_3 , CuO, and $BaCO_3$, BaO_2 or BaF_2 . Thin films were deposited by RF planar magnetron sputtering onto unheated silicon substrates. Electron microprobe analysis showed that films from targets using BaO_2 and $BaCO_3$ precursors were strongly Ba deficient and had poor run-to-run reproducibility, whereas for targets using a BaF_2 precursor films were slightly Y deficient and had improved run-to-run reproducibility. Target compositions were compensated to bring the film composition towards 1:2:3, but for targets using $BaCO_3$ and BaO_2 this was difficult. As suggested by the negative SIMS study presented in Chapter 4, the use of a BaF_2 precursor alleviated the Ba deficiency caused by O^- resputtering. Also, the use of BaF_2 was found to improve the correlation between film and target composition, compositional reproducibility and uniformity. The deviations in film compositions from target compositions were discussed in terms of resputtering by negative oxygen ions and mass-dependent angular distribution of species. The atmospheric stability of the target compounds was suggested to be an important factor determining the run-to-run reproducibility of the film composition.

As discussed in Chapter 2, the negative ion resputtering problem for the composition of sputter deposited Y-Ba-Cu-O films has been almost exclusively addressed in the literature by assuming that the high yield of O^- from $YBa_2Cu_3O_{7-x}$ targets was inevitable. The desired film compositions have been obtained by avoiding the impingement of energetic O^- on the substrate. In contrast, the combined results of this chapter and Chapter 4 have shown that rather than avoiding resputtering by O^- , the desired Y-Ba-Cu-O film composition can be obtained by controlling the yield of O^- from the target, which can be accomplished by the proper selection of target material(s).

Superconducting $YBa_2Cu_3O_{7-x}$ films were fabricated by sputter depositing from a Y_2O_3 - BaF_2 -CuO target with a 1:1.6:2.2 composition and heat treating after deposition at 900 °C in humidified oxygen. The films were characterized by resistivity versus temperature measurements, X-ray diffraction, and SEM. The superconducting properties of the films were typical of post-deposition heat treated films, with $T_{c,0} \geq 80$ K and $\Delta T \leq 8$ K. The nonidealities were discussed in terms of the presence of intergranular impurity phases in and the microstructure of the $YBa_2Cu_3O_{7-x}$ films.

CHAPTER 6

STRONTIUM TITANATE BARRIER LAYERS FOR Y-Ba-Cu-O FILMS ON SILICON AND SAPPHIRE SUBSTRATES

In this chapter is presented a study of the suitability of SrTiO_3 as a barrier layer material for the growth of superconducting Y-Ba-Cu-O films on silicon and sapphire substrates. As discussed above in Chapter 2, SrTiO_3 was chosen as a candidate barrier layer material since it is a very good bulk substrate material for the growth of high quality, superconducting $\text{YBa}_2\text{Cu}_3\text{O}_{7-x}$ films, combining good lattice matching with good chemical stability with respect to $\text{YBa}_2\text{Cu}_3\text{O}_{7-x}$. The possibility of combining one of the best substrate materials for $\text{YBa}_2\text{Cu}_3\text{O}_{7-x}$ with the most important semiconductor substrate, Si, was the motivation. This study is the first report of SrTiO_3 barrier layers for Y-Ba-Cu-O on Si, although one group had reported the use of SrTiO_3 barrier layers for Y-Ba-Cu-O films on sapphire [127]. This latter report only made a short mention of the ineffectiveness of SrTiO_3 barriers on preventing interaction between Y-Ba-Cu-O and sapphire, and no details were given.

6.1 Sample Fabrication

As discussed in Chapter 3, the Y-Ba-Cu-O and SrTiO₃ films were both deposited by RF planar magnetron sputter deposition in the same multi-source sputter deposition system. Each target was mounted in its own sputter source. For all depositions, the substrate-target distance was 6 cm and the substrates were nominally unheated and electrically floating. The (100) Si and (11 $\bar{2}$ 0) sapphire (also called A-plane sapphire) substrates were cleaned as described in Chapter 3. For SrTiO₃ deposition, a RF power of 100 W was used in conjunction with a total sputter gas pressure of 10 mTorr. The sputter gas was 10% O₂ with the balance being Ar. Attempts at depositing SrTiO₃ with 100% Ar sputter gas resulted in highly stressed films which exfoliated, presumably due to an oxygen deficiency in the film. The addition of oxygen to the sputter gas alleviated the exfoliation problem. The resulting deposition rate was 40 - 50 Å/min and the SrTiO₃ film thickness, depending on the length of the deposition, was 0.4 - 1.0 μm.

On some samples, only SrTiO₃ was deposited in order to study the properties of the SrTiO₃ films. To determine the effectiveness of SrTiO₃ on preventing interaction between Y-Ba-Cu-O and the substrates, Y-Ba-Cu-O films were deposited on top of the SrTiO₃ layers using a target with a Y:Ba:Cu composition of 1:4:4. The Y-Ba-Cu-O films were deposited

immediately after the SrTiO_3 layer without breaking vacuum. The target, identified in Table 5-1 and Chapter 5 as BaO_2 -144, was formed from starting compounds of Y_2O_3 , BaO , and CuO and fired in air at 800°C , resulting in BaCuO_2 and Y_2O_3 phases being present. The Y-Ba-Cu-O deposition parameters were identical to those used throughout this study, namely, 50 W RF and 10 mTorr Ar. The YBCO film thicknesses were $0.6 - 1.0\ \mu\text{m}$. As presented in Table 5-2, the Y-Ba-Cu-O films deposited from the BaO_2 -144 target had an average Y:Ba:Cu composition of 1.0:1.9:4.8.

The samples were removed from the deposition chamber, loaded onto a quartz boat, and placed in a tube furnace within 5 minutes. The heat treatment, performed in flowing dry O_2 , consisted of a ramp from room temperature to 850°C in 60 minutes, 60 minutes at 850°C , and a slow natural furnace cooling to below 150°C in about 12 hours.

Later in the course of this study a successful process for the growth of superconducting $\text{YBa}_2\text{Cu}_3\text{O}_{7-x}$ films on SrTiO_3 substrates had been established using a BaF_2 -based Y-Ba-Cu-O target and a post-deposition anneal in wet oxygen, as discussed above in Chapter 5. One Y-Ba-Cu-O deposition was performed using the BaF_2 -based 1:1.6:2.0 target shown in Chapter 5 to result in a composition close to 1:2:3 and good quality $\text{YBa}_2\text{Cu}_3\text{O}_{7-x}$ films on SrTiO_3 substrates. The Y-Ba-Cu-O-F films were deposited on a SrTiO_3 barrier layer on Si as discussed above. These samples were characterized

to determine if the starting film composition, the presence of BaF_2 , and/or the wet oxygen anneal at 900 °C had any effects on SrTiO_3 's ability to prevent interaction between a Y-Ba-Cu-O film and a Si substrate.

6.2 Results And Discussion

6.2.1 Y-Ba-Cu-O on Si or Sapphire Without A Barrier Layer

As-deposited Y-Ba-Cu-O films were found by four point probe measurements to be electrically insulating. Auger depth profiles of as-deposited samples showed all components to be uniformly distributed with depth, indicating that no reaction between Y-Ba-Cu-O and Si or sapphire had occurred during deposition.

After heat treatment of Y-Ba-Cu-O/Si at 850 °C, four point probe resistivity data showed the Y-Ba-Cu-O films to still be electrically insulating. In agreement with reported results [97], Ba was found to have piled up at the Si interface due to the formation of BaSiO_3 , as confirmed by AES depth profile and XRD data. The Cu-Si interfacial phases reported by Lee et al. [99] were not observed in the XRD data. In Figure 6-1 is presented an AES sputter-crater line scan across the Y-Ba-Cu-O/Si interface, in which the build-up of Ba at the interface is clearly illustrated. Peak-to-peak intensity data rather than corrected composition data are reported since Y's low sensitivity

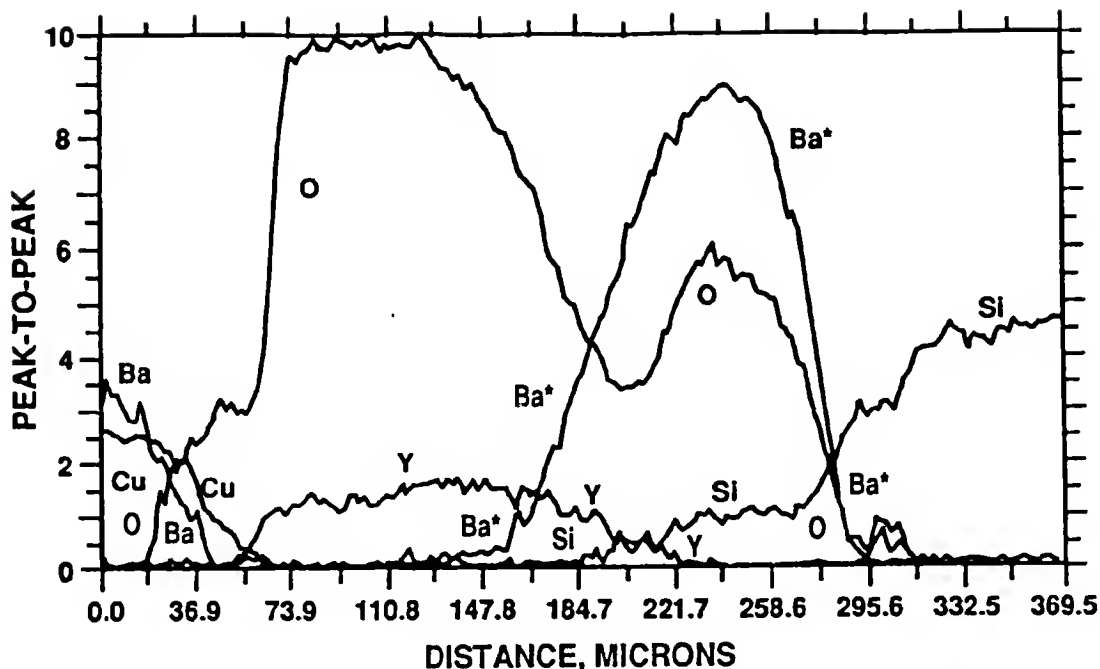


Figure 6-1. AES sputter crater line profile across the interface of Y-Ba-Cu-O/Si heat treated at 850 °C.

factor makes its detection difficult. The sputter-crater line scan was used instead of a conventional depth profile to minimize problems with charging. Because of Ba's reaction with Si, its peak energy in the interfacial layer was shifted enough to make detection of Ba at both the interface and in the Y-Ba-Cu-O film difficult when using a multiplex window. The energy of the peak for reacted Ba, designated Ba*, was determined by an AES survey at the Y-Ba-Cu-O/Si interface. A shift in the Ba peak energy of about 7 eV was common.

For Y-Ba-Cu-O/sapphire samples heat treated at 850 °C, XRD and AES data indicated the formation of an interfacial BaAl_2O_4 layer, in agreement with reported data [95]. The AES

data in Figure 6-2 clearly illustrates that Ba piled up at the sapphire interface and the Ba peak shifted as the Ba-containing compound changed from $\text{YBa}_2\text{Cu}_3\text{O}_{7-x}$ to BaAl_2O_4 . Also, the AES data illustrate that Al diffused into the overlayer film, but only as far the extent of the interfacial BaAl_2O_4 layer. The XRD data also confirmed the presence of $\text{YBa}_2\text{Cu}_3\text{O}_{7-x}$ and CuO , but no preferred orientation of the $\text{YBa}_2\text{Cu}_3\text{O}_{7-x}$ was found. Room temperature four point probe data found the Y-Ba-Cu-O film to be conducting with a resistivity of $\approx 0.02 \text{ } \Omega\text{cm}$. Resistance versus temperature tests for T_c were not performed, but the relatively high value of room temperature resistivity suggested that tetragonal semiconducting $\text{YBa}_2\text{Cu}_3\text{O}_{7-x}$ was present rather than orthorhombic superconducting $\text{YBa}_2\text{Cu}_3\text{O}_{7-x}$.

It is important to note that the reaction between Y-Ba-Cu-O and sapphire for a 850 °C heat treatment was limited in depth to a few thousand Angstroms. Therefore a sufficiently thick Y-Ba-Cu-O film on sapphire (e.g. $\geq 1 \text{ } \mu\text{m}$) could result in a superconducting transition in the top section of the film, where Al had not diffused or reacted. This explains why many early reports indicated that sapphire was a stable substrate for the growth of superconducting $\text{YBa}_2\text{Cu}_3\text{O}_{7-x}$ by post-deposition annealing. In these studies the Y-Ba-Cu-O thickness was typically 1 μm or greater, which was sufficient to result in both a non-superconducting interface reaction layer plus an unreacted superconducting surface

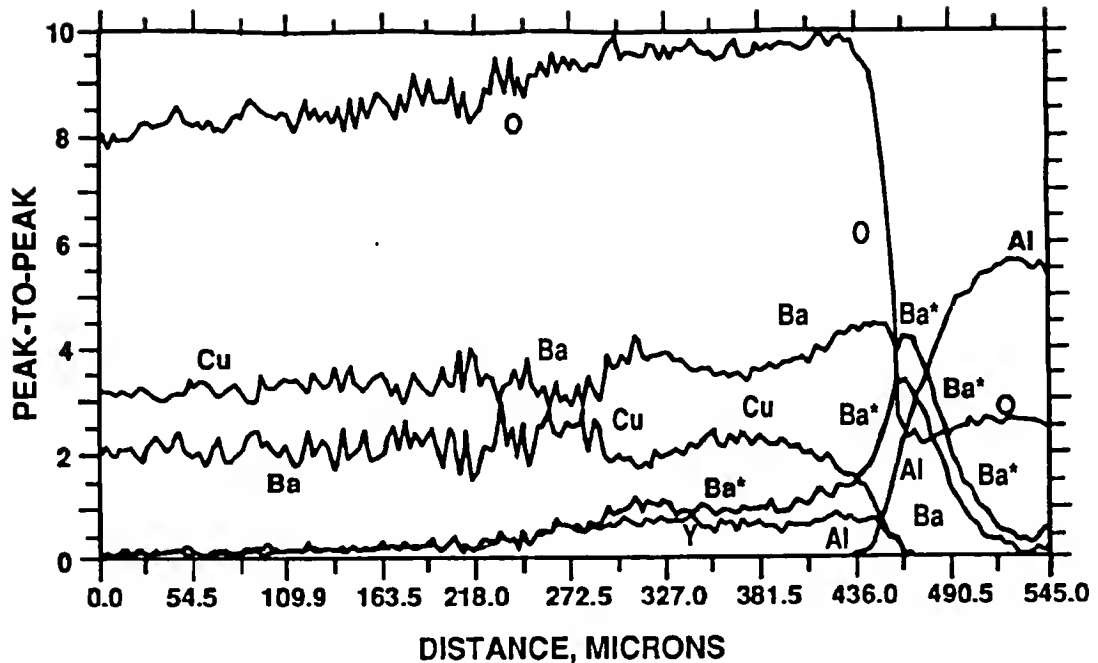


Figure 6-2. AES sputter crater line profile of Y-Ba-Cu-O/sapphire interface after 850 °C heat treatment.

layer. It is probable that the interface reaction layer would adversely influence the J_c .

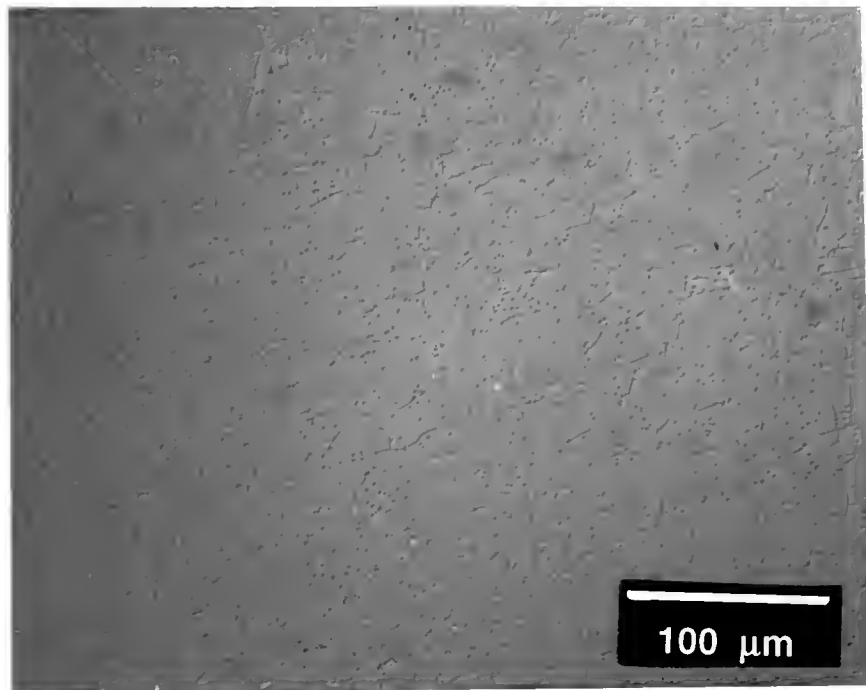
6.2.2 SrTiO₃ Films on Si and Sapphire Substrates

The composition of as-deposited SrTiO₃ films was verified by EPMA data to have a Sr:Ti ratio equal to 1:1. Films of SrTiO₃ thicker than 0.5 μm sometimes exhibited microcracks, blisters, and even exfoliation, particularly after heating on sapphire. Even well-adhering, 0.4 μm thick SrTiO₃ films on Si exhibited features which in optical microscopy appeared to be microcracks and blisters, as shown in Figure 6-3a. The "microcracks" observed with optical

microscopy were oriented randomly and criss-crossed to form cell-like areas 10 to 50 μm wide. However, under SEM examination these features were not observed to emerge at the surface, as illustrated by the micrograph in Figure 6-3b. This suggests that the features were possibly stress ridges or delaminations at the Si interface which were visible through the transparent SrTiO_3 with optical microscopy. The SEM data showed that the SrTiO_3 films were continuous, which supported AES data, discussed below, that indicated that SrTiO_3 was a barrier layer which resisted reactions between Y-Ba-Cu-O and the substrate.

Stress in the as-deposited SrTiO_3 was greatly reduced by adding 10% O_2 to the Ar sputter gas, as noted above. Heating the substrate during SrTiO_3 deposition would likely have reduced the stress as has been reported to occur for other thin films [128], but this was not attempted in this study.

On sapphire substrates, SrTiO_3 films were barely visible due to their high degree of transparency. No strongly preferred orientation for SrTiO_3 was observed in XRD data for either as-deposited or 850 $^\circ\text{C}$ heat treated films, the latter of which is illustrated in Figure 6-4. The XRD data for SrTiO_3 were nearly the same as the bulk JCPDS data for SrTiO_3 , except for a slightly larger intensity of the (200) peak. From AES data for a heat treated sample, a small amount of Al may have diffused about 0.05 μm into the



(a)



(b)

Figure 6-3. Optical micrograph (a) of SrTiO₃ film on Si showing apparent microcracks in the SrTiO₃, and SEM micrograph (b) of same region indicating no microcracks emerging at the SrTiO₃ surface.

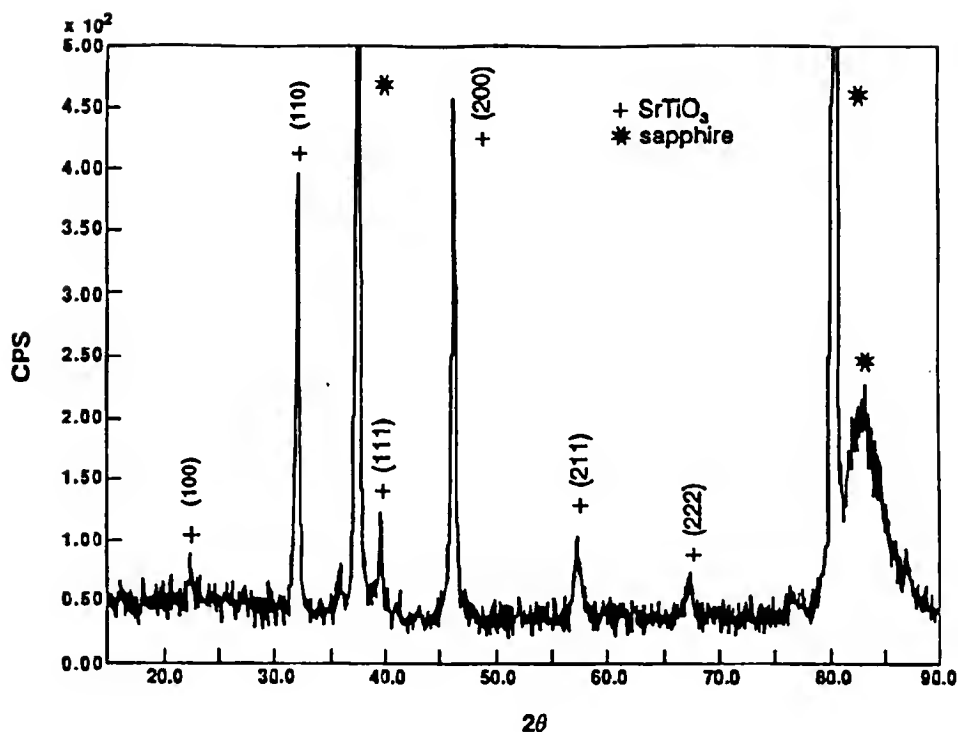


Figure 6-4. XRD data for SrTiO_3 film on sapphire substrate after 850 °C heat treatment. No strongly preferred growth orientation of the SrTiO_3 is observed.

0.4 μm SrTiO_3 thick film. The extent of this interaction was certainly far less than was seen for Y-Ba-Cu-O on sapphire. No reaction phases were detected in the XRD data in Figure 6-4, but it was possible that the diffracted intensity of such thin interfacial phases, was below noise level in the XRD data. Thus, SrTiO_3 was stable on sapphire and it could prevent interaction of Y-Ba-Cu-O and sapphire.

The fact that SrTiO_3 did not grow with a preferred orientation on A-plane sapphire is not surprising. Sapphire has a rhombohedral primitive cell, which is usually described using a simpler hexagonal representation, with

lattice parameters of $a' = 4.763 \text{ \AA}$ and $c' = 13.003 \text{ \AA}$ [129]. The face of A-plane sapphire substrates has tetragonal symmetry versus cubic symmetry for (100) SrTiO_3 , and the lattice mismatch between the $(11\bar{2}0)$ face of sapphire and (100) SrTiO_3 is 10% along $\langle 0001 \rangle$ directions. This mismatch is too large for the growth of epitaxial (100) SrTiO_3 films. Similarly, the mismatch for (110) SrTiO_3 is 9.9% along the $\langle 0001 \rangle$ directions on the face of A-plane sapphire. R-plane sapphire substrates, with a $(1\bar{1}02)$ orientation, have been found to be suitable for epitaxial growth of yttria-stabilized zirconia barrier layers [101] and also reasonable quality epitaxial $\text{YBa}_2\text{Cu}_3\text{O}_{7-x}$ films [103]. Thus it is likely that R-plane sapphire is suitable for textured or even epitaxial growth of (100) SrTiO_3 . This sapphire orientation may be useful for future study.

On Si substrates, AES depth profiling of SrTiO_3 after 850 °C heat treatment indicated no intermixing of components at the interface. In particular, no Si was found in the SrTiO_3 film. Non-reaction at the interface was supported by XRD data shown in Figure 6-5, in which no reaction products and only SrTiO_3 and Si were detected. This was in strong contrast to the case of Y-Ba-Cu-O on Si illustrated in Figure 6-1. Hence it appears that SrTiO_3 could prevent interaction of Si and Y-Ba-Cu-O.

In the as-deposited condition, SrTiO_3 films on (100) Si substrates exhibited textures with a very strong preferred

orientation of the (111) plane parallel to the face of the (100) Si substrate, as shown by the XRD data in Figure 6-5. From JCPDS powder diffraction data files, randomly oriented SrTiO_3 would have exhibited a maximum intensity for the (110) peak, while the (111) peak would only have been the fourth most intense peak with an intensity ratio $I_{(111)}/I_{(110)}$ of 0.30. However, the intensity of the (111) peak was much greater than that of any other peak. This textured growth of SrTiO_3 on Si was encouraging since it offered the possibility of the growth of textured or even epitaxial $\text{YBa}_2\text{Cu}_3\text{O}_{7-x}$ films.

The reason for the strong SrTiO_3 texture on Si is uncertain. Silicon has a diamond cubic crystal structure with a lattice parameter of 5.43 Å, while SrTiO_3 has a cubic crystal structure with a lattice parameter of 3.905 Å [129]. The lattice parameter for the (100) Si face is 5.43 Å, whereas the lattice parameter for the (111) face of SrTiO_3 is 5.52 Å. Thus the lattice mismatch between (100) Si and (111) SrTiO_3 is only 1.7%, suggesting that the (111) texture of SrTiO_3 may be due to registry between the atoms in the SrTiO_3 film and those on the surface of the Si substrate. However, the lattice matching is not very good since the (100) Si face has cubic symmetry whereas the (111) face of SrTiO_3 has hexagonal symmetry. Thus there is not good one-to-one matching for the atom positions, and many atom planes would need to be terminated by a misfit dislocation

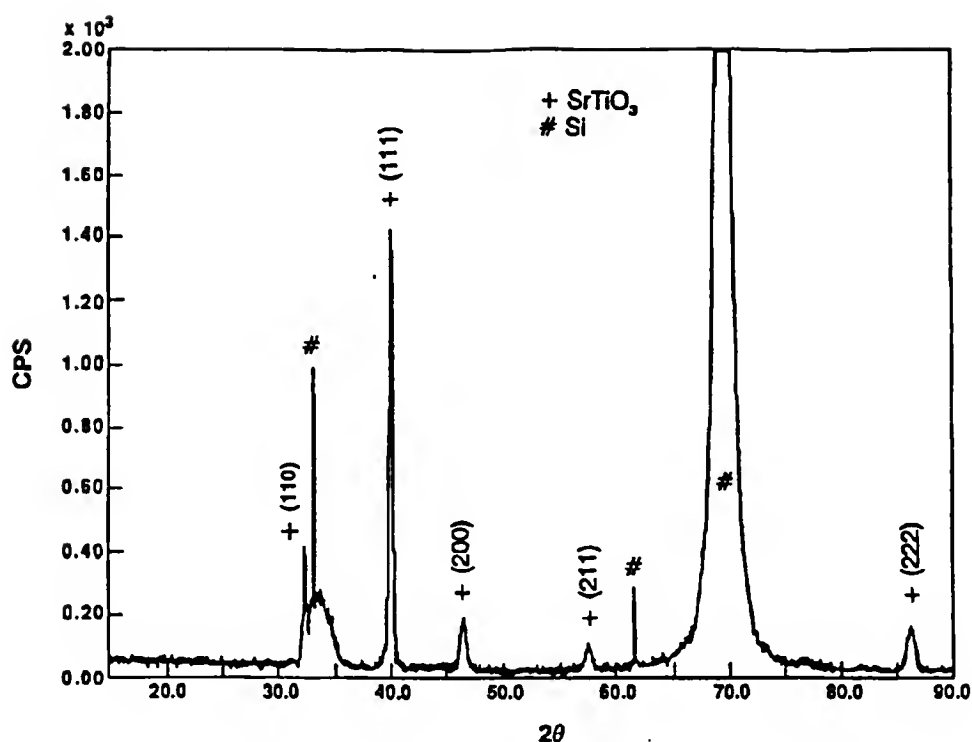


Figure 6-5. XRD data for SrTiO_3 film on (100) Si substrate, indicating strongly preferred (111) growth orientation of SrTiO_3 .

network. Thus it is unlikely that (111) preferred orientation of the SrTiO_3 film was due to registry with the Si substrate. Furthermore, approximately 10 Å of amorphous native oxide was present on the Si surface prior to the deposition of SrTiO_3 , which may have prevented any atom matching between SrTiO_3 and Si, as required for an epitaxial relationship. On the other hand, metallic Ti would be expected to reduce the native SiO_2 , especially in conjunction with the impingement of energetic particles on the substrate during sputtering. However, the Ti was oxidized and the SiO_2 would be expected to prevent atomic registry between (111) SrTiO_3 and (100) Si.

The growth of SrTiO_3 with a (111) preferred orientation on (100) Si could have been caused by surface energy effects, similar to other cubic materials, such as Al [130]. A (111) texturing is observed for the growth of Al on amorphous SiO_2 , in which atomic registry is clearly not possible. This (111) texture is attributed to the fact that the (111) face has the lowest free energy, since the atomic packing is the tightest on the close-packed plane. This surface energy effect is probably the reason that SrTiO_3 grew with a (111) preferred orientation on Si (100).

The lattice mismatch between (110) Si and the (110) face of SrTiO_3 is small since SrTiO_3 aligns well with Si along $\langle 100 \rangle$ directions, while two cells of (110) SrTiO_3 align nicely with one cell of (110) Si along the $\langle 110 \rangle$ directions. The lattice mismatch is 1.6% along $\langle 100 \rangle$ directions and 1.7% along the perpendicular direction where two SrTiO_3 cells align with a single Si cell. Thus the atomic registry and possibility for epitaxial growth of a (110) SrTiO_3 film on (110) Si are good. This effort is suggested as a profitable direction for future studies.

6.2.3 Y-Ba-Cu-O/ SrTiO_3 /Sapphire

In the as-deposited condition, the Y-Ba-Cu-O films on SrTiO_3 barrier layers on sapphire substrates were amorphous and insulating, and AES and XRD data were consistent with no interaction between any of the film or substrate components.

After heat treatment at 850 °C, the Y-Ba-Cu-O films were conducting with a room temperature resistivity of about 0.02 Ωcm . As illustrated by the AES depth profile in Figure 6-6, SrTiO_3 was found to prevent reaction between Y-Ba-Cu-O and sapphire. In contrast to Y-Ba-Cu-O directly on sapphire (Figure 6-2), Al in the Y-Ba-Cu-O film was below the AES detection limit of $\approx 1\%$. In addition, Ba was found only in the Y-Ba-Cu-O layer. The large drop in all of the profiles at the Y-Ba-Cu-O/ SrTiO_3 interface is due to substrate charging at the interface, and the apparent Ti buildup is really an artifact of this charging. The AES data were consistent with XRD data since BaAl_2O_4 was not detected while $\text{YBa}_2\text{Cu}_3\text{O}_{7-x}$, CuO, SrTiO_3 and sapphire were detected. The CuO was present because the Y-Ba-Cu-O film composition was not equal to 1:2:3. Also, no preferred orientation of the Y-Ba-Cu-O film was found by XRD, as expected from the lack of textured growth of SrTiO_3 on the A-plane sapphire.

The AES data in Figure 6-6 also show that Al migrated into the SrTiO_3 layer a distance of 0.2 μm into the 0.4 μm thick layer. This distance was greater than the extent to which Al moved into SrTiO_3 without an overlaying Y-Ba-Cu-O film (see section 6.2.2). The additional penetration of the Al into the SrTiO_3 may have been due to the presence of Y-Ba-Cu-O providing a driving force, with Al seeking to form BaAl_2O_4 . An alternative explanation is that both "apparent

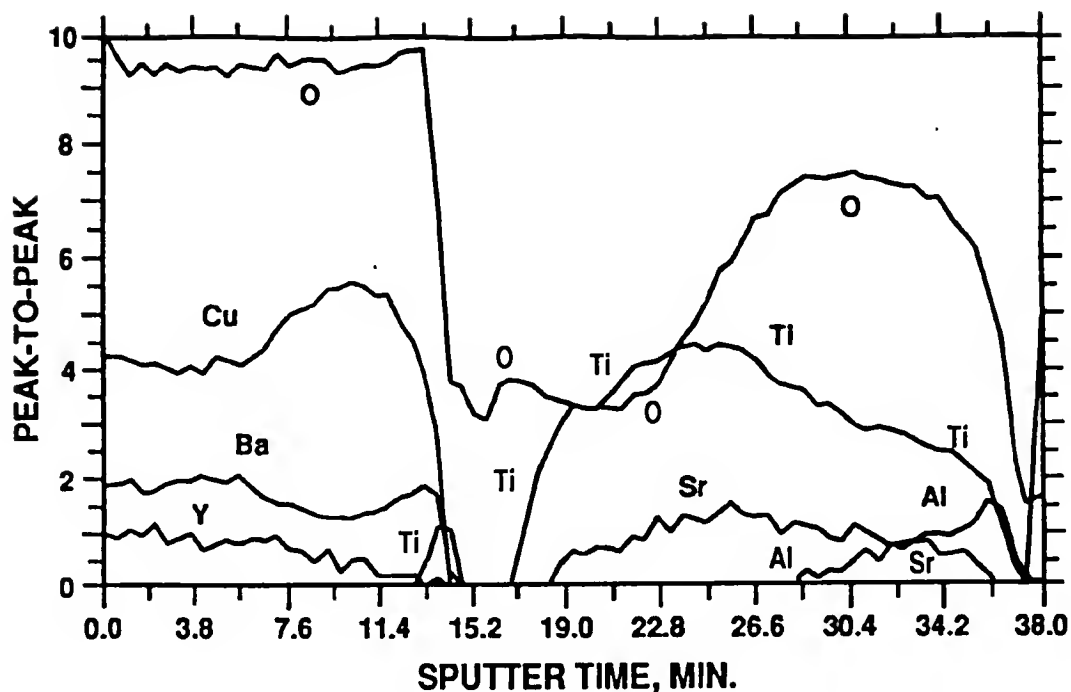


Figure 6-6. AES depth profile for Y-Ba-Cu-O/SrTiO₃/sapphire after 850 °C heat treatment.

penetrations" result from interface roughness. The data are not sufficient to prove one or the other hypotheses.

Resistance versus temperature tests of the Y-Ba-Cu-O films on SrTiO₃/sapphire indicated that the films were not superconducting even down to 77 K. Rather, the Y-Ba-Cu-O exhibited a semiconducting R-T behavior, with resistance increasing with decreasing temperature. This was consistent with the R-T data for Y-Ba-Cu-O films deposited from the same BaO₂-144 target onto SrTiO₃ substrates, as discussed in Chapter 5. Apparently the non-stoichiometric film composition, in combination with inadequate post-deposition heat treatment, prevented the formation of superconducting orthorhombic YBa₂Cu₃O_{7-x}. The semiconducting R-T data were

consistent with the presence of both tetragonal $\text{YBa}_2\text{Cu}_3\text{O}_{7-x}$ and CuO , which were identified by XRD data. Thus, the lack of a superconducting Y-Ba-Cu-O did not imply that SrTiO_3 was not a suitable barrier layer for sapphire substrates. Rather, the Y-Ba-Cu-O growth process used for this experiment was not adequate to produce superconducting films. Therefore, SrTiO_3 was an effective barrier layer and prevented interactions between Y-Ba-Cu-O and sapphire.

6.2.4 Y-Ba-Cu-O/ SrTiO_3 /Si

In the as-deposited condition, the Y-Ba-Cu-O films were insulating and both AES and XRD data indicated that no interactions had occurred between Y-Ba-Cu-O and Si. After heat treatment at 850 °C, as shown in the AES depth profile in Figure 6-7, SrTiO_3 prevented the interaction of Y, Cu, and Si, but allowed Ba to accumulate at the Si interface. X-ray diffraction data confirmed the formation of BaSiO_3 . The oxygen intensity at the Y-Ba-Cu-O/ SrTiO_3 interface drops suddenly due to sample charging at the interface. The depth profile also shows that Ba is depleted from the Y-Ba-Cu-O layer, and is concentrated at and into the SrTiO_3 layer at both the Y-Ba-Cu-O/ SrTiO_3 and SrTiO_3 /Si interfaces. This Ba profile is consistent with the fact that BaTiO_3 forms a complete solid solution with SrTiO_3 [131]. Hence Ba probably diffused through the SrTiO_3 layer, and did not simply pass through the apparent microcracks discussed above in Section

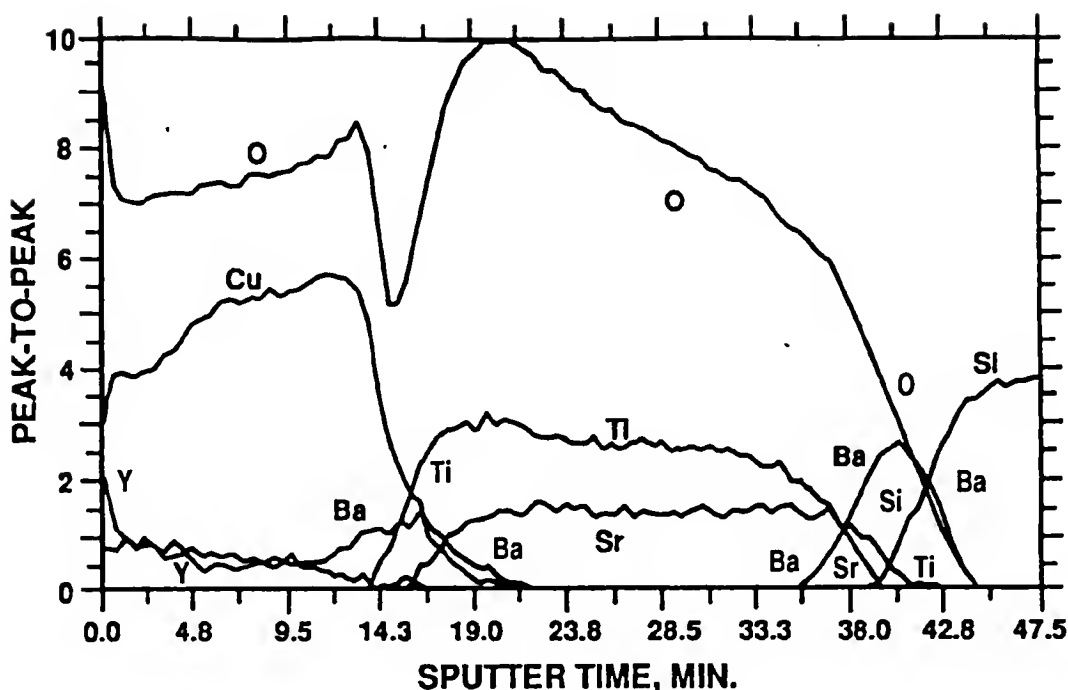


Figure 6-7. AES depth profile for Y-Ba-Cu-O/SrTiO₃/Si after 850 °C heat treatment.

6.2.2. This was confirmed by an AES line scan along 200 μm of the surface, which showed a uniform concentration of Ba or Si. No areas of high concentration were seen, as would have been expected if cracks were the transport path.

In addition to a relatively small amount of tetragonal $\text{YBa}_2\text{Cu}_3\text{O}_{7-x}$, $\text{Y}_2\text{Cu}_2\text{O}_5$ and CuO phases were detected by XRD. The presence of $\text{Y}_2\text{Cu}_2\text{O}_5$ is consistent with Ba depletion from the initially Cu-rich Y-Ba-Cu-O film, as suggested by the AES data in Figure 6-7. The presence of CuO was expected from the initial Y-Ba-Cu-O film composition of approximately 1:1.9:4.8.

In contrast to the data for 850 °C heat treated Y-Ba-Cu-O on Si, room temperature resistivity data showed that Y-Ba-Cu-O with a SrTiO₃ barrier layer was much more conducting with resistivities ranging from 0.03 to 100 Ωcm. These values were reasonable considering the presence of CuO and tetragonal YBa₂Cu₃O_{7-x}, which are both semiconducting. Resistance versus temperature data showed that the Y-Ba-Cu-O films were not superconducting down to 77 K. This was attributed to the depletion of Ba from and excess Cu in the Y-Ba-Cu-O film.

The results for Y-Ba-Cu-O/SrTiO₃/Si samples where the Y-Ba-Cu-O film was deposited from a BaF₂-based target were basically the same. Neither the presence of BaF₂ in the as-deposited film or the wet oxygen heat treatment at 900 °C prevented diffusion of Ba through the SrTiO₃ to the Si interface where it formed BaSiO₃. This was verified by AES depth profile and XRD data. The sequence of events during heat treatment with BaF₂ in the film were undoubtedly much different than with oxide targets. With fluoride targets, BaF₂ would first have been reduced in wet oxygen resulting in Ba being available for diffusion through the SrTiO₃ layer, since BaF₂ was found to be stable on Si to 900 °C in dry oxygen. However, diffusion was observed in both cases.

The data from Y-Ba-Cu-O films deposited from a BaF₂-based target were also interesting since they showed that the conclusions were the same for either a

stoichiometric or nonstoichiometric Y-Ba-Cu-O film. The extra Cu in these 1:1.9:4.8 stoichiometry films, present as CuO, did not prevent reaction of Ba in Y-Ba-Cu-O with the Si substrate. Further, a reaction with CuO was not observed. Hence the results for the barrier layer studies presented in this chapter are valid for Y-Ba-Cu-O films with a variety of stoichiometries.

Thus a 0.4 μm thick SrTiO_3 layer does not prevent but does limit the reaction between Y-Ba-Cu-O and Si during post-deposition heat treatments of 850 $^{\circ}\text{C}$ or above. This study suggests that successful barrier layer choices for Si substrates should, among other properties, have a low solubility for the components of Y-Ba-Cu-O, particularly Ba.

As discussed in Chapter 2, most present processes for the growth of superconducting $\text{YBa}_2\text{Cu}_3\text{O}_{7-x}$ films utilize an elevated substrate temperature of 650 - 800 $^{\circ}\text{C}$, followed by *in situ* cooling in oxygen to form orthorhombic $\text{YBa}_2\text{Cu}_3\text{O}_{7-x}$. Typical substrate temperatures for *in situ* deposition are about 150 $^{\circ}\text{C}$ lower than the temperatures used for post-deposition anneals. At these lower temperatures, it is possible that a SrTiO_3 layer may prevent the interaction of Y-Ba-Cu-O and Si. Thus it may be possible to determine the properties of superconducting $\text{YBa}_2\text{Cu}_3\text{O}_{7-x}$ films grown on the strongly (111) textured SrTiO_3 barrier layers on (100) Si substrates. This is suggested for future work in Chapter 7. However, it is doubtful that (111) textured SrTiO_3 would

provide a suitable surface for the growth of $\text{YBa}_2\text{Cu}_3\text{O}_{7-x}$ with the desired (00 ℓ) orientation. The situation is analogous to that discussed above in section 6.2.2 for the growth of (111) SrTiO_3 on (100) Si. The atomic arrangement of the face of (111) SrTiO_3 has hexagonal symmetry whereas the (00 ℓ) faces of $\text{YBa}_2\text{Cu}_3\text{O}_{7-x}$ have cubic symmetry. Thus the atomic registry required for the epitaxial growth of $\text{YBa}_2\text{Cu}_3\text{O}_{7-x}$ is unlikely on (111) SrTiO_3 .

As discussed in section 6.2.2, a (110) Si substrate would make a suitable substrate for epitaxial growth of a (110) SrTiO_3 film. Furthermore, a (110) oriented SrTiO_3 would be suitable for the growth of (h00) or "a-axis" oriented $\text{YBa}_2\text{Cu}_3\text{O}_{7-x}$ since the atomic arrangements are correct and the lattice match is reasonably good. The mismatch between the c axis of $\text{YBa}_2\text{Cu}_3\text{O}_{7-x}$ (see Figure 1-1) and two cells of (110) SrTiO_3 along $\langle 110 \rangle$ directions is about 5.8% and the mismatch between the b axis of $\text{YBa}_2\text{Cu}_3\text{O}_{7-x}$ and $\langle 001 \rangle$ directions on the (110) face of SrTiO_3 is about 0.4%. The 5.8% mismatch figure may seem high, but this is less than the 7% mismatch between (00 ℓ) $\text{YBa}_2\text{Cu}_3\text{O}_{7-x}$ and (100) MgO, a combination which results in high quality, superconducting $\text{YBa}_2\text{Cu}_3\text{O}_{7-x}$ films [13]. Thus it may be possible to grow epitaxial, a-axis oriented $\text{YBa}_2\text{Cu}_3\text{O}_{7-x}$ films on epitaxial (110) SrTiO_3 layers on (110) Si substrates using an *in situ* growth process for the $\text{YBa}_2\text{Cu}_3\text{O}_{7-x}$. This is suggested for future work. The growth of a-axis oriented $\text{YBa}_2\text{Cu}_3\text{O}_{7-x}$ films

is of particular interest for the fabrication of Josephson junctions [126].

6.3 Summary

The suitability of RF sputter deposited SrTiO_3 barrier layers for use in preventing interaction between RF sputter deposited Y-Ba-Cu-O films and Si or sapphire substrates during post-deposition heat treatment at 850 °C or above was investigated. The suitability of the 0.4 μm thick SrTiO_3 barrier layers was determined by AES, XRD, optical and electron microscopy, and resistivity data. The SrTiO_3 layer was found to exhibit textured growth with a (111) preferred orientation on (100) Si. Although SrTiO_3 prevented Si from reaching the Y-Ba-Cu-O films, SrTiO_3 was not a suitable barrier layer since Ba still reacted with the Si substrate after migrating through the SrTiO_3 layer. For sapphire, SrTiO_3 was a suitable barrier layer since it prevented interaction between Y-Ba-Cu-O and sapphire.

CHAPTER 7

SUGGESTIONS FOR FUTURE STUDY

Presented in this chapter are suggestions for future study suggested by the literature reviewed in Chapter 2 and by the research presented and discussed in Chapters 4, 5, and 6.

As discussed in Sections 2.1.5.3 and 5.1.4, a study of the effect of the angular distribution variations of Y, Ba, and Cu sputtered from Y-Ba-Cu-O targets on the composition of Y-Ba-Cu-O films has not been performed in which the effects of negative ion resputtering on the film composition have been removed. This study could be performed as follows. A Y-Ba-Cu-O target would be sputtered by Ar^+ from an ion source in order to avoid exposing the target and substrate to a plasma. The pressure between the target and the substrate could thus be kept at a much lower value, e.g. $\cong 1 \times 10^{-6}$ Torr, than is used in typical sputter deposition. This will result in a low probability of any sputtered specie, including O^- , being scattered in the gas phase as it travels to the substrate. If a negative bias was applied to the substrate or a grid above the substrate, the O^- would be repelled by the bias and would not strike the substrate, unlike the case for magnetron sputtering, where the O^- ions are neutralized by scattering events in the plasma, as

discussed in Section 2.1.2.4. Hence a sputter deposition situation would be established in which the substrate would not be bombarded by either O^- ions or energetic, neutral O atoms. Then, following the work of Wehner et al. [81] discussed in Section 2.1.5.3, Y-Ba-Cu-O could be deposited onto a Ta foil substrate curved into a hemispherical shape in order to collect the sputtered flux over 180° . After the deposition, the Ta foil would be flattened out and the Y, Ba, and Cu compositional profiles measured as a function of angle using an EPMA line scan. The study should first be performed using a $YBa_2Cu_3O_{7-x}$ target, but other target compositions would be of value. Of particular interest to the work presented in this dissertation would be to determine if the use of unreacted BaF_2 affects the angular distribution of Y, as suggested in Section 5.1.4.

As discussed in Section 2.1.5.2, the optical emission data of Fledderman [80] suggested that the sputter yield of Cu increased with increasing temperature. Thus, the reported decrease in the Cu concentration in Y-Ba-Cu-O films with increasing substrate temperature [58,78] could be due to a temperature-dependent resputter rate of Cu from the films. A study of this issue is suggested for future work. This could be accomplished by monitoring the yield of Cu sputtered from $YBa_2Cu_3O_{7-x}$ as a function of temperature using positive SIMS.

No mechanism has been proposed to explain why Ba is preferentially resputtered from a growing Y-Ba-Cu-O film by

O^- . It is possible that the lower vapor pressure of Ba compared to those of Y and Cu [79], which usually correlates with a higher sputter rate when all other conditions are held constant, plays a role. However, Ba is not preferentially resputtered by Ar, so an explanation based solely on vapor pressure may not hold. Perhaps the sputter rate of Ba is chemically enhanced due to sputtering with O^- , which may result from the reaction of Ba and O. In any case, the preferential resputtering of Ba by O^- is an issue which should be addressed.

As discussed in Section 4.1.4, measurements of the total sputter rates for the target materials used in the negative SIMS study were not performed nor were data available in the literature. These sputter rate data would permit interpretation of the O^- yield data from the negative SIMS study to reflect the ratio of O^- to all particles reaching the substrate, without the assumption of equal sputter rates. To perform these measurements, a portion of a target could be masked off and a sputter crater formed by sputtering with Ar^+ for a known length of time at the edge of the mask. The resultant step height could then be measured using a profilometer, and the sputter rate calculated by dividing the height by the time of sputtering. However, the unreacted targets (fired at 500 °C) used in this study were not suitable for such a measurement, since they were only $\cong 55\%$ dense and the resulting porosity would

make measurement of a step height nearly impossible. The density of the unreacted targets would need to be increased to 90% or better.

As also discussed in Section 4.1.4, it is suggested that a model for the formation of negative ions by sputtering be developed which takes into account the percent ionicity of the bonds and therefore incorporates explicitly the electronegativity differences of the elements. This is in contrast to the model for the sputtering of negative ions of Cuomo et al. [25] which assumes the solid to be completely ionic. Such a model would be not only valuable for predicting the deviation between the film and target compositions caused by resputtering by negative ions, but would also be useful for the SIMS analysis community.

In Chapter 5 it was suggested that environmental degradation of Y-Ba-Cu-O sputter targets was a controlling factor in the run-to-run reproducibility of the film composition. A negative SIMS study of environmentally degraded $\text{YBa}_2\text{Cu}_3\text{O}_{7-x}$ and other Y-Ba-Cu-O targets is suggested to explicitly test if the O^- yield depends on the extent and conditions of the degradation. Similarly, it would be useful to determine the O^- yields of the products of the environmental degradation of Y-Ba-Cu-O targets, particularly $\text{Ba}(\text{OH})_2$ and BaCO_3 . However, all Y-Ba-Cu-O films should ideally be sputter deposited using a load-locked chamber to prevent the targets from ever being exposed to atmosphere

after undergoing an initial conditioning. Also, the sputter targets should be fired in dry O_2 , and not air as was done in this work, to avoid the formation of atmospheric degradation products during firing. When targets are removed from the chamber, they should be stored in a dessicator.

Sputter deposition of Y-Ba-Cu-O films from a $YBa_2Cu_3O_6$ target should be performed to determine if the lower O^- yield of $YBa_2Cu_3O_6$, compared to that for $YBa_2Cu_3O_{7-x}$, results in improved film compositions. As discussed in Chapter 5, a $YBa_2Cu_3O_6$ target was not available for this study.

In order to improve the superconducting properties of the $YBa_2Cu_3O_{7-x}$ films prepared by sputtering from a Y-Ba-Cu-O-F target and heat treating after deposition in humid oxygen, the heat treatments require optimization. The heat treatment cycle used in this work was adequate but never optimized. For example, variables which could be adjusted include the soak temperature, the cooling rate, the flow rate of both the wet oxygen during the ramp-up and soak and the dry oxygen during the cool-down, and the temperature of the water in the bubbler (see Chapter 3). The goals would be the complete reduction of BaF_2 and formation of $YBa_2Cu_3O_6$ during the ramp-up and high temperature soak, and the complete oxygenation of $YBa_2Cu_3O_{7-x}$ during cool-down. Also, it would be valuable to try the low oxygen partial pressures during the heat treatment suggested by Feenstra et al. [74]

to determine if the same improvements would be seen for sputtered films as their evaporated films.

As discussed in Section 6.2.4, SrTiO_3 may be a stable barrier layer for the formation of $\text{YBa}_2\text{Cu}_3\text{O}_{7-x}$ on Si at the substrate temperatures typically used for the *in situ* growth of $\text{YBa}_2\text{Cu}_3\text{O}_{7-x}$ (650 - 800 °C). A study of the effectiveness of SrTiO_3 as a barrier layer between $\text{YBa}_2\text{Cu}_3\text{O}_{7-x}$ and Si during the *in situ* formation of $\text{YBa}_2\text{Cu}_3\text{O}_{7-x}$ is suggested. Thus the orientation of $\text{YBa}_2\text{Cu}_3\text{O}_{7-x}$ which grows on (111) oriented SrTiO_3 on (100) Si could be determined. However, as discussed in Section 6.2.4, it is not likely that $\text{YBa}_2\text{Cu}_3\text{O}_{7-x}$ will grow epitaxially on the surface of (111) oriented SrTiO_3 . On the other hand, since the lattice mismatch between (110) Si and the (110) face of SrTiO_3 is small, and since a-axis oriented $\text{YBa}_2\text{Cu}_3\text{O}_{7-x}$ has a good match to the face of (110) oriented SrTiO_3 , it would probably be more fruitful to study the *in situ* growth of SrTiO_3 on (110) Si and $\text{YBa}_2\text{Cu}_3\text{O}_{7-x}$ on the (hopefully) resulting (110) SrTiO_3 . This should permit the growth of epitaxial $\text{YBa}_2\text{Cu}_3\text{O}_{7-x}$ on a Si substrate using a SrTiO_3 barrier layer. The substrate temperature for the *in situ* growth of epitaxial (110) SrTiO_3 on (110) Si would have to be experimentally determined, but should be in the range 600 - 800 °C.

CHAPTER 8 SUMMARY AND CONCLUSIONS

The sputter deposition of Y-Ba-Cu-O superconductor and SrTiO_3 barrier layer thin films has been studied in an effort to develop underlying technologies which may lead to the commercial application of $\text{YBa}_2\text{Cu}_3\text{O}_{7-x}$ high temperature superconductors. This chapter contains a summary of the results of the research presented and discussed in this dissertation.

Two possible mechanisms were studied for the deviation of the composition of Y-Ba-Cu-O thin films and targets observed for sputter deposition: resputtering of the growing film by negative ions and migration of Ba to the target surface during sputtering. First, the results of a secondary ion mass spectroscopy (SIMS) study showed that the dominant negative ion sputtered from Y-Ba-Cu-O targets was O^- . The sputter yield of O^- was found to depend on the Ba compound used in the fabrication of Y-Ba-Cu-O targets and was related to the electronegativity difference between the components. The high yield of O^- from $\text{YBa}_2\text{Cu}_3\text{O}_{7-x}$ was found to depend on the target temperature and be due to the excess oxygen present. The practical implication of this was that the temperature of $\text{YBa}_2\text{Cu}_3\text{O}_{7-x}$ sputter targets must be controlled to obtain a consistent film composition. Further, the choice

of starting compounds in the sputter target was shown to influence the O^- yield. An unreacted mixture of Y_2O_3 , CuO , and BaF_2 was found to have the lowest O^- yield among targets with $Y:Ba:Cu = 1:2:3$. This suggested that unreacted sputter targets using BaF_2 as the source of Ba would give the best control of sputtered film compositions. However, it was discussed that the sputter yield of negative ions was not the only issue of importance in determining the film composition; the sputter rate of metal-containing particles as well as the deposition parameters such as the pressure and accelerating voltage were also suggested to be controlling factors.

Second, an Auger electron spectroscopy study of the surface composition of $YBa_2Cu_3O_{7-x}$ sputter targets as a function of sputter time was performed to determine if the migration of target components was contributing to the deviation between the composition of the target and films compositions. The migration of Ba to the target surface during sputtering was found not to occur.

The results of efforts to reproducibly sputter deposit Y-Ba-Cu-O films with a 1:2:3 composition from targets of a variety of compositions and subjected to different heat treatments were then presented. The targets were prepared from Y_2O_3 , CuO , and $BaCO_3$, BaO_2 or BaF_2 . Thin films were deposited by RF planar magnetron sputtering and the film compositions were measured by electron microprobe analysis. The compositions of films sputtered from targets using BaO_2

and BaCO_3 precursors exhibited a strong Ba deficiency relative to the targets, poor run-to-run reproducibilities of $\pm 25\%$ or greater, and poor correlation with changing target compositions. The reproducibility problem for $\text{YBa}_2\text{Cu}_3\text{O}_{7-x}$ targets was attributed to excess oxygen and atmospheric degradation, whereas for other Y-Ba-Cu-O targets atmospheric degradation was suggested to be the only factor. Conversely, the compositions of films sputtered from unreacted targets using BaF_2 as the source of Ba were found to exhibit no Ba deficiency, run-to-run reproducibilities of better than $\pm 6\%$, and good correlation with changing target compositions. The improvements were consistent with the decreased O^- yield for BaF_2 -based targets, as determined by the SIMS study, and also with an improved atmospheric stability for these targets. Thus it was found that the composition of sputter deposited Y-Ba-Cu-O films could be controlled by using target materials which exhibited a decreased O^- sputter yield.

Superconducting $\text{YBa}_2\text{Cu}_3\text{O}_{7-x}$ films were formed by sputter deposition of Y-Ba-Cu-O-F films from a Y_2O_3 - BaF_2 -CuO target, followed by heat treatment in humid oxygen. The superconducting properties of films on SrTiO_3 substrates were typical of post-deposition heat treated films, with $T_{c,0} \geq 80$ K and $\Delta T \leq 8$ K. The superconducting properties were discussed in terms of the presence of intergranular impurity phases in and the microstructure of the $\text{YBa}_2\text{Cu}_3\text{O}_{7-x}$ films.

The method developed in this study for the formation of superconducting $\text{YBa}_2\text{Cu}_3\text{O}_{7-x}$ films is particularly well-suited to the coating of irregularly-shaped objects with $\text{YBa}_2\text{Cu}_3\text{O}_{7-x}$. An example of such an application would be a magnetic shielding enclosure. The highest quality $\text{YBa}_2\text{Cu}_3\text{O}_{7-x}$ films are grown by *in situ* deposition, but this requires precise control of temperature uniformity which is only achievable for flat objects such as wafers. The uniformity of the substrate temperature for irregularly-shaped objects would be much easier to control during post-deposition heat treatment in a conventional tube or box furnace.

Finally, a study of the suitability of SrTiO_3 barrier layers for preventing interaction between Y-Ba-Cu-O films and substrates of Si or sapphire was presented. The SrTiO_3 layers were found to exhibit textured growth with a (111) preferred orientation on the (100) Si substrates. However, SrTiO_3 was found not to be a suitable barrier layer for Si since Ba still reacted with the Si after migrating through the SrTiO_3 layer. For sapphire, SrTiO_3 was found to be a suitable barrier layer since it prevented any interaction between the Y-Ba-Cu-O film and the sapphire substrate.

APPENDIX A HOME-BUILT MULTISOURCE SPUTTER DEPOSITION SYSTEM

All Y-Ba-Cu-O and barrier layer thin films used in this study were grown in the same home-built multisource sputter deposition system shown in Figure A-1. In this appendix a detailed description of the deposition system's hardware and operation are presented. This appendix is also presented as a manual for future users of the system. In the laboratory in which this work was conducted were other deposition systems along with this sputtering system. To identify each system easily, the practice of naming each was adopted. Hence, the multisource deposition system will be hereafter referred to by its inherited name of Rusty. It is of course traditional to name one's children.

A.1 General Description

Rusty was designed and built with the goal of depositing multicomponent films by sequential growth from up to four different sources of layers thin enough to be equivalent to having all sources directed to the same point. This was to be accomplished by moving the substrate sequentially over each source by rotation and collecting the desired component(s). For fast enough rotation, the



Figure A-1. Photograph of "Rusty", the home-built, multisource sputter deposition system used for the growth of all films in this study.

thickness of material collected over each source, depending on the deposition rate from each, would be less than an atomic layer. Thus a mixed, multicomponent film could be grown without the design complications of having all sources directed to the same point. Further, this arrangement would allow the sequential growth of distinct films without breaking vacuum, such as a Y-Ba-Cu-O/barrier layer/substrate structure. A planned early application consisted of growing Ta_5Si_3 from separate Ta and Si sources and then topping this

film with a Au contacting layer, all without breaking vacuum.

These design goals are met by Rusty's final configuration. It must be made clear that the design was not from scratch. Rather, an old evaporation system was heavily modified. Hence, much of the design work involved adding another feature where it wouldn't easily fit, leaving Rusty with a very "inside-out" appearance. Two RF and two DC planar magnetron US Gun sputter sources are mounted pointing upward in the baseplate of a diffusion-pumped high vacuum chamber. The RF sources permit the growth of films from insulating targets, while the DC sources require conducting targets. The targets in each source are the same height above the baseplate, and the sources are all positioned around a circle with a radius of about 6 inches. Thus substrates rotated about the center of this circle pass directly over each source. For growth of films from single targets, the rotation can be stopped to position the substrate holder above the desired source. It was in this mode that all of the films in this study were deposited. Baffles positioned between each source and an aperture plate resting on top of the baffles with holes directly above each source provide isolation of each source. Shutters are moved into place to cover each hole and stop the flux of material from a source independently as necessary.

A.2 Description of Equipment

Rusty's many pieces of hardware are described as they are assembled into the component subsystems of the vacuum system, gas flow and control, sputter sources and power supplies, and substrate mounting and positioning.

A.2.1 Vacuum

A schematic of the vacuum components which allow Rusty to reach its ultimate pressure of 2×10^{-7} Torr is given in Figure A-2. The pump stack, an outdated version of a Varian VHS-6 diffusion pump system, consists, from the top down, of a gate valve, a liquid nitrogen trap, a water-cooled trap, and a six inch diffusion pump. A Sputtered Films six inch throttle valve is inserted between the LN_2 trap and the water trap. Unique to sputtering systems, the throttle valve is used to decrease the pumping speed of the diffusion pump in order to maintain a constant gas pressure during sputtering. The liquid nitrogen trap is fed by an automatic fill system. The pump stack is bolted to a flanged neck which is in turn attached to the bottom of the stainless steel baseplate. The neck provides a port for installing the head of a Dycor/Ametek residual gas analyzer (RGA). The RGA is used primarily for leak checking. The outlet of the diffusion pump is connected with rubber vacuum hose to an assembly with two bellows-sealed valves. The valve assembly

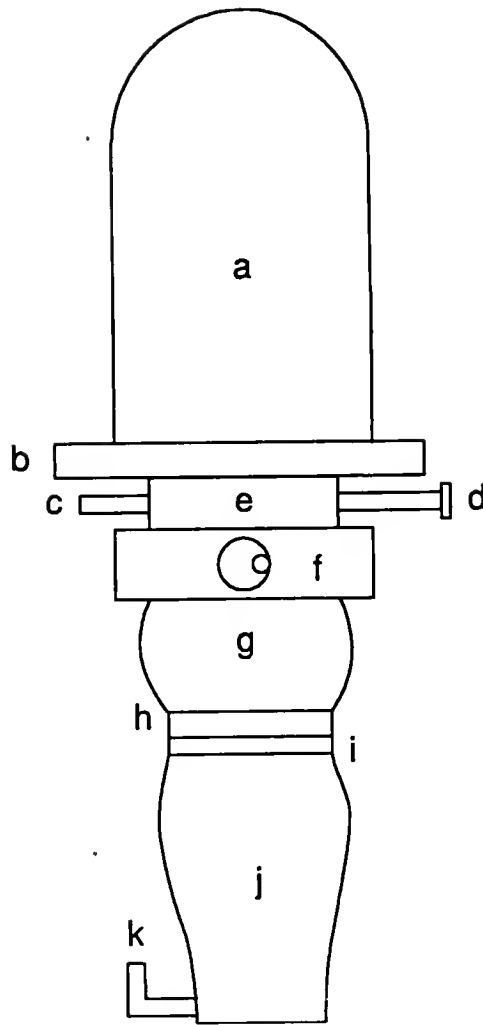


Figure A-2. Schematic illustration of Rusty's vacuum system including the a) bell jar, b) baseplate, c) roughing port, d) RGA port, e) neck, f) gate valve, g) liquid nitrogen cyrotrap, h) throttle valve, i) water-cooled baffle, j) diffusion pump, and k) foreline port.

is in turn connected to a Sargeant-Welch model 1397 mechanical pump. The valves route the pumping of the mechanical pump either to the diffusion pump (foreline) or the vacuum chamber (roughing line). A Lesker model MMA-075

foreline sorption trap near the inlet of the mechanical pump minimizes backstreaming of mechanical pump fluid.

The vacuum chamber consists of an 18 inch diameter by 30 inch high Pyrex bell jar resting with a Viton L-ring seal on the aforementioned stainless steel baseplate. A steel mesh implosion guard covers the bell jar and is in turn attached at the top by steel cables to the hoist assembly. The manual hoist employs a counter-weight to facilitate lifting of the bell jar and keeping it elevated. One inch holes in the baseplate are used for the mounting of feedthroughs for gases, electric power, pressure measurement, rotary motion, and the sputter sources. All feedthroughs and other vacuum components in the chamber are made of stainless steel.

Pressure measurements are made with a Granville-Phillips model 270 combination thermocouple gage and ionization gage controller, and by a MKS model 370 Baratron capacitance manometer head and a model 270A readout. Thermocouple gage tubes are mounted in the baseplate to monitor chamber pressure during roughing, at the outlet of the diffusion pump to make sure the foreline pressure does not exceed 200 mTorr, and at the inlet of the mechanical pump. The ionization gage tube is coupled to the chamber through the baseplate in order to measure high vacuum pressures during pumpdown. The capacitance manometer head, used to give an absolute measure of the sputter gas pressure during a deposition, is also attached to the

baseplate. A intermediary 0.5 μm filter protects the capacitance manometer head and the valve separating it from the chamber from particulates.

A.2.2 Gas Flow and Control

Maintaining a constant sputter gas pressure during deposition is critical to the reproducibility of a sputtered film process. This is accomplished by limiting the pumping speed with a throttle valve and precisely controlling the sputter gas flow rates. The flow rate of sputter gases in Rusty is regulated by microprocessor-controlled combination valve/mass-flow controllers. The flow rate of high purity (99.9999%) Ar, used exclusively in the majority of depositions, is regulated by an MKS model 248 valve, model 258 mass-flow meter, and model 246 controller/readout with a 0 - 50 sccm range. The flow rate of high purity (99.995%) oxygen, mixed in with Ar for the reactive sputtering of oxide films, is controlled by a Vacuum General model 80-4 mass-flow controller with a 0 - 10 sccm range. These flow ranges, in combination with the pumping speed of the throttled diffusion pump, give the desired sputter gas pressures of 5 - 30 mTorr.

The pressure of the tanks of Ar and O₂ is regulated down to an outlet of 30 psi from an inlet of up to 2200 psi by a two-stage regulator. The outlet of each regulator is connected to a 0.5 μm filter to limit particulate

contamination. Stainless steel tube of 0.25 inch diameter brings each gas to a flow controller. The outlet of each flow controller meets at a tee and the gases are carried in a single tube to the chamber. The sputter gas is fed into the chamber through two gas feedthroughs.

In order to bring the evacuated chamber up to ambient pressure, standard grade bottled nitrogen is backfilled into the chamber. A single-stage regulator limits the N₂ tank's outlet pressure. The N₂ gas is carried by a copper tube to a 0.5 μ m filter, through which it passes before reaching the valve to the chamber. Other functions served by the nitrogen gas include pressuring pneumatic valves and the liquid nitrogen automatic feed system, and providing filtered gas to a blow gun used to dust off samples.

A.2.3 Sputter Sources and Power Supplies

Rusty features four vertically mounted, two inch diameter US Gun planar magnetron sputter sources. Two of the sources are DC driven and can only be used to deposit from conducting targets, while the other two employ RF power and thus can sputter insulating targets as well. The location of the sources are illustrated in the photograph of the inside of Rusty's chamber given in Figure A-3. As discussed above, the guns are mounted such that the targets in each source are the same height above the baseplate, and the sources are all positioned around a circle with a radius of about 6



Figure A-3. Photograph of inside of Rusty's chamber indicating the location of the four sputter sources or guns. The guns on the right and left are RF guns, while the two in the front and back are DC guns.

inches. Thus substrates rotated about the center of this circle pass directly over each source.

One of the DC sources is powered by an Eratron model DC-1000 1 kW DC power supply, sold by US Inc. along with the

source. This DC supply features constant current control only; the sputter power is obtained by multiplying the current and voltage values read from analog meters on the supply's front panel. Power for the second DC source is provided by a far more sophisticated Advanced Energy model MDX-1K 1 kW DC supply with constant voltage, current, or power control and digital readout of all parameters. This supply was also sold by US Inc. along with the DC gun.

The RF sources are both driven by 500 W RF power supplies and tuning networks made by RF Plasma Products. One of the supplies, an older tube-based unit, combines a model HFS-500E generator, a model APCS-3 controller, and a MN-500E matching network. The other, a model RF-5 supply along with a model AM-5 tuning network, is a newer solid state unit. Likewise, the older tuning network is manual while the newer one works automatically. Power from each of the RF supplies is fed into a tuning network and then to the RF source. Each tuning network adjusts the effective impedance of the load to match the 50 ohms desired by the RF supply. If the load, made up of the RF source, plasma, and connecting cable, does not match 50 ohms, power is reflected back to the supply, which can cause heating and damage. The length of the coaxial cable from the tuning network to the source plus the length of the sputter gun is kept at an integral multiple of the 13.56 MHz RF power's wavelength in order to avoid reflection and standing waves.

The ignition of a plasma with either RF source is typically difficult without a "jump start" from an additional ion source. An 180 nm UV source inside the chamber provides the extra kick of ions that each RF source needs to ignite. The plasma above a DC source typically ignites easily, so no additional help is needed. The UV source in the chamber also provides the additional benefit of creation of ozone, which helps remove adsorbed water and hydrocarbons from the chamber walls during pumpdown.

A.2.4 Baffles and Shields

In order to isolate the plasma and flux of sputtered material of each source from the others, each is harbored in its own enclosure, as illustrated in Figure A-4. The side walls of the enclosures are comprised of stainless steel vertical baffles bent to fit around the sources while not confining the rotary motion of the shutters, as discussed below. Resting on top of the baffles is a circular stainless steel aperture plate, also shown in Figure A-4, which has a three inch hole in it directly above each sputter source and one small hole in the center through which passes the shaft of the substrate rotation assembly (see below). Thus the material flux from each sputter source is predominantly confined to the opening above each. To completely block off a source, a shutter is rotated into place to close off the hole above the source. The shutters are shown in this



Figure A-4. Photograph of inside of Rusty's chamber illustrating the location of the aperture plate, baffles, and shutters which isolate each sputter gun. (See text for description of each.)

position in Figure A-4. A shutter is present for each source, so in principal all four sources could be operating without any cross-talk of their sputtered fluxes.

In order to keep the inside surface of the Pyrex bell jar from being coated by the various materials being

deposited and also to provide an increased ground electrode area for the RF sources, two semicircular stainless steel shields are placed around the periphery of the chamber. On top of these is placed a circular lid, thereby completing a modular stainless steel "can" which fully encloses the inside of the chamber. When the bell jar is lowered, it fits snugly around the shields.

A.2.5 Substrate Mounting and Positioning

As discussed above, Rusty was designed with the ability to pass a substrate sequentially over multiple targets for many cycles. Since each sputter source is positioned around the circumference of the same circle, the desired substrate motion is accomplished by rotation about the center of this circle. This rotary motion is accomplished by the substrate rotation assembly illustrated in Figure A-5. All parts are made of stainless steel except as noted. Substrates are mounted on holders attached to one or both ends of an arm with a length equal to the diameter of the circle along which the sources lie (16 inches). The arm is attached by set screw to a vertical, center-mounted 0.25 inch diameter shaft. The shaft is held in place by two bearing assemblies in turn supported by a tripod which is fastened to the baseplate. The bottom of the shaft is coupled by gears and a chain to an A&N model 125-FTR-S rotary motion feedthrough, which is turn coupled to an externally-mounted DC gearcase

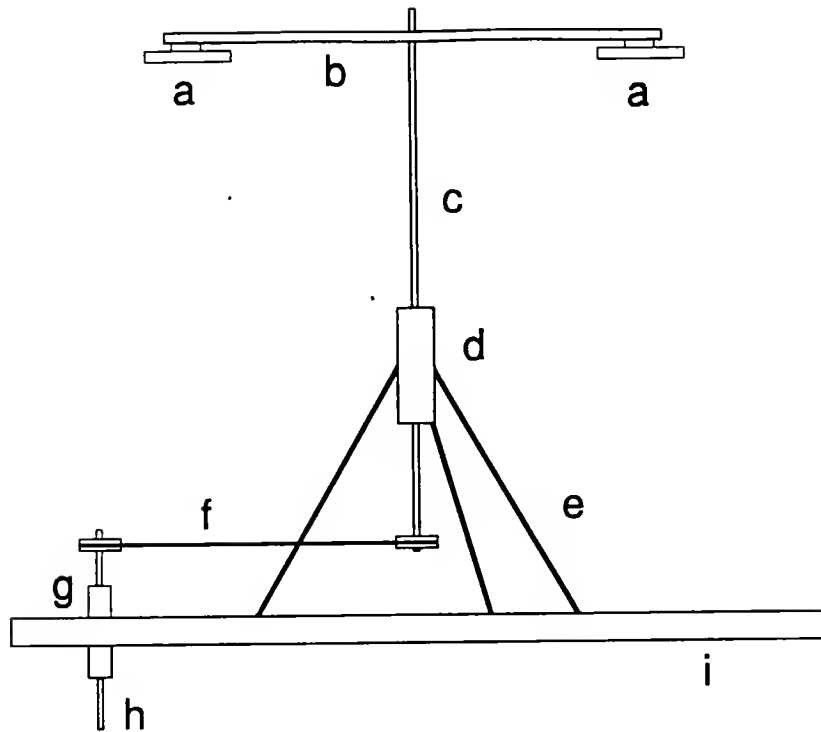


Figure A-5. Schematic illustration of substrate rotation assembly in Rusty. The component parts include the a) substrate holder, b) rotary arm, c) rotating shaft, d) bearing support, e) tripod legs, f) chain drive and gears, g) rotary feedthrough, h) coupling to drive motor, and i) chamber baseplate.

motor. A Lambda model LSC-C-01 0 - 7 V DC power supply provides the voltage to drive the motor, and a switch can be thrown to reverse the polarity of the voltage and thus the direction of motor's rotation. An on/off switch stops the rotation and allows positioning of substrates in the desired location, such as above a sputter source. This ability facilitates two different depositions from the same target with only one pumpdown, which saves a lot of time. After a first deposition, the coated substrate is moved out of the

way and the clean substrate mounted at the other end of the rotary arm is positioned over the target. Similarly, a second film can then be grown from a different target over the existing film, as was done in the barrier layer portion of this study. Thus, even though the majority of depositions in Rusty do not require continuous substrate motion, the rotation assembly is extremely useful.

The complete rotary arm and substrate holder assembly is shown above the circular aperture shield in Figure A-4, with one of the substrate holders in position above a sputter source. The substrate holder assemblies at each end of the rotary arm are removable, which allows changing of the substrates without having to remove the rotary arm. Two substrate holder assemblies are shown, one from the top and one from the bottom, in Figure A-6a. In Figure A-6b a substrate holder assembly is shown disassembled, along with a complete assembly on which is mounted a piece of a Si wafer. A mounting block, the second item from the left pictured in Figure A-6b, has one end of it machined down to a 0.25 inch diameter cylindrical plug. This plug fits into a matching socket in each end of the rotary arm and is held snug by a set screw, thereby attaching the substrate assembly to the rotary arm. This plug/socket scheme also allows tilting the substrate with respect to the target, which is useful for off-axis depositions. The substrate holder itself is a three inch diameter by 0.125 inch thick disk of aluminum with 18 or so size 76 holes drilled in it.



(a)



(b)

Figure A-6. Photographs of substrate holder assembly, viewed a) from the top (right) and bottom (left) and b) disassembled.

Aluminum was used rather than stainless steel because drilling the size 76 holes in stainless steel was extremely difficult. The small holes are for inserting the base of the 0.015 inch diameter tungsten wire, "seven-shaped" clips which hold down the substrates. The holder is fastened to the mounting block using a long bolt passed through a ceramic grommet, shown in Figure A-6b, in such a way as to electrically insulate the holder from the block, as shown on the left in Figure A-6a. This permits the substrates to be electrically floating during a deposition. The ceramic grommets are machined from Grade A LAVA, a naturally-occurring machinable ceramic, fired at 1050 °C, and slow cooled to prevent cracking. Care must be taken when fastening together the mounting block, ceramic grommet, and substrate holder to avoid cracking the grommet.

A.3 Operation

A general operating procedure will be given. There are too many small exceptions and potential disasters to include everything. The general rule: do not be afraid of mistakes; learn from them.

A.3.1 Cold Start-up

If Rusty is completely shut down, start-up will require some components to warm up over night. Turn on the foreline trap heater along with the mechanical pump in order to bake

out the foreline trap. The foreline and roughing valves should be kept closed and the diffusion pump heater kept off. Turn on the capacitance manometer readout and heater so that the head may stabilize. Be sure the valve between the capacitance manometer head and the chamber is closed. Turn on the Granville-Phillips thermocouple/ion gage readout. Allow at least eight hours for everything to stabilize.

A.3.2 Regular Start-Up

If the foreline trap heater is on, turn it off. Open the foreline valve and begin pumping on the exhaust of the diffusion pump with the mechanical pump. Turn on the cooling water to the diffusion pump and ensure that its flow rate is adequate by checking the pressure gauge. The water pressure should be at least 20 psi and preferably above 25 psi. If it is less, the element in the water filter must be changed before turning on the diffusion pump heater. If the water pressure is adequate, turn on the diffusion pump heater and allow it to warm up for at least 30 minutes. Then fill the liquid nitrogen drain reservoir with LN_2 , either manually or using the automatic feed system. This LN_2 will in turn fill the reservoir in the LN_2 trap. The LN_2 trap's reservoir should fill, as indicated by LN_2 overflow, but overfilling should be avoided to save the floor and your feet. After it has filled, allow the LN_2 trap to cool for at least 30 minutes. If the automatic feed system is used, make sure the 50 liter source tank is full and pressured with N_2 gas at 20

psi. If manually filling the drain reservoir, do so once every hour since the reservoir in the trap is small.

A.3.3 Target Mounting

All targets should first be bonded with silver epoxy to a 2 inch by 0.0625 inch thick Cu backing plate to ensure adequate cooling. Slightly oversized targets may require grinding down of their outer diameter in order to fit into the US sputter guns.

For mounting targets in either RF source, the anode cap must first be removed. Then remove the screws holding down the target clamp and lift off the target clamp and spacing ring(s). If another target is in place, carefully slide it off of the cathode. First spread a thin coat of US' conductive silver paste on the copper backing plate to ensure good thermal contact. Then place the new target in the center of the cathode. Place spacers around the target as necessary to prevent the target clamp from overstressing the edges of the target. Place the target clamp over the spacers and tighten screws down gently to avoid cracking the target. Replace the anode cap and check the spacing between it and the top of the target clamp. If they are touching or too close (see US gun manual for exact distances), a spacer needs to be installed in the anode cap or the plasma will not ignite.

Mounting targets in the DC guns is very different than in the RF sources. In the DC sources, the back of the target or backing plate is in direct contact with the cooling water. The target rests directly on the o-ring which forms the high vacuum seal between the cooling water and the chamber. This is clearly not a good design, but is workable if care is taken. First, be certain the cooling water to the guns has been shut off. Then remove the anode cap without disconnecting the ground wire if possible. Unscrew the target clamp and carefully lift off the target to avoid spilling water. Wipe any water off of the O-ring at the top of the gun. Place the new target on the O-ring and screw down the target clamp as tight as possible without cracking the target. (The conductive targets used in a DC source are almost always cast solids, so they are not nearly as brittle as the sintered insulating targets used with an RF source). Replace the anode cap and check that the ground wire is attached.

A.3.4 Sample Loading

This procedure assumes the chamber has already been vented and opened (see below). Also, substrates should be freshly cleaned and already cleaved into the desired size to avoid keeping the chamber open longer than necessary. First, remove the top and outer stainless steel shields to expose the inside of the chamber. Then disconnect the mounting block/substrate holder assembly from the end of the rotary

arm. Remove existing substrates and blow particulates off the holder surface with nitrogen gas. Place substrates and masks, if used, on the holder surface and fasten them in place with W clips. Blow particulates off of the substrates with nitrogen gas. Reattach the mounting block/substrate holder assembly to the end of the rotary arm. Replace the outer and top shields and carefully lower the bell jar. The bell jar fits rather snugly over the shields, so observe caution to avoid cracking or chipping the bottom of the bell jar.

A.3.5 Pump-Down

With the LN_2 trap full and the bell jar completely lowered, close the foreline valve and open the roughing valve so that the mechanical pump can evacuate the chamber. Let the pressure drop to at least 100 mTorr but no less than 30 mTorr to avoid backstreaming of mechanical pump fluid. Open the valve to the sputter gas line. Close the roughing valve and open the foreline valve. Open the valve which connects the capacitance manometer to the chamber. Close the throttle valve and begin to open the gate valve slowly. Monitor the foreline pressure on the thermocouple gauge and the chamber pressure on the capacitance manometer readout. Do not let the foreline pressure exceed 200 mTorr or backstreaming of diffusion pump oil can result. Continue slowly opening the gate valve until the chamber pressure drops below 5 mTorr. Then the gate valve and the throttle

valve can be fully opened. Turn on the ionization gauge tube. Continue pumping until the desired base pressure, typically 1×10^{-6} Torr, is reached. This will take about two hours. If the pressure stops at some higher value, use the RGA to check for leaks.

A.3.6 Presputtering and Deposition

After the desired base pressure has been reached, the chamber is ready to be backfilled with a steady flow of Ar sputter gas. Turn off the ionization gauge tube. Close the throttle valve, checking that the micrometer adjustment is set at 449, which has been determined as optimum for the system. Turn on the flow switch on the MKS flow controller, and then adjust the pot to establish the steady flow rate (see MKS manual) which gives the desired sputter gas pressure. Typical Ar flow rates are 5 - 7 sccm, and the standard operating pressure, as monitored by the capacitance manometer, is 10 mTorr. If oxygen is to be added to the Ar sputter gas, control the oxygen flow rate with the Vacuum General controller and monitor the pressure. A typical amount of oxygen is 10% of the sputter gas. To keep the working pressure at 10 mTorr, reduce the Ar pressure to 9 mTorr and then oxygen to bring the total pressure to 10 mTorr.

Prior to ignition of a target, turn on the cooling water to the guns. The pressure on this water line should be

about 10 psi. Ignition of the plasma above a DC source is usually easy. Increase the power to the source until a plasma is obtained, and then set the power at the desired level. The easiest way to verify plasma ignition is to look in the chamber. The Eratron DC power supply requires manual adjusting. The Applied Energy DC supply automatically ramps the power from zero to the setpoint in the time specified. For the RF sources, after applying a low power of 25 W or so, the UV source in the chamber must be turned on to jump-start the plasma. After ignition of the plasma, turn off the UV source and increase the RF power to the desired value, which is typically in the range of 50 - 150 W. The tuning network must then be adjusted to decrease the reflected power to as close to zero as possible. On the old RF supply, the tuning network must be adjusted manually. On the new supply this can be done automatically.

After ignition, presputtering is required of all targets to remove contaminants and to condition the target surface. Also, multicomponent targets must reach the steady-state condition where the component with the faster sputter yield is depleted from the surface and the resulting flux has the same composition as the bulk of the target. Presputtering is accomplished by sputtering from a source with the shutter closed. For conducting targets in the DC source, the sputter rate is usually high, so a short presputter of 10 minutes is usually sufficient. For the sintered, insulating, multicomponent targets used in the RF

sources, the sputter rates are usually much slower. Reaching the steady state surface condition for such targets can take presputters of 3 hours or more, particularly for the first use of target. The Y-Ba-Cu-O targets used in this study are particularly bad due to the slow loss of metastable oxygen.

When presputtering is complete, open the shutter over the desired target and begin deposition onto the substrate(s) positioned over the source. Monitor all relevant parameters to be certain there are no problems. Unlike evaporation, the deposition rate for sputtering remains relatively constant when a constant power is supplied to the source. Thus to obtain a desired film thickness, it is only necessary to leave the shutter open for certain length of time. Calculate the time required by dividing the desired thickness by the sputter rate. (The sputter rate is obtained by measuring a film thickness using a profilometer and dividing by the duration of the deposition. The first few depositions from a new target should be done to establish the sputter rate). When the required time has elapsed, close the shutter and then turn off power to the source.

A.3.7 Sample Removal

When all depositions are complete and power to all sources is turned off, stop the flow of Ar (and oxygen) sputter gas. Allow the chamber pressure to drop below 2

mTorr, then open the throttle valve. Close the valve between the chamber and the sputter gas feed line and also the valve to the capacitance manometer. Crank shut the gate valve to isolate the chamber. Then open the up-to-air valve, which allows N_2 gas to backfill the chamber. When the chamber is at atmospheric pressure, the L-ring seal will be broken and N_2 will flow out. Close the up-to-air valve to stop the flow of nitrogen. Lift the bell jar and remove the stainless steel shields. Disconnect the mounting block/substrate holder assembly from the rotary arm as described above. Remove W clips and substrates.

A.3.8 Shut Down

If another deposition is not planned, reconnect the substrate holder (good vacuum practice) and replace the shields. Lower the bell jar and rough pump the chamber to about 100 mTorr. Open the foreline valve and keep the diffusion pump running until the LN_2 trap warms to room temperature; this prevents water from collecting in the bottom of the diffusion pump. If a deposition is planned within a couple of days, the diffusion pump can be left heated as long as the cooling water is flowing and the mechanical pump is pumping on the foreline. For longer periods of idleness, turn off the diffusion pump heater to prolong its life. After the heater has cooled, turn off the cooling water. Close the foreline valve. If Rusty will be

used within a week or two, turn on the foreline trap heater and leave on the mechanical pump to bake out the foreline trap. For longer periods, turn off the mechanical pump and the capacitance manometer heater.

APPENDIX B HOME-BUILT RESISTIVITY VERSUS TEMPERATURE MEASUREMENT SYSTEM

This appendix contains a discussion of the the various pieces of equipment comprising the home-built R-T system used in this study, the software which automated the data acquisition, and a general operating procedure.

B.1 Description of System

All R-T data in this study were acquired using the home-built, computer-controlled system shown in Figure B-1. An APD closed-cycle He refrigeration system cooled down a sample loaded in an APD "Superconducting Characterization Cryostat" (SCC) to temperatures as low as 12 K. The SCC featured an isolated sample well which allowed changing of samples without having to warm up the cryostat's coldfinger. A Scientific Instruments model 5500-1-25 cryogenic refrigeration temperature controller changed the temperature in the sample well from 12 - 300 K by regulating a resistive heater wrapped around the cold finger. The Scientific Instruments controller also displayed the temperature measured by GaAs diode sensors mounted in the tip of the cold finger and in the sample tube. Prior to turning on the APD model HC-2 He compressor, the shroud housing the



Figure B-1. Home-built, computer-controlled resistance versus temperature measurement system used in this study.

cryostat was pumped down to 50 mTorr by a Sargent-Welch model 1397 mechanical pump. The pressure was monitored with a Kurt Lesker thermocouple gage tube and model TCC-201 readout. Resistance measurements were made using a DC four point probe method. A Keithley model 220 current source sent a constant DC current to the outer two of four collinear contacts on a sample. The voltage across the inner two contacts was measured by a Keithley model 181 nanovoltmeter. Connections among the current source, nanovoltmeter, and sample holder were made by shielded triaxial cable to

minimize noise and were wired in such a way as to avoid ground loops. To account for thermal errors in the voltage data, an average resistance from the opposite polarity voltage measurements was then calculated from [132]

$$R = \frac{(V^+ - V^-)}{2I}, \quad (B-1)$$

where V^+ and V^- were the voltage measurements at positive and negative polarity of the current I . It was very common in the high temperature superconductor literature to see the resistance data presented relatively as the fraction R/R_{rt} , where R_{rt} is resistance value at room temperature. This method of presenting the data allowed easy visualization of the superconducting transition without needing to calculate the resistivity and was used by the data collection software described below. When desired, resistivity values were calculated by multiplying the R/R_{rt} data by the room temperature resistivity measured by an Alessi four point probe station, as discussed in Chapter 3. The resistivity data from the R-T sample probe were inconsistent because of edge effects in the confined area [107]; i.e., the probe tips were often too close to the sample edge. This problem was avoided by using the Alessi probe station for room temperature resistivity measurements.

All aspects of the temperature control and data acquisition were controlled by an IBM PC, communicating with each device over a National Instruments model PC-II IEEE-488 interface. The software, written in Microsoft GW-BASIC,

instructed the temperature controller to bring the sample temperature to a desired value and then requested the current source and nanovoltmeter to perform a resistance measurement. The results were then saved in an ASCII file. This was repeated with decreasing temperature until the superconducting transition was complete and zero resistance was reached. The zero resistance value was limited by the minimum voltage measurable before noise dominates, which was 0.9 μV . The R-T data were then printed out numerically and/or plotted out graphically. For high quality R-T plots, the ASCII data file was imported into SigmaPlot version 4.1, a commercially available technical plotting program, where a plot was created and printed out.

Samples were loaded into the SCC's sample well while mounted in the home-built sample holder/four-point contact block, which was in turn positioned in the end of the sample tube. A 18-conductor electrical feedthrough was attached to the top of the sample tube. The wire connections to the GaAs diode temperature sensor and the sample holder/contact block were attached to this feedthrough, as were the cables to the temperature controller, current source and nanovoltmeter. The sample holder/contact block, designed to hold flat samples up to 0.5 inch long by 0.25 inch wide by 0.1 inch thick, is illustrated in Figure B-2. The four contacts to the sample were made by spring loaded, rhodium-tipped Augat Pogo model ASR probe tips, mounted collinearly with a spacing of 0.08 inches in a nylon block. The Teflon-coated,



Figure B-2. Sample holder/contact block for mounting samples in R-T measurement system.

size 30 wire leads were soldered to the bottom of the Pogo probe tips. The sample was held face-down on the probe tips by a small brass plate, which was then fastened by two brass screws turned into threads in the nylon block. This system of making contacts allowed quick samples changes and was suitable for general R-T measurements. More sophisticated measurements would require thin film metal contacts to be deposited on the superconductor and the wire leads to be bonded directly to these metal pads. Only the spring-loaded probe contacts were used in this study.

B.2 Operating Procedure

A general operating procedure for the R-T measurement system follows. This is provided primarily for future users. The current source, voltmeter, and temperature controller

should be turned on at least 30 minutes prior to use in order to stabilize.

1. Turn on the mechanical pump and open the valve to the SCC.
2. Pump down the SCC to 50 mTorr.
3. Flush the sample well with He. If the sample tube is loaded, remove it.
4. Check that the cooling water to the refrigerator is on.
5. Turn on the He compressor and verify the He pressure is above 300 psi.
6. Monitor the temperature of the cold finger on the temperature controller.
7. Continue pumping on the SCC with the mechanical pump to keep the pressure at 50 mTorr. If the pressure drops below 30 mTorr, close the valve to the SCC to avoid backstreaming of pump fluid. Reopen the valve if the pressure exceeds 50 mTorr. Continue this until the cryostat can hold the pressure below 50 mTorr by itself.
8. Close the valve to the SCC and turn off the mechanical pump.
9. Load the sample into the sample holder/contact block.
10. Verify that good contact has been made by applying a current and measuring a voltage.
11. Start the R-T control software on the PC and follow the instructions given. Adjust parameters if desired.

12. Verify that the cryostat has cooled to 220 K.
13. As instructed by the software, strike a key to perform a room temperature measurement.
14. Flow He into the sample well to prevent icing, quickly load the sample tube into the well, and cut off the He.
15. Strike a key on the computer keyboard and let the software run an entire measurement. The length of time required depends on parameters requested. A few hours is typical.
16. When the measurement is completed, follow the instructions given by the software and save the data collected. The data can be plotted if desired or later brought into SigmaPlot for better plotting.
17. Flow He into the sample well.
18. Quickly remove the sample tube from the well, shut the valve to the well, and cut off the He.
19. Allow sample tube and holder to warm to room temperature and remove sample.
20. Another sample can now be loaded and a measurement taken without having to warm and recool the cryostat.

REFERENCES

1. J.G. Bednorz and K.A. Muller, Z. Phys. B, Vol 64. 1986, p. 189.
2. M.K. Wu, J.R. Ashburn, C.J. Torng, P.H. Hor, R.L. Meng, L. Gao, Z.J. Huang, Y.Q. Wang and C.W. Chu, Phys. Rev. Lett., Vol 58, 1987, p. 908.
3. R. Simon and A. Smith, Superconductors: Conquering Technology's New Frontier, (Plenum Press, 1988, New York.)
4. D. Larbalestier, Phys. Today, Vol. 44, 1991, p. 74.
5. N.G. Dhere in Physics of Thin Films, Volume 16: Thin Films for Merging Applications, ed. M.H. Francombe and J.L. Vossen, (Academic Press, New York, 1992), Ch. 1.
6. R.F. Bunshah and C.V. Deshpandey, Res. and Devel., Vol. 31, 1989, p. 65.
7. R. Simon, Phys. Today, Vol. 44, 1991, p. 64.
8. D.W. Murphy, S.A. Sunshine, P.K. Gallagher, H.M. O'Bryan, and R.J. Cava, ACS Ser. 351, 1987, p. 181.
9. Y. Zhu, J. Tafto, and M. Suenaga, MRS Bull., Vol. 16, 1991, p. 54.
10. P. Chaudari, R.T. Collins, P. Freitas, R.J. Gambino, J.R. Kirtley, R.H. Koch, R.B. Laibowitz, F.K. LeGoues, T.R. McGuire, T. Penney, Z. Scchlesinger, A.P. Segmuller, S. Foner, and E.J. McNiff, Jr., Phys. Rev. B, Vol. 36, 1987, p. 8903.
11. R.H. Ono, MRS Bull., Vol. 17, 1992, p. 34.
12. T. Venkatesan, X.D. Wu, A. Inam, Y. Jeon, M. Croft, E.W. Chase, C.C. Chang, J.B. Watchman, R.W. Odom, F. Radicati, and C.A. Magee, Appl. Phys. Lett., Vol. 53, 1988, p. 1431.
13. J.K. Truman, W.R. White, P.H. Ballentine, D. Mallory, P. Borrelli, and A. Kadin, IEEE Trans. Supercon., to be published

14. J.L. Vossen and J.J. Cuomo, in Thin Film Processes, ed. J.L. Vossen and W. Kern, (Academic Press, New York, 1978) Ch. II-1.
15. D. Stauffes, Introduction to Percolation Theory, (Talyor and Francis, London, 1985).
16. J.A. Thornton, in Sputter Deposition and Ion Beam Processes, (American Vacuum Society, New York, 1984), Ch. VI.
17. W.D. Westwood and J.J. Cuomo, in Sputter Deposition and Ion Beam Processes, (American Vacuum Society, New York, 1984), Ch. IV.
18. R.K. Waits, in Thin Film Processes, ed. J.L. Vossen and W. Kern, (Academic Press, New York, 1978) Ch. II-4.
19. S.M. Rossnagel, in Thin Film Processes II, ed. J.L. Vossen and W. Kern, (Academic Press, New York, 1991) Ch. II-1.
20. R. Parsons, in Thin Film Processes II, ed. J.L. Vossen and W. Kern, (Academic Press, New York, 1991), Ch. II-4.
21. R. Kelly, in Handbook of Plasma Processing Technology, ed. S.M. Rossnagel, J.J. Cuomo, and W.D. Westwood, (Noyes, Park Ridge, NJ, 1990), Ch II-4.
22. A. Benninghoven, F.G. Rudenauer, and H.W. Werner, Secondary Ion Mass Spectroscopy: Basic Concepts, Instrumental Aspects, Applications and Trends, (John Wiley and Sons, New York, 1989).
23. G.A. Somorjai, Principles of Surface Chemistry, (Prentice-Hall, Englewood Cliffs, NJ 1972).
24. R.R. Olson, M. E. King, and G.K. Wehner, J. Appl. Phys., Vol. 50, 1979, p. 3677.
25. J.J. Cuomo, R.J. Gambino, J.M.E. Harper, J.D. Kuptsis, and J.C. Webber, J. Vac. Sci. Technol., Vol. 15, 1978, p. 281.
26. W.D. Westwood, in Handbook of Plasma Processing Technology, ed. S.M. Rossnagel, J.J. Cuomo, and W.D. Westwood, (Noyes, Park Ridge, NJ, 1990), Ch. II-9.
27. C.A. Neugebauer, in Handbook of Thin Film Technology, ed. L.I. Maissel and R. Glang, (McGraw-Hill, New York, 1970), Ch. 8.

28. R.S. Logan, in Handbook of Plasma Processing Technology, ed. S.M. Rossnagel, J.J. Cuomo, and W.D. Westwood, (Noyes, Park Ridge, NJ, 1990), Ch. II-5.
29. A. Wucher and W. Reuter, J. Vac. Sci. Technol. A, Vol. 6, 1988, p. 2316.
30. J.M.E. Harper, J.J. Cuomo, R.J. Gambino, H.R. Kaufman, and R.S. Robinson, J. Vac. Sci. Technol., Vol. 15, 1978, p. 1597.
31. J.J. Hanak and J.P. Pellicane, J. Vac. Sci. Technol., Vol. 13, 1976, p. 406.
32. L.R. Gilbert, R. Messier and R. Roy, Thin Solid Films, vol. 54, 1978, p. 129.
33. D.J. Kester and R. Messier, J. Vac. Sci. Technol. A, vol. 4, 1986, p. 496.
34. A. Kadin, P. Ballentine, J. Argana, and R. Rath, IEEE Trans. Magn., Vol. 25, 1989, p. 2437.
35. M. Leskela, J.K. Truman, C.H. Mueller, and P.H. Holloway, J. Vac. Sci. Technol. A, Vol. 7, 1989, p. 3147.
36. R.J. Lin, Y.C. Chen, J.H. Kung, and P.T. Wu, in Materials Research Society Symposium Proceedings, Volume 99: High Temperature Superconductors, ed. M.B. Brodsky, R.C. Dynes, K. Kitazawa, and H.L. Tuller, (Materials Research Society, Pittsburgh, 1988), p. 319.
37. K.C. Sheng, S.J. Lee, Y.H. Shen, X.K. Wang, E.D. Rippert, R.P. Van Duyne, J.B. Ketterson, R.P.H. Chang, J. Mater. Res., Vol. 4, 1989, p. 1312.
38. N. Savvides, C. Andrikidis, D.W. Hensley, R. Driver, J.C. McFarlane, N.X. Tan, and A.J. Bourdillon, in Materials Research Society Proceedings, Vol. 169: High Temperature Superconductors, ed. D. Christen, J. Narayan, and L. Schneemeyer, (Materials Research Society, Pittsburgh, 1990), p. 655.
39. A.K. Stamper, D.W. Greve, and T.E. Schlesinger, J. Vac. Sci. Technol. A, Vol. 9, 1991, p. 2158.
40. J.K. Truman, M.A. Leskela, C.H. Mueller, and P.H. Holloway, in High Temperature Superconducting Compounds: Processing and Related Properties, ed. S.H. Whang and A. DasGupta, (TMS, Warrendale, PA, 1989) p. 83.

41. X.X. Xi, J. Geerk, G. Linker, Q. Li, and O. Meyer, Appl. Phys. Lett., Vol 54., 1989, p. 2367.
42. J. Gao, Y.Z. Zhang, B.R. Zhao, P. Out, C.W. Yuan, and L.L. Li, Appl. Phys. Lett., Vol. 53, 1988, p. 2677.
43. S.M. Rossnagel, in Handbook of Plasma Processing Technology, ed. S.M. Rossnagel, J.J. Cuomo, and W.D. Westwood, (Noyes, Park Ridge, NJ, 1990), Ch II-6.
44. J.M.E. Harper, in Thin Film Processes, ed. J.L. Vossen and W. Kern, (Academic Press, New York, 1978), Ch. II-5.
45. P. Manini, A. Nigro, P. Romano, and R. Vaglio, in High T_c Superconducting Thin Films, Devices, and Applications, AIP Conf. Proc. No. 182, ed. G. Margarintondno, R. Joynt, and M. Onellion, (American Institute of Physics, New York, 1989), p. 90.
46. O. Michikami, H. Asano, Y. Katoh, S. Kubo, and K. Tanabe, Jpn. J. Appl. Phys., Vol. 26, 1987, p. L1221.
47. T. Aida, T. Fukuzawa, K. Takagi, and K. Miyachi, Jpn. J. Appl. Phys., Vol. 26, 1987, p. L1489.
48. J.L. Makous, L. Maritato, C.M. Falco, J.P Cronin, and G.P. Rajendran, Appl. Phys. Lett., Vol. 51, 1987, p. 2164.
49. M. Scheuermann, C.C. Chi, C.C. Tsuei, D.S. Yee, and J.J. Cuomo, Appl. Phys. Lett., Vol. 51, 1987, p. 1951.
50. R.J. Lin, Y.C. Chen, and P.T. Wu, in Materials Research Society Proceedings, Vol. 169: High Temperature Superconductors, ed. D. Christen, J. Narayan, and L. Schneemeyer, (Materials Research Society, Pittsburgh, 1990), p. 635.
51. P.L. Reydet, M. Brunel, J. Marcus, C. Escribe-Fillipine, and J.C. Bruyere, Physica C, Vol. 153, 1988, p. 806.
52. B.Y. Jin, S.L. Lee, S.N. Song, S.-J. Hwu, J. Theil, K.R. Poeppelmeier, and J.B. Ketterson, Adv. Ceramic Mat., Vol. 2, 1987, p. 436.
53. B. Hauser and H. Rogalla, in Novel Superconductivity, ed. S.A. Wolf and V.Z. Kresin, (Plenum, New York, 1987) p. 951.

54. T.I. Selinder, G. Larsson, U. Helmersson, P. Olsson, J.-E. Sundgren and S. Rudner, Appl. Phys. Lett., Vol. 52, 1988, p. 1907.
55. O. Michikami, A. Hidefumi, Y. Katoh, S. Kubo, and K. Tanabe, Jpn. J. Appl. Phys., Vol. 26, 1987, p. L1199.
56. R.F. Kwasnick, F.E. Luborsky, E.L. Hall, M.F. Garbaskas, K. Borst, and M.J. Curran, J. Mater. Res., Vol. 4, 1989, p. 257.
57. S.M. Rossnagel and J.J. Cuomo, in Thin Film Processing and Characterization of High Temperature Superconductors, AIP Conf. Proc. No. 165, ed. J.M.E. Harper, R.J. Colton, and L.C. Feldman, (American Institute of Physics, New York, 1988), p. 106.
58. J. Argana, R.C. Rath, A.M. Kadin, and P.H. Ballentine, in Thin Film Processing and Characterization of High Temperature Superconductors, AIP Conf. Proc. No. 165, ed. J.M.E. Harper, R.J. Colton, and L.C. Feldman, (American Institute of Physics, New York, 1988), p. 58.
59. A.J. Drehman and M.W. Dumais, J. Mater. Res., Vol. 5, 1990, p. 677.
60. R.L. Sandstrom, W.J. Gallagher, T.R. Dinger, R.H. Koch, R.B. Laibowitz, A.W. Kleinsasser, R.J. Gambino, R. Bumble and M.F. Chisolm, Appl. Phys. Lett., Vol. 53 1988, p. 444.
61. J. Gao, W.A.M. Aarnink, G.J. Gerritsma, and H. Rogalla, J. Appl. Surf. Sci., Vol. 46, 1990, p. 74.
62. C.B. Eom, J.Z. Sun, B.M. Lairson, S.K. Streiffer, A.F. Marshall, K. Yamamoto, S.N. Anlage, J.C. Bravman, T.H. Geballe, S.S. Laderman, R.C. Taber and R.D. Jacowitz, Physica C, Vol. 171, 1990, p. 354.
63. H. Asano, H. Yonezawa, M. Asahi, and O. Michikami, IEEE Trans. Magn., Vol. 27, 1991, p. 844.
64. N. Newman, B.F. Cole, S.M. Garrison, K. Char, and R.C. Taber, IEEE Trans. Magn., Vol. 27, 1991, p. 1276.
65. J.R. Gavaler, J. Talvacchio, T.T. Braggins, M.G. Forrester, and J. Gregg, J. Appl. Phys., Vol. 70, 1991, p. 4383.
66. W.Y. Lee, J. Salem, V. Lee, C.T. Rettner, G. Gorman, R. Savoy, V. Deline, and T. Huang, Thin Solid Films, Vol. 166, 1988, p. 181.

67. H. Adachi, K. Setsune, K. Hirochi, T. Kamada, and K. Wasa, *Physica C*, Vol. 153, 1988, p. 1696.
68. Q.Y. Ying, D.T. Shaw, and H.S. Kwok, *Appl. Phys. Lett.*, Vol. 53, 1988, p. 1762.
69. W.Y. Lee, J. Salem, V. Lee, T. Huang, R. Savoy, V. Deline, and J. Duran, *Appl. Phys. Lett.*, Vol. 52, 1988, p. 2263.
70. C.B. Lee, R.K. Singh, S. Sharan, A.K. Singh, P. Tiwari, and J. Narayan, in Materials Research Society Proceedings, Vol. 169: High Temperature Superconductors, ed. D. Christen, J. Narayan, and L. Schneemeyer, (Materials Research Society, Pittsburgh, 1990), p. 481.
71. H.W. Zandbergen, R. Gronsky, and G. Thomas, *Phys. Stat. Sol. (a)*, Vol. 105, 1987, p. 207.
72. J.D. Klein and A. Yen, *J. Vac. Sci. Technol. A.*, Vol. 8, 1990, p. 1.
73. P.M. Mankiewich, R.E. Howard, W.J. Skocpol, A.H. Dayem, A. Ourmazd, M.G. Young, and E. Good, in Materials Research Society Proceedings, Vol. 99: High-Temperature Superconductors, ed. M.B. Brodsky, R.C. Dynes, K. Kitazawa, and H.L. Tuller, (Materials Research Society, Pittsburgh, 1988), p. 119.
74. R. Feenstra, T.B. Lindemer, J.D. Budai, and M. D. Galloway, *J. Appl. Phys.*, Vol. 69, 1991, p. 6569.
75. S.W. Chan, B.G. Bagley, L.H. Greene, M. Giroud, W.L. Feldmann, K.R. Jenkin, II, and B.J. Wilkins, *Appl. Phys. Lett.*, Vol. 53, 1988, p. 1443.
76. Dangerous Properties of Industrial Materials, N.I. Sax, ed., Fifth Edition, (Van Nostrand Reinhold, New York, 1979).
77. S.H. Liou, M. Hong, J. Kwo, B.A. Davidson, H.S. Chen, S. Nakahara, T. Boone and R.J. Felder, *Appl. Phys. Lett.*, Vol. 52, 1988, p. 1735.
78. O. Auciello, M.S. Ameen, T.M. Graettinger, S.H. Rou, C. Soble, and A.I. Kington, in High T_c Superconducting Thin Films, Devices, and Applications, AIP Conf. Proc. No. 182, ed. G. Margaritondo, R. Joynt, and M. Onellion, (American Institute of Physics, New York, 1989), p. 61.
79. J.F. O'Hanlon, A User's Guide to Vacuum Technology, (John Wiley and Sons, New York, 1980).

80. C.B. Fleddermann, J. Appl. Phys., Vol. 67, 1990, p. 3815.
81. G.K. Wehner, Y.H. Kim, D.H. Kim and A.M. Goldman, Appl. Phys. Lett., Vol. 52, 1988, p. 1187.
82. D. Burbidge, P. Mulhern, S. Dew, and R. Parsons, in Thin Film Processing and Characterization of High Temperature Superconductors, AIP Conf. Proc. No. 165, ed. J.M.E. Harper, R.J. Colton, and L.C. Feldman, (American Institute of Physics, New York, 1988), p. 87.
83. Y. Kageyama and Y. Taga, Appl. Phys. Lett., Vol. 55, 1989, p. 1035.
84. N. Terada, H. Ihara, M. Jo, M. Hirabayashi, Y. Kimura, K. Matsutani, K. Hirata, E. Ohno, R. Sugise, and F. Kawashima, Jpn. J. Appl. Phys., Vol. 27, 1988, p. L639.
85. S.I. Shah and P.F. Garcia, in Thin Film Processing and Characterization of High Temperature Superconductors, AIP Conf. Proc. No. 165, ed. J.M.E. Harper, R.J. Colton, and L.C. Feldman, (American Institute of Physics, New York, 1988), p. 50.
86. M. Migliuolo, R.M. Belan, and J.A. Brewer, Appl. Phys. Lett., Vol. 56, 1990, p. 2572.
87. A. Benninghoven and L. Wiedmann, Surf. Sci., Vol. 41, 1974, p. 483.
88. M. Leskela, C.H. Mueller, J.K. Truman, and P.H. Holloway, Mater. Res. Bull., Vol. 23, 1988, p. 1469.
89. J.C. Bruyere, J. Marcus, P.L. Reydet, C. Esribe-Filippini and C. Schlenker, Mater. Res. Bull., Vol. 23, 1988, p. 1907.
90. T. Buyukliamanli, Ph.D. dissertation, University of Florida, 1991.
91. P.M. Mankiewich, J.H. Scofield, W.J. Skocpol, R.E. Howard, A.H. Dayem, and E. Good, Appl. Phys. Lett., Vol. 51, 1987, p. 1753.
92. J.H. Simmons, University of Florida, unpublished communication, 1992.
93. R.P. Vasquez, B.D. Hunt, and M.C. Foote, Appl. Phys. Lett., Vol. 54, 1989, p. 2373.
94. J.D. Klein and A. Yen, to be published.

95. J.J. Cuomo, M.F. Chisolm, D.S. Lee, D.J. Mikalsen, P.B. Madakson, R.A. Roy, E. Geiss, and G. Scilla, in Thin Film Processing and Characterization of High Temperature Superconductors, AIP Conf. Proc. No. 165, ed. J.M.E. Harper, R.J. Colton, and L.C. Feldman, (American Institute of Physics, New York, 1988), p. 141.
96. K. Mizuno, M. Miyauchi, K. Setsune, and K. Wasa, Appl. Phys. Lett., Vol. 54, 1989, p. 383.
97. A. Mogro-Campero, B.D. Hunt, L.G. Turner, M.S. Burrell, and W.E. Balz, Appl. Phys. Lett. Vol. 52, 1988, p. 584.
98. A. Inam, X.D. Wu, T. Venkatesan, D.M. Hwang, C.C. Chang, R. Ramesh, S. Miura, S. Matsubara, Y. Miyasaka, and N. Shotaha, Solid State Technol., Vol. 33, 1990, p. 113.
99. S.Y. Lee, B. Murdock, D. Chin, and T. VanDuzer, in Thin Film Processing and Characterization of High Temperature Superconductors, AIP Conf. Proc. No. 165, ed. J.M.E. Harper, R.J. Colton, and L.C. Feldman, (American Institute of Physics, New York, 1988), p. 427.
100. S. Hatta, H. Higashino, K. Hirochi, H. Adachi, and K. Wasa, Appl. Phys. Lett. Vol. 53, 1988, p. 148.
101. X.D. Wu, R.E. Muenchausen, N.S. Nogar, A. Pique, R. Edwards, B. Wilkens, T.S. Ravi, D.M. Hwang, and C.Y. Chen, Appl. Phys. Lett. Vol. 58, 1991, p. 301.
102. C. Cheung and T. Ruckenstein, J. Mater. Res., Vol. 4, 1989, p. 1.
103. K. Char, D.K. Fork, T.H. Geballe, S.S. Laderman, R.C. Taber, R.D. Jacowitz, F. Bridges, G.A.N. Cornell, and J.B. Boyce, Appl. Phys. Lett., Vol. 56, 1990, p. 785.
104. XRD Powder Diffraction File, Joint Commission on Powder Diffraction Standards, (International Center for Diffraction Data, Swathmore, PA, 1981).
105. M. Naito, R.H. Hammond, B. Oh, M.R. Hahn, J.W.P. Hsu, P. Rosenthal, A.F. Marshall, M.R. Beasley, T.H. Geballe, and A. Kapitulnik, J. Mater. Res., Vol. 2, 1987, p. 713.
106. D.B. Tanner, University of Florida, unpublished communication, 1992.

107. L.I. Maissel, in Handbook of Thin Film Technology, ed. L.I. Maissel and R. Glang, (McGraw-Hill, New York, 1970), Ch. 13.
108. M.L. Knotek and P.J. Feibelman, *Phys. Rev. Lett.*, Vol. 40, 1978, p. 964.
109. CRC Handbook of Chemistry and Physics 66th Edition, ed. R.C. Weast, (CRC Press, Cleveland, 1985).
110. Y. Ikuma and S. Akiyoshi, *J. Appl. Phys.*, vol. 64, 1988, p. 3915.
111. Y. Zhu, J. Tafto, and M. Suenaga, *MRS Bull.*, Vol. XVI, 1991, p. 54.
112. J.-M. Tarascon and B.G. Bagley, *MRS. Bull.*, Vol XIV, 1989, p. 53.
113. L. Pauling, The Nature of the Chemical Bond and the Structure of Molecules and Crystals: An Introduction to Modern Structural Chemistry, 3rd edition, (Cornell University Press, Ithaca, NY, 1960).
114. H.B. Michaelson, *IBM Jour. Res. Dev.*, Vol. 22, 1978, p. 73.
115. D.M. De Leeuw, C.A.H.A. Mutsaers, C. Langereis, H.C.A. Smoorenburg and P.J. Rommers, *Physica C*, Vol. 152, 1988, p. 39.
116. I.D. Raistrick, D.W. Cooke, J.G. Beery, F.H. Garzon, H. Javadi, M.P. Maley, A.D. Rollett, T. Roy, D.N. Sinha, and D.K. Wilde, in Materials Research Society Proceedings, Vol. 169: High Temperature Superconductors, ed. D. Christen, J. Narayan, and L. Schneemeyer, (Materials Research Society, Pittsburgh, 1990), p. 695.
117. F. H. Garzon, I.D. Raistrick, and D.R. Brown, *Jour. Electr. Mater.*, Vol. 21, 1992, p. 483.
118. R.J. Cava, B. Batlogg, C.H. Chen, E.A. Reitman, S.M. Zahuraki, and D. Werder, *Phys. Rev. B*, Vol. 10, 1987, p. 5719.
119. B. D. Cullity, Elements of X-ray Diffraction, (Addison-Wesley, Reading, MA, 1978).
120. P.R. Broussard, in Science and Technology of Thin Film Superconductors, ed. R.D. McDonnel and S.A. Wolf, (Plenum Press, New York, 1989), p. 91.

121. G.J. Fisanick, P. Mankiewich, W. Skocpol, R.E. Howard, A. Dayem, R.M. Fleming, A.E. White, S.H. Liou, and R. Moore, in Materials Research Society Proceedings, Vol. 99: High-Temperature Superconductors, ed. M.B. Brodsky, R.C. Dynes, K. Kitazawa, and H.L. Tuller, (Materials Research Society, Pittsburgh, 1988), p. 703.
122. R. Feenstra, L.A. Boatner, J.D. Budai, D.K. Christen, M.D. Galloway, and D.B. Poker, Appl. Phys. Lett., Vol. 54, 1989, p. 1063.
123. J. Halbritter, Int. J. Modern. Phys., Vol. 3, 1989, p. 719.
124. S.N. Basu, A.H. Carim, and T.E. Mitchell, J. Mater. Res., Vol 6., 1991, p. 1823.
125. R.M. Rose, L.A. Shephard, and J. Wulff, The Structure and Properties of Materials, Volume IV: Electronic Properties, (John Wiley and Sons, New York, 1966).
126. C.B. Eom, A.F. Marshall, S.S. Laderman, R.D. Jacowitz, and T.H. Geballe, Science, Vol. 249, 1990, p. 1549.
127. H.C. Li, G. Linker, F. Ratzel, R. Smithey, and J. Geerk, Appl. Phys. Lett., Vol. 52, 1988, p. 1098.
128. D.S. Campbell, in Handbook of Thin Film Technology, ed. L.I. Maissel and R. Glang, (McGraw-Hill, New York, 1970), ch. 12.
129. K. Wasa, M. Kitabatake, H. Adachi, K. Setsune, and H. Adachi, in Thin Film Processing and Characterization of High Temperature Superconductors, AIP Conf. Proc. No. 165, ed. J.M.E. Harper, R.J. Colton, and L.C. Feldman, (American Institute of Physics, New York, 1988), p. 38.
130. S. Mader, in Handbook of Thin Film Technology, ed. L.I. Maissel and R. Glang, (McGraw-Hill, New York, 1970), Ch. 9.
131. E.M. Levin, C.R. Robbins, and H.W. McMurdie, Phase Diagrams for Ceramists, (American Chemical Society, Columbus, OH, 1974), p. 195.
132. W. Pelster, Res. and Devel., Vol. 30, 1988, p. 80.

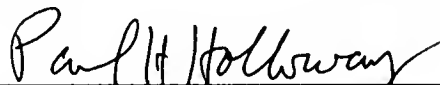
BIOGRAPHICAL SKETCH

James Kelly Truman was born on October 8, 1960, in East Chicago, Indiana, to Suzanne J. Truman (now Higgins) and Edward J. Truman. He graduated from Lake Central High School in St. John, Indiana, in 1978 and was ranked third in a class of over 450 students. In 1982 he graduated cum laude from the University of Notre Dame in Notre Dame, Indiana, with a Bachelor of Science degree in metallurgical engineering and materials Science. During the summers while a student at the University of Notre Dame, Kelly worked as an Intern Metallurgical Engineer at the Inland Steel Company in East Chicago, Indiana. He received the Master of Science degree in materials Science and engineering at the University of Florida in 1984. His master's research, which was performed primarily while he was a student intern at Tektronix, Incorporated in Beaverton, Oregon, was under the direction of Dr. Paul H. Holloway. The area of research was the high temperature stability of refractory metal silicide Schottky barrier contacts to gallium arsenide. In 1984 he assumed a full time position as a Materials Engineer in the Display Device Organization of Tektronix, where his primary responsibility was the development of thin film materials for a resistive touch-panel application. In late 1985 he

returned to the University of Florida to pursue a doctorate in materials science and engineering under the direction of Dr. Paul H. Holloway and to get married. His initial area of research was high temperature stable electrical contacts to gallium arsenide. He remained working in this area until 1987, during which time he held student intern positions at Bell-Northern Research in Ottawa, Ontario, Canada, and at IBM T.J. Watson Research Center in Yorktown Heights, New York. In late 1987 he was swept by the tide of excitement and money into the field of high temperature superconducting materials. His doctoral research concentrated on the sputter deposition of high temperature superconductor and barrier layer thin films. In 1990, before completing his doctoral dissertation, he took a position out of economic necessity as Materials Scientist at CVC Products in Rochester, New York. At CVC he managed three government research contracts: two in the area of high temperature superconducting thin films and one in the area of thin film high dielectric constant materials for RAM devices. While at CVC, he also continued to work on his doctoral dissertation, albeit slowly, which is presented here. As of November, 1992, Kelly will assume a position at Conductus, Incorporated in Sunnyvale, California, where he will be responsible for the development of thin film growth processes for the application of high temperature superconducting thin films as interconnects in multi-chip modules.

Kelly married Cristina Logan in Palm Beach, Florida, on December 28, 1985. His wife and he became parents on March 10, 1989, when their daughter Isabel was born in Gainesville, Florida.

I certify that I have read this study and that in my opinion it conforms to acceptable standards of scholarly presentation and is fully adequate, in scope and quality, as a dissertation for the degree of Doctor of Philosophy.



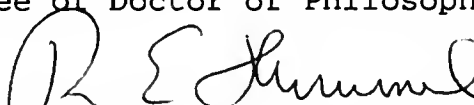
Paul H. Holloway, Chair
Professor of Materials Science
and Engineering

I certify that I have read this study and that in my opinion it conforms to acceptable standards of scholarly presentation and is fully adequate, in scope and quality, as a dissertation for the degree of Doctor of Philosophy.



Joseph H. Simmons
Professor of Materials Science
and Engineering

I certify that I have read this study and that in my opinion it conforms to acceptable standards of scholarly presentation and is fully adequate, in scope and quality, as a dissertation for the degree of Doctor of Philosophy.



Rolf E. Hummel
Professor of Materials Science
and Engineering

I certify that I have read this study and that in my opinion it conforms to acceptable standards of scholarly presentation and is fully adequate, in scope and quality, as a dissertation for the degree of Doctor of Philosophy.



Robert T. DeWoff
Professor of Materials Science
and Engineering


I certify that I have read this study and that in my opinion it conforms to acceptable standards of scholarly presentation and is fully adequate, in scope and quality, as a dissertation for the degree of Doctor of Philosophy.



David B. Tanner
Professor of Physics

This dissertation was submitted to the Graduate Faculty of the College of Engineering and to the Graduate School and was accepted as partial fulfillment of the requirements of the degree for Doctor of Philosophy.

December 1992


for Winfred M. Phillips
Dean, College of Engineering

Madelyn M. Lockhart
Dean, Graduate School

UNIVERSITY OF FLORIDA



3 1262 08554 0523